Low Noise Microwave Feedback Amplifier Design with Simultaneous Signal and Noise Matching

Luciano Boglione

Submitted in accordance with the requirements for the degree of Doctor of Philosophy,
Institute of Microwaves and Photonics, School of Electronic and Electrical Engineering,
The University of Leeds.

The candidate confirms that the work submitted is his own and that appropriate credit has been given where reference has been made to the work of others.

January 1998

Abstract

This thesis looks into the problem of simultaneous signal and noise match at the input port of low noise amplifiers; feedback LNAs are considered because previous works show that they can achieve the simultaneous match condition.

The investigation analyses the influence of both parallel and series feedback elements on the amplifier. Matrices are used to describe signal and noise parameters of each component of the model – parallel admittance, series impedance, active device. This approach allows the analysis to be applied to a wide range of networks, as long as noise and signal matrices are available. For this reason, the results are not limited to active devices in the microwave region of the spectrum but they are applicable to any linear 2–port circuit.

The noise parameters of feedback networks are investigated thoroughly. Analytical expressions are worked out as functions of the feedback immittances and have been used to support experimental evidence previously published. A duality property for feedback networks is pointed out; new circles for constant equivalent noise resistance are devised; optimum values for the feedback impedance are determined; an investigation of a well–known noise model is carried out and its validity is extended.

Based on the closed form expressions of the noise parameters, an original analytical procedure for the design of the optimum noise source reflection coefficient is presented. To the author's knowledge, no technique was available before. The design for simultaneous signal and noise match is now possible, because the input reflection coefficient can be set independently by properly choosing the load. Different devices are considered and their different behaviour is highlighted. A remarkable feature of the new design technique is to avoid the need of input matching when designing low noise amplifiers.

Finally, experimental results are also presented and the performance of a 1 GHz single stage BJT LNA is shown. The fundamental achievement is that the noise figure of the LNA is equal to its minimum value within the measurement uncertainty.

Acknowledgments

I still remember my excitement when I found Roger's message on my answering machine, about four years ago. It was the beginning of an adventure I firmly wanted and which is now coming to an end. During my PhD at the University of Leeds, I came across a large number of people, who may not find their name mentioned in these few lines: I hope they will forgive me.

Prof. Roger Pollard has been my first supervisor. His guidance and help have been exceptional, from the very start, when he arranged an interview for me with Filtronic Comtek plc to sponsor my PhD; I thank them for their indispensable financial support. Prof. Pollard put me in touch with a number of people; he supported my idea of fabricating a MMIC LNA – for which I am also indebted to Hewlett Packard Microwave Technology Division, Santa Rosa, USA. Apart from technical discussions, hints and suggestions for my research throughout these years, I hope I have learnt something from his professional attitude toward me. I saw my PhD as a job, not as yet another University course; I often felt this view was shared by him. I will always treasure my years as Prof. Pollard's PhD student.

Many people come under the heading of the Institute of Microwaves and Photonics, part of the School of Electronic and Electrical Engineering. I would like to mention Prof. Christopher M. Snowden as Head of the School and my second supervisor, Dr. Vasil Postoyalko.

The people of the workshop have been extremely helpful coping with my requests whenever a new circuit had to be fabricated. I am not going to write down their names, not because I do not remember them, but because they are a team and it is to the team that I am grateful.

There are other teams in the School. I would like to mention Moyra Culbert, Judith Watson and Gill Cooper, to whom I asked the most unexpected requests and I always had them answered, with wonderful smiles: thank you! John Sheard and Sunalini Ekbote, who have kept my work going despite all my unpredictable computer–related problems. A special mention to Albert Payne with whom I have enjoyed many, many laughs and jokes every time our paths crossed over, especially near the photocopier machine.

I also want to remember the other PhD students who will soon be *doctors* and with whom I have spent these years. In particular, Nafisa Khan and Pallavi Sandhiya, whose proof reading of my thesis has been an invaluable help for me: I just hope she forgives me for the hard time she went through. The errors which may still be present in the following pages are my fault only.

A special remark goes to Richard Roper, librarian at the Combined Mechanical Engineering Library, whom I took over during his lunch break and I shared many laughs with.

Finally, these years have revealed to me the true feelings of many people back home. A joyful testimony beyond any expectation has come from my sister, Elisa, and my brother–in–law, Alessandro: without their love and friendship, many things would have been impossible for me to achieve and one thesis would not be enough to mention all they did for me. I wish my father and my mother could share my happy memories, too.

I want to finish this page with a poem [1] which I learnt many years ago when I did not know what my fate would be today. I am sorry if these words are not in English: I have done my best to ensure that they are the only foreign ones in this dissertation.

Ognuno sta solo sul cuore della Terra,
trafitto da un raggio di sole.
Ed é subito sera.

Salvatore Quasímodo,
from *Acque e Terre*, 1930
(Nobel Laureate in Literature, 1959)

Now it's time to move on.

Contents

List of Figures

List of Tables

List of Symbols

DC	Direct Current
LNA	Low Noise Amplifier
MMIC	Monolithic Microwave Integrated Circuit
SSNM	Simultaneous Signal and Noise Match
SWR	Voltage standing wave ratio
BJT	Bipolar Junction Transistor
HBT	Heterojunction Bipolar Transistor
FET	Field Effect Transistor
MESFET	Metal–Semiconductor Field Effect Transistor
HEMT	High Electron Mobility Transistor
$\Re e\,[z]$	Real part of complex number z
$\Im m\,[z]$	Imaginary part of complex number z
$\mid z \mid$	Magnitude of complex number z
$\angle z$	Phase of complex number z
$z^{\star}$	Complex conjugate value of z
^{T}	Transponse operator
v^{+}	Hermitian conjugate of complex vector v, $v^{+} = (v^{\star})^{T} = \left(v^{T}\right)^{\star}$
f_o	Test frequency
T_o	Standard temperature, $T_o = 290$ K
Z_o	Characteristic impedance
Z_s	Feedback series impedance at f_o
R_s	Feedback series resistance at f_o, $R_s = \Re e\,[Z_s]$
r_s	Feedback series resistance normalised to Z_o, $r_s = \Re e\,[Z_s/Z_o]$
X_s	Feedback series reactance at f_o, $X_s = \Im m\,[Z_s]$

x_s	Feedback series reactance normalised to Z_o, $x_s = \Im m\left[Z_s/Z_o\right]$
$X_{s_{min}}$	Feedback series reactance at f_o for $R_n = R_{n_{min}}$
$X_{s_{max}}$	Feedback series reactance at f_o for $R_n = R_{n_{max}}$
Y_p	Feedback parallel admittance at f_o
G_p	Feedback parallel conductance at f_o, $G_p = \Re e\left[Y_p\right]$
B_p	Feedback parallel susceptance at f_o, $B_p = \Im m\left[Y_p\right]$
$\mathbf{M}$	Matrix
M_{ij}	Element of the matrix $\mathbf{M}$ at row i, column j
$\mathbf{T}$	Transmission matrix
$\mathbf{C}_M$	Correlation matrix for M – matrix representation
$\mathbf{C}_n$	Correlation matrix for transmission representation
R_n	Equivalent noise resistance
g_n	Equivalent noise conductance
ρ_{n_o}	Noise correlation factor
ρ_n	Correlation matrix off–diagonal element
$Z_{S_{opt}}$	Optimum source noise impedance for minimum noise figure at f_o
$R_{S_{opt}}$	Optimum source noise resistance for minimum noise figure at f_o for $R_{S_{opt}} = \Re e\left[Z_{S_{opt}}\right]$
$X_{S_{opt}}$	Optimum source noise reactance for minimum noise figure at f_o for $X_{S_{opt}} = \Im m\left[Z_{S_{opt}}\right]$
Γ_{in}	Input reflection coefficient
Γ_L	Load reflection coefficient
$\Gamma_{S_{opt}}$	Optimum source noise reflection coefficient for minimum noise figure
$SSNM$	SSNM definition, $SSNM\left(\Gamma_L\right) = \Gamma_{in}\left(\Gamma_L\right) - {\Gamma_{S_{opt}}}^{\star}$
Γ_L^{SSNM}	Load reflection coefficient for $SSNM = 0$

Chapter 1

Introduction

Wireless communications are of paramount importance in everybody's life and perhaps are the best example of microwave engineering. Few years ago, microwave applications were primarily for the military. Income from commercial applications such as mobile phones, satellite television and radars for car detection allowed the microwave industry to transform and target the general public when the demand from the military began to decrease.

In order to guarantee a reliable wireless communication system, a compound of different expertise is required. Microwave engineering primarily deals with the hardware (transmitters, receivers, propagation of electromagnetic waves, and so on) and is not concerned with the handling of the information to be transported from one point to another.

A radio–link is used as example in order to gradually focus on the various aspects of noise and on the problem of simultaneous power match. This feature is one important characteristic associated with low noise amplifiers, which are indispensable subsystems for radio–communications. The design of low noise amplifiers and the simultaneous power match is the topic on which this dissertation reports.

1.1 Wireless Microwave Communications

Any unwanted signal, frequently without any repetitive pattern, can be considered as electric noise. Since noise lacks in coherence, it is often described in term of average power superimposed on the information travelling from the source to the destination.

Any wireless system may be described as a chain of three stages, each of which is prone to introduce unwanted noise power and to degrade the quality of the message:

- *the transmitter*: the signal may be affected by noise before leaving the antenna;
- *the link*: noise power from sources other than the transmitter reaches the receiver and worsen the signal–to–noise (S/N) power ratio at the input of the receiver;
- *the receiver*: the S/N power ratio after the antenna has detected the incoming wave decreases further due to the noise generated by the receiver itself.

Proper design of the transmitter will guarantee that the noise contribution from this stage is negligible; the link stage is discussed in the next section; the receiver stage, in particular the front end amplifier located immediately after the antenna, constitutes the bulk of this dissertation. It will be introduced in section 1.3.

1.2 Noise in Radio–Links

This section focuses on general aspects related to noise in radio–links and is based on reports made by the International Radio Consultative Committee (CCIR). The CCIR carries out technical research on behalf of the International Telecommunication Union (ITU) which regulates the spectrum management and exploitation among Countries of the world. The task of keeping up with technological improvements makes CCIR update its reports on a regular basis. The reports cited in this section refer to a thorough discussion of the spectrum management carried out by Withers [2]; a footnote is added to point out the exact reference.

Often the radio–link noise generated between transmitter and receiver is the main cause of degradation for the overall S/N ratio of wireless systems. Noise power sources detectable by any receiving antenna can be classified as follows:

- *atmospheric* noise, generated by lightning discharges;
- *man–made noise*, generated by electrical man–made sources;
- *thermal noise*, generated by any body whose temperature is above 0 K. This class may be split in:
  - *terrestrial sources*: the radiating bodies are the ground and the atmosphere of the Earth;
  - *extra–terrestrial sources*: this class includes a vast number of extra–terrestrial physical entities, such as stars or radiation.

Some of the above noise sources may form the actual information to be detected: the Sun, planets, galactic noise, cosmic background radiation, etc. are targets for radio–astronomers. These targets may be extremely weak; the power detected by the receiving antenna often is far below the noise floor of the LNA at ambient temperature. Cooling systems are used to lower the receiver temperature to few tens of Kelvin in order to minimise its noise contribution. This highly specialised area forms another branch of microwave engineering, related to devices for very low noise amplification [3]. Solid state transistors [4], [5], [6], [7] have demonstrated very low noise performance when cooled down to cryogenic temperatures (77 K or 12.5 K) and they have shown new phœnomena to account for [5]. As a matter of fact, cryogenic amplifiers have obviously limited applications and do not have a major impact in economic terms. Therefore, this dissertation will not further investigate this topic and the radio–link noise is assumed to be undesired power, degrading the S/N ratio available at the receiver antenna.

Atmospheric Noise

Lightening discharges occur primarily in thunderstorms. The power is not distributed evenly over the frequency spectrum: the maximum occurs below 10 kHz but significant power still is available in the very high frequency (VHF) range, between 30 and 300 MHz. The power can be transmitted by ionospheric propagation mechanisms to locations far away from the storm. Large, rapid fluctuations of received power level characterise atmospheric radio noise; if averaged over several minutes, this noise power[1] is nearly constant within ±2 dB. Changes of the average value are related to the solar activity cycle and other atmospheric phœnomena whose importance has often not been quantified.

Man–made Noise

Man–made apparatus are likely to radiate power in a narrow band and the signal waveform is usually coherent. This is not the case for man–made electrical equipments such as electric traction systems, overhead electric power systems, ignition systems of petrol–driven motor vehicles, etc. The noise power delivered from man–made noise sources[2] decreases as frequency increases; quantification is somewhat controversial among experts. Man–made noise is the main source of link degradation in the frequency range from 10 MHz to over 1 GHz,

[1] *Characteristics and applications of atmospheric radio noise data*, CCIR Report 322–3, ITU, Geneva, 1988

[2] *Man–made radio noise*, CCIR Report 258–4, ITU, Geneva, 1986, Volume VI

particularly in heavily populated areas.

Terrestrial Thermal Noise

Terrestrial thermal noise[3] is important in the range of frequency over 300 MHz. Any state in which water can be found, gases in the atmosphere and the Earth's surface radiate incoherent power, often called *sky noise*. The noise power emitted by our planet depends on its temperature as well as on its surface characteristics. The surroundings of an antenna affect its equivalent noise temperature[4]; the antenna equivalent noise temperature is also called *brightness temperature*.

The brightness temperature of the Earth's surface depends in a complex fashion on frequency as well as on its temperature, roughness and permittivity of the ground. The brightness temperature of the sea is lower than its physical temperature – about 100 K in the microwave range, slightly higher at millimetre wave frequency. Land surface brightness temperature is about 90% of the physical temperature of the ground for high angles of elevation; it may diminish if the elevation decreases, or if the ground is made of very wet soil.

Gases in the atmosphere, such as oxygen and water vapour, interfere with any electromagnetic wave by absorbing power; they radiate thermal noise, too. The atmosphere brightness temperature T_{atm} for a given gas under clear sky conditions can be calculated at any given frequency by:

$$\frac{T_{atm}}{T_m} = 1 - 10^{A/10}$$

where T_m is the mean temperature in Kelvin of the atmospheric gas and A is the attenuation in dB at the given frequency along the principal axis of the antenna. The same expression also applies to rain up to 10 GHz. Above this frequency, T_{atm} may be overestimated because scattering occurs and increases the attenuation; however, scattering does not contribute to the brightness temperature.

When considering these contributions together, some considerations on the antenna equivalent noise temperature T_{ant} due to terrestrial thermal noise can be made.

1. In general, T_{ant} is usually below 300 K and will not have major effects on radio–links which do not require low noise performance.

[3] *Radio emission from natural sources in the frequency range above about 50 MHz*, CCIR Report 720–2, Recommendations and Reports of the CCIR, 1986, Volume V (ITU, Geneva, 1986)

[4] The definition of *equivalent noise temperature* will be introduced in chapter 2.

2. A point–to–point terrestrial link is likely to receive half power of the total incoming power from the side lobes of the antenna; the total equivalent noise temperature of the antenna being in the 200–250 K range. These values often exceed either the man–made noise for frequencies above 1 GHz, even in populated areas; or the galactic noise above 0.6 GHz in scarcely populated areas. Therefore, for low noise first stage amplifiers, terrestrial thermal noise may be dominant. In heavy rain as well as in the millimetre wave absorption bands, the equivalent antenna noise temperature raises to 300 K.

3. Well–designed antennas pointing to the sky[5] will not see bright surroundings (brightness temperature of around 20 K). This value is likely to increase up to 50–150 K in the range 10–15 GHz when raining, or even when only clouds are present above 15 GHz. Absorption of signal power at 22.3 GHz due to water vapour does not significantly affect the radio–link but is an important source of noise; oxygen is a further noise source. Indicatively, these two noise sources make the antenna equivalent noise temperature range from 130 to 290 K between 45 and 350 GHz.

4. For antennas located on space crafts or satellites watching the Earth, thermal noise coming from the ground will be seen by the main lobe; however, the brightness temperature will be lower than 290 K because seas cover most of the Earth surface, except for those frequencies where atmosphere gas absorption occurs.

Extra–terrestrial Thermal Noise

Radio noise is generated within the Milky Way by sources such as interstellar gas or other physical mechanisms[6]. The Sun is a powerful source of electromagnetic waves; some values of its brightness temperature vs. frequency are shown in Figure 1.1. Large increments in its brightness are produced when the Sun is not quiet.

The Moon has a brightness temperature, seen from the Earth, between 150 and 370 K; other planets or stars may have brightness temperatures up to 600 K. These values vary with frequency as well as with other causes, such as the gain of the antenna (low gain antennas

[5] *Radio emission from natural sources in the frequency range above about 50 MHz*, CCIR Report 720–2, Recommendations and Reports of the CCIR, 1986, Volume V (ITU, Geneva, 1986); *Form of the hypothetical reference circuit and allowable noise standard for frequency division multiplex telephony and television in the fixed–satellite service*, CCIR Report 208–6, Recommendations and Reports of the CCIR, 1986, Volume V (ITU, Geneva, 1986); *Earth station antennas for the fixed–satellite service* CCIR Report 390–5, *ibid.*, Volume IV–1

[6] *Radio emission from natural sources in the frequency range above about 50 MHz*, CCIR Report 720–2, Recommendations and Reports of the CCIR, 1986, Volume V (ITU, Geneva, 1986); *Earth station antennas for the fixed–satellite service* CCIR Report 390–5, Recommendations and Reports of the CCIR, 1986, (ITU, Geneva, 1986), Volume IV–1

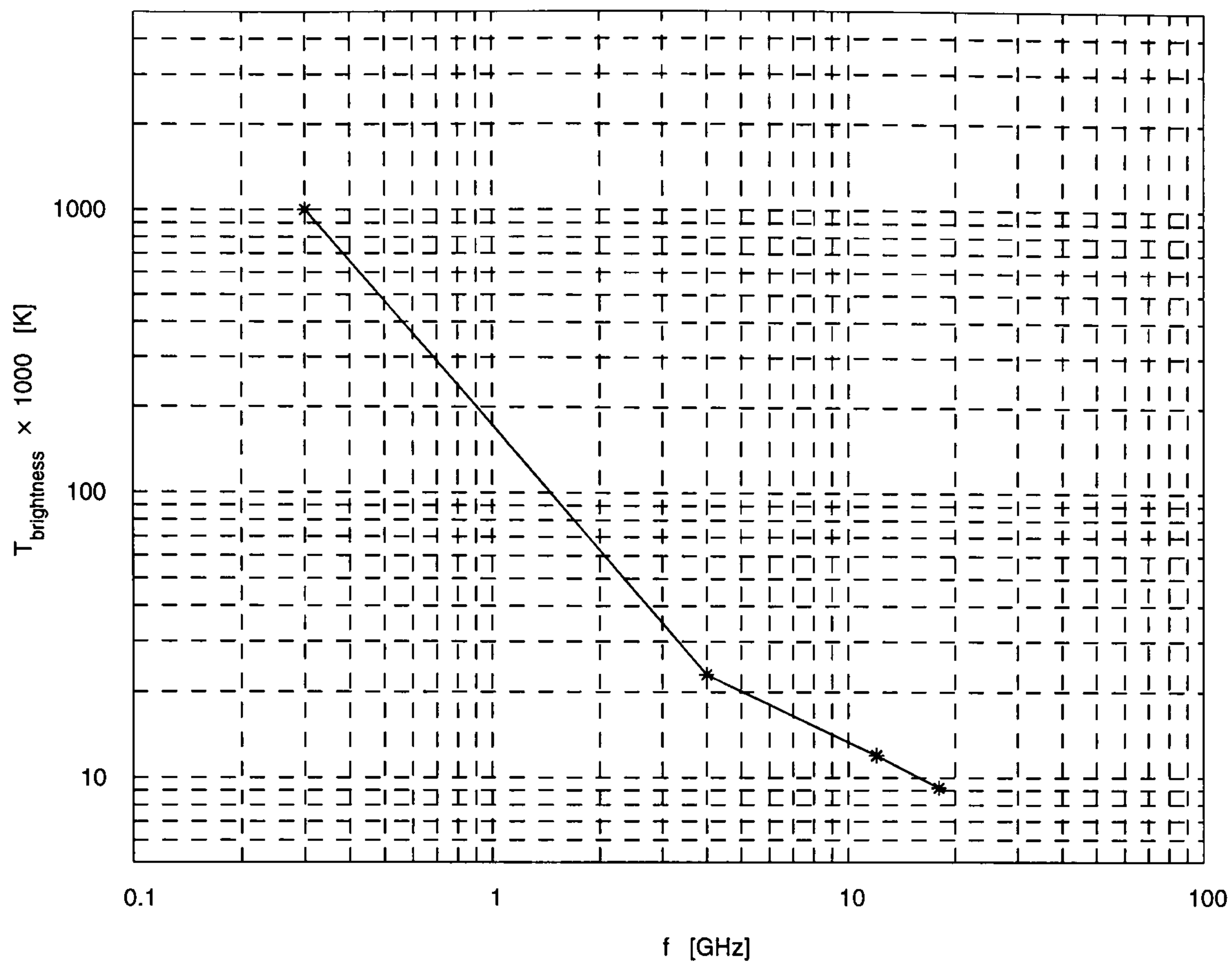

Figure 1.1 Sun brightness temperature vs. frequency in quiet conditions.

do not focus on a given spot; instead, they average the detected power over a large area of space). At frequencies up to 1 GHz, galactic noise can be important, in particular for antennas located in sparsely populated areas where there is little contribution from man–made noise. Unless the Sun, the Moon or other noise sources are specifically tracked by the antenna, their noise contribution lasts for a few minutes per day - if the antenna beam can see that object. Consequently, the equivalent noise temperature is not heavily affected by any of the above sources in particular. Extra–terrestrial noise sources are significant in the ultra high frequency (UHF) range, from 300 MHz to 3 GHz, but are less significant in the upper part of the 3 to 300 GHz range. A noteworthy point is that the brightest part of the Milk Way (located in the direction of the constellation Sagittarius) is never in alignment with the geostationary satellites and the Earth. The Sun is lined with a geostationary satellite and its Earth antenna, for no longer than tens of minutes per year. Properly oriented ground antennas are likely to receive no noise power from any extra–terrestrial source.

Finally, it is worth mentioning than an antenna with very low side lobes, looking at the deep space at its zenith, will see a very cold sky whose brightness temperature is as small as

2.7 K. This is the cosmic background radiation level and it is the ultimate noise floor level in radio–links.

1.3 Low Noise Amplifiers for Microwave Links

When an antenna detects an electromagnetic wave, the first active stage to process the incoming signal is a low noise amplifier (LNA). A filter may be located in front of the amplifier in order to properly define the bandwidth of the signal [8]. For instance, microwave applications for mobile communications occupy the spectrum at 900 MHz and 1.8–1.9 GHz; a typical GSM system bandwidth is 35 MHz. State–of–the–art circuits have shown that the antenna and the device can be integrated on the same substrate in order to reduce size and improve the electrical performance [9].

Therefore, the signal–to–noise power ratio S_i/N_i is set at the input of the LNA and is a known quantity. Since the signal and noise powers are small, non–linearities in the first stage of the receiver are not important and the assumption that linearity holds, is taken for granted. The previous section has highlighted some contributions to the noise power N_i. The signal power S_i available at the output terminal of the antenna depends upon the transmitter power, the gain of the transmitting and receiving antennas and the distance between them; other phœnomena related to the propagation of electromagnetic waves affect the delivered power as well [10].

Communication systems often have a characteristic impedance Z_o of 50 Ω and both signal and noise measurements are referred to this value. Scattering parameters [11] are widely used to characterise the electrical performance of wireless communication subsystems. However, design techniques, in particular concerning LNAs, are normally based on current and voltages; low frequency network topologies are used (for instance, [12], [13]) and mixed with distributed elements for matching purposes. Microwave monolithic integrated circuit (MMIC) technology allows the designer to apply low frequency techniques at high frequencies as well as increase repeatability and reliability [14]. These features are indispensable to achieve the high yields necessary for mass production.

As the frequency crosses the 1 GHz threshold, majority carrier active devices tend to dominate over minority carrier devices because of their better noise performance. Gallium arsenide field effect transistors (FETs) have demonstrated their superiority over silicon devices. However, silicon is less expensive than gallium arsenide and is extremely attractive for low cost, high yield commercial applications. Hetero–junction bipolar transistors (HBTs) show very good microwave characteristics and have revived the use of bipolar homo–junction transistors (BJTs) at microwave frequencies.

Both FETs and BJTs show a predominantly capacitive input though for different physical reasons [15]. The device input impedance must be transformed in order to achieve the desired electrical LNA performance at the known characteristic impedance Z_o of the microwave system. This is usually carried out by matching networks. Simple as well as more sophisticated techniques have been devised in order to cope with the requirement that the entire available signal power S_i should be delivered to the device for amplification. Since the LNA cannot distinguish between information and noise, the input available noise power N_i is amplified, too. The input S_i/N_i ratio would not degrade if the LNA could be noiseless. This is not the case in practice: the LNA adds its own noise power to the incoming noise N_i so that the output signal–to–noise power ratio S_o/N_o is smaller than the input S_i/N_i ratio.

The causes of noise differ in active devices such as BJTs or FETs. The former tend to suffer from many sources of noise: self–heating effects may affect the lattice temperature (which cannot be assumed to be equal to the room temperature) [16]; and shot noise is an intrinsic source of noise in n–p junctions [17]. The main cause of noise for FETs is the thermal contribution from the channel.

1.3.1 The Mismatch at the Input Port

Whatever the device in use, experiments demonstrate that the output S_o/N_o ratio at the LNA output port shows a minimum for a value of source impedance which does not yield the maximum power gain at the same time. The source impedance is the small signal Thevenin equivalent impedance of the source feeding the LNA at its input port. The experimental evidence is explained by noise theory [18]. Device manufacturers aim to produce transistors which can provide maximum gain and minimum S_o/N_o with the same source impedance. It should also be pointed out that the optimum noise source impedance rarely is the characteristic impedance Z_o of the system at the frequency of interest. Matching techniques are used to furnish a simultaneous solution for these requirements.

1.4 The Contribution of this Work

It is evident that LNA designers want the amplifier to show as high gain as possible; and as little degradation of the output signal–to–noise ratio as possible with comparison to the input signal–to–noise ratio.

How to achieve those goals simultaneously is the topic which this research has been investigating: it has been named SSNM for *Simultaneous Signal and Noise Match.* The SSNM condition is to be achieved for a given value of source impedance connected to the LNA input port; a further requirement is that the optimum impedance also is the characteristic impedance of the system.

Many results which will be discussed in this dissertation are new as well as original: some are new because they improve the understanding of previous achievements; some are original because no previous description is available in the literature to the author's knowledge.

The new contributions of this thesis are about:

- the SSNM condition and the constraints it imposes on the final LNA when an input matching circuit is used. It will be shown that the SSNM requirement is achievable only with lossy (noisy) input matching networks, which are likely to degrade the noise performance of the overall LNA. This conclusion has driven to formalise the new concept of LNA design without input matching circuit;

- the analysis of microwave feedback amplifiers. The analysis has produced a set of closed form equations for the noise parameters which account for both parallel and series feedback immittances as well as their thermal noise contributions if real parts are present;

- the extension and validation of a well-known noise model to extrinsic and packaged FETs.

The original contributions deal with:

- the design of the optimum source impedance for minimum noise figure with feedback amplifiers. To the author's knowledge, no previous analytical design procedure was available in the literature before;

- the extension of the previous original design procedure to lossy series feedback elements. The result shows that, theoretically, series feedback elements can still lower the minimum noise figure while designing the optimum noise source impedance.

An experimental validation of the original design technique has also been published.

1.5 Structure of the Thesis

This thesis is structured as follows:

- chapter 2 reviews the previous contributions to the field of noise and design techniques for low noise amplifiers. Particular attention is paid to the SSNM topic;
- chapter 3 describes the new analysis of feedback amplifiers as well as the interaction between LNA and input matching circuit within the SSNM constraint;
- chapter 4 extends the analysis to inductors at the device input port. The Pospieszalski noise model for intrinsic FETs is modified to account for parasitics and a discussion on the validity of the new approach outlined;
- chapter 5 presents the original noise design technique for feedback amplifiers as well as its extension to lossy series feedback elements. The experimental validation with a 1 GHz single stage LNA is also reported;
- chapter 6 concludes this dissertation and points out some directions for future investigations of the SSNM topic.

Appendices as well as a copy of the publications this work has generated, follow along with the list of references.

1.6 Conclusion

The complexity of a microwave wireless communication system as well as the causes of noise which affect any given wireless system have been sketched out. The importance of low noise amplifiers within the system has been outlined and the problem of simultaneous signal and noise match at the input port of the LNA has been focused upon. Finally, the contributions of this research on the SSNM topic as well as the structure of the thesis have been presented.

Chapter 2

Noise and Low Noise Amplifier Design

Noise is an extremely broad area in microwave engineering and its understanding is of paramount importance for designing low noise amplifiers. In this chapter, some aspects of noise are introduced and critically reviewed, focusing on those parts which are essential for the understanding of the following chapters. This is accomplished by surveying the results available in the microwave engineering literature.

2.1 Noise Figure

The noise figure is a powerful tool quantifying the noise performance of any 2–port network. Friis [19] defined the noise figure in 1944. In his paper, he first introduces some concepts such as source available power (power delivered from the source to a matched load), 2–port network available gain (the ratio of available power at the output port to the available power at the input port) and effective bandwidth B:

$$B\,G_{av}\left(f_o\right) = \int G_{av}\left(f\right)\,df$$

where f_o is a convenient reference frequency and the integral is evaluated between proper limits. Then, Friis' noise figure definition is *The ratio of the available signal–to–noise ratio at the signal generator terminals to the available signal–to–noise ratio at its output terminals*

([19], page 420):

$$F = \frac{(S_i/N_i)}{(S_o/N_o)} \tag{2.1}$$

The noise figure of two or more networks in cascade is analysed, as well. It is important to bear in mind that the noise figure deals with available powers. This fact brings together two consequences: the noise figure is dependent only on the source impedance; and the noise figure definition is based on a worst case approach. The first point is reported in plain words; the second point is implied by Friis' statement related to footnote 5 ([19], page 419): *In amplifier input circuits a mismatch condition may be beneficial due to the fact that it may decrease the output noise more than the output signal.*

The noise figure definition (2.1) shows that F depends on the (available) power N_i delivered by the noise source to the network. Johnson and Nyquist [20] in two papers demonstrated that the available power from a resistance R at frequency f_o, temperature T and in the bandwidth $B \ll f_o$ independent of f_o, is directly proportional to the temperature T:

$$N = k\,B\,T \tag{2.2}$$

where k is the Boltzmann constant. Friis assumes that the reference temperature of the noise source at which (2.1) is to be considered is $T = T_o = 290$ K.

An equivalent representation of the Friis' noise figure can be done with equivalent temperatures on the basis of (2.2). Rewrite (2.1) as:

$$N_o = F\,G_{av}\,N_i \tag{2.3}$$

where $G_{av} = S_o/S_i$. The available noise power N_i from the source is given by (2.2) with $T = T_o = 290$ K as required by Friis [19]. N_o is the noise power detected at the output of the 2–port network and consists of two uncorrelated contributions: the amplified noise power $G_{av}\,N_i$ coming from the noise source; and the noise power N_n from the 2–port network. It is common practice to refer the available power N_n to the input of the network before being amplified:

$$N_n = G_{av}\,N_{eq}$$

where N_{eq} is a fictitious noise source to be added to N_i. Finally, it is straightforward to associate N_{eq} with an equivalent noise temperature T_{eq} by means of (2.2). The equivalent noise temperature T_{eq} is a different way of expressing the noise figure definition; their linking expression is:

$$F = 1 + \frac{T_{eq}}{T_o} \tag{2.4}$$

The equivalent noise temperature is also known as effective noise temperature [21]

Years later, the IRE Subcommittee 7.9 on Noise [21] detailed the theory for representing in the frequency domain an ergodic and stochastic process such as noise. The problem of representing a process extending over all time and with infinite energy content in the frequency domain can be described with either Fourier transform or Fourier series. The process $f(t)$ can be sampled in the time window $-T/2 < t < +T/2$ in order to make its energy finite; then, the Fourier transform can be calculated. On the other hand, the process can be sampled in a similar time window and a new periodic function $f(t;T)$ can be defined by repeating the sampled function every T seconds. Finally, the Fourier series of $f(t;T)$ is computed. The larger T, the better the approximation of the frequency content of the original process $f(t)$. In the case of electrical random processes, however, one is interested in its spectral densities. As a matter of fact, only 2 spectral densities ($\overline{|v|^2}$ and $\overline{|i|^2}$) and one cross–spectral density ($\overline{i\,v^\star}$) are sufficient for the complete noise characterisation of any 2–port network. The spectral densities describe average powers related to current and voltage and eventually they lead to the definition of noise parameters.

Some techniques for the measure of the noise figure are outlined in [21]. In particular, the Y factor technique is discussed here because commercially available noise figure meters are based on it [22]. Consider a 2–port network and measure its output (available) noise power in a small band B around the test frequency f_o when the available power of the source is $k\,B\,T_s$:

$$N_o = N_n + G_{av}\,k\,B\,T_s.$$

Assume that the source temperature can be switched between 2 values, T_c and $T_h > T_c$ and refer the contribution N_n of the network to its input port: $N_n = G_{av}\,N_{eq} = G_{av}\,k\,B\,T_{eq}$. If the output noise power N_o is measured to be N_h at T_h and N_c at T_c, the equivalent noise temperature T_{eq} is:

$$T_{eq} = \frac{T_h - Y\,T_c}{Y - 1}$$

where $Y = N_h/N_c$.

The Y factor technique is particularly attractive when solid state noise sources are employed for compact and handy test sets [23]. However, there are some drawbacks such as the noise source output impedance may vary between the hot ($T = T_h$) and the cold state ($T = T_c$) as well as the output impedance of the 2–port under test may not be matched to the noise figure meter. The noise source can be substituted by a real resistor whose temperature is physically varied between two known temperatures (hot and cold technique). This option gives very good results with skilled operators.

2.2 Noise Measure

The noise figure of 2 networks in cascade is discussed by Friis in [19]. If network A precedes network B, the total noise figure is:

$$F_{AB} = F_A + \frac{F_B - 1}{G_A} \tag{2.5}$$

where G_A is the available gain of the first stage. It is clear that only if G_A is large, $F \approx F_A$, otherwise the second stage will deteriorate the total noise figure.

Haus and Adler [24] extend the definition of available gain and noise figure in order to define and examine the noise measure of amplifiers. With some assumptions related to input and output impedances, they answer the following question: given 2 networks, say A and B, which is the cascaded network, say AB for A preceeding B (BA for B preceeding A), that minimises the total noise figure (2.5) ? The answer leads to the definition of noise measure:

$$M = \frac{F - 1}{1 - 1/G_{av}}$$

where F and G_{av} are, respectively, the noise figure and the available gain of the 2–port network under consideration.

It should be noticed that the noise measure can be used to compare two amplifiers to decide which should be used as first stage. The connection of two (or more) networks does not leave the noise measure M_{AB} of the final amplifier unaffected. As a matter of fact, if M_A and $M_B > M_A$ are the noise measures of each stage and G_A and G_B their respective available gains, the total noise measure is [25]:

$$M_{AB} = M_A + (M_B - M_A)\,\frac{G_B - 1}{G_A\,G_B - 1} \tag{2.6}$$

(2.6) demonstrates that:

- $M_A < M_{AB} < M_B$ as long as $G_A G_B > 1$;
- if $M_A = M_B$ and $G_A \neq G_B$, the total noise measure is independent of the available gains of each stage; and
- since the product $G_A G_B$ is the same for either order of cascading, the smallest M_{AB} is achieved by placing first the amplifier with the lowest individual noise measure.

In the general case that $G_A \neq G_B$, (2.6) predicts that either cascade of amplifiers makes the noise measure deteriorate.

The noise measure is a better way of describing the noise performance of any 2–port network rather than the noise figure only because it takes into account gain and noise figure at the same time. However, literature does not seem to stress this fact as much as it deserves. Fukui [26] showed that available gain, noise figure and noise measure can be drawn as circles on the source impedance planes; some of his expressions were later revised by Tucker [27]. Further analysis concerning the noise measure has been carried out by Poole and Paul [28] who presented some results for a microwave low noise amplifier. However, their design does not take the input matching circuit into consideration. This approximation is widely accepted even though an input matching circuit, either lossless or lossy, affects the noise performance of the overall final low noise amplifier; this point will be reconsidered later in this chapter.

2.3 Noise Parameters

In the early 60s, the Institute of Radio Engineers (IRE) defined a standard approach for modelling and measuring noise of 2–port networks.

The measurement of the noise performance of a 2–port network is discussed in [29], where the definitions of spot and average noise figure are stated. The former deals with the degradation of the signal–to–noise ratio at any given frequency according to Friis' definition [19]. The latter drops the assumption $B \ll f_o$ extending the spot noise figure concept to large bandwidths; an effective input noise temperature is then defined and related to the noise figure as in (2.4).

Any noisy linear 2–port network at frequency f_o is described by a set of 4 numbers (2 real and 1 complex), called noise parameters [18]; they relate the noise figure of the network to three physical quantities characterising the network itself – two noise sources and the correlation between them. Depending on the chosen representation, different sets of noise parameters can be worked out; when an admittance matrix representation is selected, the set F_{min}, $Y_{S_{opt}} = G_{S_{opt}} + jB_{S_{opt}}$ and R_n is typical. Their measurement is also outlined in [29]:

1. measure the (spot) noise figure F for a number of source admittances $Y_s = G_s + j\,B_s$ with G_s kept constant;

2. plot F vs B_s and find the minimum $B_{S_{opt}}$;

3. measure F for a number of G_s with $B_s = B_{S_{opt}}$;

4. plot F vs G_s and find the minimum $G_{S_{opt}}$. The optimum source admittance is $Y_{S_{opt}} = G_{S_{opt}} + j\,B_{S_{opt}}$;

5. plot F vs $x = \mid Y_s - Y_{S_{opt}} \mid^2 / G_s$; they should lie on a straight line $F = F_{min} + R_n\,x$. The intercept point defines the value of F_{min}; the slope, R_n.

This procedure will be discussed later on when dealing with other measurement techniques.

The noise parameters definition of the IRE Subcommittee as well as the reasons for their measurement procedure find their foundations in an earlier publication by Rothe and Dalke in the Proceedings of IRE in 1956 [18]. That classic paper develops the noise characterisation for linear 2–port networks in transmission matrix representation [30]. Two correlated noise sources, $v\,(t)$ and $i\,(t)$, take account of voltages and currents measurable at the network terminals when no signal generators are connected; the noise figure is given in terms of the spectral densities $\overline{\mid v\,(t)\mid^2}$, $\overline{\mid i\,(t)\mid^2}$ and $\overline{i\,(t)\,v\,(t)^\star}$ related to those noise sources: the noise parameters are directly defined from those average quantities. Notice that the noise parameters are given in the frequency domain, even though the time t may appear in the notation. Hillbrand and Russer [30] have introduced a matrix form (correlation matrix) for representing the noise performance – and hence the noise parameters – of any 2–port network. A correlation matrix is a compact way of describing the noise contribution from linear networks; with them, it is easy to show that cascaded linear networks combine their noise parameters non-linearly. Correlation matrices have been used extensively in the thesis; more details will be given in chapter 3.

Rothe and Bauer also described the noise performance of the network in terms of scattering parameters and noise power waves in another paper in German. Penfield [31] is the first one to make their achievements available to the English speaking community. Their use leading to a new scattering matrix definition is outlined by Kurokawa in a paper published a few years later [32].

As Penfield reports, both noise wave generators a_n and b_n are located between the source and the input port of the 2–port network. These generators are uncorrelated ($\overline{a_n\, b_n{}^{\star}} = 0$) if the complex characteristic impedance Z_o for the scattering parameters is equal to $Z_{S_{opt}}$, the optimum source noise impedance for minimum noise figure. This point is remarkable because that choice ($Z_o = Z_{S_{opt}}$) makes the corresponding correlation matrix diagonal. Furthermore, complex normalising impedances are best dealt with by power waves rather than the usual voltage waves.

The fact that the noise sources are uncorrelated, simplifies the task of writing the noise figure: only two noise temperatures are required, $T_a = \overline{\mid a_n \mid^2}/k\,B$ and $T_b = \overline{\mid b_n \mid^2}/k\,B$, where k is the Boltzmann constant and $B \ll f_o$ is the bandwidth around the frequency of interest f_o. The noise figure at f_o is:

$$F = 1 + \frac{T_a + \mid \Gamma_S \mid^2 T_b}{T_o\,(1 - \mid \Gamma_S \mid^2)}$$

where:

$$\Gamma_S = \frac{Z_S - Z_o{}^{\star}}{Z_S + Z_o}$$

is the source reflection coefficient of the source impedance Z_S normalised to Z_o according to [32].

The efforts of describing the noise performance of a microwave network in terms of scattering–related rather than voltage and current–related parameters multiply as technology reaches higher and higher frequencies.

Meys [33] acknowledges that the expression of the noise figure in terms of F_{min}, $\Gamma_{S_{opt}}$ and R_n is a hybrid representation and presents a set of noise parameters totally associated with (voltage) noise waves. This representation causes the noise performance of a network to be described in terms of equivalent temperatures: T_a and T_b are respectively associated with the incoming and the outgoing noise waves; a complex term $T_c e^{j\,\Phi_c}$ accounts for the correlation between a_n and b_n in the general case – as opposed to the particular case analysed by Penfield in [31].

Hecken [34] redevelops IRE and Rothe's concepts on a scattering–based approach. Starting from the assumption that noise is a stationary stochastic process, voltage noise waves are defined as a new random process related to $v\,(t)$ and $i\,(t)$, voltage and current noise sources respectively. Even if not stated plainly, these noise waves are not power waves because it is implied that the normalising impedance Z_o is real; furthermore, the reflection coefficients are defined as $\Gamma = (Z - Z_o)/(Z + Z_o)$. Hecken's analysis is very straightforward and achieves an important result: it shows that losses as small as 0.25 dB at 2 GHz in the input matching circuit of very low noise amplifiers can degrade the noise figure of the overall network dramatically.

The noise parameters, as defined by Rothe and Dalke [18], are a natural consequence of both the linearity of the 2–port network and Friis' definition of noise figure [19]. The most popular set of noise parameters in use for characterising active devices is the minimum noise figure F_{min}, the optimum noise source reflection coefficient $\Gamma_{S_{opt}}$ corresponding to $F = F_{min}$ and the equivalent noise resistance R_n:

$$F(\Gamma_S) = F_{min} + \frac{4\,R_n/Z_o}{\mid 1 + \Gamma_{S_{opt}} \mid^2} \frac{\mid \Gamma_S - \Gamma_{S_{opt}} \mid^2}{1 - \mid \Gamma_S \mid^2} \tag{2.7}$$

where Γ_S is the source reflection coefficient.

Other representations can be used [35], depending on the particular matrix used for describing the 2–port network [30]. For instance, when using a transmission matrix $\mathbf{T} = \begin{bmatrix} A & B \\ C & D \end{bmatrix}$, the obvious choice is the set R_n, g_n and ρ_n; they are respectively the equivalent noise resistance, the equivalent noise conductance and the correlation coefficient between them. A complex correlation admittance $Y_{cor} = G_{cor} + j\,B_{cor}$ making the noise sources uncorrelated, can also be devised [18].

2.3.1 Measurement of the Noise Parameters

The noise figure expressed in terms of the noise parameters demonstrates that a paraboloid–like surface is generated from (2.7) on the source reflection coefficient plane Γ_S. It is possible to show theoretically [18] that the minimum noise figure is achieved by independently tuning real and imaginary parts of the source impedance in order to find $\Gamma_{S_{opt}}$. This is the foundation for the noise parameters measurement technique by IRE [29] described earlier on in the previous section. However, the procedure is tedious and time–consuming [36] and it is not appropriate for automatic applications.

The most popular measurement technique has been proposed by Richard Q. Lane [37], who starts from a hint by Fukui [38] (the linearisation of the expression for the noise figure in admittance representation) in order to minimise the error between (2.7) and measured noise figure with a least squares fit, for a number $i = 1, \ldots, N$ of input source admittances at the test frequency f_o. The author warns about a high sensitivity related to the determination of R_n; he also includes weighting coefficients W_i *... to be used if certain data are known to be less reliable than the average* ([37], page 1461).

Lane does not face some important issues: the selection of the input source admittances, i.e. the position of the input source reflection coefficients $\Gamma_{S_{opt}}$ on the Smith chart; the number N of measurements required for the least squares fit to deliver the correct set of noise parameters; and expressions for the weighting factors W_i.

Caruso and Sannino [36] and Sannino [39] tackle the issue of positioning the input source reflection coefficients $\Gamma_{S_{opt}}$ on the Smith Chart. They show in two different linearisations of (2.7) that the least squares fit does not have a solution when a row or column of the matrix delivering the coefficients for the least squares fit is a linear combination of the remaining rows or columns. This is the case when every Γ_S has the same magnitude (all of them lie on a circle centred on $\Gamma_S = 0$). The solution to this problem is to select different magnitudes for each Γ_S.

The number N of measurements required for the least squares fit still is an open issue. Since there are four noise parameters, $N \geq 4$; it is common practice to repeat the measurement for at least 7 different Γ_S. Recent evidence [40] pushes this minimum value up to 20–25.

The selection of the weighting coefficients W_i directly affects the results of the fit. Lane might have included this further degree of freedom in order to tackle the problem of the sensitivity of R_n. The choice $W_i = 1/(F_i)^2$, where F_i is the measured noise figure, has been suggested by Escotte *et al.* [41] and named modified Lane method (MLane).

Mitama and Katoh [42] acknowledge that the Lane method does not minimise the error between the surface determined by (2.7) and the actual surface. Referring to Figure 2.1, the Lane method minimises the distance $\epsilon_i^{'}$ between the inferred value of the i^{th} noise figure and the measured F_i; the shortest distance (error) for any $(G_{si}; B_{si})$ is accounted for by Mitama, whose method minimises ϵ_i. The drawback of the proposed technique is that it needs a starting set of values for the noise parameters, which is provided by the Lane procedure: the Mitama method is not independent of the Lane method.

Other techniques have been proposed. Wedge and Rutledge [43] base their analysis of 2–port networks on noise waves and propose a setup for measuring noise temperatures which does not require a tuner. The method totally relies on a scattering wave–oriented approach which makes it suitable for millimetre applications. Escotte *et al.* [41] collects and compares techniques stemming from Lane's approach. Some of them require a starting guess of noise parameters, others such as the MLane method, do not. The paper suggests to use 10 different source impedances and to position them evenly on the Smith chart since the position of $\Gamma_{S_{opt}}$ is not known beforehand. However, this reasoning looks weak if one

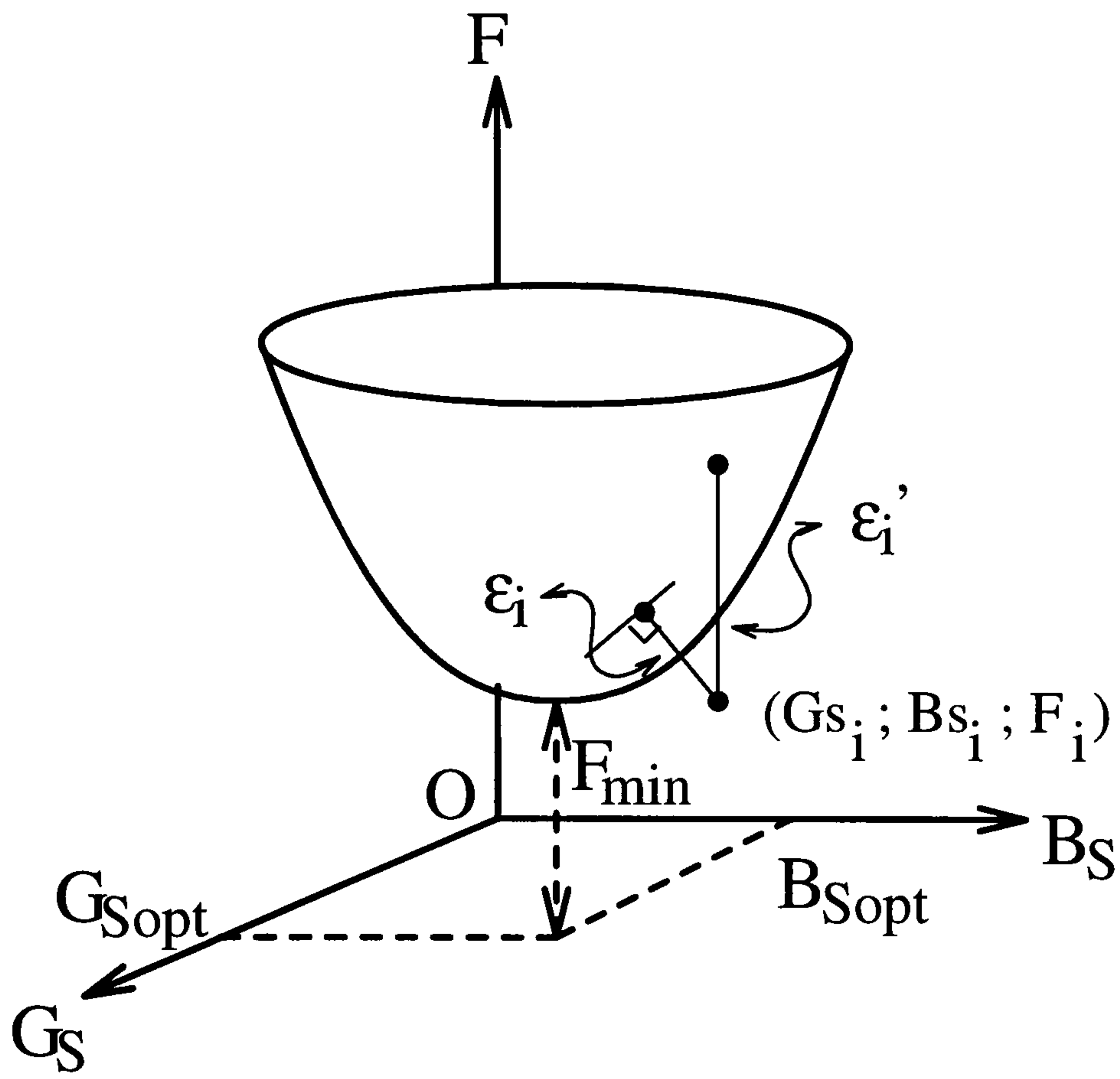

Figure 2.1 Visualisation of the error ϵ_i' minimised by the Lane method and the error ϵ_i minimised by the Mitama method when (2.7) is expressed in admittance representation.

considers that computer simulations along with valid noise and signal device models allow the designer to predict the circuit performance in advance.

A slightly different approach listed in Escotte's paper is proposed by Vasilescu [44]. He states that the linearisation of the noise figure (2.7) affects the accuracy of the measured noise parameters, which Lane tackles with an increase in the number of measured data. Vasilescu solves a system of four non-linear equations such as (2.7), in order to determine the four noise parameters. The solution allows the uncertainty ΔF related to the noise figure to be assessed quite easily under the condition that the uncertainties related to the real and imaginary parts of the source admittances are the same: $\Delta G_{si}/G_{si} = \Delta B_{si}/B_{si}$. However, some basic errors are made in the paper. Vasilescu solves the system

$$M = \frac{N!}{4!\,(N-4)!}$$

times, M being the number of combinations of 4 measured data out of the $N \geq 4$ measurements. Then the best solution is selected. The method is very time–consuming and not suitable for automatic applications. For instance, $M = 35$ different combinations must be considered for only $N = 7$ different source admittances.

The techniques above are quite general because they can be applied to any linear 2–port network. However, an actual measurement faces some practical problems. One common aspect is the need for a computer to manage the data and calculate the results. Martines and Sannino [45] describe an automatic measurement system based on the Lane method for the evaluation of the noise parameters; this system also takes into consideration the mismatch at the output port [40].

The noise figure meter, also called a receiver, contributes to the measured noise figure according to (2.5). This contribution must be taken into account through the calibration (or characterisation) of the receiver before the actual measurement. Adamian and Uhlir [46] determine the noise parameters of the receiver by a series of measurements, only one of which requires the source at a different temperature. The procedure requires that the input impedance of the receiver be known. The contributions from different parts of the noise measurement setup can be described with correlation matrices [30]. Pospieszalski [7], [47] reports that the condition:

$$T_{min} \leq 4\,N\,T_o \tag{2.8}$$

derives directly from the Hermitian and non–negative definite properties for correlation matrices, as appendix A.1 demonstrates. T_{min}, N and T_o in (2.8) are respectively the minimum noise temperature, the Lange invariant (discussed in section 2.3.2) and the reference temperature 290 K. (2.8) should be included in Lane algorithms in order to obtain acceptable results.

2.3.2 Invariance of the Noise Parameters

The problem of characterising the electrical performance of any network has always been a major topic of investigation [48], because it is indispensable for quantitative comparisons. As far as noise is concerned, lossless components do not inject further noise in the circuit, but they shape the frequency response of the noise parameters. It is obvious that the noise figure cannot uniquely characterise a given device because it may be affected by embedding elements as well as by the source impedance.

Lange [49] shows that the quantity:

$$N = R_n \,\Re e \left[Y_{S_{opt}} \right]$$

is invariant to lossless transformations applied to the input port of any noisy network. $Y_{S_{opt}}$ is the source admittance for minimum noise figure. Hartmann [50] shows that any passive noise–free circuit preceeding a noisy 2–port network does not change F_{min} and notices that a noise–free network cascaded after the noisy 2–port does not affect any noise parameters. Correlation matrices [30] easily prove this statement.

Following Hartmann and Lange, F_{min} and N uniquely characterise any given device, since they do not change when connecting a lossless network to its input port. Reciprocity is also a requirement in [49] and [50]. This is the case when noise figure measurements are carried out with a lossless tuner between source and device [47].

The noise measure is also constant to lossless embedding. This point seems controversial: it stems from a statement by Engberg [51], which researchers have used to support their results [14], [52] with series feedback amplifiers. However, Engberg refers to Haus [25] who analyses [24] the noise behaviour of n–port networks and faces the problem of noise characterisation. His mathematical analysis shows that for any 2–port amplifier, the noise figure F must satisfy the condition:

$$F - 1 \geq \frac{\lambda_1}{kT_o \Delta f} \left(1 - \frac{1}{G_{av}} \right),$$

where G_{av} is the available gain of the amplifier and λ_1 is the smallest (positive) eigenvalue of the matrix:

$$\mathbf{N} = -\frac{1}{2} \left(\mathbf{Z} + \mathbf{Z}^{+} \right)^{-1} \overline{v\, v^{+}}.$$

There, $\mathbf{N}$ is called *the characteristic–noise matrix*, $\mathbf{Z}$ is the impedance matrix of the network, v is the 2×1 voltage noise vector of the amplifier and the term $\overline{v\, v^{+}}$ is the impedance representation correlation matrix [30]. The term:

$$M_{opt} = \frac{\lambda_1}{kT_o \Delta f}$$

is the smallest optimum noise measure value; Haus proves that M_{opt} for any network is invariant to lossless embeddings.

2.4 Noise CAD Software

Computer aided design software is an indispensable tool for designing low noise networks. Efforts have been made to analyse the noise performance of arbitrarily connected multi–ports: Rizzoli and Lipparini [53] and Dobrowolski [54] present a solution in admittance and scattering matrix representation, respectively. Kanaglekar *et al.* [55] make use of the complex temperatures defined by Meys [33]. CAD allows the designer to optimise the network in order to achieve one or more goals [56]; they may also extract some specific information from measured data [57].

2.5 Active Device Noise Models

In light of the particular approach used in this thesis – any active device is considered as a noisy 2–port network – only a brief sketch of the fundamental noise properties of field effect transistors (FETs) – such as metal semiconductor FETs (MESFETs) or high electron mobility transistors (HEMTs) – and bipolar transistors – such as homojuction (BJTs) or heterojunction transistors (HBTs) – are outlined. Device models are reviewed and their capability of simulating the device noise performance is discussed.

Most of this section concentrates on field effect transistors because they are the state–of–the–art devices for best noise performance available nowadays. Among noise models, the *Pospieszalski noise model* has been successfully applied in a number of low noise amplifier designs because of its simplicity. The Pospieszalski model deals with intrinsic devices; this may constitute a limitation, partially overcome by Hughes [58]. Its application to extrinsic and packaged MESFETs [59] is further extended in chapter 4 of this study with the results of chapter 3.

2.5.1 Bipolar Transistor Noise Models

In 1966, Fukui [38] developed the expressions for the BJT noise parameters. His analysis is based on Giacoletto's intrinsic model in common emitter configuration [60]. The noise sources are due to shot noise at the emitter and collector junctions as well as the thermal noise from the base resistance. Fukui linearises the expressions for the noise parameters before applying the IRE standard method for noise parameter measurement [29] and acknowledges the importance of parasitics as the frequency of operation increases.

Vendelin [15] summarises some characteristics of small signal and noise models for homojuction bipolar transistors. A simplified small signal model for narrow band applications resembles the field effect transistor model; when large bandwidths are required, the model must account for the BJT physical structure which is inherently different from the field effect transistor structure. Therefore, the two models differ.

In line with Fukui, Vendelin recognises two main causes of noise: the emitter shot noise and the collector partition noise, due to the random direction taken by charges flowing from the emitter to the base or the collector. These noise sources are strongly correlated and DC current–dependent. A thorough description of physical noise sources in both n–p junctions and bipolar transistors is carried out by Van der Ziel [17].

Bipolar transistors have been revived in the microwave range by heterojunction bipolar transistors [16]. HBTs can be fabricated on GaAs substrates; heterojunctions such as AlGaAs–GaAs between base and emitter are then grown. The heterojunction increases the energy barrier between base and emitter, which decreases the number of majority carriers drifting from the base to the emitter. The base can be doped more heavily and made thinner without the risk that the emitter–base depletion region can reach the collector. The noise behaviour of HBTs is dependent on self–heating effects. They increase the lattice temperature which cannot be assumed to be equal to the ambient temperature; consequently, thermal noise sources associated with resistive components are affected by the higher temperature.

2.5.2 Field Effect Transistor

The study of the noise sources within field effect transistors is important for device designers. Noise models focus on intrinsic devices after peeling off the parasitics [61]. The importance of parasitics as part of an optimum device noise design seems to be overlooked or underestimated and left for CAD software to simulate. Finally, it should be pointed out how the chosen representation of the intrinsic transistor has influenced the way researchers have reported on noise measurements: noise currents have been used at both input and output ports until recently, when a hybrid representation has also stimulated new approaches to noise measurement techniques.

In 1952, Shockley [62] in a famous paper analysed FETs analytically. However, he did not deal with their noise properties: only DC and small–signal characteristics were described before the onset of the saturation region occurs under the gate.

Van Der Ziel Noise Model

In 1962, Van der Ziel tackled noise in the conducting channel of junction gate FETs for the first time. Closed form expressions are worked out under Shockley's constraint that carrier velocity is proportional to the electric field along the whole length L of the gate [63]. Any region of the channel between x and $x + dx$ $(0 \leq x \leq L)$ is associated with an uncorrelated thermal noise source. Then, based on Shockley's analysis, the expressions for the noise powers of two current sources in admittance representation are derived. In particular, the drain noise current consists of two contributions: the thermal noise power produced by the DC output conductance and the thermal noise power generated by the RF output conductance. Coefficients allow noise powers to be expressed relatively to either the DC output conductance or the maximum transconductance. The source R_s and drain R_d access resistances are accounted for and their effect on the current sources is assessed. Van der Ziel also validates the coefficients in the saturated region of operation experimentally.

At low frequency, shot noise affects the gate current: oppositely charged carriers leave and enter the gate–channel junction, producing a small noise current uncorrelated to the channel thermal noise. Shot–noise is fairly constant with frequency. However, capacitive coupling between channel and gate occurs at high frequencies of operation [64]. The coupling effect between channel and gate produces a displacement current. In particular, the displacement current is measurable when an admittance representation is chosen to describe the noise performance of the transistor. The magnitude of the gate displacement current is proportional to ω^2, and quickly overcomes the intensity of the shot noise current as frequency increases. Channel and gate noise sources are partially correlated because of the capacitive coupling. Van der Ziel's expressions support the experimental evidence that the drain current is independent of frequency, the gate current is proportional to ω^2 and the correlation factor is imaginary and proportional to ω.

Brunncke [65] validates Van der Ziel's model experimentally. Finally, it is noticeable that Van der Ziel's choice of using an admittance representation in order to model the device noise performance has not been challenged by researchers for many years.

Pucel Noise Model

In 1975, Pucel *et al.* [66] presented a comprehensive analysis of field effect transistors. Researchers had been investigating FET noise performance during the years between Van der Ziel and Pucel. The main limitation in Van der Ziel's analysis is that carrier ' velocity is proportional to the electric field under the gate. This is not true in general and in particular for devices fabricated on substrates like gallium arsenide (GaAs) whose mobility vs. electric field relationship shows a typical peak before achieving a constant value as the electric field increases [67].

Pucel bases his noise analysis on Van der Ziel's with some important new features:

- the channel length L under the gate is divided in two regions:

  1. the ohmic region, from $x = 0$ to $x = L_1 < L$;
  2. the velocity saturated region, from $x = L_1$ to $x = L$.

  The condition $L = L_1 + L_2$ holds, where L_2 is the length of the saturated region;

- a two–piece linear velocity vs. electric field approximation is assumed and the peak in the GaAs velocity vs. electric field relationship is neglected. In the ohmic region, the carrier velocity v is proportional to the electric field magnitude E through a constant mobility coefficient μ_o; in the velocity saturated region, the carrier velocity v_{sat} is constant:

$$\begin{aligned} v &= \mu_o E & \quad \text{if } E \leq E_{sat} \\ v &= v_{sat} & \quad \text{if } E \geq E_{sat} \end{aligned}$$

  where $v_{sat} = \mu_o E_{sat}$ and E_{sat} is the magnitude of the electric field occurring in the channel region at $x = L_1$. The two–piece linear approximation is supported by experimental measurements on FETs;

- the noise temperature T_n of the carriers is a strong function of the electric field E in the channel under the gate.

The latter point is worth expanding. Baechtold [68] demonstrates for GaAs devices that:

$$\frac{T_n}{T_o} = 1 + \delta \left(\frac{E}{E_{sat}} \right)^3$$

where $T_o \approx 300$ K is assumed. The electric field dependent noise temperature is due to the intervalley scattering process: when $E \approx E_{sat}$, carriers are scattered from the GaAs central valley to a satellite valley. There, mobility is very small and so is the contribution from carriers in the satellite valley to the total current. The carrier mean lifetime in a satellite valley is approximately 2 ps; this value sets the importance of intervalley scattering on the noise temperature to frequencies above 10 GHz.

Pucel obtains analytical expressions for the intrinsic device noise performance within the above assumptions; the input gate–source terminals are short–circuited and the output drain–source terminals are open–circuited. However, interestingly enough, he presents his results in admittance representation, as Van der Ziel did. The saturated region may reach very deep into the channel and is not confined to the drain end of the FET as previously supposed. Therefore, the noise contribution from the saturated region becomes predominant.

The saturated region makes the noise analysis very involved. Thermal noise originates in the ohmic region, as Van der Ziel assumed. However, when carriers enter the velocity saturated region, their velocity cannot change in magnitude any further. This makes the position L_1 vary in order to absorb the noise voltage fluctuations. Carriers in the velocity saturated region proceed at constant velocity v_{sat} but the direction of their velocity vector varies randomly. The noise associated with this process can be attributed to charge displacements produced by the random changes in direction of the carriers. The charge displacement results in the formation of an electric dipole layer travelling at constant speed. The dipole would disappear if enough time and space is given. This is not the case in practical devices: it is the low frequency approximation, which takes into account only the first term of the spatial Fourier transform of the drifting dipole layer potential. Summarising, Pucel identifies two separate causes of noise: thermal noise in the ohmic part of the channel; and diffusion noise in the saturated part of the channel. The noise in the ohmic part also affects the position $x = L_1$ where velocity saturation occurs.

Gate noise stems from the capacitive coupling between gate and channel; both regions under the channel induce noise current in the gate. Under short–circuit conditions, the gate current i_g is frequency dependent and the correlation coefficient is purely imaginary as in Van der Ziel's analysis. The presence of a saturated region complicates the expressions but no new noise sources are introduced in order to model the gate noise.

Pucel applies his analysis to the transistor noise figure because a direct verification with experimental data is possible. Accounting for diffusion noise explains the minimum in the noise figure vs. drain current. However, Pucel voluntarily neglects the series source inductance in his analysis of the noise figure, even though he acknowledges that better noise figure values can be achieved if this component is accounted for. Despite the fact that his analysis works out the open–circuit drain voltage noise source, he also does not investigate a hybrid representation of the device noise performance as Pospieszalski does a few years later. It could be of interest to rearrange Pucel's results for an hybrid representation and make a comparison with Pospieszalski's model.

Fukui Noise Model

Fukui's approach to MESFET modelling is somewhat different from the previous ones. Semi–empirical expressions are given and validated on an experimental basis. For this reason, device designers have found Fukui's formulæ extremely useful.

In 1979, Fukui presented a set of expressions to characterise a GaAs MESFET [69]. He wanted to determine the basic properties of the active channel – i.e. the effective gate length L, the channel thickness a and the carrier concentration N – from DC measurements. The effective channel length can be shorter or longer than the physical gate length, depending on the gate junction topology. Then, maximum output power and minimum noise figure are also obtained from the DC–evaluated parameters with expressions validated experimentally.

A more comprehensive analysis of GaAs MESFET minimum noise figure F_{min} is carried out in [70]. Again attention is focused on empirical expressions for either the equivalent circuit of the transistor or the geometrical and material parameters of the device. The starting point is Pucel's analysis [66]: Fukui acknowledges that his own empirical expression for F_{min} can be obtained as a particular case of Pucel's F_{min}. The terms in F_{min} are entirely determined with measurements at $V_{gs} = 0$ and DC operating point. It is also found that both source access R_s and gate R_g resistances have very little frequency dependence. Then, the quantities in the F_{min} expression are given as functions of both device geometry and material parameters – effective gate length L, gate width Z, carrier concentration N. As mentioned in [69], Fukui specifies that the effective gate length L is equal to the physical gate length L_g only for plain gates on planar channels; recessed gate devices show $L < L_g$, a necessary condition for lowering F_{min}. However, that condition is not sufficient because the gate width Z is to be smaller than a critical value Z_m in order to reduce F_{min}. The gate width Z_m is determined by setting $R_s = R_g$ and it is shown to be dependent on L_g. Therefore, the minimum noise figure decreases as the gate is shortened only if the condition $R_g < R_s$ is satisfied at the same time. Another interesting fact is Fukui's comparison between BJT and GaAs MESFET minimum noise figures in an appendix of his paper. The derivative $\partial F_{min}/\partial f$ (where f is the frequency) varies proportionally with frequency for BJT but is a constant for MESFETs. Therefore, in the microwave region, BJTs are bound to be noisier than MESFETs.

Cappy's Contribution

Device technology has provided for constant improvements in device noise performance. In 1988, Cappy† compared MESFETs and HEMTs, the state–of–the–art devices for achieving

† Alain Cappy, "Noise modelling and measurement techniques", *IEEE Trans. on Microwave Theory and Techniques*, vol. 36, No. 1, pp. 1–10, January 1988.

minimum noise figures as small as possible. Cappy's contribution is important in order to evaluate some points the previous noise models have brought up.

First of all, the noise performance can be modelled only if a small signal equivalent circuit and the noise sources – along with their correlation coefficient – are known. This is what can be named a *circuit approach* as opposed to a *system approach* which makes use of 2–port signal and noise data at each frequency of interest – for instance, a set of scattering and noise correlation matrices. As far as the noise is concerned, Cappy still refers to an admittance representation, consisting of two correlated noise current sources $\overline{\mid i_g \mid^2}$ and $\overline{\mid i_d \mid^2}$ at the gate and the drain ports respectively; the correlation coefficient is ρ_{n_o}.

The noise sources are to be determined by analysing the physics of the device. Cappy refers to Shockley's impedance field method which allows the determination of the local voltage source $v_d(x)$ at the position x in the channel. The spectral power densities at the frequency f can be calculated if the small signal impedance $Z(x; f)$ between the point x and the drain end of the channel is known. As Pucel did, once $\overline{\mid v_d \mid^2}$ is known, it is possible to determine $\overline{\mid i_d \mid^2}$. Of course, the main drawback of this method is that it is applicable only to ohmic channels.

Once the noise sources are known, the noise parameters can be obtained with standard noise theory [18]. Two cases are considered:

- the gate current i_g is neglected and Van der Ziel's expression for $\overline{\mid i_d \mid^2}$, containing the parameter P, is applied. P depends on technological parameters as well as on the DC bias and strongly affects the noise parameters;
- the gate current i_g is taken into account as well as the correlation coefficient ρ_{n_o}. A coefficient R plays the same role in $\overline{\mid i_g \mid^2}$ as P in $\overline{\mid i_d \mid^2}$.

In the first case, the expression for F_{min} shows that low minimum noise figure can be obtained if the device shows high cut–off frequency $f_t = g_m/2\pi C_{gs}$, small total access resistance $R_s + R_g$ and small value of P. The second case shows that F_{min}, which is proportionally dependent on frequency, is affected by the gate noise current source even at low frequencies. Furthermore, i_g makes $F_{min} > 1$ even if the total access resistance $R_s + R_g \to 0$. Finally, the correlation coefficient further reduces the minimum noise figure.

It should be noticed that the device equivalent circuit does not include the gate–drain capacitance C_{gd} as far as the previous considerations are concerned. Taking it into account makes the drain noise current source frequency dependent.

Based on the previous considerations as well as technological notes, Cappy compares

HEMT and MESFET performance by considering the main noise quantities P, R, ρ_{n_o} and the total access resistance $R_g + R_s$. High cut-off frequency is a requirement in order to improve noise performance. HEMTs have high f_t for two reasons: high carrier mobility corresponds to high average velocity and eventually in larger transconductance g_m; parasitics are less important than for MESFETs. The influence of R_g can be evaluated precisely because it is related to the gate fabrication process and device layout; on the contrary, the HEMT structure involves several conductive layers which do not allow an analytical approach for R_s. In conclusion, lowering F_{min} for field effect transistors requires increasing both f_t and the value of the correlation coefficient ρ_{n_o}.

Pospieszalski Noise Model

In 1989, Pospieszalski [7] proposed a simple noise model for intrinsic MESFETs and HEMTs; it is derived from experiments, not from theoretical analysis, as Danneville *et al.* [71] have noticed.

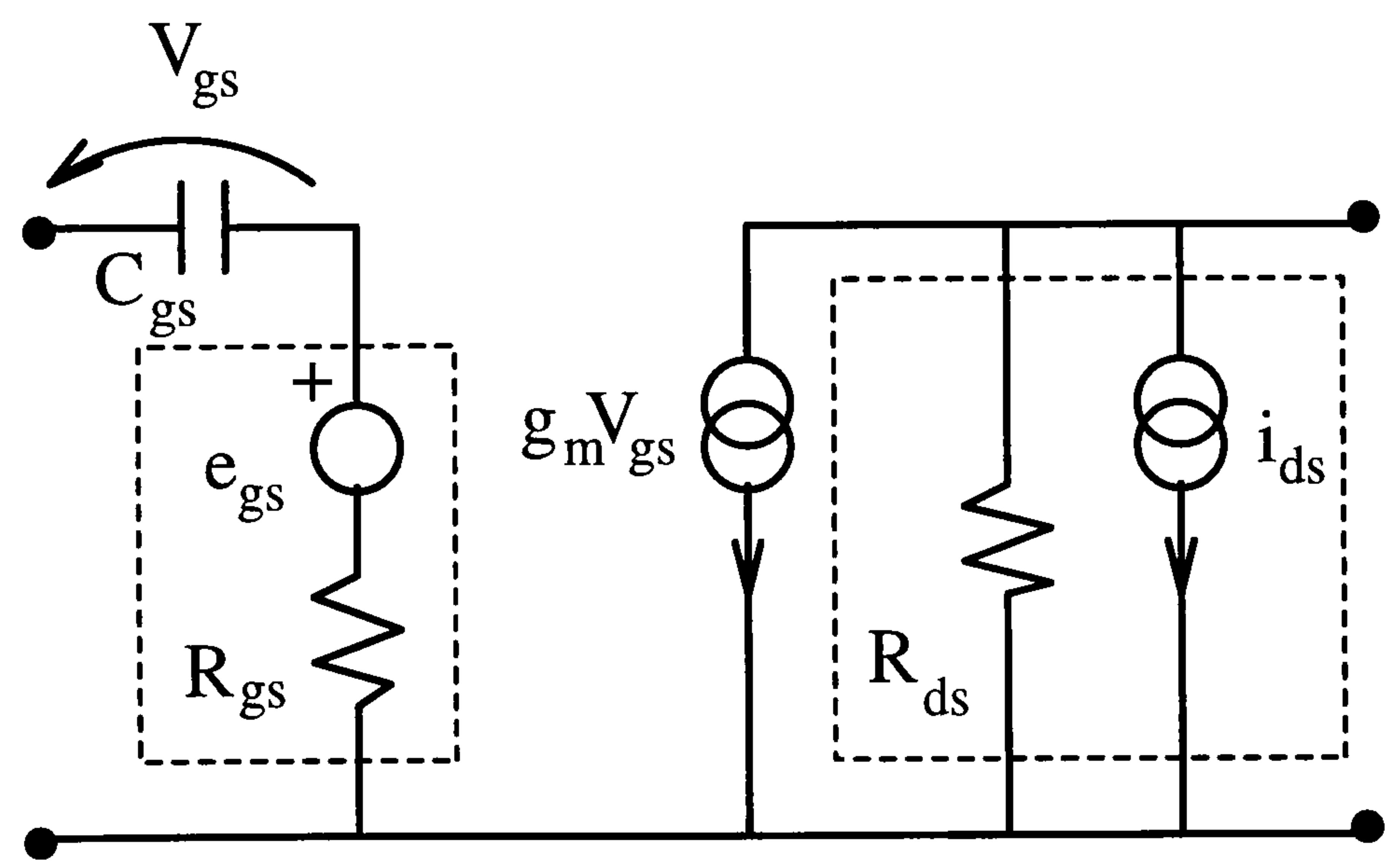

Figure 2.2 Pospieszalski noise model for intrinsic MESFETs and HEMTs; the dashed boxes are the resistor noise models consisting of the same noiseless resistor and a voltage/current noise source, $\overline{\mid e_{gs} \mid^2} = 4\,k\,B\,T_{gs}\,R_{gs}$ and $\overline{\mid i_{ds} \mid^2} = 4\,k\,B\,T_{ds}\,(1/R_{ds})$ respectively.

The Pospieszalski noise model for common source intrinsic FETs (Figure 2.2) consists of four elements, namely the gate capacitance C_{gs}, the gate resistance R_{gs}, the transconductance g_m and the drain resistance R_{ds}. The value of each component is extracted from scattering parameter measurements with a de-embedding procedure which determines and accounts for the influence of the extrinsic elements. Parasitic resistances (access resistances such as the source resistor R_s) are thermal noise sources [20] proportional to the room temperature T_{room}. Their contributions are taken off the noise data and, eventually, signal and noise data are referred to the intrinsic model only. Then, Pospieszalski shows that an extremely good fit is obtained if two equivalent noise temperatures T_{gs} and T_{ds} are associated with R_{gs} and R_{ds} respectively. Furthermore, he proves with noise measurements vs. temperature that:

1. $T_{gs} \approx T_{room}$;
2. $T_{ds} \gg T_{room}$; and
3. the noise sources e_{gs} and i_{ds} associated with T_{gs} and T_{ds} respectively are uncorrelated.

The model is very attractive because it is simple and provides a powerful tool for both design and analysis. Independent validations have been published; for instance, the expression for the optimum noise source reactance, $X_{S_{opt}} = 1/\omega C_{gs}$, where $\omega = 2\pi f_o$, has been experimentally confirmed by Tasker *et al.* [72].

The Pospieszalski noise model has also been very successful. Particularly remarkable is a series of papers by Hughes, demonstrating that:

- the model can be extended to extrinsic FETs [58] by properly choosing T_{ds};
- MESFET or HEMT design can be based on the Pospieszalski noise model [73]. The aim is to have a noise figure close to its minimum value and as insensitive as possible to changes in the input mismatch $\mid \Gamma_S - \Gamma_{S_{opt}} \mid$; and
- the model provides a theoretical explanation as to the reason why the minimum noise figure in dB is linearly dependent on frequency [74].

Finally, Hughes *et al.* [75] applied the Pospieszalski model to monolithic microwave integrated circuit (MMIC) low noise amplifier design after making it bias-dependent.

Hughes' investigation shows that the noise figure of any gain matched extrinsic FET is likely to be approximately 2 (3 dB). Consider the Pospieszalski noise model in Figure 2.2; the noise figure definition (2.1) is mainly determined by the noise power from both source and input gate resistance because the device gain under the gain match condition is very high. The Pospieszalski noise model predicts that $T_{gs} \approx T_{source} = T_o$, where T_{source} is the source impedance temperature and the output resistor temperature T_{ds} is approximately

500 K for extrinsic devices. Therefore,

$$F = \frac{(T_{source} + T_{gs})\ G_{av} + T_{ds}}{T_{source}\, G_{av}} \approx \frac{(T_o + T_o)\ G_{av}}{T_o\, G_{av}} = 2.$$

2.5.3 Noise Model Unification

Danneville *et. al* [71] have unified the Pucel and Pospieszalski FET noise models. The channel under the gate between the position x and $x + dx$ is modelled as a small signal active circuit consisting of four components: transconductance, resistance, coupling capacitance and noise source $i_n(x)$; a capacitive coupling with the gate is also accounted for at each position x. These components are embedded by the extrinsic circuit; access resistances R_s and R_g are important generators of thermal noise. Transconductance, resistance and coupling capacitance at x are defined from physical properties of the device (sheet carrier density, electrical field, average carrier velocity, etc.); the associated noise source is calculated from sheet carrier density and diffusivity. The achievements are remarkable: Pucel and Pospieszalski noise models are derived by properly choosing the matrix representation – admittance for Pucel, hybrid for Pospieszalski. Furthermore, in the Pospieszalski case, the correlation coefficient is shown to be very small but not negligible. This is due to the non–uniformity of the channel ($\partial/\partial x \neq 0$); the edge effects around the gate; and the influence of the parasitic resistances R_s and R_g. In particular, the feedback resistance R_s in Danneville's expression of the correlation coefficient is shown to reduce the correlation between gate voltage and drain current source.

The condition $\overline{v_{gs}\, i_{ds}{}^{*}} = 0$ in the Pospieszalski noise model has been proven somewhat controversial even though it has not discredited the model. Hau and Lee [76] extracted from measurement a non–zero correlation coefficient. The imaginary part increases with frequency at the expense of the real part; however, the latter has an opposite sign to the one predicted by Danneville [71].

2.6 Device Noise Parameter Measurements

The test procedure for measuring the noise parameters of a device does not differ from the procedure discussed in section 2.3.1. However, two competing features can be recognised:

- accessing the intrinsic device allows the equivalent circuit to be simple. Depending on the noise model in use, further assumptions can be made in order to speed up the test;

- modern noise parameter measurements, such as the Lane method [37], require both signal and noise parameter tests in order to characterise each and every component of the setup. Connecting and disconnecting equipment is not advisable, in particular when wafer probes and on–wafer device are involved because the repeatability of the test may be of some concern.

Furthermore, noise parameter measurement is inherently a lengthy process which is not easily subject to automatisation and high production yields of devices. An effort has been made to improve and automate the measurement process [36].

Gupta *et al.* [77] take advantage of the simplicity of the Pospieszalski noise model and tailor the complexity of signal and noise on–wafer setup [78] for production and yield purposes in order to evaluate MESFETs and HEMTs F_{min}. The on–wafer device model is simplified: only 4 lumped components and one frequency–independent current noise source at the output – described by the equivalent noise temperature T_{ds} – is considered; T_{gs} is set equal to the room temperature value. Full advantage of the frequency independence is taken and validated experimentally; low frequency noise sources such as $1/f$ noise and recombination–generation noise are avoided by carrying out the test in the UHF – low microwave band.

Dambrine [79] reports on the intrinsic FET noise parameters in admittance representation. His conclusions are that a single noise figure measurement would allow the intrinsic FET noise parameters to be calculated; the obvious application is for on–wafer measurements where the access to the intrinsic device is not too difficult.

Riddle [80] adopts a matrix correlation extraction technique in admittance representation in order to calculate Van der Ziel's noise coefficients P, R and the correlation coefficient ρ_{n_o}. Parasitic influence is de–embedded from the measured data. The set P, R and ρ_{n_o} are rarely used because of their sensitivity; furthermore, commercial simulators often do not provide noise models based on P, R and ρ_{n_o} and no simple extraction technique has been devised. Riddle's procedure systematically reduces the transistor to the intrinsic device so that the admittance correlation matrix can be written and the noise coefficients can be identified; only terminal parasitics must be known a priori for this procedure to be carried out. Finally, he finds out that the correlation coefficient scales the minimum noise figure and that changes in the noise coefficients cause the noise parameters to vary. In particular, R affects $\Gamma_{S_{opt}}$ and P affects both R_n and F_{min}.

Byzery [81] extracts the FET noise parameters for the intrinsic device and finds that the Pospieszalski noise model is valid for frequencies $f < 18$ GHz; in this range the correlation coefficient is negligible. He also finds that gate T_{gs} and drain T_{ds} temperatures are proportional for a given DC bias condition.

Caddemi *et al.* [82] reach similar conclusions to Dambrine [79]. Based on a Pospieszalski noise model paired with a small signal model of the transistor, they measure the noise parameters from a single noise figure measurement carried out at 50 Ω. Then, the noise behaviour vs. temperature of the noise parameters is determined; Byzery's [81] relation between T_{gs} and T_{ds} is confirmed.

2.7 Low Noise Amplifiers

Low noise amplifiers (LNAs) provide the initial amplification of the incoming signal in a microwave receiver. A typical LNA must achieve three main goals:

- high gain;
- low noise figure;
- stability.

High gain ensures that the noise contribution of the following stages is negligible and that the total noise figure is determined mainly by the noise figure of the first stage. Stability is necessary in order to prevent unwanted oscillations [83], [84]; therefore, stability is often mentioned in connection with LNA techniques.

Low noise devices are available [85]; however, standard design procedures [15], [86] do not allow the design of simultaneously high gain, low noise amplifiers. This is due to the fact that devices do not have the input reflection coefficient Γ_{in} equal to the conjugate of the optimum noise source reflection coefficient $\Gamma_{S_{opt}}$. Different topologies have been investigated in order to overcome this problem.

An isolator connected before the device reduces the power mismatch at the LNA input port and the active device can be designed for minimum noise figure. This concept is extended to balanced amplifiers where input and output 3 dB couplers [87] embed two equal LNAs connected in parallel. These solutions are not very popular because they are expensive and they occupy more area of the given substrate.

Typical applications make use of distributed amplifiers and feedback amplifiers; these topologies are well suited for integration.

2.7.1 Distributed Amplifiers

A distributed amplifier [88], [89], [90] consists of a cascade of transistors whose input and output are connected to two separate lines. Theoretically, these lines are lossless and they introduce only a phase–delay. In the input line, the travelling signal is picked up by every device which delivers it amplified to the output line. This line is such that each contribution from the devices is vectorially added without cancellation. The lines are matched at their ends in order to avoid unwanted reflections. An optimum number of devices exists.

Distributed amplifiers show large bandwidth [91] because device components (such as the FET input gate capacitance C_{gs}) become part of the input/output lines. The noise performance of distributed amplifiers has not generally been investigated in depth. Niclas [92] reports his results and points out that the noise figure for a distributed amplifier is close to its minimum noise figure ($F \approx F_{min}$). Output power as high as 250 dBm has been measured in the 2–20 GHz frequency range [93].

2.7.2 Feedback Amplifiers

Feedback amplifiers find many applications at low frequencies where very high gain is achievable [60]. This is not the case when high frequencies are considered. In this region, devices do not amplify enough for the gain G to be determined by the classical expression

$$G = \frac{A}{1+\beta A} \approx \frac{1}{\beta}$$

where A is the gain of the stage to which the feedback β is applied. The analysis therefore becomes more involved.

The main setback is that the gain of the device is lowered but the advantages that series or parallel feedback provide, such as:

- improving the input mismatch between Γ_{in} and $\Gamma_{S_{opt}}{}^{\star}$;
- widening the frequency response over many octaves;

often cause the designer to opt for this type of amplifier. Some details of microwave feedback amplifiers are presented [94]; a basic introduction to feedback systems can be found in [60].

Parallel Feedback Amplifiers

Parallel feedback microwave amplifiers usually consist of a passive admittance connected between the input and output ports of a transistor. An example is shown in Figure 2.3

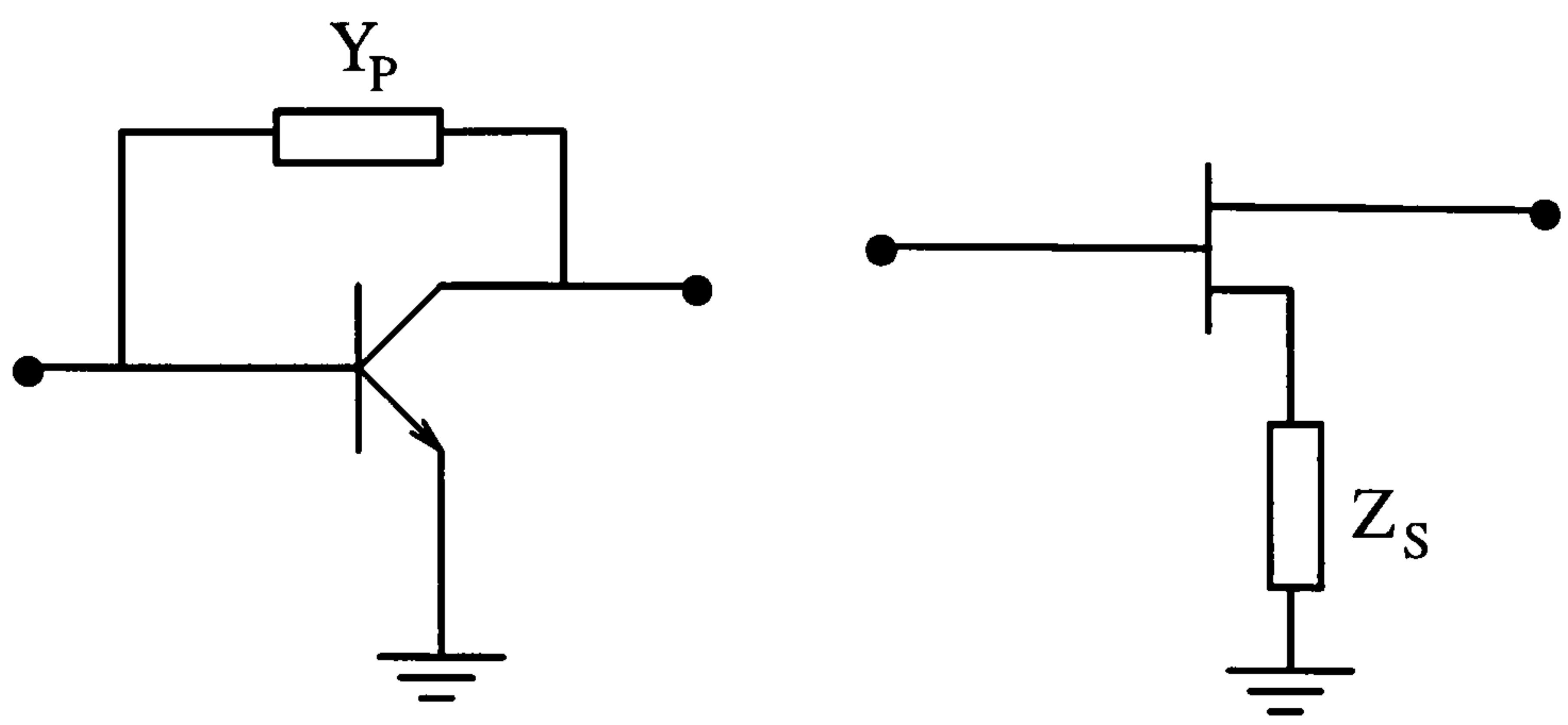

Figure 2.3 Basic topology for parallel feedback (left) and series feedback (right).

where the active device is a BJT; the parallel admittance Y_p makes the gain flat over a broad bandwidth and decreases the magnitudes of input and output reflection coefficients. A desirable by–product of parallel feedback is the improved stability at low frequencies. Narhi [95] develops an interesting graphical approach to select the parallel admittance on the Smith chart for a given value of the desired magnitude of the scattering parameter S_{ij}; this approach is also carried out with series feedback amplifiers [96].

Perez and Ortega [97] describe two graphical methods for the design of parallel feedback amplifiers in order to obtain gain equalisation and unconditional stability; or to get flat $| S_{21} |$ over a wide band and to control the S–parameters.

The exact expression for the noise figure of a noisy parallel feedback with lossy matching circuits has been obtained by Niclas [98]. His investigation on parallel feedback is further extended and a small signal gain better than 40 dB and a noise figure better than 4 dB over 2-8 GHz for a five–stage, single–ended MESFET amplifier is reported [99]; input and output standing wave ratios (SWRs) are better that 1.8. An ultra wide–band GaAs MESFET with parallel feedback [100] has shown a gain better than 4 dB and an output power of 13 dBm over the range 350 MHz – 14 GHz. Input and output SWR tends to degrade as frequency increases: $| S_{11} |$ goes up to ≈ 0.7 (SWR = 5.6) and $| S_{22} |< 0.3$ (SWR = 1.9).

Pavio [101] reports on the design of 2–18 GHz three–stage parallel feedback amplifiers. Their gain is better than ≈ 10 dB. The design relies on an accurate model of the substrate as well as the parasitics. Other examples of parallel feedback amplifiers are found in [102] and [103].

Series Feedback Amplifier

Series feedback amplifiers consist of a 2–port active device, whose third terminal is connected to ground through an impedance Z_s. An example is shown in Figure 2.3 where the active device is a FET. This LNA topology will be discussed extensively as part of the solution for simultaneous signal and noise match.

2.7.3 LNAs and the Design for Simultaneous Match

The design for simultaneous signal and noise match (SSNM) is a paramount objective in microwave engineering. Wireless communications, radars and measurement equipment may be required to discern a faint signal over the noise floor; their first stages must provide for amplification and little deterioration of the input signal–to–noise ratio of the incoming radio frequency. This is not achievable with FETs or BJTs at the same time because they show different values for Γ_{in} and $\Gamma_{S_{opt}}{}^{\star}$; the mismatch can be quantitatively described by the complex number $SSNM$ at each frequency f of interest:

$$SSNM = \Gamma_{in} - \Gamma_{S_{opt}}{}^{\star} \tag{2.9}$$

Many contributions from various researchers tackle the SSNM problem with a different degree of accuracy. Graphical techniques have been devised for the design of LNAs. Sierra [104] analyses gain, match and noise limitations on the selection of the source and load impedances. Albisson [105] carries out his investigation on the load Γ_L plane. A set of equations are developed and used to visualise the constant noise figure circles and the input stability circles on the Γ_L plane along with other circles already defined on the same plane. This is possible because a match at the input port is assumed: $\Gamma_{in}(\Gamma_L) = \Gamma_{S_{opt}}{}^{\star}$. Bor *et al.* [106] extends Albinsson's and Sierra's works by considering circles for constant noise figure, gain, stability, along with the circles for $\Gamma_{in}(\Gamma_L) = \Gamma_{S_{opt}}{}^{\star}$ on the load plane or for $\Gamma_{out}(\Gamma_S) = \Gamma_L{}^{\star}$ on the source plane. A similar approach is taken by Liu [107]. Edwards *et al.* [108] embrace the previous work in order to design conditionally stable amplifiers. Again, circles are defined on either the source or the load plane; they ensure that the source (load) reflection coefficient corresponds to passive input and output reflection coefficients ($|\Gamma_{in}| \leq 1$ and $|\Gamma_{out}| \leq 1$).

Another class of papers tackles the LNA design analytically. Anastassiou and Strutt [109], [110] and Vendelin [111] consider the effect on the noise figure of a source inductance applied to FETs. Link and Gudimetla [112] give expressions for the noise figure vs. frequency at a specified available gain; and for the available gain vs. frequency at a specified noise figure in order to highlight the trade–offs between noise and gain.

Some papers address the SSNM issue directly. Engberg [51] develops a computer–based technique which guarantees $SSNM = 0$ and $F = F_{min}$. This is achieved with lossless parallel and series feedback elements along with a careful choice of the load impedance. In fact, feedback elements affect $\Gamma_{S_{opt}}$ of the device and the load affects Γ_{in} which can be moved on the Smith chart onto $\Gamma_{S_{opt}}{}^{\star}$. Engberg's paper provides a tool for the designer to satisfy the SSNM condition; he does not state, however, that a further requirement is to obtain $\Gamma_{in} = \Gamma_{S_{opt}}{}^{\star} = 0$ (which is a particular case of $SSNM = 0$) even though the graphic results he shows are for unity input SWR.

Besser [113] follows Engberg's approach to the SSNM problem with a mixture of mapping techniques, computer optimisation and stability considerations. He acknowledges that lossless feedback affects both gain and noise figure of the device and he suggests that the noise measure should be considered.

Lehmann and Heston [14] tackle the SSNM issue starting from Engberg's analysis. For the first time, a three–stage LNA at 10 GHz (30 dB gain, 1.8 dB noise figure, 1.2:1 input SWR) is fabricated using monolithic technology which guarantees repeatable results. Similar achievements have been reported later on by Shiga *et al.* [52] with a four–stage 0.5 μm gate GaAs MESFET at 12 GHz (24 dB gain, 1.67 dB noise figure, 1.3:1 input SWR). Both papers demonstrate that series feedback is the key factor in order to achieve the SSNM condition. However, they do not underline the influence of input matching circuits and they do not rely on any analytical technique to calculate the feedback element.

Recently, Ko and Lee [114] have again relied on monolithic technology to fabricate a simultaneously matched LNA; the approach they use is in line with the previous papers discussed above. Interestingly, they make use of parallel feedback with a cascode configuration of two GaAs MESFETs. This configuration allows the use of a large value of resistive parallel feedback which is thought not to inject too much thermal noise. The signal and noise performance of this single stage cascode LNA is 17 dB gain, 2 dB noise figure and input/return losses better than 14–18 dB at 1.57 GHz.

Many state–of–the–art LNAs are reported in the literature. Remarkable are the achievements of Kobayashi [12], [13], [115], [116], who counts on state–of–the–art monolithic technology to fabricate BJTs and FETs on the same chip. Series feedback is widely used for MMIC applications [117]. Monolithic LNAs have been fabricated at many frequencies: Camilleri *et al.* [118] test a gain better than 7 dB and a noise figure less than 7.5 dB over a 40–60 GHz bandwidth for a 2–stage LNA; Hughes *et al.* [75] measure 25.6 dB gain and 1.6 dB noise figure at 12 GHz for a 3–stage LNA; Lunden *et al.* [119] claim a noise figure of 4.8 dB and gain in excess of 15 dB for 4 and 6–stage LNAs at 60 GHz with commercially available HEMTs. Wang *et al.* [120] have shown a monolithic LNA with 5 dB gain in the range 138–145 GHz.

2.8 Input Matching Circuit

An input matching circuit is required in order to match the device input reflection coefficient to a given source reflection coefficient. The choice is typically between either maximum available gain (gain match) or minimum noise figure (noise match). As a matter of fact, a basic assumption underlying standard input matching circuit design techniques, is linearity. This explains why only one single match (either for noise or for gain) is achievable.

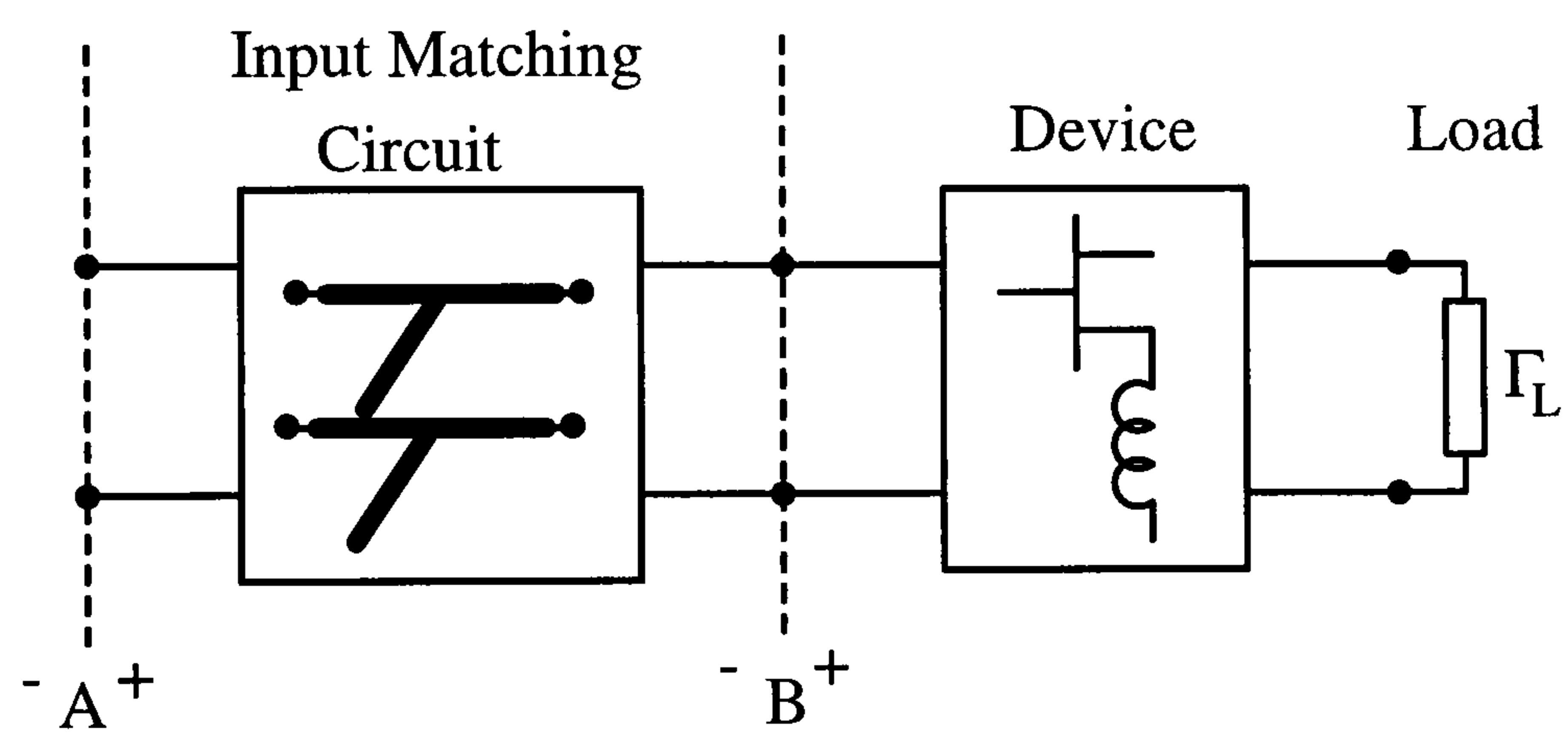

Figure 2.4 Basic structure for an input matching circuit to provide for the require match; the load models following stages.

Consider Figure 2.4. The input matching circuit should fulfill two requirements at the design frequency f_o: to deliver the given reflection coefficient Γ_S looking from plane B toward plane A (referred to as match at plane ^-B); and to ensure a power match at plane A when looking toward plane B (referred to as match at plane A^+). The former copes with noise ($\Gamma_S = \Gamma_{S_{opt}}$) or gain ($\Gamma_S = \Gamma_{in}{}^*$) requirements; the latter ensures a power match between the source power and the cascaded stages. As long as a device is such that $SSNM = \Gamma_{in} - \Gamma_{S_{opt}}{}^* \neq 0$, the simultaneous match is impossible.

Design techniques for input matching circuits can arbitrarily be split in two broad classes: standard design techniques; and non–standard design techniques. A critical approach to the use of input matching circuits will follow after reviewing some investigations of the topic available in the literature.

2.8.1 Standard Design Techniques

Text book techniques, as described, for instance, by Vendelin [15], Collins [121] or Pengelly [122], are here named standard design techniques. These procedures are the basis for the microwave designer. The reflection coefficient required at plane ^{-}B is usually transformed into $Z_o = 50\ \Omega$ by lossless transmission lines and open or short–circuit stubs. Maximum gain or minimum noise figure for the second stage is ensured if $\Gamma_{in}{}^{*}$ or $\Gamma_{S_{opt}}$, respectively, is designed. This corresponds to movements along a circle of constant reflection coefficient magnitude and then along a circle of constant resistance on the Smith chart at the design frequency. Notice that standard designs are carried out in two logical steps (*2–step design*): first, design the LNA so that the required reflection coefficient is determined; then, design the input matching circuit. Linearity allows an exact and manageable control of each design step.

However, a flaw related to the standard design techniques is detectable. Standard procedures ensure that the desired reflection coefficient looking towards ^{-}B is achieved. After designing the matching circuit, nothing can be said about the reflection coefficient seen at A^{+} in either the gain or noise match cases. In light of the SSNM problem, if an input matching circuit is to be used, the simultaneous match should be designed at the plane of interest, which is plane A in Figure 2.4. Since the matching circuit is designed from a *signal point–of–view* ($\Gamma_{S_{opt}}$ and Γ_{in} are treated the same), the noise contribution of the input matching circuit to the overall network performance is not considered. This is not strictly correct since the noise parameters of the final network do not transform as the signal parameters, on which the design is based. In fact, even though the input matching circuit is noiseless, some of the noise parameters (R_n and $\Gamma_{S_{opt}}$) change. In order to clarify this statement, consider Figure 2.4 and assume that a transmission matrix [30] representation is used. Let the signal and noise matrices of the input matching circuit be respectively $\mathbf{T}_i$ and $\mathbf{C}_i$. Similarly, let the signal and noise matrices of the LNA be $\mathbf{T}_a$ and $\mathbf{C}_a$.

Signal Analysis – Linearity

The cascade of input matching circuit and LNA is described by:

$$\mathbf{T}_{net} \quad = \quad \mathbf{T}_i\,\mathbf{T}_a \qquad (2.10.a)$$

where the transmission matrix $\mathbf{T}_{net}$ is the known design objective to be achieved and the LNA signal matrix $\mathbf{T}_a$ is known. The input matching circuit signal matrix $\mathbf{T}_i$ to be designed is easily calculated from (2.10.a).

Noise Analysis – Non–linearity

The overall noise parameters in transmission matrix representation are represented by the matrix $\mathbf{C}_{net}$:

$$\mathbf{C}_{net} = \mathbf{C}_i + \mathbf{T}_i\,\mathbf{C}_a\,\mathbf{T}_i{}^{+} \tag{2.10.b}$$

The Hermitian conjugate is represented by $^+$. Here, the objective of the design is $\mathbf{C}_{net}$, the matrices to be designed are $\mathbf{C}_i$ (noise parameters) and $\mathbf{T}_i$ (signal parameters). The noise behaviour of the LNA is known and described by $\mathbf{C}_a$.

Discussion about the Standard 2 Step Design Technique

The noise design of a cascade of two networks is a non–linear problem as (2.10.b) demonstrates. It should be remembered that the noise matrix $\mathbf{C}$ of passive networks can be derived from the network signal parameters [123] with simple matrix equations if the proper representation is chosen [30]. Therefore, $\mathbf{C}_i$ in (2.10.b) can theoretically be written in terms of $\mathbf{T}_i$ (or in any other more suitable representation) and (2.10.b) solved. It is clear, though, that the task may be very demanding because of the non–linearity involved.

Standard design techniques are valuable tools forthe LNA designer.However, they are not very likely to contribute to the solution to the SSNM problem as shown. Only one value of reflection coefficient at plane ^-B can be transformed into another value with the 2–step design technique. Furthermore, it is often assumed that lines and stubs are noiseless and that their noise contribution is negligible. The noise parameters of a transmission line are available in the literature [35]; the assumption that the noise generated by the input matching circuit feeding the following LNA is negligible, may be questionable [34]. As a matter of fact, computer optimisation often gives the designer an easy way to override these points.

2.8.2 Non–standard Design Techniques

Researchers have demonstrated various ways of achieving good match, high gain and low noise with microwave amplifiers. Three different analytical design techniques will be outlined:

- matched amplifiers;
- lossy matched amplifiers; and
- active matching circuits.

All of these techniques stem from the work of Niclas; later on, Kobayashi applies the active matching technique to monolithic technology. A noticeable fact is that Niclas always starts his analysis in matrix form disregarding what is inside the 2–port networks (system approach). Later on, the equivalent model for the active device is introduced and discussed.

Matched Amplifiers

According to Niclas [100], a matched amplifier exploits negative parallel feedback in order to control the gain and both input and output reflection coefficients. Niclas designs a broadband MESFET amplifier and he suggests the use of a series drain inductance, in order to tune out the capacitive output impedance at the high frequency limit of the amplifier (< 18 GHz) and an inductor in series with the resistive parallel feedback in order to compensate for the loss in gain as frequency increases. However, the concept he introduces, maybe involuntarily, is that an amplifier can theoretically be designed without matching circuits. Had he not been presenting a broadband technique, no input matching circuit perhaps would have been necessary.

Lossy Matched Amplifiers

Lossy matched amplifiers [98], [124] consist of a 2–port network with lossy admittances connected at both input and output ports and ground – Y_G at the input and Y_D at the output respectively. The admittance matrix is the natural choice of parameters for the signal analysis. Since the device electrical performance is described by admittance parameters, the formulæ do not depend on the device in use. Niclas' achievements are remarkable:

1. when considering Y_G and Y_D, an expression for $\mid S_{21} \mid$ is given in terms of S_{11} and S_{22}; it is verified that the more reflective the ports, the higher the gain;
2. perfect input and output match can be achieved if $\Re e\,[Y_{in}] \ll Y_o$ and $\Re e\,[Y_{out}] \ll Y_o$, where Y_{in} and Y_{out} are respectively the input and the output admittance when Y_o, the normalising admittance for the scattering parameters, is connected to the other port.

Improvement in S_{11} and S_{22} can still be obtained with the reactive parts of Y_{in} and Y_{out} even though those conditions are not satisfied;

3. as frequency increases, simplifications do not hold. In this case, external standard matching circuits are required; the inter–stage circuit between amplifying stages is seen as a particular case of external matching circuit.

4. the lossy elements at each port are connected to ground with stubs in order to diminish their effects as the frequency increases and the device gain drops.

The matching circuit still comes into play because a broadband amplifier is investigated. However, Niclas' achievement is to show that a low noise figure can be obtained with noisy elements if particular conditions are met.

Active Matching Circuits

Active matching circuit performance has been analysed by Niclas in 1985 [125]. His results are described because, recently, Kobayashi has based some of his MMIC designs on them.

Consider a FET characterised as a 2–port network in common source configuration. The input active circuit consists of a common gate FET between source and common source device. Since this configuration is prone to oscillate careful design and external components – such as series impedance Z_s between gate and ground; parallel admittance Y_p between input and output port; and input Y_G and output Y_D admittance connected between each port to ground – are included. These elements are noisy and are accounted for in the determination of the noise parameters. They affect stability, and shape the gain as well as improve the output match. Niclas' results are:

1. the signal parameters – in admittance form – simplify if the condition

$$Z_s \Delta_y \ll Y_{22} \tag{2.11}$$

   is verified for both real and imaginary parts. Y_{22} is an element of the admittance matrix of the device in common source configuration, whose determinant is Δ_y;

2. after adding the surrounding elements Y_p, Y_G and Y_D, the new signal parameters are calculated again. It is shown that at low frequencies where $Y_{11} \approx 0$ and $Y_{12} \approx 0$, gain and noise figure are not affected by Z_s;

3. the noise parameters are described by very complicated expressions and a study with a real series impedance $Z_s = R_s$ which satisfies (2.11) is carried out;

4. extreme simplification is obtained if $Y_D = 0$.

This analysis must comprise the following common source stage for two reasons: the elements surrounding the active matching stage heavily affect the network stability as well as gain, which may be extremely small as frequency goes up; the common source stage provides most of the amplifier gain and therefore is an important component in determining its noise performance.

Summarising, Niclas' results are:

1. active input matching circuit allows good noise and signal performance over a broad range of frequencies;

2. lossy components are able to control the noise figure despite the injection of thermal noise;

3. the analysis of input stage cannot be performed independently of the following stage because the input reflection coefficient depends on the load.

It should also be pointed out that Niclas makes use of admittance parameters as measured from a common source configuration in order to calculate the common gate parameters. The underlying hypothesis is that the network is a 2–port, or equivalently, no path to ground from any internal (parasitic) components exists when characterising the device in common source configuration. Niclas' analysis is not acceptable if this condition is not verified.

Active matching circuits are particularly attractive for two reasons: they can be easily implemented with monolithic circuits and the active device allows electrical control of the signal and noise performance of the amplifier through its DC biasing point. Kobayashi [115] demonstrates these points with heterojunction bipolar transistors (HBTs). The topology of the input matching circuit is the one described by Niclas; the 3 dB bandwidth may be greater than 5 GHz with the proper choice of biasing conditions and the overall noise figure is smaller than the expected noise figure from the Darlington configuration of the second amplifying stage. Small chip area consumption is also claimed. The same topology but with a common gate HEMT input device is shown by the same author in [126].

Other special topologies have been demonstrated. In [13], a monolithic integrated circuit comprising HEMTs and HBTs manages to combine the low noise performance of the HEMT along with the high linearity and output drive capability of the HBT. The HEMT forms the low noise input stage and it is followed by two HBTs in Darlington configuration; resistive feedback injects radio–frequency current from the input into the first Darlington

HBT emitter. The gain and the noise figure are respectively $\approx$ 20 dB and $<$ 3 dB over a 2–10 GHz band. This circuit also shows how advantageous it is to have the capability of fabricating FETs and BJTs structures on the same chip; only resistors and one capacitor are used. The input radio–frequency is fed directly into the HEMT gate input.

In [12], Kobayashi presents another example of a low noise amplifier. He makes use of two input HEMTs in cascode configuration followed by a source follower output stage; a parallel feedback provides broad bandwidth and good noise figure. An HBT current regulator is also designed for biasing the amplifier. The gain and the noise figure are respectively $\approx$ 13 dB and $<$ 1.9 dB in the 1–8 GHz range. Kobayashi's amplifiers are examples of state–of–the–art monolithic amplifiers; they do not make use of standard input matching techniques.

2.9 Conclusion

This chapter has reviewed some concepts about noise and LNA design through a literature survey. It has been shown that state–of–the–art LNAs often take advantage of the series feedback topology in order to achieve low noise performance and high gain. At frequencies above 1 GHz, a LNA is typically three stages because of the limited gain available from single devices. Finally, the attention has been focused on input matching circuits: passive and active realisations have been presented and a critical approach to their standard design has been discussed.

Chapter 3

Microwave Feedback Amplifier Analysis

The noise parameters when both series and parallel feedback immittances are connected to a 2–port network are studied at the given frequency f_o. The analysis allows the real part of the feedback elements to be associated with thermal noise sources.

The investigation described in this chapter stems from pioneering work by Engberg [51] and extends it to provide a solid theoretical model applicable to published data [111]. This forms the basis of a new approach to circuit modelling which will be described in this work [127].

3.1 Definitions and Analysis

Any linear and noisy network can be modelled with a set of two linear equations [18]; in matrix form:

$$s_{out} \quad = \quad \mathbf{M}\, s_{in} + n_{out} \tag{3.1}$$

This expression is general and aims to summarise different possible ways of describing a linear 2–port circuit: s_{out}, s_{in} and n_{out} are 2×1 vectors and $\mathbf{M}$ is a 2×2 matrix. Table 3.1 collects some applications of (3.1) applied to specific representations, one of which is shown in Figure 3.1. It is also very important to bear in mind that (3.1) models linear noisy networks only. As a consequence of linearity, two separate items contribute independently

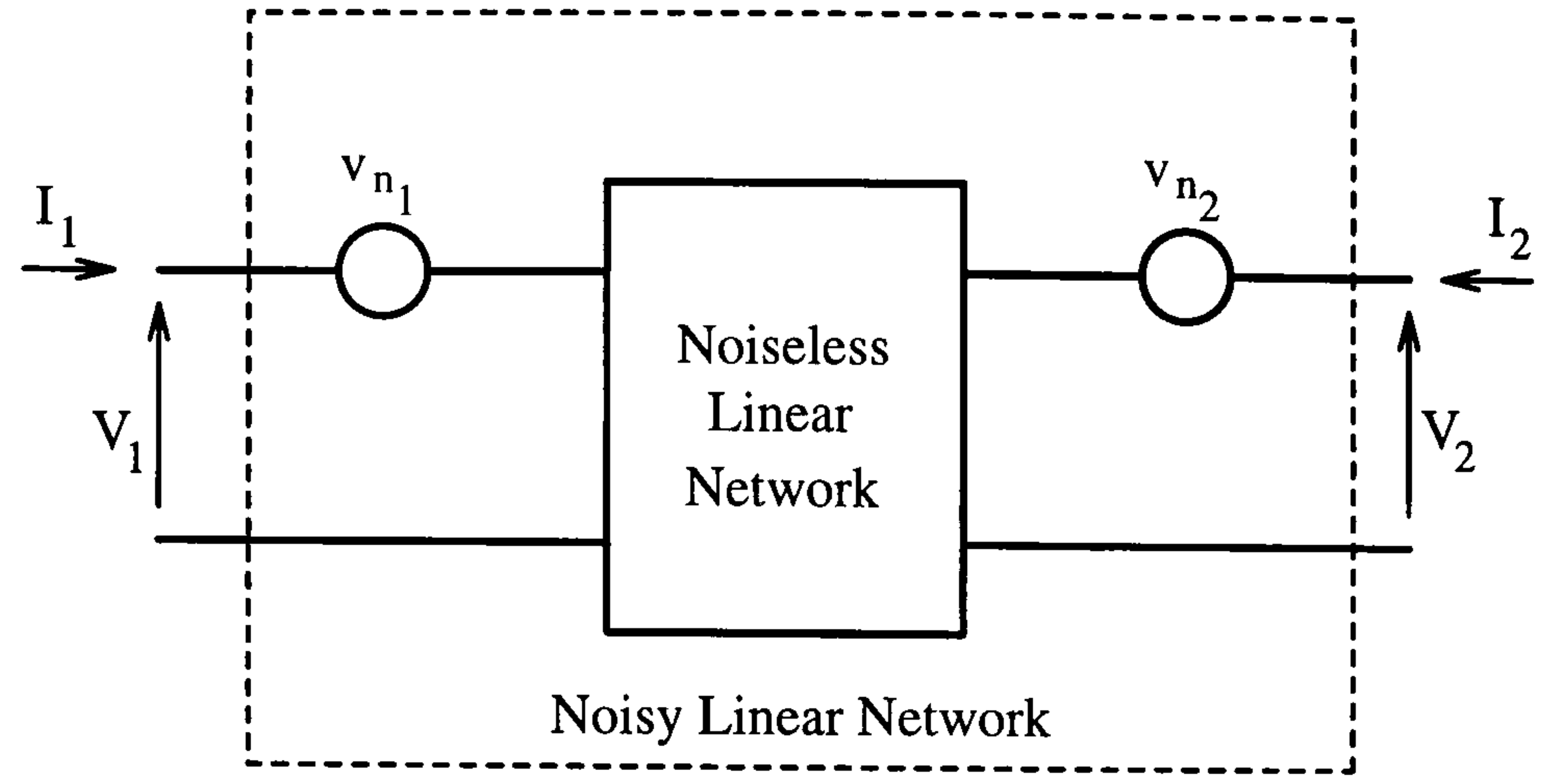

Figure 3.1 Impedance representation of a noisy linear network.

to s_{out} in (3.1): the signal vector s_{in} through the matrix $\mathbf{M}$; and the noise vector n_{out}, which accounts for the internal noise contributions of the network. Furthermore, if it were possible to switch off every noise source of the 2–port circuit, its signal performance would still be modelled by the same signal matrix $\mathbf{M}$. In fact, if $n_{out} = 0$, then (3.1) is simply $s_{out} = \mathbf{M}\, s_{in}$; in other words, $\mathbf{M}$ can be determined by standard signal measurements, independently of the noise sources.

Table 3.1 Collection of different representations for linear networks; the superscript ^{T} stands for the transpose operation.

Representation	Output	M	Input	Noise
Impedance	$V = [V_1 \quad V_2]^T$	$\mathbf{Z}$	$I = [I_1 \quad I_2]^T$	$v_n = [v_{n_1} \quad v_{n_2}]^T$
Admittance	$I = [I_1 \quad I_2]^T$	$\mathbf{Y}$	$V = [V_1 \quad V_2]^T$	$i_n = [i_{n_1} \quad i_{n_2}]^T$
Transmission	$s_{out} = [V_1 \quad I_1]^T$	$\mathbf{T}$	$s_{in} = [V_2 \quad -(I_2)]^T$	$n_n = [v_n \quad i_n]^T$
Scattering	$b = [b_1 \quad b_2]^T$	$\mathbf{S}$	$a = [a_1 \quad a_2]^T$	$b_n = [b_{n_1} \quad b_{n_2}]^T$
Chain Scattering	$c_{out} = [a_1 \quad b_1]^T$	$\mathbf{\Phi}$	$c_{in} = [a_2 \quad b_2]^T$	$c_n = [a_n \quad b_n]^T$
Hybrid	$p_{out} = [V_1 \quad I_2]^T$	$\mathbf{H}$	$p_{in} = [I_1 \quad V_2]^T$	$p_n = [v_{1_n} \quad i_{2_n}]^T$

Other remarkable consequences of linearity applicable to this work are:

1. it is possible to switch between representations with linear combinations of the vectors s_{in} and s_{out}; and
2. the noise vector n_{out} can be evaluated by setting the signal source vector s_{in} off, in a fashion similar to the one utilised to work out each element of the signal matrix $\mathbf{M}$.

Point 1 above is discussed now; point 2 will be dealt with when describing the actual analysis of feedback amplifiers later on.

In order to switch between representations, matrix algebra is used [30][1], [87]. The transformation from impedance to transmission representation is detailed as shown in the following example; any other transformation can be obtained in a similar manner. Consider Figure 3.1 and use:

$$V \;=\; \mathbf{Z}\, I + v_n \tag{3.2}$$

to describe the electrical behaviour of the noisy linear network; vectors V, I and v_n are defined in Table 3.1. Let $\mathbf{R}$, $\mathbf{r}$, $\mathbf{L}$ and $\mathbf{l}$ be equal to:

$$\mathbf{R} = \begin{bmatrix} 0 & 1 \\ 0 & 0 \end{bmatrix} \mathbf{r} = \begin{bmatrix} 0 & 0 \\ 0 & 1 \end{bmatrix} \qquad \mathbf{L} = \begin{bmatrix} 1 & 0 \\ 0 & 0 \end{bmatrix} \mathbf{l} = \begin{bmatrix} 0 & 0 \\ 1 & 0 \end{bmatrix}$$

respectively. The sought transformation is found by carefully modifying sign and position of $V = s_{out}$ and $I = s_{in}$ elements in (3.2):

$$\begin{aligned}
\begin{bmatrix} V_1 \\ V_2 \end{bmatrix} &= \mathbf{Z} \begin{bmatrix} I_1 \\ I_2 \end{bmatrix} + v_n \\
\mathbf{L} \begin{bmatrix} V_1 \\ I_1 \end{bmatrix} + \mathbf{l} \begin{bmatrix} V_2 \\ -(I_2) \end{bmatrix} &= \mathbf{Z} \left(\mathbf{R} \begin{bmatrix} V_1 \\ I_1 \end{bmatrix} - \mathbf{r} \begin{bmatrix} V_2 \\ -(I_2) \end{bmatrix} \right) + v_n \\
(\mathbf{L} - \mathbf{Z}\,\mathbf{R}) \begin{bmatrix} V_1 \\ I_1 \end{bmatrix} &= -(\mathbf{l} + \mathbf{Z}\,\mathbf{r}) \begin{bmatrix} V_2 \\ -(I_2) \end{bmatrix} + v_n \\
\mathbf{C}_{Z\to T}^{-1} \begin{bmatrix} V_1 \\ I_1 \end{bmatrix} &= -(\mathbf{l} + \mathbf{Z}\,\mathbf{r}) \begin{bmatrix} V_2 \\ -(I_2) \end{bmatrix} + v_n
\end{aligned}$$

Therefore, the transmission matrix is:

$$\mathbf{T} = -\mathbf{C}_{Z\to T}\, (\mathbf{l} + \mathbf{Z}\,\mathbf{r})$$

where:

$$\mathbf{C}_{Z\to T} = (\mathbf{L} - \mathbf{Z}\,\mathbf{R})^{-1}$$

and the new noise vector is:

$$n_n = \mathbf{C}_{Z\to T}\, v_n$$

This approach gives the same results as the usual conversion tables – see [87] or [128] for

[1] Pucel *et al.* ([61], footnote 4, page 2016) point out the correct use of the off–diagonal elements

signal matrices and [30] for noise correlation matrices, respectively. Its compact form makes it easily implementable with computer programs.

Table 3.2 tabulates the results for other conversions. If a desired pair of matrices is not found there, two transformations can be used; the case $\mathbf{Z} \to \mathbf{T} \to \mathbf{S}$ is equivalent to $\mathbf{Z} \to \mathbf{S}$ and each step corresponds to a matrix multiplication from the left–hand side: for instance, $\mathbf{C}_{Z\to S} = \mathbf{C}_{T\to S}\,\mathbf{C}_{Z\to T}$.

Table 3.2 Matrices for converting representation A into B ($Z_o = 50\ \Omega$).

A → B	$\mathbf{C}^{-1}_{A\to B}$	B
Y → **Z**	$-\mathbf{Y}$	$-\mathbf{C}_{Y\to Z}$
Z → **Y**	$-\mathbf{Z}$	$-\mathbf{C}_{Z\to Y}$
Z → **T**	$(\mathbf{L}-\mathbf{Z}\,\mathbf{R})$	$-\mathbf{C}_{Z\to T}\ (\mathbf{l}+\mathbf{Z}\,\mathbf{r})$
T → **Z**	$(\mathbf{L}-\mathbf{T}\,\mathbf{R})$	$-\mathbf{C}_{T\to Z}\ (\mathbf{l}+\mathbf{T}\,\mathbf{r})$
S → **T**	$\frac{1}{2\sqrt{Z_o}}\ [(\mathbf{1}-\mathbf{S})\ \mathbf{L}-Z_o\ (\mathbf{1}+\mathbf{S})\ \mathbf{R}]$	$-\frac{1}{2\sqrt{Z_o}}\ \mathbf{C}_{S\to T}\ [(\mathbf{1}-\mathbf{S})\ \mathbf{l}+Z_o\ (\mathbf{1}+\mathbf{S})\ \mathbf{r}]$
T → **S**	$\sqrt{Z_o}\ \left[(\mathbf{L}-\mathbf{T}\,\mathbf{R})-\frac{1}{Z_o}\ (\mathbf{l}+\mathbf{T}\,\mathbf{r})\right]$	$-\sqrt{Z_o}\,\mathbf{C}_{T\to S}\ \left[(\mathbf{L}-\mathbf{T}\,\mathbf{R})+\frac{1}{Z_o}\ (\mathbf{l}+\mathbf{T}\,\mathbf{r})\right]$
T → **H**	$(\mathbf{L}+\mathbf{T}\,\mathbf{r})$	$-\mathbf{C}_{T\to H}\ (\mathbf{l}+\mathbf{T}\,\mathbf{R})$
H → **T**	$(\mathbf{L}-\mathbf{H}\,\mathbf{R})$	$\mathbf{C}_{H\to T}\ (\mathbf{r}+\mathbf{H}\,\mathbf{l})$

The vector n_{out} in (3.1) carries the information about the noise performance of the network; from it, the correlation matrix for the given representation [30] is easily obtained:

$$\mathbf{C}_M = \overline{n_{out}\,n_{out}{}^{+}} = \begin{bmatrix} C_{M11} & C_{M12} \\ C_{M21} & C_{M22} \end{bmatrix} \tag{3.3}$$

The bar represents the statistical average of the random noise sources in n_{out} and $^+$ is the Hermitian operator; since 2–port networks are investigated, the correlation matrix has 2 rows and 2 columns.

Matrix $\mathbf{C}_M$ is Hermitian:

$$\mathbf{C}_M = \mathbf{C}_M{}^{+} \tag{3.4}$$

This condition implies that:

1. the diagonal elements $C_{M_{ii}}$ $(i = 1, 2)$ are real and positive:

$$\Im m\,[C_{M_{ii}}] = 0$$
$$C_{M_{ii}} > 0$$

2. the off–diagonal elements are complex conjugated:

$$C_{M_{21}} = (C_{M_{12}})^{\star}$$

3. the correlation coefficient ζ of the random processes $C_{M_{11}}$ and $C_{M_{22}}$ is proportional to the off–diagonal element $C_{M_{21}}$ [30] according to:

$$\zeta \;=\; \frac{C_{M_{21}}}{\sqrt{C_{M_{11}} C_{M_{22}}}} \tag{3.5}$$

4. the correlation matrix of a 2–port network is semi–positive definite. In particular its determinant is always positive:

$$\Delta_{\mathbf{C}_M} \;=\; C_{M_{11}} C_{M_{22}} - \mid C_{M_{21}} \mid^2 \;>\; 0 \tag{3.6}$$

or it is zero for lossless networks.

From (3.5) and (3.6), it follows that if $\Delta_{\mathbf{C}_M} > 0$, then $\mid \zeta \mid < 1$ and vice versa. In fact, (3.6) can be rewritten as:

$$C_{M_{11}} C_{M_{22}} \left(1 - \frac{\mid C_{M_{21}} \mid^2}{C_{M_{11}} C_{M_{22}}}\right) = C_{M_{11}} C_{M_{22}} \left(1 - \mid \zeta \mid^2\right) > 0.$$

Generally speaking, diagonal elements of $\mathbf{C}_M$ are related to noise sources properly located at the network ports. For instance, impedance, admittance, hybrid and scattering parameter representations have one noise source at the input and one at the output port; transmission and chain scattering parameter representations have no sources at the output port of the network. $C_{M_{21}}$ always measures the degree of correlation between them.

This mathematical tool has been applied to the analysis of feedback networks. The model under investigation is shown in Figure 3.2. The embedded 2–port may be an active device such as field effect transistors (JFETs, MESFETs or HEMTs) or junction transistors (homo or hetero–junction). However, passive networks can be considered, too. A parallel admittance $Y_p = G_p + jB_p$ is connected between the input and output and a series feedback impedance $Z_s = R_s + jX_s$ couples the device to ground. The feedback elements are sources of thermal noise [20] if their real part is not zero at the given frequency f_o.

One assumption is tacitly made in Figure 3.2: there is no direct path to ground from the 2–port network. This may be questionable at microwave frequencies [129] but it is a reasonable assumption that measurements have shown to be legitimate. This hypothesis

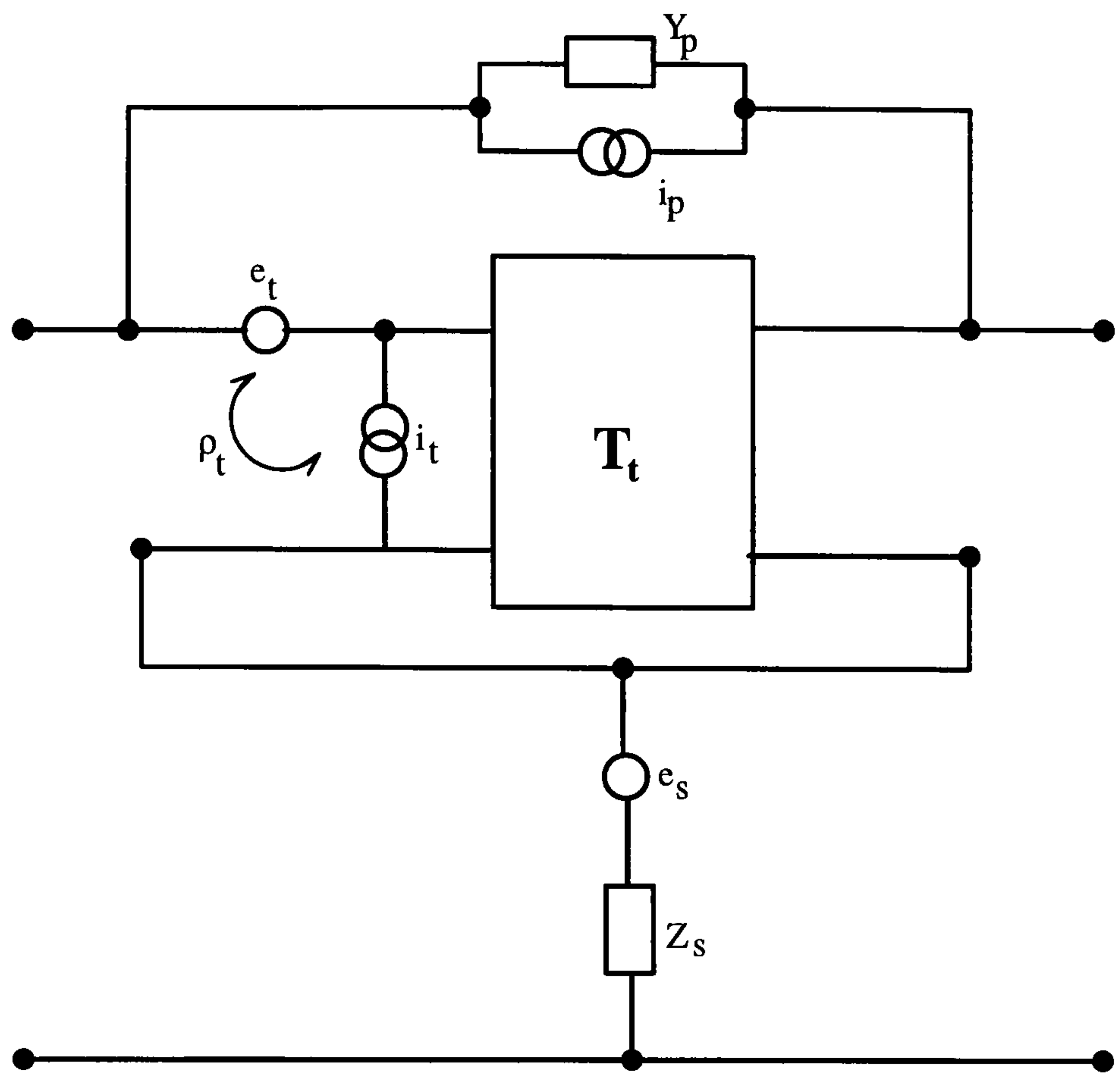

Figure 3.2 Feedback network under analysis.

allows the analysis to make use of transistor manufacturers' data books [85], [130].

The selection of which representation is to be used is not critical; the most reasonable choice should be the one which minimises the effort to obtain the desired results. At microwave frequencies, device handbooks generally resort to scattering parameters S_{ij} and the set F_{min}, R_n and $\Gamma_{S_{opt}}$ in order to characterise signal and noise behaviours, respectively; standard characteristic impedance usually is $Z_o = 50\ \Omega$. New representations can easily be obtained.

The goal of the analysis is to determine the signal and noise matrices of the final network, whose equivalent circuit is shown in Figure 3.3. Its electrical behaviour is described by an expression similar to (3.1), where the elements of the matrices $\mathbf{M}$ and $\mathbf{C}_M$ are functions of the feedback immittances as well as the signal and noise parameters of the embedded 2–port.

Matrix or circuit analysis techniques are available to work out the final signal and noise matrix elements. The first approach may be the most elegant and compact. It has been used in [127] and makes use of Table 3.2; the signal matrix of the feedback amplifier will be derived using this method. The second approach is considered here as far as the noise parameters are concerned and consists of different steps:

- define the notation for both signal and noise quantities;
- switch off the noise sources in Figure 3.2 and determine the signal matrix of the final network of Figure 3.3 (signal analysis);
- switch off the signal generators in Figure 3.2 leaving the internal noise sources turned on. Then, determine the overall noise performance for the final network of Figure 3.3 (noise analysis).

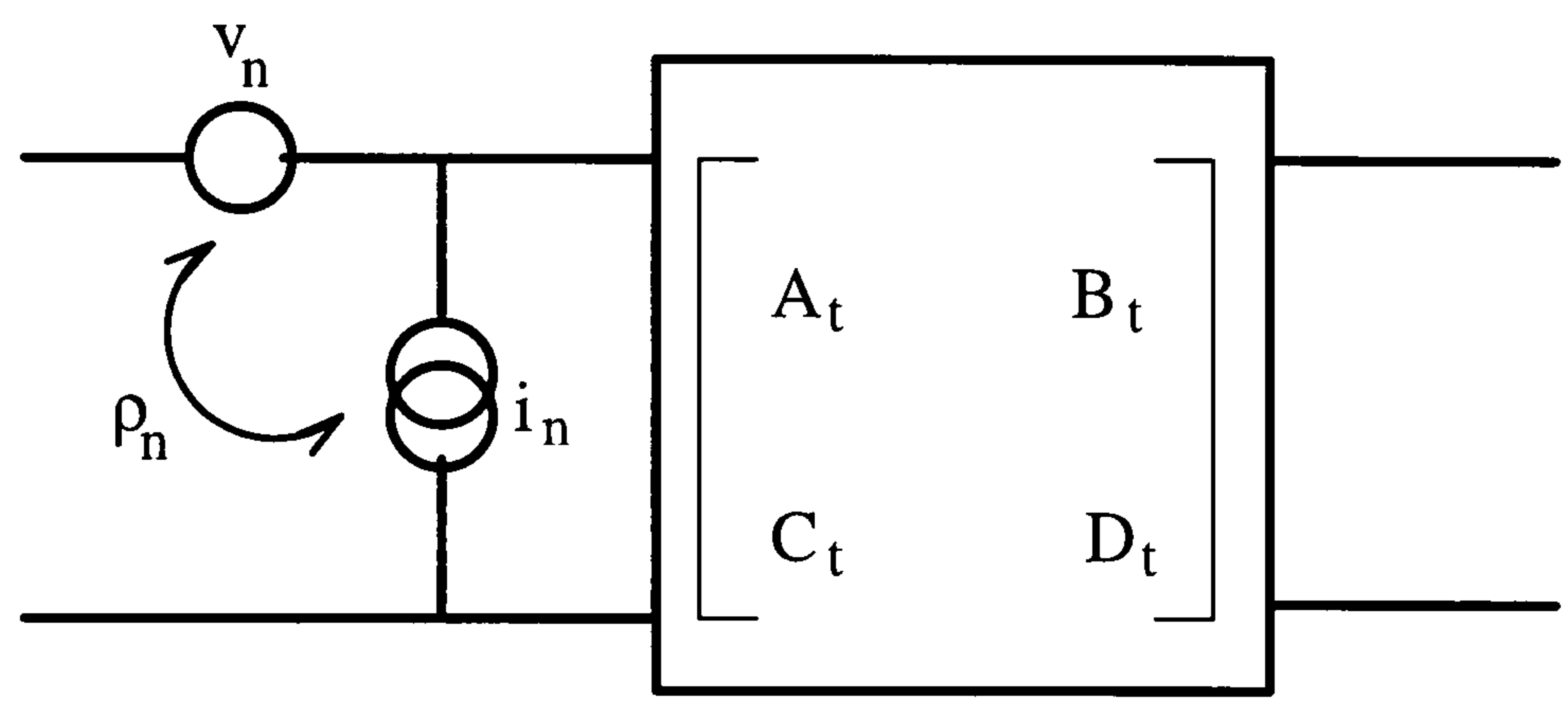

Figure 3.3 Final equivalent model of the feedback network.

3.1.1 Symbols Definition

A transmission representation models the noisy 2–port circuit of Figure 3.2; a subscript t is associated with its parameters. Since this analysis is going to be applied to LNAs, t may be assumed to stand for *transistor*. Subscripts s and p identify quantities of the series and parallel feedback elements respectively.

The device transmission matrix is:

$$\mathbf{T}_t = \begin{bmatrix} A_t & B_t \\ C_t & D_t \end{bmatrix} \tag{3.7}$$

and its noise sources e_t and i_t have root mean squared (rms) values [20] equal to:

$$\overline{\mid e_t \mid^2} = 4kT_oR_t\Delta f \tag{3.8}$$

$$\overline{\mid i_t \mid^2} = 4kT_og_t\Delta f \tag{3.9}$$

Their correlation coefficient is:

$$\rho_t = \frac{\overline{i_t\, e_t^\star}}{\sqrt{\overline{i_t^2}\,\overline{e_t^2}}} \tag{3.10}$$

Here, k is the Boltzmann constant[2], T_o is the (standard) temperature of the system; the bandwidth Δf in which the noise power is measured, spans around the test frequency f_o. The constraint $\Delta f / f_o \ll 1$ is assumed also.

Both parallel $Y_p = G_p + jB_p$ and series $Z_s = R_s + jX_s$ feedback immittances are noisy because their real parts, if present, are sources of thermal noise [20]. Therefore, a current noise source i_p is associated with the conductance G_p and a voltage noise source e_s with the resistance R_s. Their rms values are:

$$\overline{\mid i_p \mid^2} = 4kT_oG_p\Delta f \tag{3.11}$$

$$\overline{\mid v_s \mid^2} = 4kT_oR_s\Delta f \tag{3.12}$$

It is assumed that feedback immittance noise sources are correlated neither between each other nor with the noise sources of the transistor; only e_t and i_t are correlated. This hypothesis is allowed for by:

$$x = [i_t \quad e_t \quad i_p \quad e_s]^T \tag{3.13}$$

which holds every noise source of the starting network; the associated correlation matrix:

$$\overline{x\, x^+} = \begin{bmatrix} \overline{\mid i_t \mid^2} & \overline{e_t\, i_t^\star} & 0 & 0 \\ \overline{i_t\, e_t^\star} & \overline{\mid e_t \mid^2} & 0 & 0 \\ 0 & 0 & \overline{\mid i_p \mid^2} & 0 \\ 0 & 0 & 0 & \overline{\mid e_s \mid^2} \end{bmatrix} \tag{3.14}$$

defines the correlation coefficients among the four noise sources.

3.1.2 Signal Analysis

The signal behaviour of linear feedback amplifiers has been studied extensively, both at low frequencies [60] and microwave frequencies [86] where the gain of the amplifier drops. For the purposes of this section, matrix analysis is used.

Consider Figure 3.4 where the noise sources in the network have been switched off. The

[2] The approximated numerical value of the Boltzmann constant is 1.381×10^{-23}; its dimensions are $\mathrm{J{\cdot}K^{-1}}$.

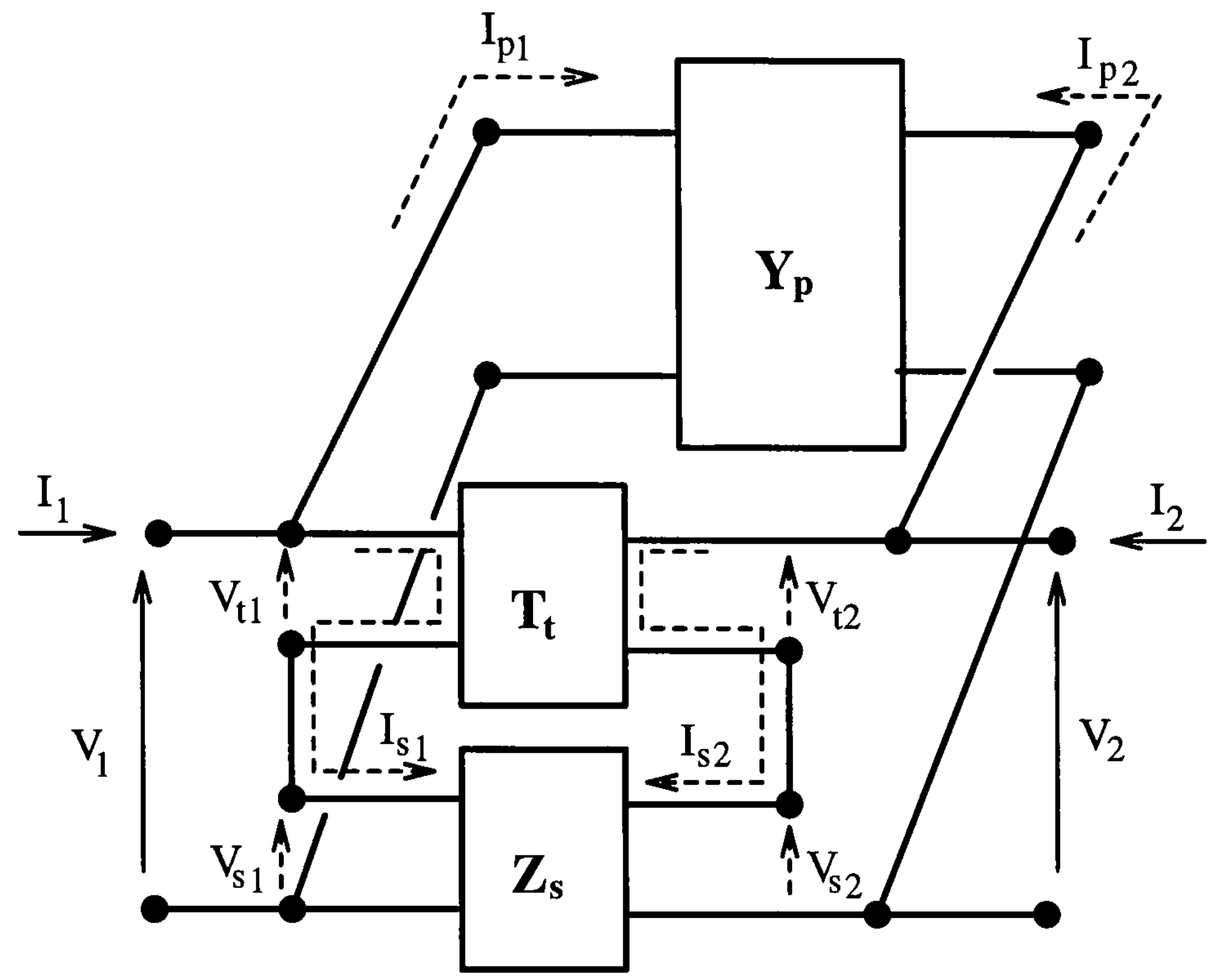

Figure 3.4 Definitions for the signal analysis of the feedback amplifier.

transistor matrix $\mathbf{T}_t$ (3.7), the series impedance matrix $\mathbf{Z}_s$,

$$\mathbf{Z}_s = Z_s \begin{bmatrix} 1 & 1 \\ 1 & 1 \end{bmatrix} \tag{3.15}$$

and the parallel admittance matrix $\mathbf{Y}_p$,

$$\mathbf{Y}_p = Y_p \begin{bmatrix} 1 & -1 \\ -1 & 1 \end{bmatrix} \tag{3.16}$$

are the components of the network; Z_s and Y_p are the series and parallel immittance, respectively. (3.7), (3.15) and (3.16) are used to link voltages and currents of Figure 3.4:

$$\begin{bmatrix} V_{t_1} \\ I_{t_1} \end{bmatrix} = \mathbf{T}_t \begin{bmatrix} V_{t_2} \\ I_{t_2} \end{bmatrix} \tag{3.17}$$

$$\begin{bmatrix} V_{s_1} \\ V_{s_2} \end{bmatrix} = \mathbf{Z}_s \begin{bmatrix} I_{s_1} \\ I_{s_2} \end{bmatrix} \tag{3.18}$$

$$\begin{bmatrix} I_{p_1} \\ I_{p_2} \end{bmatrix} = \mathbf{Y}_p \begin{bmatrix} V_{p_1} \\ V_{p_2} \end{bmatrix} \tag{3.19}$$

Other quantities which do not appear in Figure 3.4 are easily expressed in terms of those defined in the same figure:

$$\begin{cases} V_1 & = V_{p_1} = V_{t_1} + V_{s_1} \\ I_1 & = I_{p_1} + I_{s_1} \\ V_2 & = V_{p_2} = V_{t_2} + V_{s_2} \\ I_2 & = I_{p_2} + I_{s_2} \\ I_{t_2} & = -I_{s_2} \end{cases} \tag{3.20}$$

Finally, the transmission matrix $\mathbf{T}_t$ of the device is transformed into its equivalent impedance matrix $\mathbf{Z}_t$ (Table 3.2):

$$\begin{bmatrix} V_{t_1} \\ V_{t_2} \end{bmatrix} = \mathbf{Z}_t \begin{bmatrix} I_{t_1} \\ -(I_{t_2}) \end{bmatrix} \tag{3.21}$$

where

$$\mathbf{Z}_t = -\mathbf{C}_{T\to Z}\ (\mathbf{l} + \mathbf{T}_t\,\mathbf{r})$$

The analysis is carried out by making use of (3.18), (3.19), (3.20), (3.21) and the unit matrix

$$\mathbf{1} = \begin{bmatrix} 1 & 0 \\ 0 & 1 \end{bmatrix}$$

It consists of 4 steps:

Step 1:

$$\begin{bmatrix} I_{p_1} \\ I_{p_2} \end{bmatrix} = \mathbf{Y}_p \begin{bmatrix} V_1 \\ V_2 \end{bmatrix} = \mathbf{Y}_p \begin{bmatrix} V_{t_1} + V_{s_1} \\ V_{t_2} + V_{s_2} \end{bmatrix} = \mathbf{Y}_p\,[\mathbf{Z}_t + \mathbf{Z}_s] \begin{bmatrix} I_{s_1} \\ I_{s_2} \end{bmatrix}$$

Step 2:

$$\begin{bmatrix} I_1 \\ I_2 \end{bmatrix} = \begin{bmatrix} I_{p_1} \\ I_{p2} \end{bmatrix} + \begin{bmatrix} I_{s_1} \\ I_{s_2} \end{bmatrix} = [\mathbf{Y}_p\ (\mathbf{Z}_t + \mathbf{Z}_s) + \mathbf{1}] \begin{bmatrix} I_{s_1} \\ I_{s_2} \end{bmatrix}$$

Step 3:

$$\begin{bmatrix} I_{s_1} \\ I_{s_2} \end{bmatrix} = [\mathbf{1} + \mathbf{Y}_p\ (\mathbf{Z}_t + \mathbf{Z}_s)]^{-1} \begin{bmatrix} I_1 \\ I_2 \end{bmatrix}$$

Step 4:

$$
\begin{aligned}
\begin{bmatrix} V_1 \\ V_2 \end{bmatrix} &= \begin{bmatrix} V_{t_1} \\ V_{t_2} \end{bmatrix} + \begin{bmatrix} V_{s_1} \\ V_{s_2} \end{bmatrix} \\
&= [\mathbf{Z}_t + \mathbf{Z}_s]\,[\mathbf{1} + \mathbf{Y}_p\,(\mathbf{Z}_t + \mathbf{Z}_s)]^{-1} \begin{bmatrix} I_1 \\ I_2 \end{bmatrix}
\end{aligned}
$$

The impedance matrix of the final equivalent circuit is:

$$
\mathbf{Z}_n = [\mathbf{Z}_t + \mathbf{Z}_s]\,[\mathbf{1} + \mathbf{Y}_p\,(\mathbf{Z}_t + \mathbf{Z}_s)]^{-1} \tag{3.22}
$$

The subscript n identifies quantities related to the final network of Figure 3.3. Once $\mathbf{Z}_n$ is known, any kind of signal matrix, such as transmission or scattering matrix, can easily be worked out with the help of Table 3.2. The task of determining the signal performance of the feedback amplifier is thus completed.

3.1.3 Noise Analysis

The noise parameters are determined with circuit analysis techniques: Kirchoff laws on voltages and currents are applied to the noisy network of Figure 3.2. This technique is outlined by Hillbrand [30]; the equivalent matrix approach is described in [127].

Consider Figure 3.2 and Figure 3.3; the latter shows the equivalent feedback network resulting from signal and noise analysis of the former. Switch off the signal sources: $s_{in} = [\,V_2 \quad I_2\,]^T = 0$. For a transmission matrix representation, $s_{in} = 0$ reduces (3.1) to:

$$
\begin{bmatrix} V_1 \\ I_1 \end{bmatrix} = \begin{bmatrix} A_n & B_n \\ C_n & D_n \end{bmatrix} \begin{bmatrix} 0 \\ 0 \end{bmatrix} + \begin{bmatrix} e_n \\ i_n \end{bmatrix} = \begin{bmatrix} e_n \\ i_n \end{bmatrix}
$$

Voltage and current at the input port of the final circuit (when the output port quantities are set to zero) are equal to the equivalent voltage and current noise sources, e_n and i_n respectively. Since the nodes defining input and output ports of the final network are the same as the starting circuit, $[\,V_2 \quad I_2\,]^T = 0$ is applied to the circuit of Figure 3.2 and voltage and current at the input port are worked out as functions of the noise source vector x (3.13). Because of linearity, it is possible to state that the matrix $\mathbf{n}$ that links $x = [\,i_t \quad e_t \quad i_p \quad e_s\,]^T$ to $s_{in} = [\,e_n \quad i_n\,]^T$ has 8 elements n_{ij} arranged in 2 rows and 4 columns:

$$
\begin{bmatrix} e_n \\ i_n \end{bmatrix} = \mathbf{n}\; x \tag{3.23}
$$

where

$$\mathbf{n} = \begin{bmatrix} n_{11} & n_{12} & n_{13} & n_{14} \\ n_{21} & n_{22} & n_{23} & n_{24} \end{bmatrix} \tag{3.24}$$

The elements n_{ij} have different dimensions:

- n_{11} and n_{13} unit is Ω because they link currents to voltages;
- n_{22} and n_{24} relate voltages to currents; therefore, they are measured in S;
- the remaining elements are dimensionless coefficients of proportionality because they couple similar generators.

For circuit analysis approach, the unknowns are to be defined. With reference to Figure 3.5, nine unknowns are required: five currents ($I_1 = i_n$, I_{11}, I_{22}, I_3, I_4) and four voltages ($V_1 = e_n$, V_{11}, V_{22}, V_4). The noise analysis begins by applying Kirchoff laws to the network

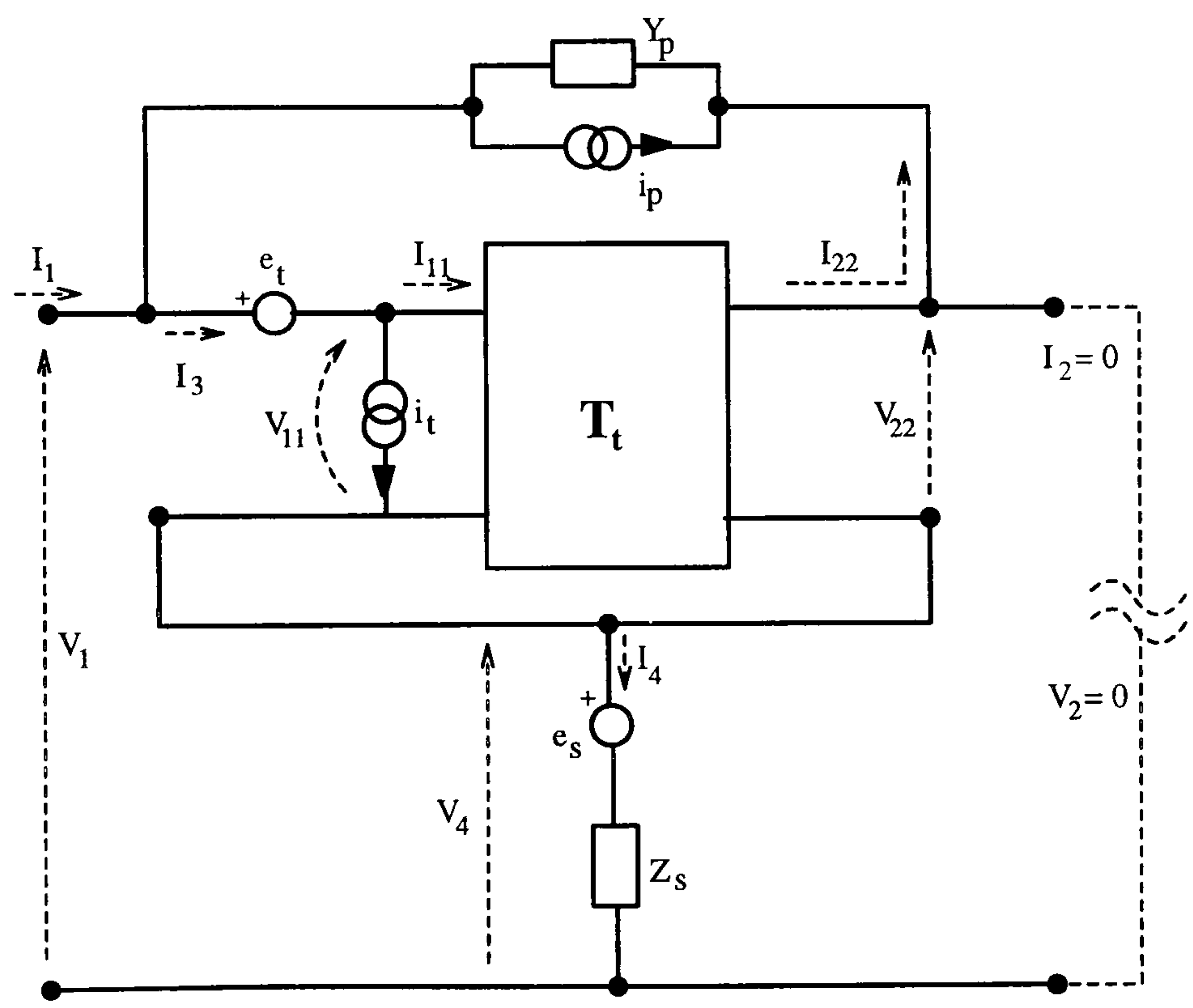

Figure 3.5 Definitions for the noise analysis of the feedback amplifier.

nodes:

$$\begin{cases} I_1 + I_{22} & = I_3 \\ I_3 & = I_{11} + i_t \\ V_{11} & = A_t V_{22} + B_t I_{22} \\ I_{11} & = C_t V_{22} + D_t I_{22} \\ -Y_p V_1 & = I_{22} + i_p \\ V_{22} + V_4 & = 0 \\ V_4 & = e_s + Z_s I_4 \\ I_3 & = I_4 + I_{22} \\ V_1 & = e_t + V_{11} + V_4 \end{cases} \tag{3.25}$$

The reduction of (3.25) to (3.23) requires a lengthy process of substitutions, as outlined in appendix B.1. The final result is:

$$y = \mathbf{n}\, x \tag{3.26}$$

where

$$\begin{aligned} y &= \begin{bmatrix} e_n & i_n \end{bmatrix}^T \\ x &= \begin{bmatrix} i_t & e_t & i_p & e_s \end{bmatrix}^T \\ \mathbf{n} &= \mathbf{A}^{-1}\mathbf{N} && (3.26.a) \\ \mathbf{A} &= \begin{bmatrix} 1 + B_t Y_p & -(1 - A_t)\, Z_s \\ -(1 - D_t)\, Y_p & 1 + C_t Z_s \end{bmatrix} && (3.26.b) \\ \mathbf{N} &= \begin{bmatrix} 0 & 1 & -B_t & 1 - A_t \\ 1 & 0 & 1 - D_t & -C_t \end{bmatrix} && (3.26.c) \end{aligned}$$

(3.26.a) shows that $\mathbf{n}$ is the product of 2 matrices, $\mathbf{A}^{-1}$ and $\mathbf{N}$; $\mathbf{A}$ is a transmission matrix and so is its inverse. If (3.22) is converted into transmission matrix $\mathbf{T}_n$, the determinant of $\mathbf{A}$ is the same as that of the signal matrix of the final circuit. This is demonstrated in appendix B.2. Therefore, the denominator of $\mathbf{n}$ is equal to $\Delta_{\mathbf{T}_n}$, the determinant of the final transmission matrix. $\mathbf{N}$ can be interpreted as the linear combination that reduces the $4{\times}1$ noise source vector x to the $2{\times}1$ vector:

$$\chi = \mathbf{N}\ x$$

located at the output port of a noiseless network represented by matrix $\mathbf{A}$. Its inverse gives the required input vector y:

$$y = \mathbf{A}^{-1}\chi.$$

$\mathbf{A}$ is such that the characteristic equation for noise and signal parameters in transmission representation of the network of Figure 3.2 is the same, even though $\mathbf{A} \neq \mathbf{T}_n$.

3.1.4 Noise Parameters Expansion

The transmission representation correlation matrix [30] is readily obtained from (3.26):

$$\mathbf{C}_n = \overline{y\,y^+} = \overline{(\mathbf{A}^{-1}\mathbf{N}\,x)\,(\mathbf{A}^{-1}\mathbf{N}\,x)^+} = \mathbf{A}^{-1}\,\mathbf{N}\,\overline{x\,x^+}\,\mathbf{N}^+\mathbf{A}^{-1^+} \tag{3.27}$$

The 4×4 matrix $\overline{x\,x^+}$ is the correlation matrix (3.14) of the noise sources in Figure 3.3. Some remarks about (3.27) are necessary:

1. $\mathbf{C}_n$ is in substance a power–related matrix [30], even though its element dimensions may not be homogeneous. For scattering parameter representation, the correlation matrix collects available powers only [31], [33]. As far as (3.27) is concerned, the diagonal element units are Volt or Ampere; and the off–diagonal terms are in Watts;

2. any voltage or current noise generator mean squared value can be made proportional to an equivalent resistance $R = \overline{\mid e \mid^2}/4kT_o\Delta f$ or to an equivalent conductance $g = \overline{\mid i \mid^2}/4kT_o\Delta f$, respectively [20]. Cross products are proportional to $4kT_o\Delta f$ as clearly seen from the definition of correlation coefficient if (3.10) is rewritten as $\overline{i\,e^\star} = \rho\sqrt{\overline{\mid e \mid^2}\;\overline{\mid i \mid^2}}$. Equivalent considerations can be applied to the noise sources in x. Therefore, a common term $4kT_o\Delta f$ can be collected out of $\mathbf{C}_n$ and $\overline{x\,x^+}$ in (3.27) and then dropped for simplicity.

The matrix approach cannot deliver the goal aimed, i.e. to have closed form expressions of the noise parameters: therefore, (3.27) must be expanded. This boring and time consuming task has been carried out:

$$\begin{aligned} R_n &= \mid n_{11} \mid^2 g_t + \mid n_{12} \mid^2 R_t + 2\,\Re e\,[n_{11}n_{12}{}^\star\rho_{t_o}] \\ &\quad + \mid n_{13} \mid^2 G_p + \mid n_{14} \mid^2 R_s \end{aligned} \tag{3.28}$$

$$\begin{aligned} g_n &= \mid n_{21} \mid^2 g_t + \mid n_{22} \mid^2 R_t + 2\,\Re e\,[n_{21}n_{22}{}^\star\rho_{t_o}] \\ &\quad + \mid n_{23} \mid^2 G_p + \mid n_{24} \mid^2 R_s \end{aligned} \tag{3.29}$$

$$\rho_{n_o} = n_{21}n_{11}{}^\star g_t + n_{22}n_{12}{}^\star R_t + n_{22}n_{11}{}^\star \rho_{t_o}{}^\star + n_{21}n_{12}{}^\star\rho_{t_o}$$

$$+n_{23}n_{13}{}^{\star}G_p + n_{24}n_{14}{}^{\star}R_s \tag{3.30}$$

where $\rho_{t_o} = \rho_t \sqrt{g_t R_t}$ and ρ_t is the correlation coefficient of the 2–port device.

This is an intermediate step because the dependence on Z_s and Y_p is not explicit; however, it shows that the feedback immittances, even if noiseless, shape the frequency response of the final network through the terms n_{ij} of (3.26.a) [19], [18], [35], [131]. The terms $R_s = \Re e\,[Z_s]$, $G_p = \Re e\,[Y_p]$ in (3.28), (3.29) and (3.30), correspond to the noise generators e_s and i_p, respectively. In fact, when the noise sources e_s and i_p in x are switched off, Z_s and Y_p still relate voltage and current at their terminals; however, they do not produce noise power proportional to $4kT_oR_s\Delta f$ and $4kT_oG_p\Delta f$ any longer. Switching the noise sources off is equivalent cooling their temperatures down, ideally to $T_{room} = T_o = 0$ K. When this is done, $e_s = 0$ and $i_p = 0$ as desired, even though their V–I relation at the immittance terminals is not affected. In conclusion, the n_{ij} terms are purely signal terms and R_s and G_p in (3.28), (3.29) or (3.30), refer to their noise generators; the feedback immittance V–I relationship is accounted for by n_{ij} only. This reasoning applies to the embedded 2–port network as well. $T_{room} = 0$ K makes only the noise parameters R_t, g_t, ρ_{t_o} equal to zero; it does not affect the signal elements of the transmission matrix $\mathbf{T}_t$. Consequently,

$$n_{ij} = n_{ij}\left(R_s; X_s; G_p; B_p; \mathbf{T}_t\right)$$

The closed form expressions of (3.28), (3.29) and (3.30) are finally obtained [127]:

$$R_n = \frac{r_1 \mid Z_s \mid^2 + r_2 R_s + r_3 X_s + r_4}{\mid \Delta_A \mid^2} \tag{3.31}$$

$$g_n = \frac{g_1 \mid Y_p \mid^2 + g_2 G_p + g_3 B_p + g_4}{\mid \Delta_A \mid^2} \tag{3.32}$$

$$\rho_{n_o} = \frac{c_1 Z_s{}^{\star} + c_2 Z_s{}^{\star} Y_p + c_3 Y_p + c_4 Z_s{}^{\star} G_p + c_5 R_s Y_p + c_6 G_p + c_7 R_s + \rho_{t_o}}{\mid \Delta_A \mid^2} \tag{3.33}$$

where

$$\begin{aligned}
r_1 &= g_t \mid a \mid^2 + 2\Re e\,[a\rho_{t_o} C_t{}^{\star}] + \mid C_t \mid^2 R_t + \mid \Delta \mid^2 G_p \\
r_2 &= 2\left(\frac{1}{2} \mid a \mid^2 + \Re e\,[a\rho_{t_o} + R_t C_t + G_p \Delta B_t{}^{\star}]\right) \\
r_3 &= -2\Im m\,[a\rho_{t_o} + R_t C_t + G_p \Delta B_t{}^{\star}] \\
r_4 &= \mid B_t \mid^2 G_p + R_t \\
g_1 &= R_t \mid d \mid^2 + 2\Re e\,[d\rho_{t_o}{}^{\star} B_t{}^{\star}] + \mid B_t \mid^2 g_t + \mid \Delta \mid^2 R_s \\
g_2 &= 2\left(\frac{1}{2} \mid d \mid^2 + \Re e\,[d\rho_{t_o}{}^{\star} + g_t B_t + G_p \Delta C_t{}^{\star}]\right)
\end{aligned}$$

$$
\begin{aligned}
g_3 &= -2\Im m\left[d\rho_{t_o}{}^{\star} + g_t B_t + R_s \Delta C_t^{\star}\right] \\
g_4 &= \mid C_t \mid^2 R_s + g_t \\
c_1 &= g_t a^{\star} + \rho_{t_o} C_t^{\star} \\
c_2 &= \left(g_t a^{\star} + \rho_{t_o} C_t^{\star}\right) B_t + \left(\rho_{t_o}{}^{\star} a^{\star} + R_t C_t^{\star}\right) d \\
c_3 &= \rho_{t_o} B_t + d R_t \\
c_4 &= -d\Delta^{\star} \\
c_5 &= -a^{\star}\Delta \\
c_6 &= -d B_t{}^{\star} \\
c_7 &= -a^{\star} C_t \\
\Delta_A &= (1 + B_t\, Y_p)\,(1 + C_t\, Z_s) - a\, d\, Z_s Y_p \\
\Delta &= -\left[1 - a - d - (A_t D_t - B_t C_t)\right] \\
a &= 1 - A_t \\
d &= 1 - D_t
\end{aligned}
$$

The task of working out the expressions of the noise parameters as functions of the noisy feedback immittances, is completed. The study of these expressions reveals interesting results.

3.1.5 The Duality Property

This section points out a property of feedback networks which, to the author's knowledge, has not been reported before. It has been named *duality property* because it allows the expressions (3.31), (3.32) and (3.33) of the noise parameters to switch from one to another by swapping their terms appropriately.

Consider (3.31) and suppose (3.32) is to be derived. A simple way to obtain it is to scan (3.31) and whenever any parameter is found, replace it with the one pointed by the double arrow in Table 3.3: R_n swaps with g_n, G_p with R_s and so forth. According to the duality rules, the dual of ρ_{n_o} is $\rho_{n_o}{}^{\star}$; some entities such as Δ_A in (3.31), are equal to their dual in the sense of Table 3.3.

A consequence of duality is that a property of R_n (or g_n), holds for g_n (R_n) when considering the dual network; this is defined as the network which is obtained by switching elements according to Table 3.3. For instance, a series feedback network is the dual of a parallel feedback network: $Z_s = R_s + jX_s \Rightarrow Y_p = G_p + jB_p$. A pure series feedback

Table 3.3 Duality rules for the noise parameters of the feedback network.

R_n	ρ_{n_o}	A_t	B_t	ρ_{t_o}	R_s	X_s
$\Updownarrow$	$\Updownarrow$	$\Updownarrow$	$\Updownarrow$	$\Updownarrow$	$\Updownarrow$	$\Updownarrow$
g_n	$\rho_{n_o}{}^{\star}$	D_t	C_t	$\rho_{t_o}{}^{\star}$	G_p	B_p

amplifier is such that $Z_s \neq 0$ and $Y_p = 0$; a pure parallel amplifier with $Z_s = 0$ and $Y_p \neq 0$ is its dual circuit. It will be shown, later in this chapter, that R_n for a pure series feedback amplifier has a particular behaviour and reaches a minimum and a maximum. Based on the duality principle, the same behaviour is expected from g_n of a pure parallel feedback amplifier [127].

3.1.6 Noise Parameters Extremes

The behaviour of the noise parameters as functions of the feedback elements at a given frequency is now investigated. This subject has been analysed previously; in particular, the positive effects of series feedback LNAs on the simultaneous match have been assessed [109], [110], [132]. Various works have been produced about the noise performance of series feedback amplifiers when the feedback element is varied: Shiga [52] enhances Lehmann's first series feedback MMIC LNA [14] with another MMIC realisation of a MESFET LNA based on a noise simulation when the series impedance is varied.

Some of the achievements by Lehmann [14] and Shiga [52] are summarised here:

1. MMIC microwave amplifiers are investigated;
2. only one feedback element, the series stub between source and ground, is considered;
3. the results about the influence of the series feedback impedance on the noise parameters are extrapolated out of state-of-the-art LNAs and a frequency simulation supports the tested results;
4. noise parameter characteristic behaviours are reported (reduction of F_{min} vs. feedback value in [14], page 1562; saturation of R_n vs. feedback value in [52], page 1990) on the basis of the measurements but no model supports them;
5. the results are confined to the particular design frequency, 10 and 12 GHz for [14] and [52], respectively;

In relation to the above features, this chapter is going to focus upon the following points:

1. the investigation is not related to any type of device as long as its signal and noise matrices are available;
2. feedback elements can be both parallel Y_p and series Z_s immittances. Series feedback amplifiers are readily investigated by setting $Y_p = 0$;
3. the analysis which leads to the noise parameters (3.31), (3.32) and (3.33) is not bound to any type of realisation of the feedback elements, as long as they are linear and expressible as Z_s and Y_p;
4. noise parameter closed form equations are obtained and they can be studied analytically. The consequence is the opportunity to find *optimum points* which can be exploited for LNA designs;
5. both analysis and optimum points are not depending on the particular value of the frequency at which the investigation is carried out.

Those points are considered when (3.31), (3.32) and (3.33) are adapted in the case of pure series feedback networks ($Z_s = jX_s$ and $Y_p = 0$) [127]. The reasons of this choice are:

- series feedback reactance is renowned to achieve extremely good noise performance;
- the need for series feedback LNA modelling, independent of technology and frequency, has been addressed by Shiga[3] but no works have stemmed from his suggestion to tackle this point;
- optimum points for LNA design based on a valid and useful model are not available.

Furthermore, the results for series amplifiers are extendable to parallel LNAs on the basis of the duality principle.

The expressions of the noise parameters when $Z_s = jX_s$ and $Y_p = 0$ are obtained from (3.31), (3.32) and (3.33):

$$R_n = \frac{r_1^{(s)} X_s^2 + r_3^{(s)} X_s + R_t}{\mid 1 + jC_t X_s \mid^2} \tag{3.34}$$

$$g_n = \frac{g_t}{\mid 1 + jC_t X_s \mid^2} \tag{3.35}$$

$$\rho_{n_o} = \frac{-c_1^{(s)} X_s + \rho_{t_o}}{\mid 1 + jC_t X_s \mid^2} \tag{3.36}$$

where

[3] [52], page 1982: *A detailed examination of the relation between FET [noise] parameters and series inductance has not been extensively reported.*

$$
\begin{aligned}
\rho_{n_o} &= \rho_n \sqrt{g_n R_n} \\
r_1^{(s)} &= g_t \mid a \mid^2 + 2\Re e\left[a\rho_{t_o} C_t^\star\right] + \mid C_t \mid^2 R_t \\
r_3^{(s)} &= -2\Im m\left[a\rho_{t_o} + R_t C_t\right] \\
c_1^{(s)} &= g_t a^\star + \rho_{t_o} C_t^\star \\
c_7^{(s)} &= -a^\star C_t \\
a &= 1 - A_t
\end{aligned}
$$

Some features of the noise parameters can be stated at once:

1. R_n and g_n are ratios of polynomials with same degree in X_s; for large values of $\mid X_s \mid$, they tend to:

$$
\begin{aligned}
R_{n_{sat}} &= \lim_{X_s \to \infty} R_n = \frac{r_1^{(s)}}{\mid C_t \mid^2} \\
g_{n_{sat}} &= \lim_{X_s \to \infty} g_n = 0
\end{aligned}
$$

2. the identity

$$
r_1^{(s)} = R_t \mid C_t + aY_{cor} \mid^2 + g_t \mid a \mid^2 \left(1 - \mid \rho_t \mid^2\right)
$$

   holds; $Y_{cor} = \rho_t \sqrt{g_t/R_t}$ is the correlation admittance [18]. $r_1^{(s)} > 0$, together with a positive denominator, guarantees $R_{n_{sat}} > 0$, as expected;

3. g_n decreases as $\mid X_s \mid$ increases.

Physically, $R_{n_{sat}} \neq 0$ and $g_{n_{sat}} = 0$ are noise sources located between the input and the output port of the final network (Figure 3.3). $R_{n_{sat}}$ is equivalent to the whole 2–port circuit of Figure 3.2 when the series feedback is an open circuit and therefore the 2–port device is not coupled to ground. On the basis of the duality rules, this statement can be adapted to a pure parallel feedback network in order to state that, when the feedback admittance is a short circuit, $g_{n_{sat}} \neq 0$ models the whole device as a series conductance connected to ground.

Based on (3.34), the analytical behaviour of R_n for pure series feedback networks can be studied exactly. If $dR_n/dX_s = 0$ is calculated, one maximum $R_{n_{max}}$ and one minimum $R_{n_{min}}$ are found at $X_{s_{max}}$ and $X_{s_{min}}$, respectively [127]. The expression to solve is:

$$
A X_s^2 + B X_s + C = 0 \tag{3.37}
$$

where:

$$A = |C_t|^2 \Im m[a\rho_{t_o}] - |a|^2 g_t \Im m[C_t] - 2\Im m[C_t] \Re e[a\rho_{t_o} C_t^*] \quad (3.37.a)$$

$$B = |a|^2 g_t + 2\Re e[a\rho_{t_o} C_t] \quad (3.37.b)$$

$$C = -\Im m[a\rho_{t_o}] \quad (3.37.c)$$

$$\rho_{t_o} = \rho_t \sqrt{g_t R_t}$$

It is worth pointing out that these results have been achieved for a given f_o. By varying the feedback value at constant frequency, optimum points are visualised. It is also possible to state that if the device signal and noise parameters do not vary dramatically with frequency, the analysis might be mirrored in the frequency domain for a fixed feedback value. This statement has to be taken very carefully. However, if remembered, it may suggest an explanation about the reason why the curves which characterise the noise parameters vs. series feedback in the following chapters, look quite similar to the curves for the same noise parameters in the frequency domain.

The data published in [111] has been used in [127] to validate the R_n analysis: the experimental $R_{n_{min}}$ as well as $R_{n_{sat}}$ perfectly match the values obtained with the new R_n analysis. This independent validation allows the discussion to proceed with confidence.

3.2 Discussion of the Results

The results on R_n are discussed and applied to different types of 2–port circuits. Since the analysis requires signal and noise parameters of the 2–port network to which the feedback immittances are applied, real and complex matrices are examined separately.

A simple T attenuator will be used first. It is a very simple but enlightening example and the results from it are to be taken as suggestions for further investigations as well as hints of features typical of active devices, as shown later on.

3.2.1 Noisy T Attenuator

The first T attenuator under consideration (Figure 3.6) consists of 3 real lossy elements $Z_1 = R_1$, $Z_2 = 1/G_2$ and $Z_3 = R_3$. Each element is source of thermal noise $\overline{|e_i|^2} = 4kT_oR_i\Delta f$, $i = 1, 3$, $\overline{|i_2|^2} = 4kT_oG_2\Delta f$, uncorrelated to each other. The network can easily be described in terms of $\mathbf{T}$ matrices [11]:

$$\begin{aligned}
\mathbf{T}_t &= \mathbf{T}_1\,\mathbf{T}_2\,\mathbf{T}_3 \\
&= \begin{bmatrix} 1 & R_1 \\ 0 & 1 \end{bmatrix} \begin{bmatrix} 1 & 0 \\ G_2 & 1 \end{bmatrix} \begin{bmatrix} 1 & R_3 \\ 0 & 1 \end{bmatrix} \\
&= \begin{bmatrix} 1+R_1\,G_2 & R_3 + R_1\,(1+R_3\,G_2) \\ G_2 & 1+R_3\,G_2 \end{bmatrix}
\end{aligned} \tag{3.38}$$

and its correlation matrix [30] can be written as easily as (3.38):

$$\mathbf{C}_t = \mathbf{C}_1 + \mathbf{T}_1\,\mathbf{C}_2\,\mathbf{T}_1{}^{+} + \mathbf{T}_1\,\mathbf{T}_2\,\mathbf{C}_3\,\mathbf{T}_2{}^{+}\,\mathbf{T}_1{}^{+} \tag{3.39}$$

where

$$\begin{aligned}
\mathbf{C}_i &= 4kT_o\Delta f \begin{bmatrix} R_i & 0 \\ 0 & 0 \end{bmatrix} \quad (i=1,3) \\
\mathbf{C}_2 &= 4kT_o\Delta f \begin{bmatrix} 0 & 0 \\ 0 & G_2 \end{bmatrix}
\end{aligned}$$

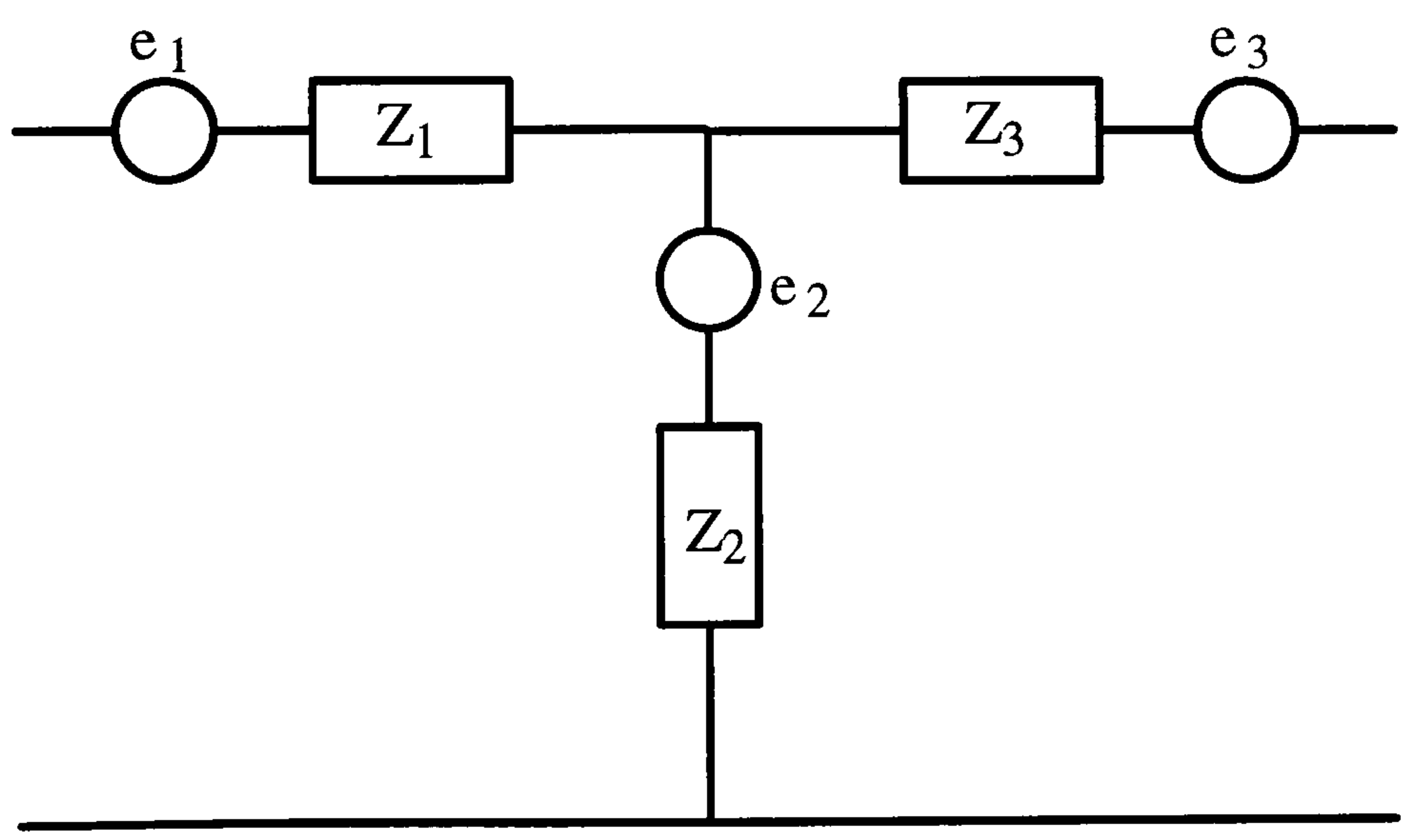

Figure 3.6 Noisy T attenuator.

The signal (3.38) and noise (3.39) matrices are real because the network is comprised of resistances only. Assume that a pure series feedback $Z_s = jX_s$ is applied to the attenuator and look at the coefficients for $R_{n_{min}}$, in particular (3.37.a) and (3.37.c): $A = C = 0$ and the only term that survives in (3.37) is B. The solution of (3.37) is unique and achieved for $X_s = 0$; its value is equal to R_t and it is usually a maximum: a comparison with the value $R_{n_{sat}}$ resolves this uncertainty. The interesting result is that resistive attenuators (real $\mathbf{T}_t$

and $\mathbf{C}_t$ matrices) have no minimum in R_n. Figure 3.7 shows the typical behaviour of R_n vs. X_s.

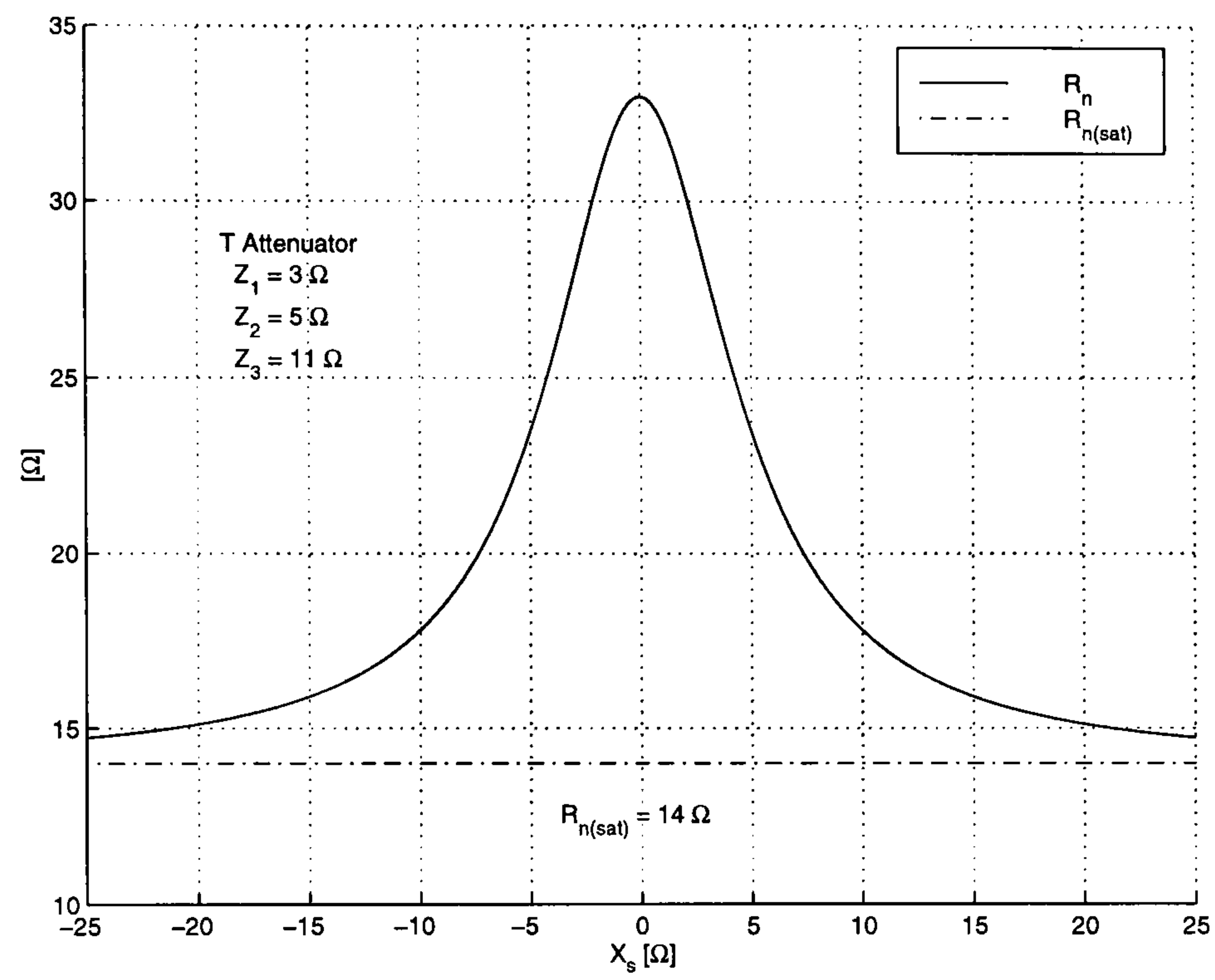

Figure 3.7 R_n vs. the series feedback reactance for a T attenuator.

Now, consider the same attenuator but with reactive elements at frequency f_o. If $Z_1 = R_1 + jX_1$, $1/Z_2 = Y_2 = G_2 + jB_2$ and $Z_3 = R_3 + jX_3$, then

$$\mathbf{T}_t = \mathbf{T}_1\,\mathbf{T}_2\,\mathbf{T}_3 = \begin{bmatrix} 1 + Z_1\,Y_2 & Z_3 + Z_1\,(1 + Z_3\,Y_2) \\ Z_2 & 1 + Z_3\,Y_2 \end{bmatrix}$$

and its correlation matrix is still expressible as in (3.39). When a pure series feedback is applied, coefficients (3.37.a), (3.37.b) and (3.37.c) are not equal to zero and both minimum and maximum values in R_n are expected. If further investigation is carried out, it is found that:

1. the only signal parameters occurring in (3.37) are $a = 1 - A_t = -Z_1/Z_2$ and $C_t = 1/Z_2$
2. the noise parameters of the attenuator are obtained from (3.39):

$$\begin{aligned} R_t &= R_1 + R_2\,\frac{|\,Z_1\,|^2}{|\,Z_2\,|^2} + \frac{R_3}{|\,Z_3\,|^2}\;|\,Z_1 + Z_3\,|^2 \\ g_t &= \frac{R_2 + R_3}{|\,Z_2\,|^2} \end{aligned}$$

$$\rho_{t_o} = \rho_t \sqrt{g_t R_t} = \frac{R_3}{|Z_2|^2}(Z_1 + Z_2)^\star$$

All of them depend on Z_1, Z_2 and $R_3 = \Re e\,[Z_3]$; only R_t depends on both real and imaginary part of Z_3. However, R_t does not appear in (3.37) except through ρ_{t_o}, whose expression does not depend on $\Im m\,[Z_3]$;

3. g_t does not depend on the imaginary part of Z_3.

Therefore, R_n extremes for Figure 3.6 complex T attenuators, are independent of $\Im m\,[Z_3]$.

Bearing those comments in mind, some values are assigned to Z_1, Z_2 and Z_3: prime numbers are chosen in order to minimise the chances of possible simplifications of the above equations. $R_{n_{min}}$ and $R_{n_{max}}$ at $X_{s_{min}}$ and $X_{s_{max}}$, respectively, have been tabulated in Table 3.4 vs. the sign of the imaginary part of Z_1 and Z_2; since the noise parameters are independent of $\Im m\,[Z_3]$, its sign and value do not affect the results of Table 3.4.

Table 3.4 T attenuator R_n extremes vs. the sign of the imaginary part of Z_i, $i = 1, 2$ ($Z_3 = 11 \pm X_3$).

Case	$Z_1 = 3 \pm j2$ Ω	$Z_2 = 5 \pm j7$ Ω	$R_{n_{min}}$ Ω	$X_{s_{min}}$ Ω	$R_{n_{max}}$ Ω	$X_{s_{max}}$ Ω
1	+	+	13.13	-32.44	36.38	-6.02
2	+	-	13.13	-18.44	36.38	7.98
3	-	+	13.13	18.44	36.38	-7.98
4	-	-	13.13	32.44	36.38	6.02

The aim of Table 3.4 is to look at the positions of $X_{s_{min}}$ and $X_{s_{max}}$, as well as the sign of the reactance required to achieve $R_{n_{min}}$, as functions of the impedances Z_i. R_n extremes do not change in magnitude but they are achieved for different X_s: in case 1 and 2, $X_{s_{min}} < X_{s_{max}}$ and $X_{s_{min}}$ is capacitive; in case 3 and 4, $X_{s_{min}} > X_{s_{max}}$ and $X_{s_{min}}$ is inductive.

Inductive input reactances are associated with case 1 and 2 ($\Im m\,[Z_1] > 0$); capacitive Z_1 with case 3 and 4 ($\Im m\,[Z_1] < 0$). If Z_1 is inductive (capacitive), then $X_{s_{min}} < X_{s_{max}}$ ($X_{s_{min}} > X_{s_{max}}$). Z_2 can be considered as a feedback branch between the common node of Z_1 and Z_3. The sign of $\Im m\,[Z_2]$ does not affect the relative position of $X_{s_{min}}$ and $X_{s_{max}}$, but seems to be related to the sign of $X_{s_{max}}$. The application of external feedback reactance X_s modify $\Im m\,[Z_2]$. Finally, these results are independent of $\Im m\,[Z_3]$.

3.2.2 Amplifiers

The noise parameter analysis is now applied to active 2–port networks, such as BJTs or FETs, since the analysis has been developed independently of the type of 2–port device in use. Transistors show complex matrices for both signal and noise parameters. Their noise properties will be outlined with particular attention to the behaviour of R_n in the light of further development for design applications of LNAs.

FET

The field effect transistor under consideration is a Hewlett Packard MESFET ATF21186 [85]. The following considerations have influenced the choice of HP MESFET devices:

1. LNA receivers for mobile communications in the range 1 – 2 GHz take advantage of their low noise characteristics [7], [66], [69];
2. HP devices are widely used by many manufacturers of communications systems and subsystems (for instance, see [133]);
3. noise parameters in the HP data book usually are more reliable than those of other manufacturers – the transformation to new sets with Table 3.2 give acceptable results.

The last point is very important because LNA designers often rely on parameters detailed in data books.

The HP ATF21186 is a typical MESFET for low noise applications around 1 GHz. Its signal and noise data vs. frequency provided by the manufacturer [85] are given in Table 3.5 and Table 3.6, respectively.

Table 3.5 Hewlett Packard ATF21186 data book signal performance ($Z_o = 50\ \Omega$).

f GHz	$\mid S_{11} \mid$ –	$\angle S_{11}$ deg	$\mid S_{21} \mid$ –	$\angle S_{21}$ deg	$\mid S_{12} \mid$ –	$\angle S_{12}$ deg	$\mid S_{22} \mid$ –	$\angle S_{22}$ deg
0.5	0.98	-49	3.77	147	0.069	62	0.34	-55
1.0	0.92	-61	3.42	133	0.092	54	0.33	-63
2.0	0.81	-87	2.85	108	0.131	39	0.32	-81
4.0	0.64	-143	2.11	61	0.178	13	0.26	-135
6.0	0.61	162	1.59	19	0.189	-8	0.28	162
8.0	0.65	123	1.25	-14	0.200	-20	0.37	129

Notice that $R_n = R_t$ decreases down to 2 Ω at 6 GHz where the gain is $\mid S_{21} \mid = 4$ dB; an interpretation of this minimum will be suggested later on. $\Gamma_{S_{opt}}$ displays a similar trend which reaches a minimum value at the same frequency as R_n.

Table 3.6 Hewlett Packard ATF21186 data book noise performance ($Z_o = 50\ \Omega$).

f GHz	F_{min} dB	$\mid \Gamma_{S_{opt}} \mid$ –	$\angle \Gamma_{S_{opt}}$ deg	R_t Ω
0.5	0.50	0.91	31	34.0
1.0	0.55	0.87	40	24.5
2.0	0.65	0.77	63	20.0
4.0	0.84	0.66	111	14.5
6.0	1.13	0.65	171	2.0
8.0	1.23	0.79	-141	5.5

When a series feedback reactance is applied, the equivalent noise resistance assumes a value between maximum and minimum extremes. ATF21186 R_n extremes are tabulated in Table 3.7; signal and the other noise parameters in Table 3.8 and Table 3.9, respectively. Figure 3.8 and Figure 3.9 show two examples of R_n vs. frequency.

Table 3.7 Extremes in the equivalent noise resistance R_n for HP ATF21186 at the required series reactance X_s.

f GHz	$R_{n_{min}}$ Ω	$X_{s_{min}}$ Ω	$R_{n_{max}}$ kΩ	$X_{s_{max}}$ kΩ	$R_{n_{sat}}$ Ω	$-\left(\frac{R_{n_{min}}-R_t}{R_t}\right)$ %
0.5	1.29	223.54	6.02	-0.43	122.21	96.20
1.0	1.18	169.34	2.85	-0.33	89.03	95.17
2.0	1.62	98.98	1.12	-0.23	91.90	91.92
4.0	2.45	46.49	0.34	-0.15	92.87	83.13
6.0	1.77	5.51	0.10	-0.15	63.55	11.26
8.0	0.57	-24.86	0.05	-1.57	49.42	89.71

Some remarks can be stated when comparing Table 3.6 with Table 3.7:

1. the equivalent noise resistance R_t of the transistor can be lowered when applying a pure series feedback;

2. the smallest relative decrease in R_n (11.26%) occurs at the frequency where R_t is minimum without feedback (6 GHz);

3. $R_{n_{max}}$ always precedes $R_{n_{min}}$: $X_{s_{min}} > X_{s_{max}}$;

4. the feedback reactances for $R_{n_{min}}$ and $R_{n_{max}}$ are inductive and capacitive respectively at any frequency except at 8 GHz, where both $R_{n_{min}}$ and $R_{n_{max}}$ are achieved with capacitive feedback;

Table 3.8 ATF21186 scattering parameters and available gain vs. frequency when the feedback is $Z_s = jX_{s_{min}}$ and the source is 50 Ω.

f GHz	$\mid S_{11} \mid$ –	$\angle S_{11}$ deg	$\mid S_{21} \mid$ –	$\angle S_{21}$ deg	$\mid S_{12} \mid$ –	$\angle S_{12}$ deg	$\mid S_{22} \mid$ –	$\angle S_{22}$ deg	G_{av} dB
0.5	0.93	-11.34	0.56	81.01	0.19	87.15	0.95	-7.67	10.70
1.0	0.88	-15.31	0.72	77.50	0.24	84.62	0.91	-10.29	9.60
2.0	0.72	-25.80	1.08	70.29	0.34	80.97	0.77	-16.66	9.34
4.0	0.29	-81.39	1.55	48.50	0.45	66.61	0.37	-44.94	8.94
6.0	0.56	160.69	1.57	18.30	0.21	14.05	0.24	163.53	8.43
8.0	0.67	131.06	1.25	-14.08	0.42	-77.56	0.36	128.92	5.11

Table 3.9 ATF21186 noise parameters vs. frequency at $Z_s = j\,X_{s_{min}}$.

f GHz	$X_{s_{min}}$ Ω	F_{min} dB	$\mid \Gamma_{S_{opt}} \mid$ –	$\angle\Gamma_{S_{opt}}$ deg	$R_{n_{min}}$ Ω
0.5	223.54	0.37	0.02	17.56	1.29
1.0	169.34	0.39	0.06	176.54	1.18
2.0	98.98	0.46	0.21	-179.97	1.62
4.0	46.49	0.69	0.45	-179.65	2.45
6.0	5.51	1.11	0.64	-179.91	1.78
8.0	-24.86	1.10	0.80	179.58	0.57

5. reactive series feedback values for $R_{n_{min}}$ at low frequencies are quite large. For instance, 71 nH at 0.5 GHz, 27 nH at 1 GHz, 8 nH at 2 GHz. At 8 GHz the feedback capacitance is 0.8 pF;

6. X_s makes F_{min} decrease (Table 3.9). This may occur when the feedback is capacitive, too;

7. $\mid \Gamma_{S_{opt}} \mid < 0.1$ for $f \leq 1$ GHz (Table 3.9);

8. the higher the frequency, the closer $R_{n_{max}}$ to the value $R_{n_{sat}}$.

BJT

A Hewlett Packard AT41486 BJT is investigated; a comparison with the previous FET behaviour is also outlined. Signal and noise data [85] of the transistor are tabulated in Table 3.10 and Table 3.11, respectively.

Across the frequency range outlined in the data book, the BJT equivalent noise resistance shows a smoother behaviour than the ATF21186's (compare Table 3.6 and Table 3.11); however, a decreasing trend is noticeable: R_t reaches its minimum at approximately 1–2

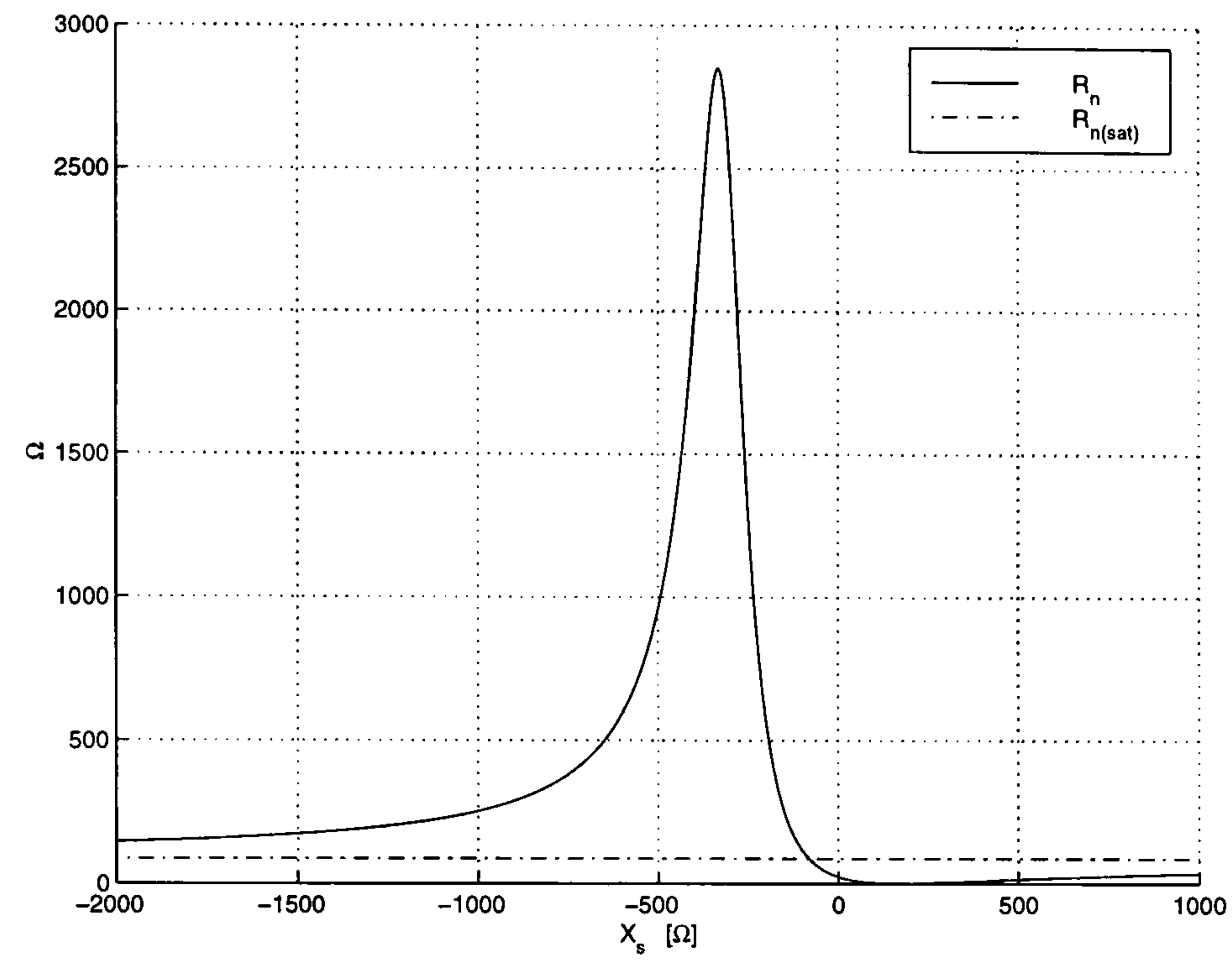

Figure 3.8 R_n vs. series feedback element X_s at 1 GHz with ATF21186 MESFET.

Table 3.10 Hewlett Packard AT41486 data book signal performance ($Z_o = 50\ \Omega$).

f GHz	$\mid S_{11} \mid$ –	$\angle S_{11}$ deg	$\mid S_{21} \mid$ –	$\angle S_{21}$ deg	$\mid S_{12} \mid$ –	$\angle S_{12}$ deg	$\mid S_{22} \mid$ –	$\angle S_{22}$ deg
0.1	0.74	-38	25.46	157	0.011	68	0.94	-12
0.5	0.59	-127	12.63	107	0.031	47	0.60	-29
1.0	0.56	-168	6.92	84	0.041	46	0.49	-29
2.0	0.62	152	3.61	56	0.058	43	0.42	-39
4.0	0.71	113	1.80	16	0.106	48	0.35	-70

GHz. In order to determine its frequency, the magnitude of the optimum reflection coefficient $\Gamma_{S_{opt}}$ is checked: its smallest value occurs at 1 GHz, as in the case of ATF21186. Therefore, the minimum in R_t is associated with $f = 1$ GHz instead of $f = 2$ GHz.

When a series feedback reactance X_s is applied, both scattering and noise parameters vary; optimum points for R_n are detailed in Table 3.12. The variation of R_n with respect to R_t is within 2% up to 2 GHz and the minimum value is at 1 GHz (if the result at 0.1 GHz is neglected). The variation range is quite small in comparison to the MESFET case in Table 3.7. There, the smallest value is about 11% at 6 GHz (the frequency where R_t is the smallest) and variations are in the order of 100%. The feedback reactance almost reduces the value of the noise resistance to zero. As a consequence, the BJT can be assumed to be

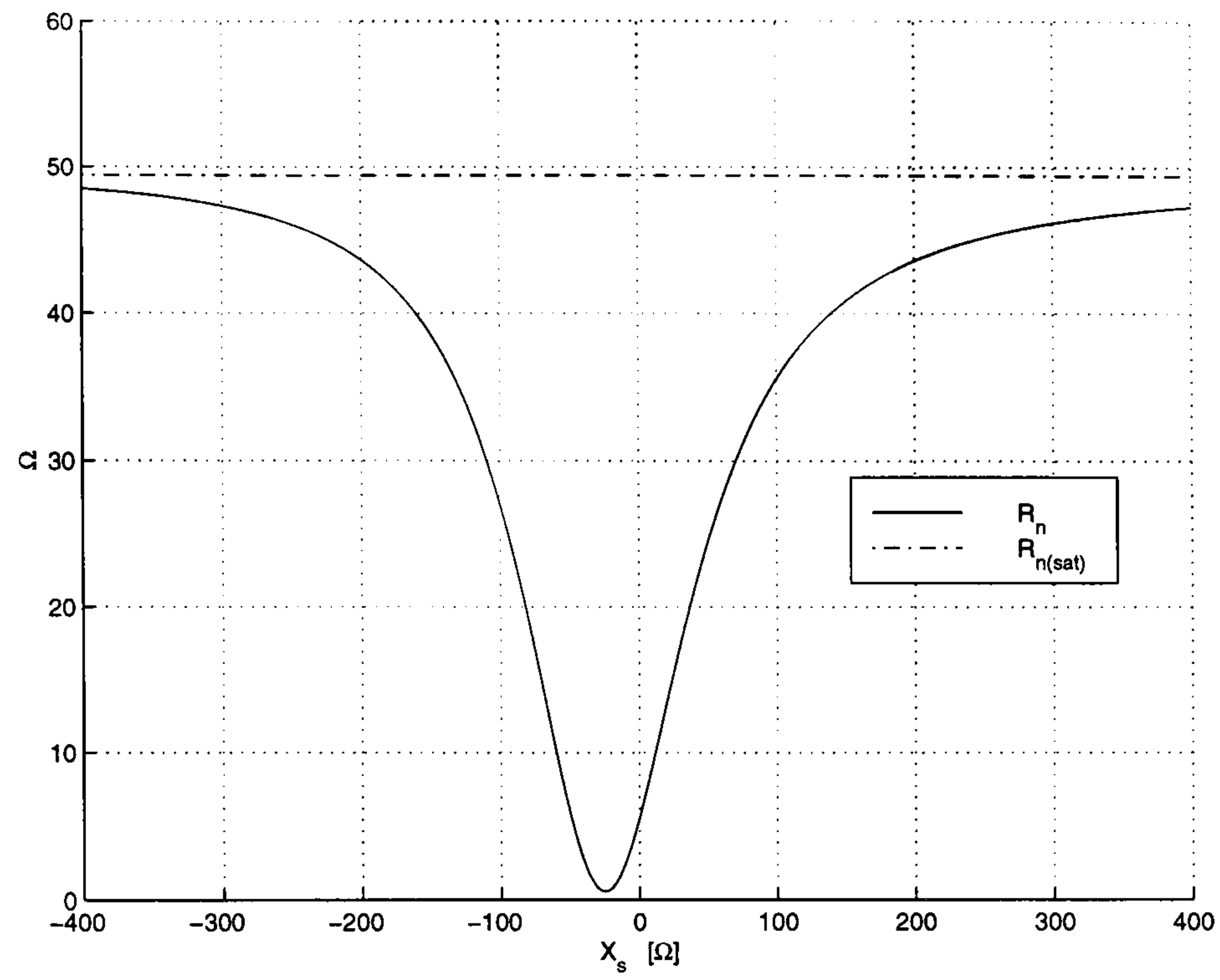

Figure 3.9 R_n vs. series feedback element X_s at 8 GHz with ATF21186 MESFET.

Table 3.11 Hewlett Packard AT41486 data book noise performance ($Z_o = 50\ \Omega$).

f GHz	F_{min} dB	$\mid \Gamma_{S_{opt}} \mid$ –	$\angle\Gamma_{S_{opt}}$ deg	R_t Ω
0.1	1.3	0.12	3	8.5
0.5	1.3	0.10	16	8.5
1.0	1.4	0.04	43	8.0
2.0	1.7	0.12	-145	8.0
4.0	3.0	0.44	-99	20.0

tuned for smallest dependence of the noise figure on the input mismatch $\mid \Gamma_S - \Gamma_{S_{opt}} \mid$ [19], [73]. Even though series feedback does not improve R_t dramatically, it substantially affects the final **S** matrix, in particular S_{11} as Table 3.13 demonstrate.

Some conclusions can be drawn:

1. the equivalent noise resistance R_t of the transistor decreases when applying a pure series feedback, but less dramatically than in the MESFET case;

2. $R_{n_{min}}$ is always met after $R_{n_{max}}$ as X_s sweeps from -∞ to +∞: $X_{s_{max}} < X_{s_{min}}$;

3. the feedback element at $R_{n_{min}}$ is inductive, while it is capacitive at $R_{n_{max}}$. As in the MESFET case, $X_{s_{max}} < X_{s_{min}}$ even when R_n minimum is achieved with a capacitive

Table 3.12 Extremes in the equivalent noise resistance R_n for HP AT41486 and the required series reactance X_s.

f GHz	$R_{n_{min}}$ Ω	$X_{s_{min}}$ Ω	$R_{n_{max}}$ kΩ	$X_{s_{max}}$ kΩ	$R_{n_{sat}}$ kΩ	$-\left(\frac{R_{n_{min}}-R_t}{R_t}\right)$ %
0.1	8.499	0.840	23030	-7.34	113.08	0.02
0.5	8.473	3.455	118.82	-1.32	3.91	0.32
1.0	7.976	3.003	12.64	-0.68	1.18	0.31
2.0	7.843	-6.021	1.31	-0.38	0.44	1.97
4.0	8.792	-32.560	0.23	-0.44	0.21	56.04

Table 3.13 AT41486 scattering parameters and available gain vs. frequency when the feedback is $Z_s = jX_{s_{min}}$ and the source is 50 Ω.

f GHz	$\mid S_{11} \mid$ –	$\angle S_{11}$ deg	$\mid S_{21} \mid$ –	$\angle S_{21}$ deg	$\mid S_{12} \mid$ –	$\angle S_{12}$ deg	$\mid S_{22} \mid$ –	$\angle S_{22}$ deg	G_{av} dB
0.1	0.649	-31.628	23.216	146.438	0.011	72.117	0.912	-10.310	35.059
0.5	0.224	-88.266	9.015	99.251	0.038	75.988	0.670	-15.748	21.686
1.0	0.301	-164.768	5.804	82.116	0.054	68.136	0.561	-21.780	16.915
2.0	0.995	155.070	4.355	56.046	0.064	-34.188	0.305	-54.590	13.204
4.0	1.471	125.440	2.270	12.399	0.463	-86.805	0.106	-142.313	7.168

reactance ($X_{s_{min}} < 0$);

4. the inductances associated with $X_{s_{min}}$ are far smaller than the values for the ATF21186 device: 1.34 nH, 1.10nH, 0.48 nH at 0.1 GHz, 0.5 GHz, 1.0 GHz respectively. The feedback capacitances are 13.22 pF and 1.22 pF at 2 GHz and 4 GHz;

5. positive series feedback reactances do not affect noticeably F_{min};

6. $\mid \Gamma_{S_{opt}} \mid$ changes very little when applying the feedback and it remains smaller than 0.1 at 1 GHz;

Table 3.14 AT41486 noise parameters vs. frequency at $Z_s = jX_{s_{min}}$.

f GHz	F_{min} dB	$\mid \Gamma_{S_{opt}} \mid$ –	$\angle \Gamma_{S_{opt}}$ deg	$R_{n_{min}}$ Ω
0.1	1.302	0.120	0.54	8.498
0.5	1.297	0.097	3.11	8.473
1.0	1.395	0.031	-30.55	7.975
2.0	1.721	0.111	-175.34	7.842
4.0	3.130	0.305	177.37	8.791

7. $R_{n_{max}}$ approaches the value of $R_{n_{sat}}$ at the highest frequency only; otherwise, the two values are quite far apart.

The behaviour of R_n at 1 GHz is shown in Figure 3.10. Notice again the characteristic shape of the curve.

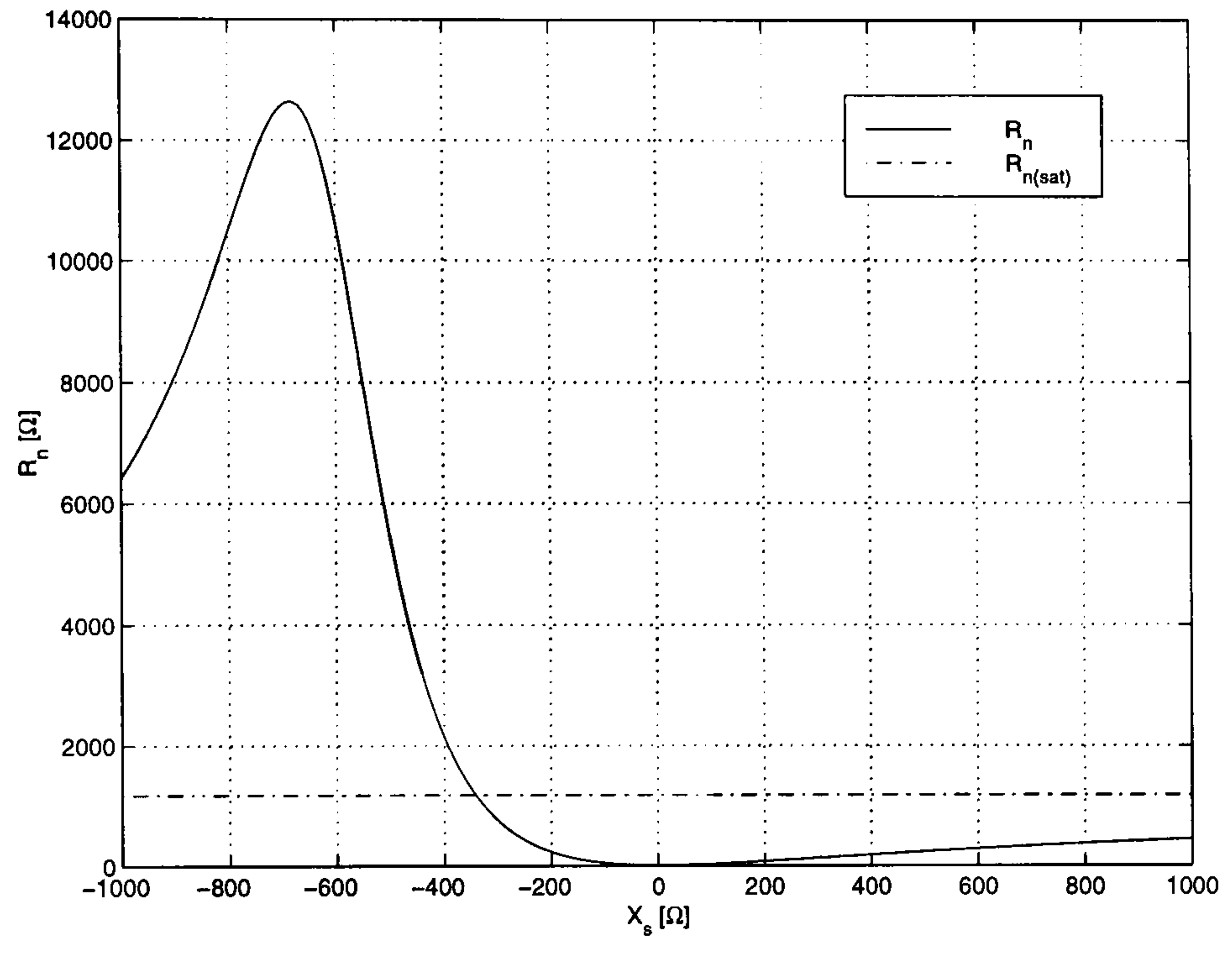

Figure 3.10 R_n vs. series feedback element X_s at 1 GHz with HP AT41486 BJT.

3.3 Application to the Design of Low Noise Amplifiers

LNA design can benefit from the previous results. Designer's experience plays a fundamental role in this process together with computer optimisation: small values of reactance are typical (around 1 nH in the 1 GHz range, less for higher frequencies). A sound and designer–independent approach is preferable. The analysis above reveals that larger values of reactance may be required, as in the MESFET case, in order to make the noise figure as insensitive to the input mismatch as possible. It is clear that this is only one aspect out of many when meeting the required specifications and designer's experience does and always will play an important role.

3.3.1 Noise Parameter Circles

The availability of closed expressions for the noise parameters allows an original graphic technique to be devised for choosing either the feedback impedance Z_s or the feedback admittance Y_p. It makes use of circles on the feedback immittance plane. Series feedback impedance circles are considered here; the duality principle (section 3.1.5) facilitates the task of working out parallel feedback admittance circles, if required.

Narhi [96] published a set of scattering parameter circles on the feedback element plane[4]. They map the loci where the feedback element $Z_s = R_s + jX_s$ provides constant magnitude of the scattering parameters S_{ij}. The intersection between one or more of these circles and the unity circle (here also called *the Smith chart area*) is the region where a passive feedback impedance simultaneously satisfies up to four specifications, one for each scattering parameter S_{ij}. For instance, two requirements could be $\mid S_{11} \mid < -20$ dB and $\mid S_{21} \mid > 15$ dB. Here, constant R_n circles are defined on the same plane on which Narhi describes his constant $\mid S_{ij} \mid$ circles.

For any given R_{n_o}, the region of the Smith chart area where $R_n < R_{n_o}$ at the design frequency f_o is found. If (3.31) is substituted into the equation $R_n = R_{n_o}$ after setting $Y_p = 0$,

$$\mid Z_s - Z_c \mid^2 \quad = \quad r^2 \tag{3.40}$$

is obtained on the impedance plane Z_s. Centre Z_c and radius r are:

$$Z_c \quad = \quad R_c + jX_c = \frac{2\,\Re e\,[C_t]\;R_{n_o} - r_2}{2\,D} - j\,\frac{2\,\Im m\,[C_t]\;R_{n_o} + r_3}{2\,D} \tag{3.40.a}$$

$$r \quad = \quad \sqrt{\frac{R_{n_o} - R_t}{D} + \mid Z_c \mid^2} \tag{3.40.b}$$

$$a \quad = \quad 1 - A_t \tag{3.40.c}$$

$$D \quad = \quad r_1 - R_{n_o} \mid C_t \mid^2 \tag{3.40.d}$$

$$\rho_{t_o} \quad = \quad \rho_t \sqrt{g_t R_t}$$

The terms r_1, r_2 and r_3 come from (3.31). A computer program can readily transform the circles from the complex impedance plane Z_s to the Smith chart plane $\Gamma_s = (Z_s - Z_o)/(Z_s + Z_o)$ referred to Z_o. The designer must be aware of 2 issues:

1. the range of acceptable values for R_{n_o};

[4] Narhi's expressions are revised in appendix B.3.

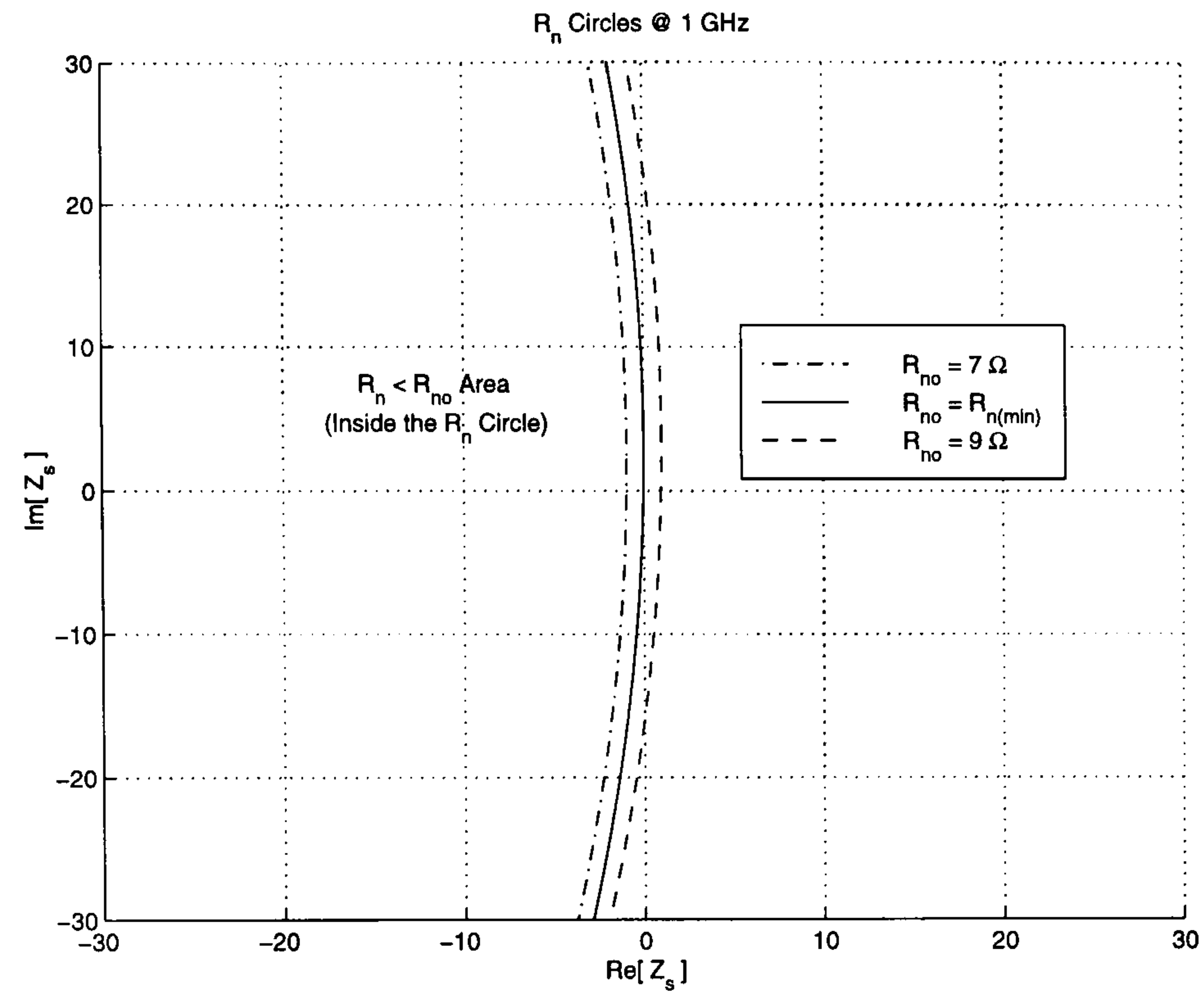

Figure 3.11 Hewlett Packard AT41486 R_n circles on the series feedback element plane Z_s plane around $R_{n_{min}} \approx 7.97\ \Omega$.

2. if the range of series impedances which satisfies $R_n < R_{n_o}$ lies inside or outside the circle described by (3.40).

The first point has been addressed in the R_n analysis [127] when a series feedback reactance X_s is applied (section 3.1.6). There, it has been demonstrated that for complex signal matrices such as for microwave transistors, one minimum $R_{n_{min}}$ and one maximum $R_{n_{max}}$ in R_n occur at $X_s = X_{s_{min}}$ and $X_s = X_{s_{max}}$, respectively.

Figure 3.11 shows the case $R_{n_o} = R_{n_{min}}$ and suggests that:

- smaller values than $R_{n_{min}}$ cannot be achieved with passive series feedback impedances;
- for the particular choice $Z_s = j\, X_{s_{min}}$, the condition $r = -\Re e\,[Z_c]$ holds.

Therefore, $R_{n_{min}}$ at $X_{s_{min}}$ is an absolute minimum for the 2–port network to which the feedback is applied, because the presence of a positive resistive part in Z_s does not let R_n achieve its minimum value. Table 3.15 tabulates noise circles vs. frequency at $R_{n_{min}}$ for the Hewlett Packard low noise BJT AT41486. Its signal and noise parameters are taken from Table 3.10 and Table 3.11.

The second point is about the determination of the region of elements Z_s satisfying $R_n < R_{n_o}$. The sign of the term D (3.40.d) determines whether that region is inside

Table 3.15 R_n circles vs. frequency for HP AT41486 when $Z_s = j\,X_{s_{min}}$ achieving $R_{n_{min}}$ is applied.

f GHz	R_t Ω	$R_{n_{min}}$ Ω	$X_{s_{min}}$ Ω	$R_{n_{max}}$ kΩ	$X_{s_{max}}$ Ω	$\mid Z_c \mid$ Ω	$\angle Z_c$ deg	r Ω
0.1	8.5	8.499	0.84	230299	-7342.08	257.60	179.81	257.60
0.5	8.5	8.473	3.45	118.818	-1326.82	231.43	179.14	231.41
1.0	8.0	7.975	3.00	12.638	-684.30	188.96	179.09	188.94
2.0	8.0	7.842	-6.02	1.309	-382.21	108.51	-176.82	108.35
4.0	20.0	8.791	-32.56	0.233	-445.74	56.22	-144.61	45.83

or outside (3.40). Equivalently, the value of R_n for a known series feedback, for instance $Z_s = 50\ \Omega$, can be checked, as standard textbooks suggest when dealing with stability circles [87].

It is also important to analyse the case $R_{n_o} = N_r / \mid C_t \mid^2$ which makes $D = 0$ in (3.40.d). For this particular value, (3.40) is not valid any longer. The region $R_n = R_{n_o}$ collapses to a straight line:

$$\begin{aligned}
\alpha\, \Re e\,[Z_s] &- \beta\, \Im m\,[Z_s] = \gamma \qquad (3.41)\\
\alpha &= \Re e\,[C_t]\, R_{n_o} - \left(1/2 \mid a \mid^2 + \Re e\,[a\,\rho_o + R_t\, C_t]\right)\\
\beta &= \Im m\,[C_t]\, R_{n_o} - \Im m\,[a\,\rho_o + R_t\, C_t]\\
\gamma &= \frac{R_t - R_{n_o}}{2}
\end{aligned}$$

Notice that straight lines still map circles on the Smith chart because of the bilinear transformation $\Gamma_s = (Z_s - Z_o)/(Z_s + Z_o)$.

At this point it is possible to plot signal circles for constant values of the feedback LNA scattering parameters along with the R_n noise circles on the feedback impedance plane and select the series feedback impedance at the design frequency.

Figure 3.12 shows an example with the AT41486 BJT. The BJT case is straightforward because the value of R_t (the equivalent noise resistance of the transistor) is already close to $R_{n_{min}}$ and the $\mid S_{11} \mid$ circle overlaps the Smith chart. The series feedback position can be chosen on the basis of the R_n and $\mid S_{11} \mid$ circles at the same time.

Figure 3.13 presents a more complex case with the ATF21186 MESFET. In fact, the circle still helps the designer to choose a series feedback that makes $R_n < R_{n_o}$; if $L_s \approx 27$ nH is assumed, then $S_{11} = 0.885 \angle -15.308$ for the feedback amplifier. This procedure seems to fail because the $\mid S_{11} \mid < 0.1$ circle does not overlap the Smith circle area. What the

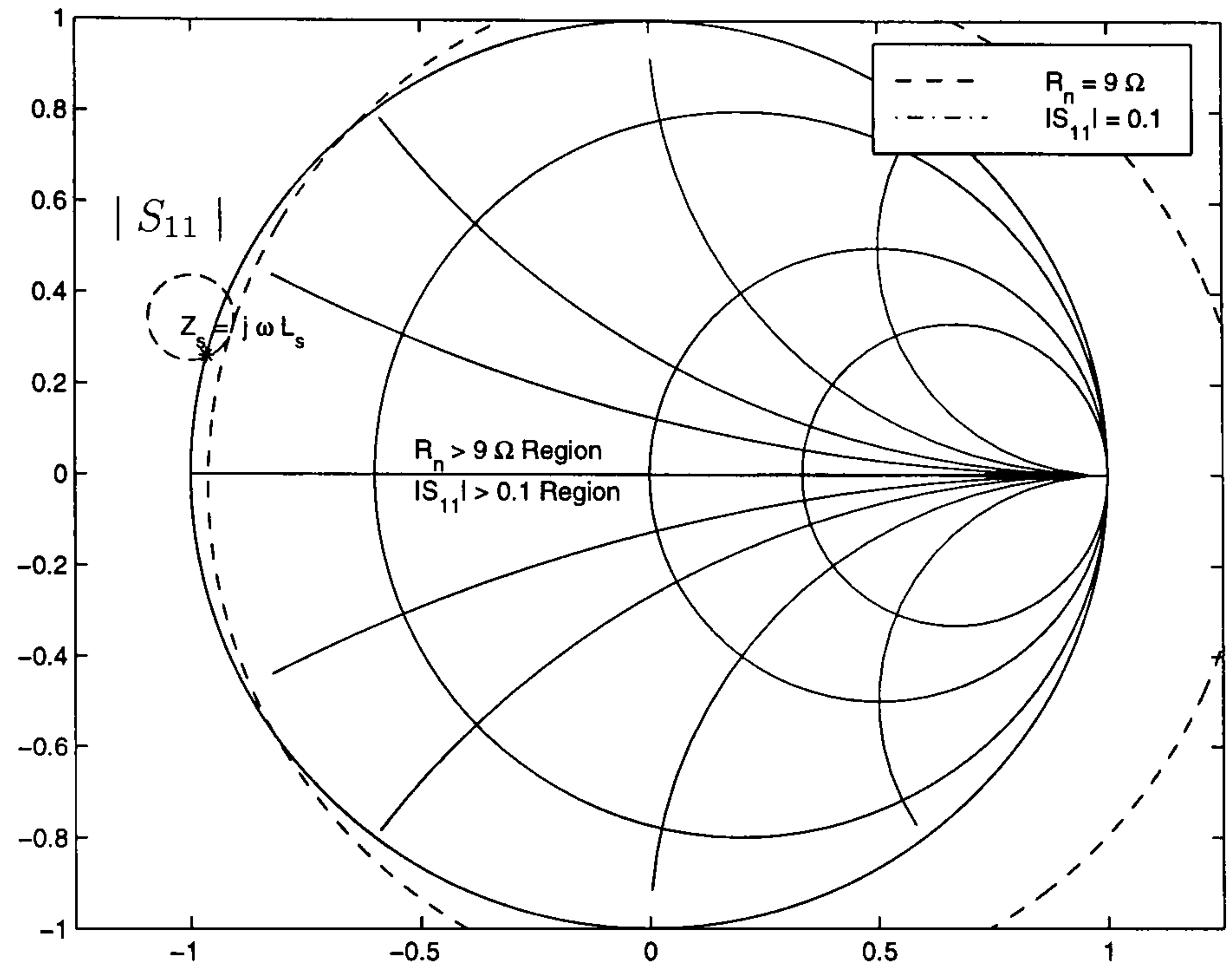

Figure 3.12 Hewlett Packard AT41486 R_n and S_{11} circles on the series feedback element plane Γ_s at 1 GHz ($L_s \approx 1$ nH).

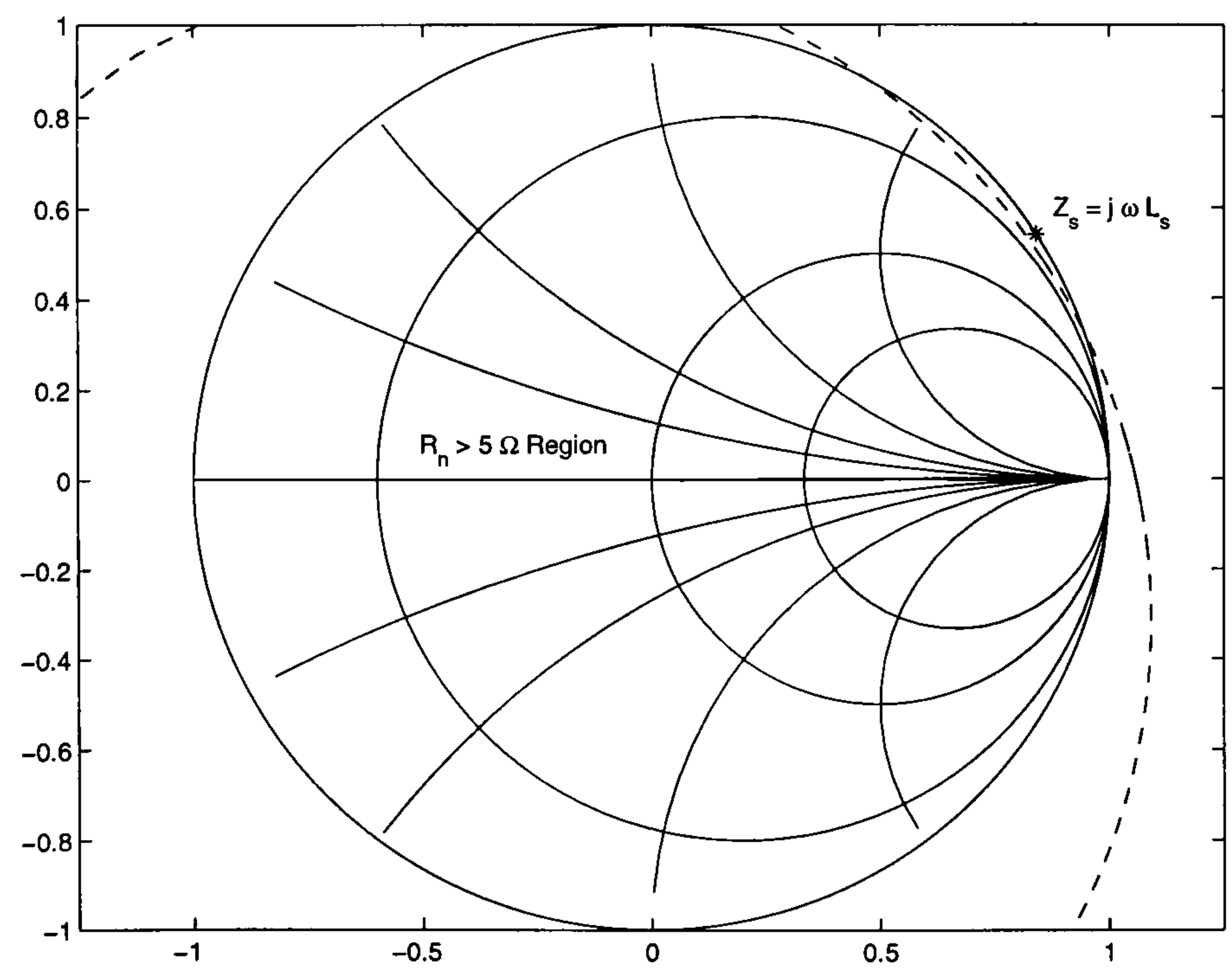

Figure 3.13 Hewlett Packard ATF21186 $R_n < 5\ \Omega$ circle on the series feedback element plane Γ_s at 1 GHz; $L_s = 27$ nH.

designer must remember is that there is still one degree of freedom for his design: the load Γ_L which defines the input reflection coefficient Γ_{in} of the feedback amplifier. The graphic design with R_n circles is useful but it is just another tool for the LNA designer and it should be used skilfully.

3.3.2 Design for Minimum R_n

The R_n analysis can be adapted to outline an analytical design procedure, consisting of three main steps: definition of starting values, simulation and test. A low noise amplifier with an HP ATF21186 MESFET at the centre frequency $f_o = 1$ GHz and ± 35 MHz range has been designed and tested.

The goals outlined in this section are: to highlight some setbacks related to standard design approaches [87]; and to direct the research towards new possible solutions.

Table 3.16 ATF21186 design for $R_{n_{min}}$ at $f_o = 1$ GHz.

L_s	26.952	nH
$\mid S_{11} \mid$	0.885	–
$\angle S_{11}$	-15.310	deg
$\mid S_{12} \mid$	0.246	–
$\angle S_{12}$	84.624	deg
$\mid S_{21} \mid$	0.719	–
$\angle S_{21}$	77.502	deg
$\mid S_{22} \mid$	0.910	–
$\angle S_{22}$	-10.291	deg
F_{min}	0.390	dB
$\mid \Gamma_{S_{opt}} \mid$	0.058	–
$\angle \Gamma_{S_{opt}}$	176.54	deg
R_n	1.182	Ω
$\mid \Gamma_L^{SSNM} \mid$	0.911	–
$\angle \Gamma_L^{SSNM}$	9.164	deg
G_t	4.762	dB

Definition of the starting values

The design is carried out at $X_s = X_{s_{min}}$ for $R_n = R_{n_{min}}$. Once the device signal and noise matrices are given, the numerical value of the feedback reactance is worked out with (3.37). For the ATF21186, the feedback is inductive:

$$L_s = \frac{X_{s_{min}}}{2\,\pi\, f_o},$$

and the final LNA signal and noise parameters are detailed in Table 3.16. There, the reflection coefficient Γ_L^{SSNM} is the load that makes:

$$SSNM = \Gamma_{in}(\Gamma_L) - \Gamma_{S_{opt}}{}^{\star} \qquad (3.42)$$

equal to 0. $SSNM$ stands for simultaneous signal and noise matching; it is a measure of how far apart the signal and noise reflection coefficients are at the input port [106] and hence how far the power match is. As already pointed out by Engberg [51], two degrees of freedom can be associated with the goal $SSNM = 0$ when applying feedback elements at a constant frequency: the feedback immittance affects both $\Gamma_{S_{opt}}$ and scattering parameters S_{ij} of the final network; the input reflection coefficient Γ_{in} depends on S_{ij} as well as on the load Γ_L:

$$\Gamma_{in} = S_{11} + \frac{S_{12}\,S_{21}\,\Gamma_L}{1 - S_{22}\,\Gamma_L} \qquad (3.43)$$

Therefore, the designer can select feedback immittance and Γ_L independently. The load Γ_L^{SSNM} that makes:

$$SSNM = \Gamma_{in}\left(\Gamma_L^{SSNM}\right) - \Gamma_{S_{opt}}{}^{\star} = 0$$

is found with (3.42) and (3.43) to be:

$$\Gamma_L^{SSNM} = \frac{S_{11} - \Gamma_{S_{opt}}{}^{\star}}{(S_{11}\,S_{22} - S_{12}\,S_{21}) - S_{22}\,\Gamma_{S_{opt}}{}^{\star}} \qquad (3.44)$$

Usually, the value determined by (3.44) is unacceptable without any feedback immittance ($\Gamma_L^{SSNM} = 1.52\,\angle - 149.70$ deg for ATF21186 from Table 3.5 and Table 3.6). When the feedback is applied, Γ_L^{SSNM} moves inside the Smith chart area.

Since the load Γ_L^{SSNM} is unlikely to power–match the output port, it is pointless to describe the gain of the LNA in terms of available gain. Table 3.16 shows the value of the transducer power gain (ratio of power delivered to the load to the power available from the source) [87] which takes account of the mismatch at output port. This gain is well–suited for the characterisation of SSNM LNA stages because the SSNM condition ensures the power–match at the input port. In general, even if (3.42) is 0, $\Gamma_{in} = \Gamma_{S_{opt}}{}^{\star} \neq 0$ and therefore an input matching circuit is still required; however, it is typical of SSNM design that when $R_{n_{min}}$ occurs, $\Gamma_{S_{opt}}$ is very small. This point will be resumed for discussion later on.

Simulation

The network of Figure 3.14 has been fabricated on 0.031" Duroid 5880 substrate[5]. Distributed elements are used because they can easily design the required value; commercially available lumped components do not give the designer any control whatsoever. MMIC realization should be the best option in order to realise feedback amplifiers.

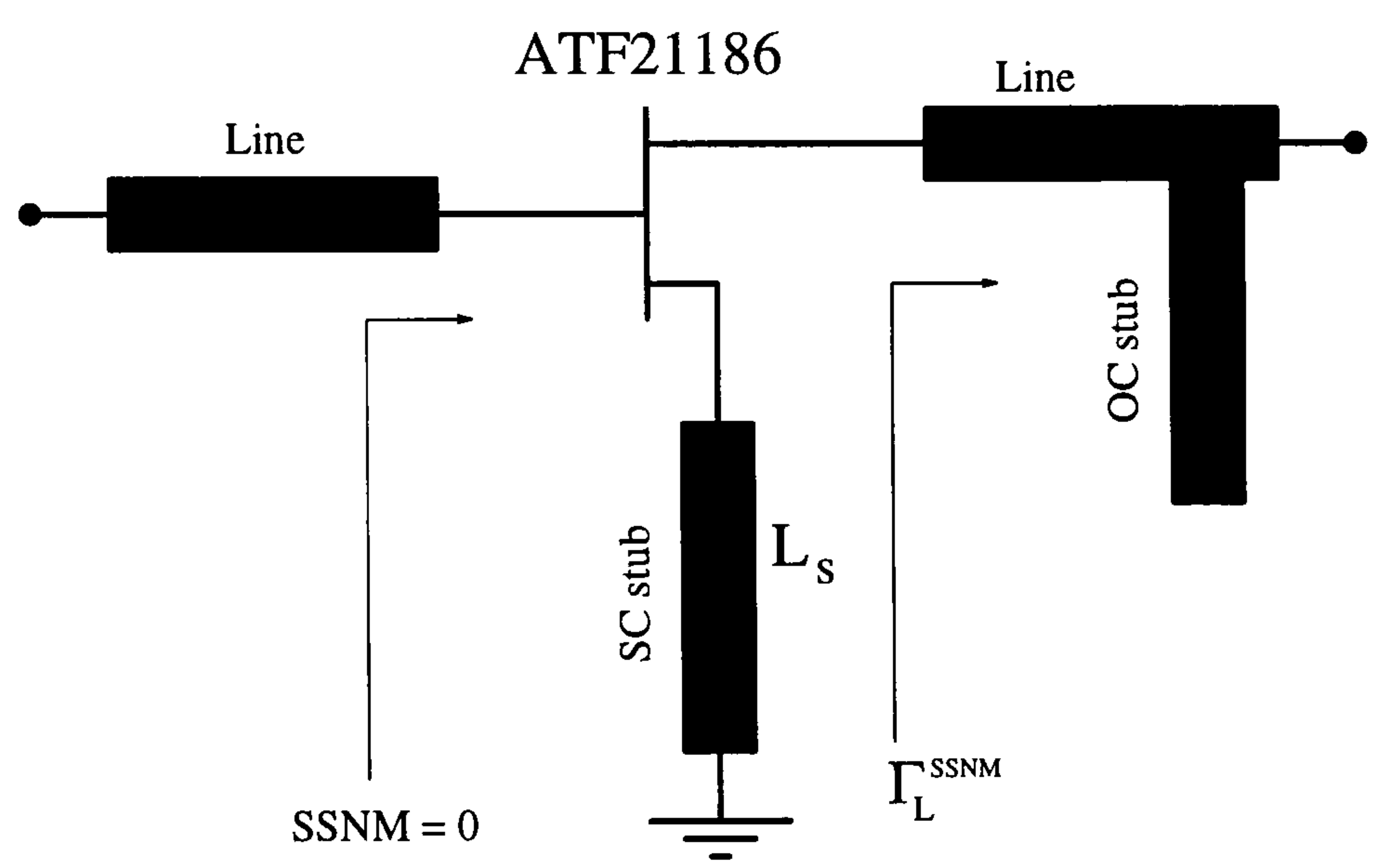

Figure 3.14 ATF21186 feedback LNA network to be used with optimiser. OC stands for Open Circuit, SC for Short Circuit.

There is perfect agreement at the design frequency between the performance predicted by the analysis (3.34) and the one accomplished by the simulator. This is not the case when real lossy lines are simulated. An extensive investigation has been carried out and different realizations of the input and output matching circuits have been looked into. Each available solution for a stub plus transmission line matching circuit has been considered. An impedance transformer ($\lambda/4$ long transmission line) as input matching circuit has been considered as well.

The circuit has been optimised at f_o. The dimensions of every line have been allowed to vary. Constraints have been defined for the optimiser to take into account: minimum realizable line width (0.55 mm); transistor leg and connector launcher width (0.5 mm). Lines of the output matching circuit have equal width. The results of this design study are:

- the optimiser can reach the SSNM condition along with high input return loss at the design frequency;

[5] RT/duroid and Duroid are registered trademarks of Rogers Corporations.

- the largest variation in dimensions occurs in the input matching circuit – as large as +635% of the starting length in one occasion, round about +200% in average;
- the feedback open circuit stub shrinks by about 5% of the starting length;
- the output matching circuit variations are in the region of ±10%;
- when an impedance transformer is used as input matching circuit, width and length decrease by only 60–70%;
- when feed lines[6] between connector and matching circuit have been allowed to vary in length, the optimiser has reduced their lengths dramatically, down to negligible values.

Based on these results, the network of Figure 3.14 with a transformer at the MESFET gate is selected because it showed the smallest variations after optimisation.

Test

The final dimensions are tabulated in Table 3.17. Notice that a short circuit stub is used as series feedback in order to allow the DC current to flow from the source lead to the ground. DC bias is provided by two external biasing T's through the connectors.

Table 3.17 Final dimension for the SSNM LNA design with ATF21186.

feedback short circuit stub	44.224 mm long 0.998 mm wide
output transmission line	57.440 mm long 0.586 mm wide
output open circuit stub	44.169 mm long 0.586 mm wide
input transmission line	18.466 mm long 0.687 mm wide
input/output feed lines	5.000 mm long 2.400 mm wide

A 50 Ω noise figure and $| S_{21} |$ of about 0.56 dB and 5 dB, respectively, are expected at 1 GHz. The simulation ranges from 0.965 to 1.035 GHz, typical bandwidth for mobile communication systems. Tested and simulated scattering parameters at $V_{DS} = 2$ V, $I_{DS} =$ 15 mA are compared in Figure 3.15: the shapes of the scattering parameter magnitude are consistent.

[6]Here, the term *feed line* denotes a short transmission line used to house the launcher of the SMA connector; it acts as a buffer area for the connections to be fabricated without affecting the next component.

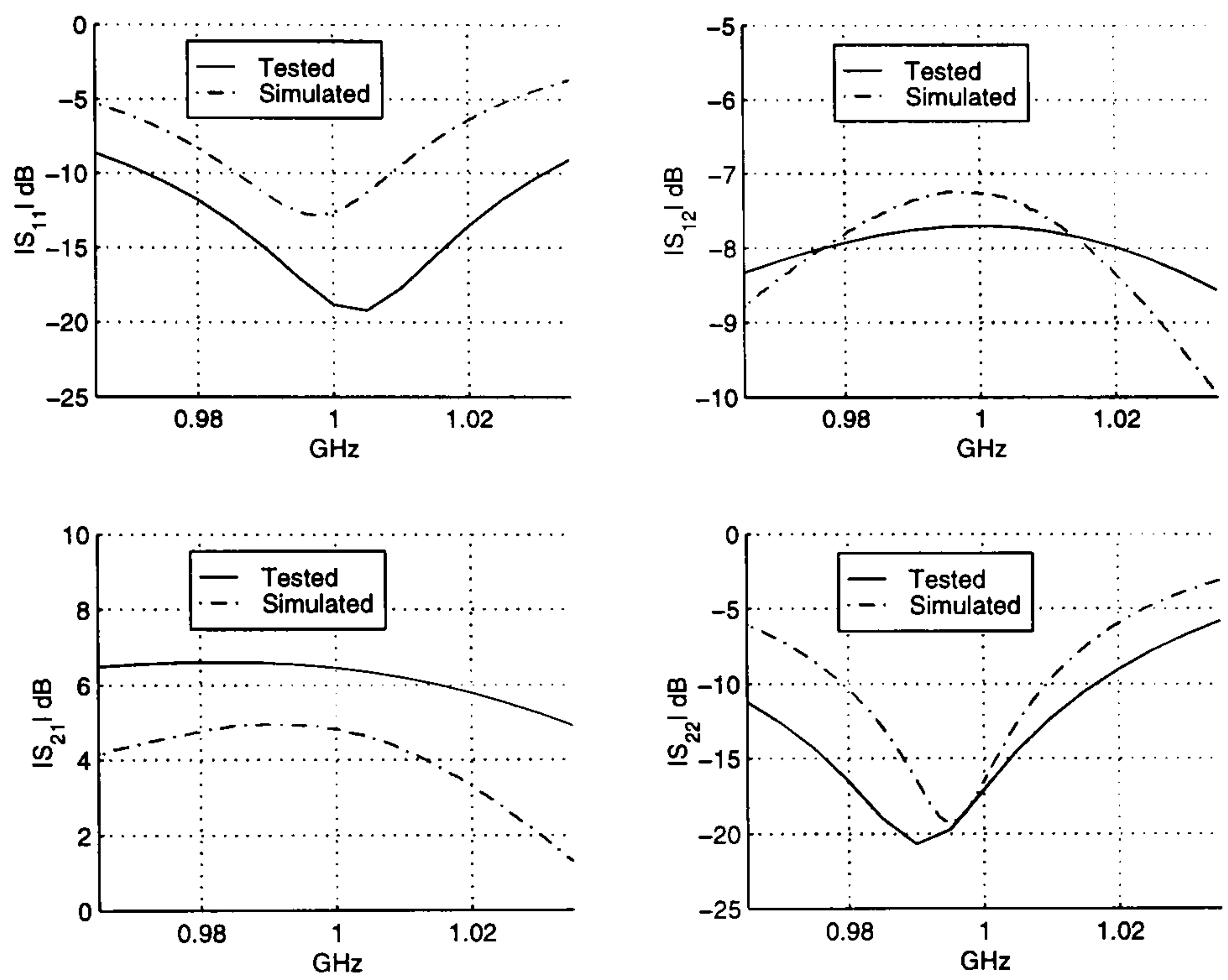

Figure 3.15 Magnitude of the tested scattering parameters for ATF21186 LNA designed at $R_{n_{min}}$.

A noise figure of 0.6 dB was measured with a HP8970A noise figure meter and a HP346 noise source. The noise parameters could not be evaluated [37] because the amplifier is not stable when high reflective loads are connected to its ports (Figure 3.16). On the contrary, in a 50 Ω system, it does not oscillate (Figure 3.17). This can explain why the noise figure can be tested while the noise parameters cannot.

The circuit failed to achieve its main goal, i.e. validation of the R_n analysis. However, some considerations about this failure have contributed to the progress of the research.

The design has been implemented with distributed components. This approach makes the circuit very large at this frequency. Efforts have been made to use lumped components for successive designs in the range around 1 GHz.

The optimisation has highlighted that LNA performance is strongly dependent on the transmission lines, in particular at the input port of the transistor. As long as lossless lines are simulated, a perfect match at the design frequency can be achieved. If the lines are lossy, a solution at the design frequency $f_o = 1$ GHz is found; however, it seems extremely difficult to increase the bandwidth around f_o within the simultaneous match constraint.

What the simulations suggest is that the input matching circuit design is troublesome and it has been a mistake to try to further reduce $| S_{11} | \approx -20$ dB. The reason is that

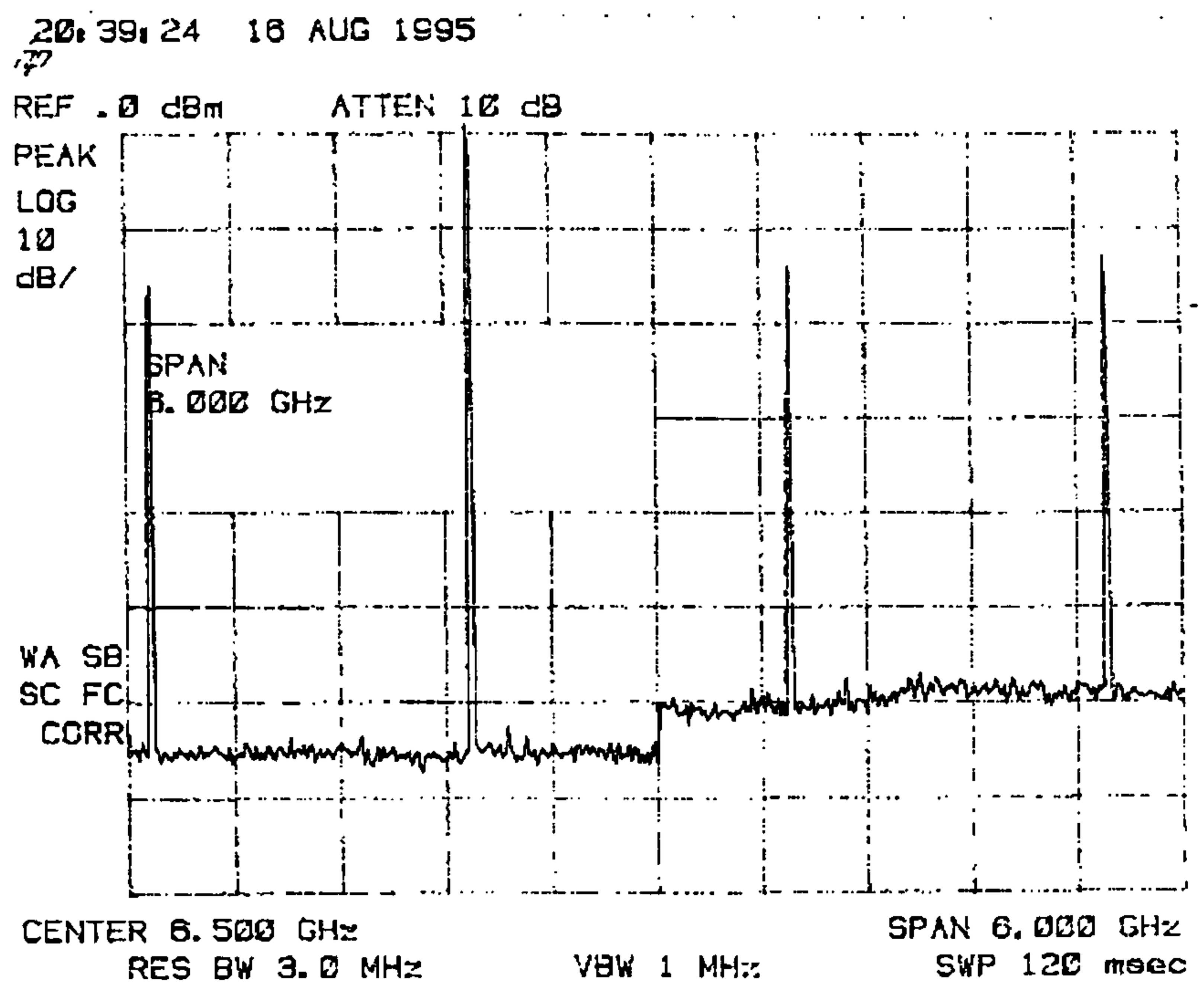

Figure 3.16 Output frequency spectrum for the ATF21186 LNA when the input port is left open (I_{DS} = 28 mA, $V_{GS} = -1.60$ V).

standard design techniques for either noise or signal match [15], [87] deal with the matching problem from a genuine signal point–of–view. For example, minimum noise figure is achieved when the output port of the input matching circuit supplies $\Gamma_{S_{opt}}$. This fails to consider the input matching network as a part of the LNA [30]; section 3.4 will address this point again.

3.3.3 Design for Minimum SSNM

The simultaneous signal and noise match $SSNM$ has been defined in (3.42) as that complex number that quantifies how far apart input reflection coefficient and optimum noise source reflection coefficient are from supplying the simultaneous signal and noise power match at the input port of any linear network. It has also been pointed out that it is a function of both feedback immittances and load Γ_L.

Consider the following simulation for a pure series feedback $Z_s = jX_s$ at f_o GHz:

1. work out signal and noise parameters for the overall series feedback network in terms of scattering parameters and the set F_{min}, R_n and $\Gamma_{S_{opt}}$;

2. noise–match the input port for minimum noise figure, $\Gamma_S = \Gamma_{S_{opt}}$;

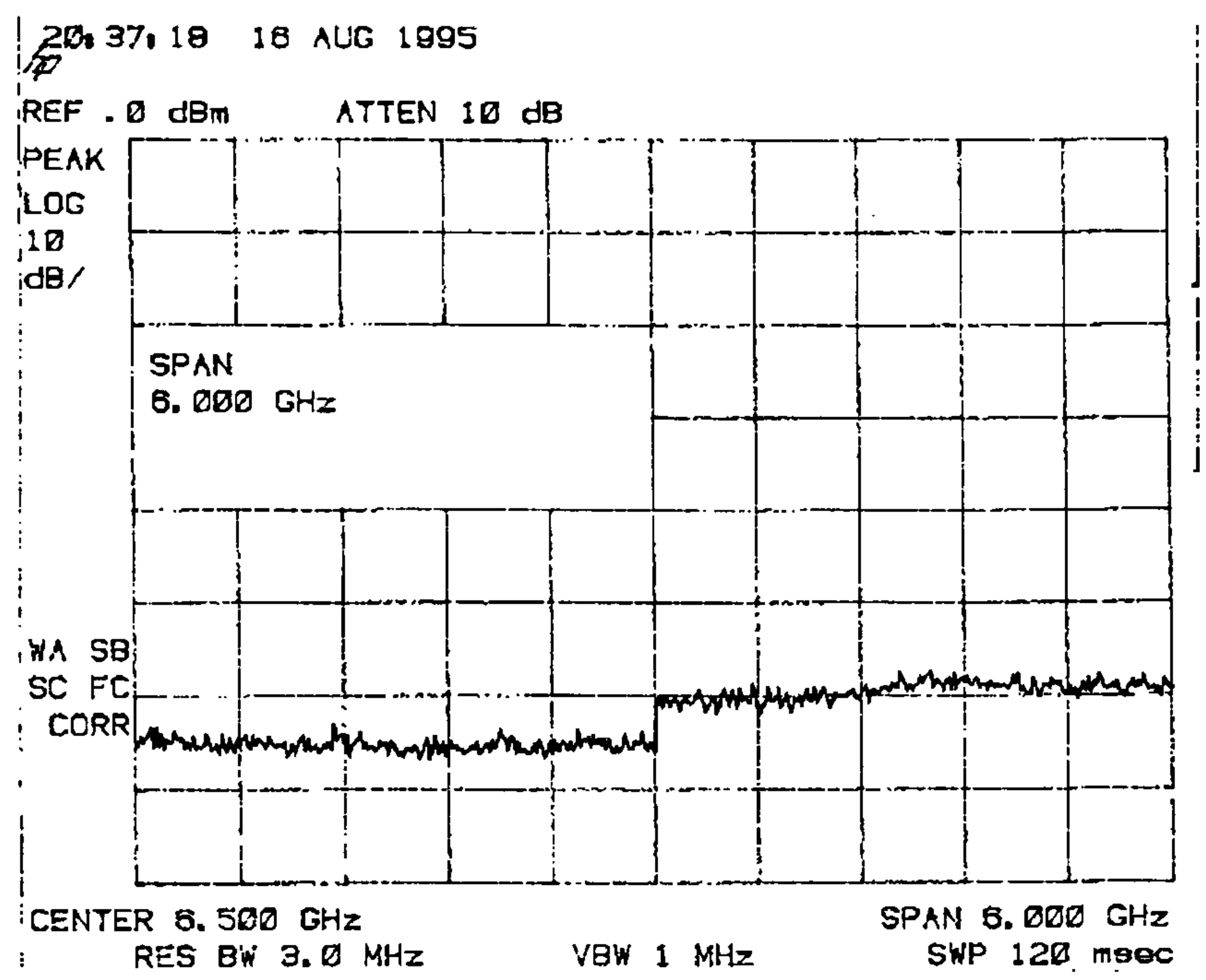

Figure 3.17 Output frequency spectrum for the ATF21186 LNA with 50 Ω at the input port (I_{DS} = 15 mA, V_{GS} = −1.37 V).

3. signal–match the output port for maximum power transfer,

$$\Gamma_L \;=\; \Gamma_{out}^{\star} = \left(S_{22} + \frac{S_{12}\,S_{21}\,\Gamma_{S_{opt}}}{1 - S_{11}\,\Gamma_{S_{opt}}}\right)^{\star} \tag{3.45}$$

4. evaluate $SSNM$.

This procedure can easily be implemented and evaluated for different X_s and/or f_o; input data for the routine to work are signal and noise matrices of the device.

Figures 3.18 and 3.19 show ATF21186 MESFET $SSNM$ vs. X_s at 1 GHz. They demonstrate that:

- feedback reactance can improve the SSNM condition within the given boundary conditions ($\Gamma_S = \Gamma_{S_{opt}}$ and $\Gamma_L = \Gamma_{out}^{\star}$);
- at $X_s = X_{s_{min}}^{SSNM}$, a minimum in $SSNM$ occurs:

$$SSNM_{min} = SSNM\left(X_{s_{min}}^{SSNM}\right),$$

and it can be evaluated numerically for design purposes;

- $0 < X_{s_{min}}^{SSNM} < X_{s_{min}}$ usually, where $R_n\left(X_{s_{min}}\right) = R_{n_{min}}$;

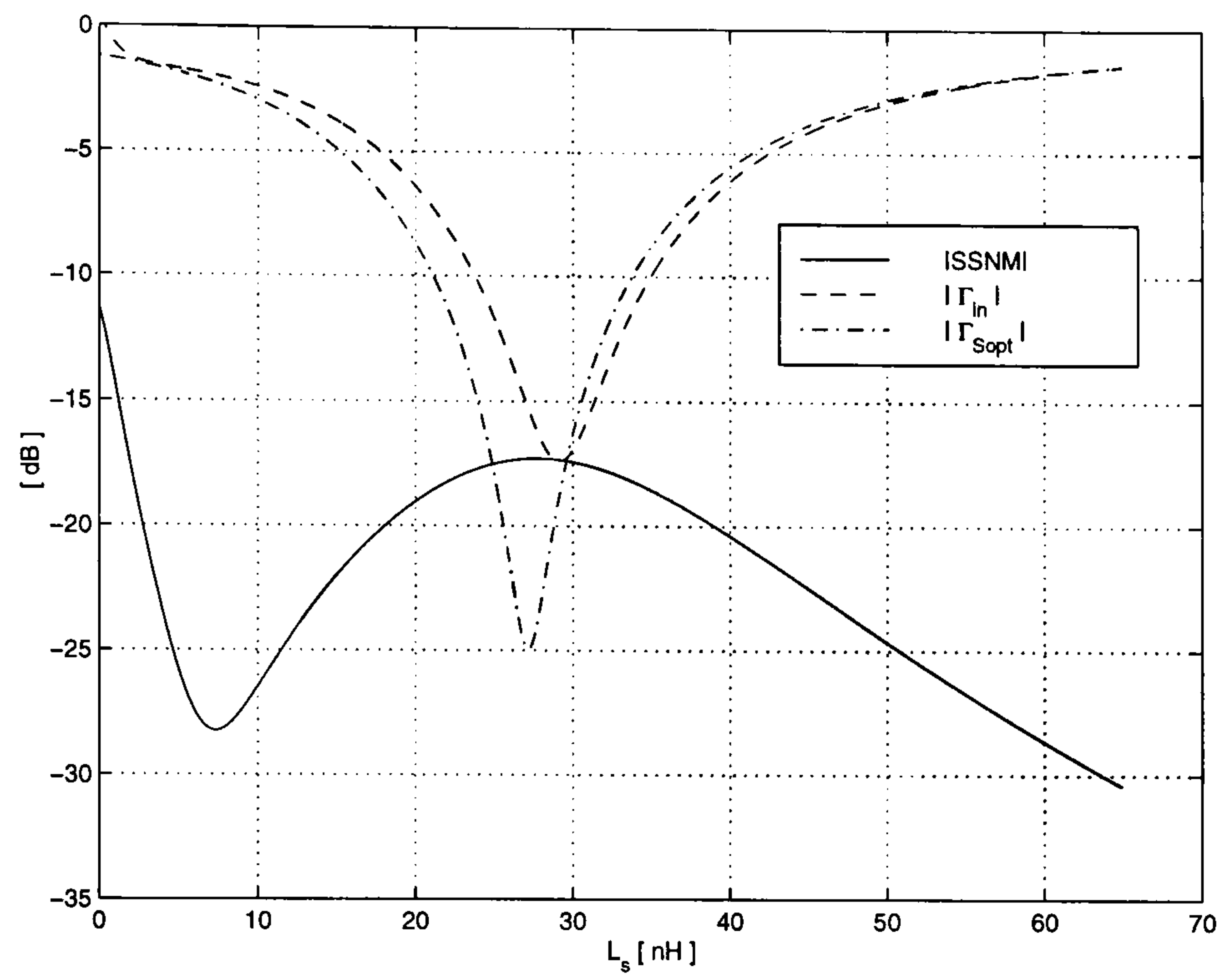

Figure 3.18 Behaviour of $| SSNM |$ vs. a pure series feedback for HP ATF21186 at 1 GHz.

- the input reflection coefficient magnitude of the feedback network is larger than 1 for very small values ($L_s < 0.3$ nH) of X_s.

Notice that the load (3.45) is the one that power–matches the output port of the amplifier and is different from Γ_L^{SSNM} which makes $SSNM = 0$. It is important to specify the boundary conditions when dealing with (3.42).

Figure 3.20 describes the behaviour of HP AT41486 BJT $SSNM$ vs. X_s at four different frequencies. It is clear that the design for $SSNM_{min}$ is not appealing in that case. However, some remarks are worthwhile:

1. for positive reactances ($0 < L_s < 65$ nH), the SSNM decreases without showing any significant minimum; and the gain $| S_{21} |$ decreases as both feedback and frequency increase;

2. negative feedback reactance corresponds to a capacitance

$$C = -\frac{1}{2\pi f_o X_{s_{min}}}$$

and in this region the amplifier is always very unstable;

Results for $X_s < 0$ should be considered carefully because the axis corresponds to very large

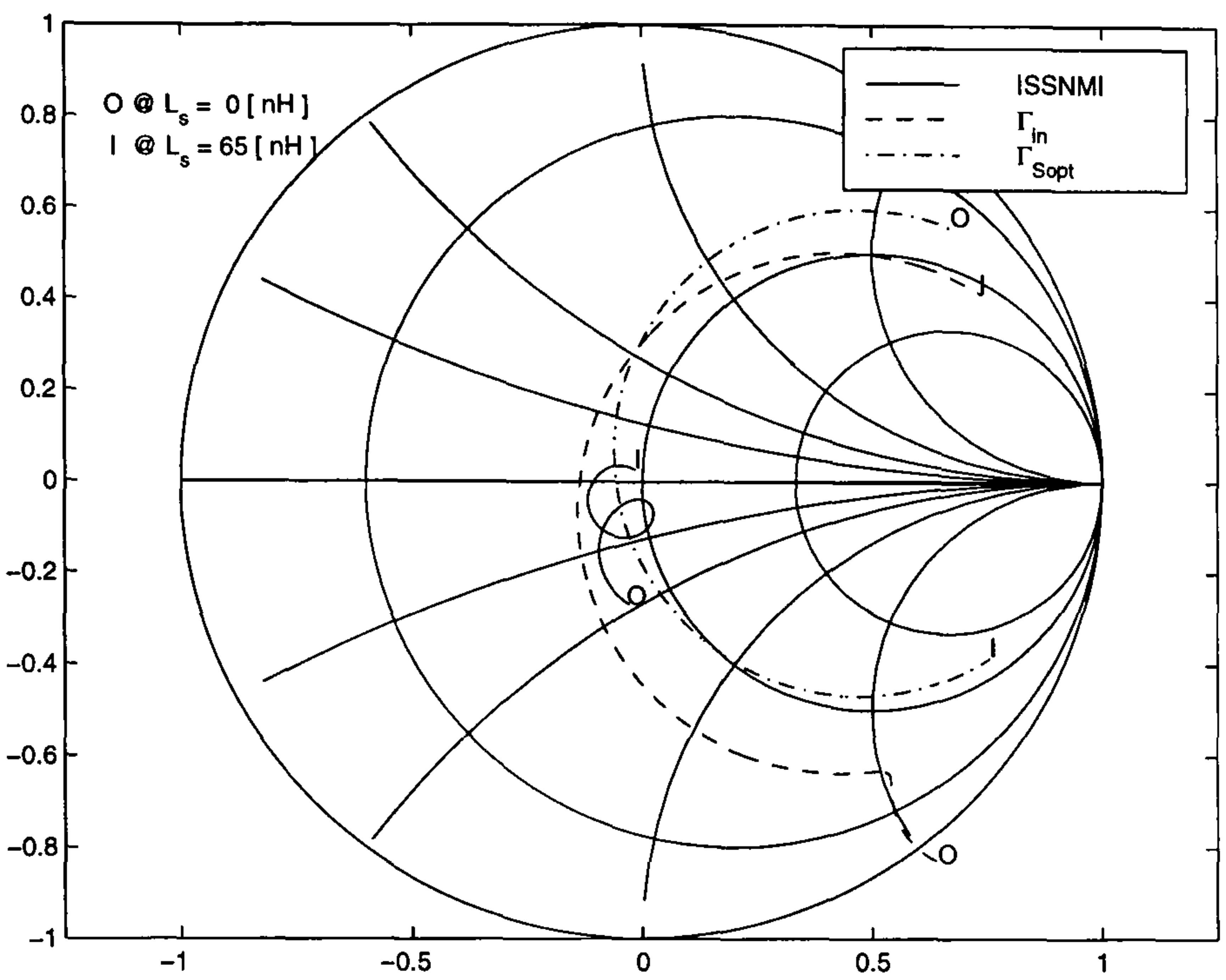

Figure 3.19 *SSNM* vs. a pure series feedback for HP ATF21186 at 1 GHz on the Smith chart plane.

capacitances as $X_s \to 0$ and to small capacitances as $X_s \to -\infty$.

The comparison between MESFET and BJT highlights the differences between their noise behaviours. As discussed earlier on, those devices show similarities as far as their equivalent noise resistance R_t is concerned. However, the frequency at which the BJT reaches the optimum condition $R_{t_{min}}$ without feedback is 1 GHz, while the value for the MESFET is 6 GHz. The required feedback reactance which make R_n decrease to $R_{n_{min}}$ is to be much larger than the one for the BJT. According to the previous results of this study, the MESFET ATF21186 needs the smallest reactive series feedback at 6 GHz, the BJT AT41486 at 1 GHz. Finally, the design for $SSNM_{min}$ is another option for the LNA designer but depends heavily on the selected device.

3.4 Effects of the Input Matching Network on the Noise Performance of the Amplifier

Here, the importance of input matching circuit for low noise applications is discussed by means of a new and straightforward theoretical analysis [123] which points out the weakness of standard noise design [87]; and suggests why very simple matching circuits should be used

Table 3.18 ATF21186 design for $SSNM_{min}$ at $L_s \approx 7.3$ nH and $f_o = 1$ GHz.

L_s	7.333	nH
$\mid S_{11} \mid$	0.696	–
$\angle S_{11}$	-22.630	deg
$\mid S_{12} \mid$	0.202	–
$\angle S_{12}$	92.042	deg
$\mid S_{21} \mid$	1.627	–
$\angle S_{21}$	89.591	deg
$\mid S_{22} \mid$	0.708	–
$\angle S_{22}$	-2.371	deg
F_{min}	0.701	dB
$\mid \Gamma_{S_{opt}} \mid$	0.769	–
$\angle \Gamma_{S_{opt}}$	50.860	deg
R_n	15.600	Ω
$\mid \Gamma_L \mid$	0.7656	–
$\angle \Gamma_L$	36.124	deg
$\mid \Gamma_{in} \mid$	0.798	–
$\angle \Gamma_{in}$	-52.836	deg
$\mid SSNM_{min} \mid$	0.040	–
$\angle SSNM_{min}$	-94.631	deg

for low noise amplifiers [75].

Figure 3.21 shows an input matching network followed by an active stage; the exact behaviour of the noise parameters can be predicted by means of matrix algebra [30]. Standard minimum noise figure design requires an input matching circuit in order to achieve $\Gamma^I_{out} = \Gamma^A_{S_{opt}}$. However, a comprehensive approach for low noise applications should also take into account:

1. the source mismatch at the matching circuit input port; and

2. the fact that the source is unlikely to correspond to the optimum source for minimum noise figure of the cascaded network.

When considering the design of matching circuits from a noise point–of–view, it should be remembered that the input network is going to be part of the final LNA; its contribution must allow for both noise and signal parameters and LNA designers should look into the cascade of input matching circuit and active device. This seems to make computer optimisation indispensable. A deeper understanding about how the input matching circuit affects the following LNA is worthwhile.

In order to keep the problem simple, the noise contribution of the output stage which

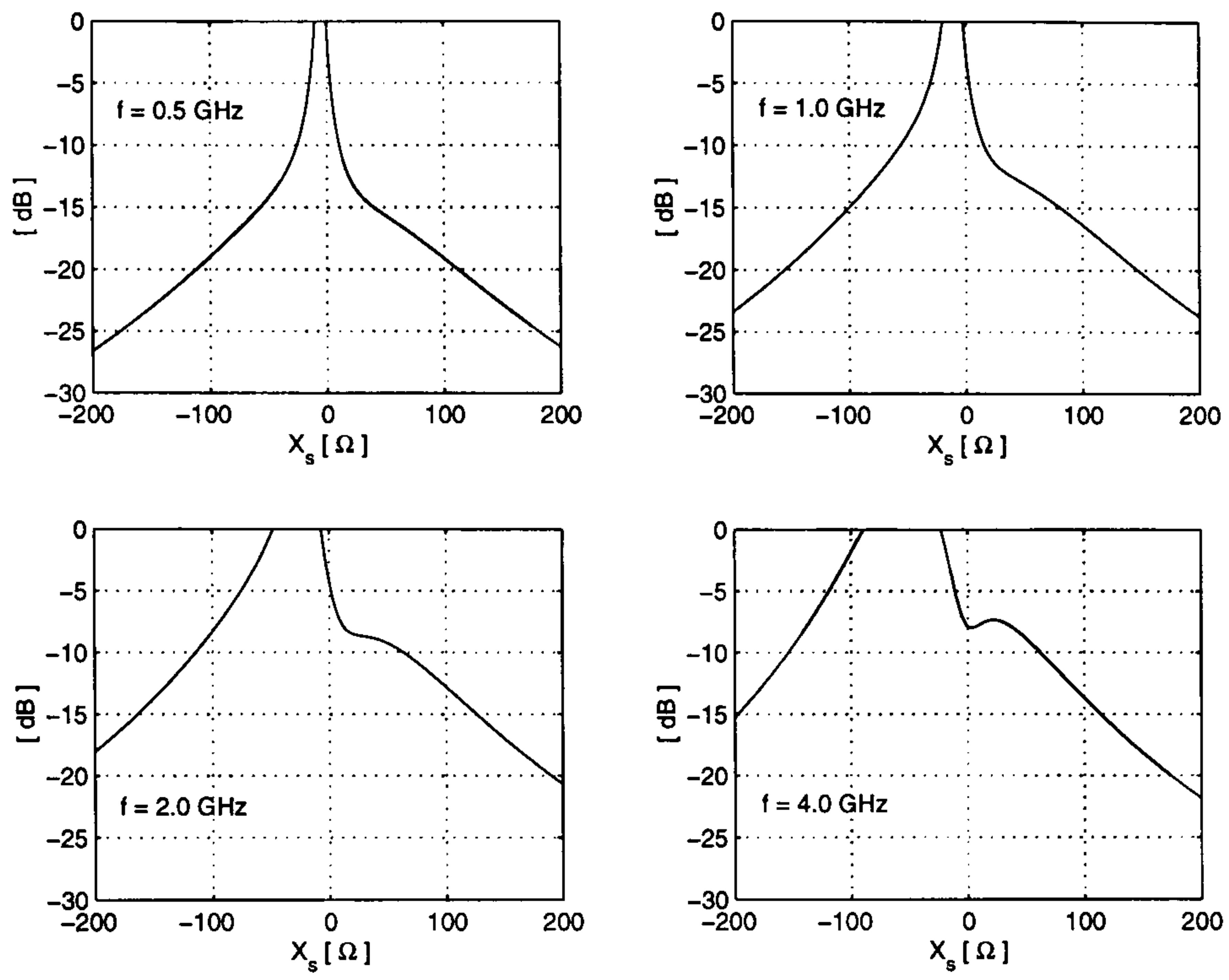

Figure 3.20 *SSNM* behaviour for HP AT41486 BJT.

supplies Γ_L is ignored on the basis that the gain of the active device is large enough to make its noise contribution negligible [19].

The superscripts:

- I for quantities related to the input matching circuit;
- A for the feedback (active) network; and
- IA for the cascade of the input matching circuit and the active stage,

are defined. A transmission representation describes the 2–port network under investigation:

$$\mathbf{C}^{IA} = \begin{bmatrix} R_n^{IA} & \widetilde{\rho_n^{IA}}^{\star} \\ \widetilde{\rho_n^{IA}} & g_n^{IA} \end{bmatrix} = \mathbf{C}^I + \mathbf{T}^I\,\mathbf{C}^A\,\mathbf{T}^{I+} \tag{3.46}$$

$$\mathbf{T}^{IA} = \begin{bmatrix} A^{IA} & B^{IA} \\ C^{IA} & D^{IA} \end{bmatrix} = \mathbf{T}^I\mathbf{T}^A \tag{3.47}$$

The active device in Figure 3.21 has a series feedback which guarantees $SSNM^A = 0$ when the output is loaded by Γ_L^{SSNM}. Therefore, stage A is such that:

$$\Gamma_{in}^A = \Gamma_{S_{opt}}^{A}{}^{\star} \tag{3.48}$$

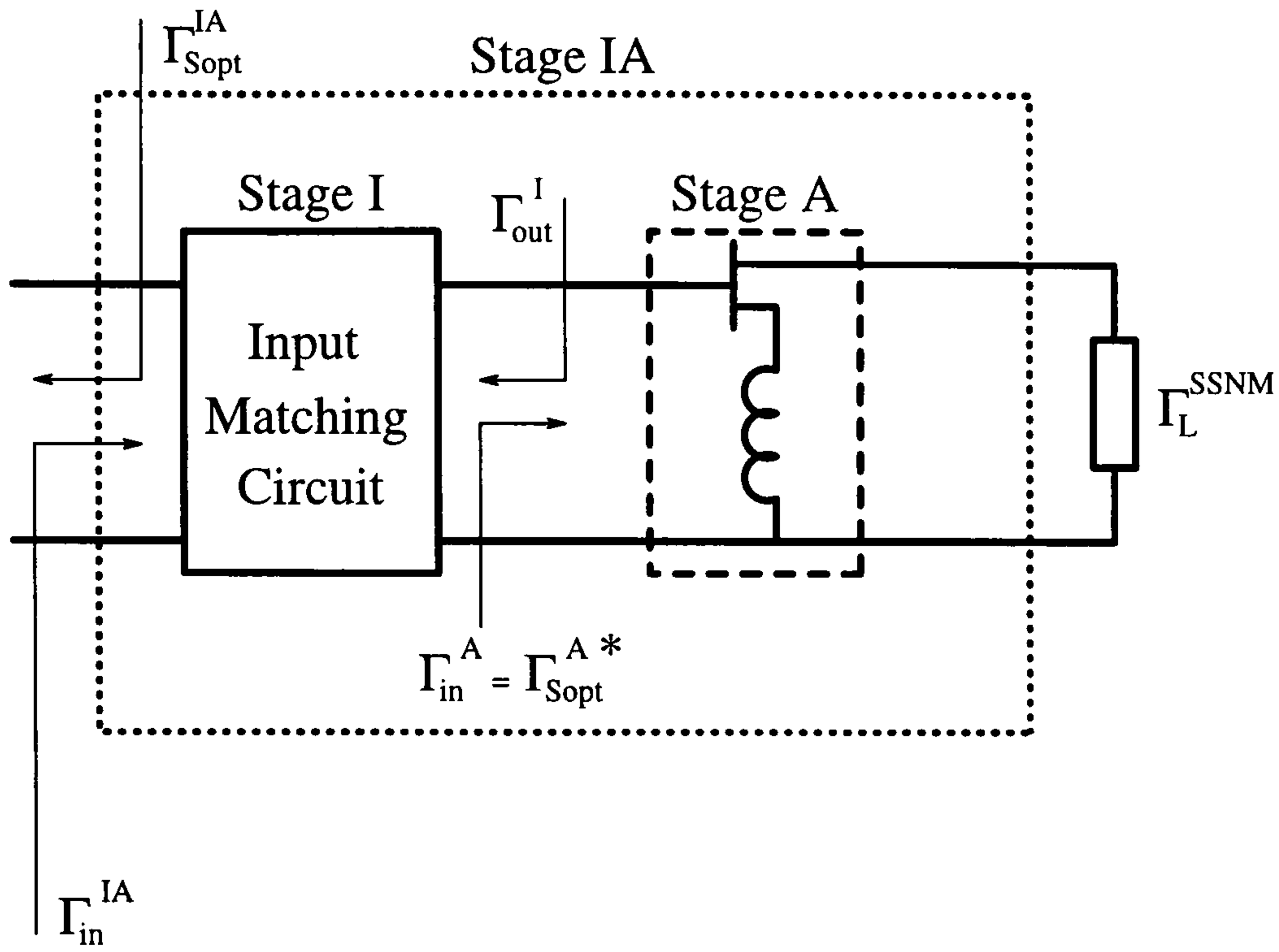

Figure 3.21 Requirements for designing an input matching circuit for simultaneous signal and noise match.

and it is assumed that $|\Gamma^A_{in}| = |\Gamma^A_{S_{opt}}|$ is large (for example 0.5): an input matching circuit is required. A unique and original method to achieve (3.48) and a reason why Γ_{in} and $\Gamma_{S_{opt}}$ magnitudes may be large, is presented in chapter 5.

The input matching system within SSNM constraint must satisfy 3 goals:

$$\Gamma^{IA}_{S_{opt}} = 0 \tag{3.49.a}$$

$$\Gamma^{IA}_{in} = 0 \tag{3.49.b}$$

$$\Gamma^{I}_{out} = \Gamma^{A\ *}_{S_{opt}} \tag{3.49.c}$$

Each reflection coefficient (3.49) is normalised to Z_o; the same value is associated with the source impedance and is assumed to be real. In case of complex Z_o, the same reasoning can be restated in terms of power waves [32].

System (3.49) must be satisfied at the design frequency f_o. Its physical interpretation is:

(3.49.a) ensures that the minimum noise figure F^{IA}_{min} of the cascaded network is achieved;

(3.49.b) causes the available signal power to be delivered by the source to the network;

(3.49.c) imposes that the noise figure of the second stage is equal to its minimum value; (3.48) guarantees that maximum power transfer between stages is achieved at the same time.

The following facts are noteworthy:

- (3.49.a) and (3.49.b) are equivalent to impose the SSNM condition on the overall network with the further requirement that both reflection coefficients are zero:

$$\begin{aligned} SSNM^{IA} &= \Gamma_{in}^{IA} - \Gamma_{S_{opt}}^{IA\;\star} = 0 \\ \Gamma_{in}^{IA} &= 0 \end{aligned}$$

- (3.48) is indispensable for (3.49.c) because a 2–step design procedure is assumed: first, the design of the active device is carried out; then, the input matching circuit is added to it. Different results may be expected if simultaneous design of active device and input matching circuit is carried out – for instance, by varying the series feedback element in Figure 3.21;

- there is no assumption in (3.49) on the nature of the input matching circuit – passive or active, distributed or lumped.

The complex system (3.49) has been expanded in [123] with the substitution of terms obtained from (3.46) and (3.47). The resulting system is:

$$\begin{aligned}
0 &= Z_o\left(g_n^I + R_n^A \mid C^I \mid^2 + 2\Re e\left[\widetilde{\rho_n^A} C^{I\star} D^I\right] + g_n^A \mid D^I \mid^2\right) \\
&\quad - Y_o\left(R_n^I + R_n^A \mid A^I \mid^2 + 2\Re e\left[\widetilde{\rho_n^A} A^{I\star} B^I\right] + g_n^A \mid B^I \mid^2\right) && (3.50.a) \\
0 &= \Im m\left[\widetilde{\rho_n^I} + R_n^A A^{I\star} C^I + \widetilde{\rho_n^A}^{\star} B^{I\star} C^I + \widetilde{\rho_n^A} A^{I\star} D^I + g_n^A B^{I\star} D^I\right] && (3.50.b) \\
0 &= \left[1 + \left(\Gamma_{S_{opt}}^A\right)^\star\right] A^I + \left[1 - \left(\Gamma_{S_{opt}}^A\right)^\star\right] (B^I Y_o) \\
&\quad - \left[1 + \left(\Gamma_{S_{opt}}^A\right)^\star\right] (C^I Z_o) - \left[1 - \left(\Gamma_{S_{opt}}^A\right)^\star\right] D^I && (3.50.c) \\
0 &= \left[1 + \Gamma_{S_{opt}}^A\right] A^I - \left[1 - \Gamma_{S_{opt}}^A\right] (B^I Y_o) \\
&\quad + \left[1 + \Gamma_{S_{opt}}^A\right] (C^I Z_o) - \left[1 - \Gamma_{S_{opt}}^A\right] D^I && (3.50.d)
\end{aligned}$$

There are seven unknowns in (3.50) with the superscript I related to the input matching circuit to be designed: four signal and three noise parameters. They are not independent of one another, as clarified by the following examples:

1. the noise parameters of any passive 2–port network can be expressed as functions of its signal parameters [30], [123];

2. suppose the input matching circuit is made of N distributed elements such as stubs and transmission lines on the same substrate: their lengths and widths set both signal and noise behaviour of the stage. Therefore, seven unknowns depend on $2 \times N$ physical dimensions;

3. if the input matching circuit is made of lumped RLC components and the topology of the network is known, analytical expressions for signal and noise parameters can be worked out.

Hence, (3.50) requires the knowledge of the dependence of the unknowns on either the physical parameters or the components of the input matching circuit: this is an area of research worth being further investigated. As a consequence, the noise parameters can be expressed as functions of the complex transmission matrix elements A^I, B^I, C^I and D^I, chosen to be the set of independent unknowns in (3.50) or, equivalently, in (3.49). In fact, 3 complex equations[7] form (3.49); therefore, the system can be solved by any network with $7 - 3 = 4$ independent parameters at least. The network must be non–reciprocal, because reciprocity imposes a fourth condition. In transmission matrix representation:

$$\Delta_{\mathbf{T}^I} = \mid \mathbf{T}^I \mid = A^I \, D^I - B^I \, C^I = 1$$

A reciprocal network must provide 4 complex degrees of freedom z_i, $i = 1, \ldots, 4$ for its $\mathbf{T}^I$ matrix:

$$\begin{aligned} A^I &= A^I \, (z_1; z_2; z_3; z_4) \\ B^I &= B^I \, (z_1; z_2; z_3; z_4) \\ C^I &= C^I \, (z_1; z_2; z_3; z_4) \\ D^I &= D^I \, (z_1; z_2; z_3; z_4) \end{aligned}$$

The fundamental conclusions of this analysis are:

1. a standard distributed stub plus transmission line of an input matching circuit for noise application has, at the most, four real unknowns to be set (length and width of each distributed component), once the substrate is chosen. There are not enough unknowns for solving (3.50);

[7] (3.50.a) and (3.50.b) are real and imaginary part of (3.49.a).

2. if the matrix $\mathbf{T}^I$ is to have complex elements for solving (3.50), then the input matching network must be lossy. A lossless network transmission matrix $\mathbf{T}^I$ has either real or imaginary elements and cannot provide for SSNM 2–step design requirements;

3. the solution of (3.50) guarantees $SSNM^{IA} = 0$ and $\Gamma^{IA}_{S_{opt}} = 0$. However, F^{IA}_{min} is likely to increase if the matching circuit is bound to be made of lossy components.

Two options can be pursued by the designer at this point: considering non–reciprocal input matching networks, such as active input stages, or eliminating the input matching circuit itself. Since the design without input matching networks has never been formalised, this option will be investigated in chapter 5. In that case,

$$\mathbf{C}^{IA} = \mathbf{C}^{A}$$

and every effort focuses on designing the active stage.

3.5 Conclusion

An analysis of a 2–port network with both series and parallel feedback elements has been developed. Plain expressions for the noise parameters have been obtained and discussed extensively. Their application to the design of low noise amplifiers has been examined in detail and a critical approach to input matching circuits has been considered as a basis for further developments.

Chapter 4

Microwave Feedback Amplifiers Analysis with an Input Series Inductor

The influence on the noise parameters of an inductor connected at the input port of an active device is investigated. The goal is to improve the understanding of parasitic inductances. The findings of chapter 3 are taken into account. Examples with MESFETs and HEMTs are presented and a noise model for intrinsic MESFETs is examined and its validity extended to extrinsic and packaged devices.

The importance of inductors in modelling MESFETs and HEMTs is highlighted. Design guidelines are pointed out throughout this chapter.

4.1 Input inductor analysis

Signal and noise analysis of an ideal inductor L_g connected at the input port of a linear 2–port device is carried out at the given angular frequency $\omega = 2\pi f_o$; the circuit under investigation is shown in Figure 4.1. The analysis can easily be extended to any kind of input reactance by substituting $X_g = \omega L_g$.

A transmission representation [30] is used for each stage in Figure 4.1. Subscripts g, n and n_{tot} refer to the input inductor L_g, the (active) network and the overall circuit, respectively. Every block of Figure 4.1 is linear; in particular, the second stage may consist of either one device or a feedback amplifier.

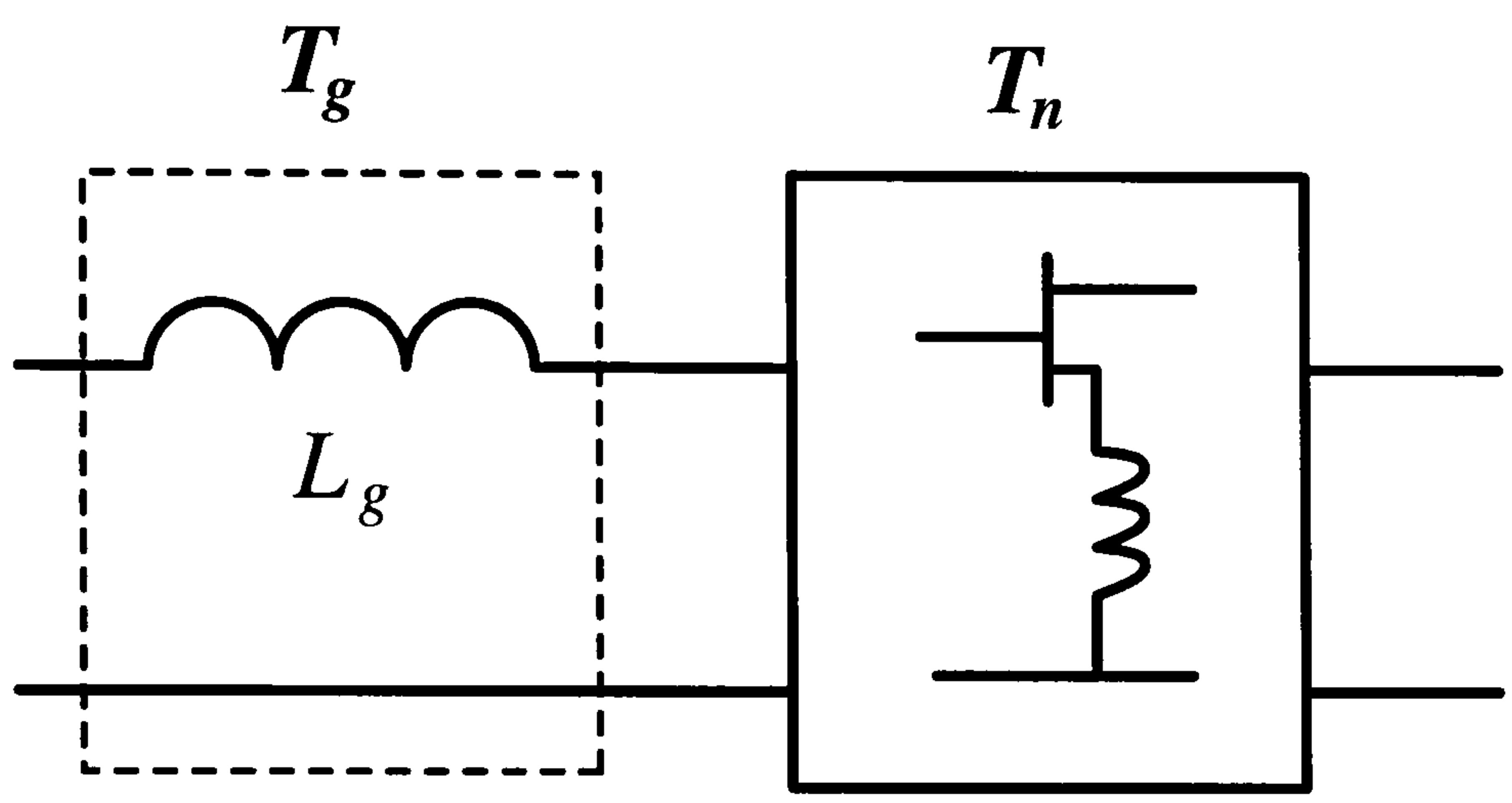

Figure 4.1 Cascade of lossless inductance and 2–port network (amplifier).

Signal Analysis

Define the transmission matrices $\mathbf{T}_g$ for the input inductor stage, $\mathbf{T}_n$ for the second stage and $\mathbf{T}_{n_{tot}}$ for the overall network as:

$$\mathbf{T}_g = \begin{bmatrix} 1 & j\,\omega\,L_g \\ 0 & 1 \end{bmatrix} \tag{4.1}$$

$$\mathbf{T}_n = \begin{bmatrix} A_n & B_n \\ C_n & D_n \end{bmatrix} \tag{4.2}$$

$$\mathbf{T}_{n_{tot}} = \mathbf{T}_g\,\mathbf{T}_n = \begin{bmatrix} A + j\,\omega\,L_g\,C_n & B + j\,\omega\,L_g\,D_n \\ C_n & D_n \end{bmatrix} \tag{4.3}$$

Transform (4.3) into scattering representation – with Table 3.2 for instance:

$$\mathbf{S}_{n_{tot}} = \frac{1}{\Delta_d} \begin{bmatrix} S_{n_{11}} & 2\,(A_n\,D_n - B_n\,C_n) \\ 2 & S_{n_{22}} \end{bmatrix} \tag{4.4}$$

where:

$$S_{n_{11}} = A_n + B_n/Z_o - C_n\,Z_o - D_n + j\,\omega\,L_g\,(C_n + D_n/Z_o)$$

$$S_{n_{22}} = -A_n + B_n/Z_o - C_n\,Z_o + D_n - j\,\omega\,L_g\,(C_n - D_n/Z_o)$$

$$\Delta_d = A_n + B_n/Z_o + C_n\,Z_o + D_n + j\,\omega\,L_g\,(C_n + D_n/Z_o)$$

and Z_o is the characteristic impedance.

The determinant of $\mathbf{T}_{n_{tot}}$ is:

$$\mid \mathbf{T}_{n_{tot}} \mid \; = \; \mid \mathbf{T}_g \mid \cdot \mid \mathbf{T}_n \mid \; = \; \mid \mathbf{T}_n \mid$$

and is equal to the determinant of the transmission matrix $\mathbf{T}_n$ of the second stage since $\mid \mathbf{T}_g \mid \; = \; 1$.

Noise Analysis

By making use of correlation matrices for transmission representation, the overall network noise parameters are:

$$\mathbf{C}_{tot} = \begin{bmatrix} R_{n_{tot}} & \widetilde{\rho_{n_{tot}}}^{\star} \\ \widetilde{\rho_{n_{tot}}} & g_{n_{tot}} \end{bmatrix} \; = \; \mathbf{T}_g \, \mathbf{C}_n \, \mathbf{T}_g{}^{+} \tag{4.5}$$

where $^{+}$ represents the Hermitian conjugate operation, (4.1) defines $\mathbf{T}_g$ and:

$$\mathbf{C}_n \; = \; \begin{bmatrix} R_n & \rho_{n_o}{}^{\star} \\ \rho_{n_o} & g_n \end{bmatrix} \tag{4.6.a}$$

$$\rho_n \; = \; \frac{\rho_{n_o}}{\sqrt{g_n \, R_n}} \tag{4.6.b}$$

(4.6.b) is the correlation coefficient between R_n and g_n. No correlation matrix is associated with L_g in (4.5) since the component is lossless and ideal.

The expansion of (4.5) determines the noise parameters of the overall network:

$$R_{n_{tot}} \; = \; R_n + \omega^2 \, L_g^2 \, g_n + 2 \, \omega \, L_g \, \Re e \left[j \, \rho_{n_o} \right] \tag{4.7}$$

$$g_{n_{tot}} \; = \; g_n \tag{4.8}$$

$$\widetilde{\rho_{n_{tot}}} \; = \; \rho_{n_o} - j \, \omega \, L_g \, g_n \tag{4.9}$$

The correlation coefficient is $\rho_{n_{tot}} = \widetilde{\rho_{n_{tot}}} / \sqrt{R_{n_{tot}} \, g_{n_{tot}}}$. The optimum noise source impedance $Z_{S_{opt}}$ can be expressed as [35]:

$$Z_{S_{opt}} \; = \; \frac{\sqrt{R_{n_{tot}} \, g_{n_{tot}} - \Im m \left[\widetilde{\rho_{n_{tot}}} \right]^2} + j \, \Im m \left[\widetilde{\rho_{n_{tot}}} \right]}{g_{n_{tot}}}$$

and tailored to this investigation by making use of (4.7), (4.8) and (4.9):

$$\Re e \left[Z_{S_{opt}} \right]^2 \; = \; \frac{R_n \, g_n - \Im m \left[\rho_{n_o} \right]^2}{g_n^2} \tag{4.10.a}$$

$$\Im m\left[Z_{S_{opt}}\right] = \frac{\Im m\left[\rho_{n_o}\right] - \omega\, L_g\, g_n}{g_n} \qquad (4.10.b)$$

The set (4.10) demonstrates that L_g affects the imaginary part of $Z_{S_{opt}}$ only; and that $\Re e\left[Z_{S_{opt}}\right]$ of the final network is independent of L_g and equal to the real part of the optimum noise source impedance of the stage after the inductor.

4.1.1 Discussion of the analysis

The impact of an input inductance on the noise parameters of the final network is described by (4.7), (4.8), (4.9) and (4.10). A non–linear dependence of the noise resistance $R_{n_{tot}}$ on L_g is shown; (4.9) is proportional to the imaginary part of the optimum noise impedance (4.10.b): for any 2–port network, an ideal input inductance decreases $\widetilde{\rho_{n_{tot}}}$ at the given frequency and allows the optimum noise source impedance for minimum noise figure to be a real number either for a given value of L_g at f_o or for a given frequency f_o if L_g is known.

Either (4.9) or (4.10.b) suggest how to design the value of the input inductor for simultaneous match purposes, independently of what the active stage contains. Consider again the HP ATF21186 MESFET at $f_o = 1$ GHz (Table 3.5, chapter 3) and transform its noise parameters to the set R_n, g_n and ρ_n:

$$\begin{aligned} R_n &= 24.500\ \Omega \\ g_n &= 1.345\ \text{mS} \\ \rho_n &= 0.160 + j\,0.977 \end{aligned}$$

Assume that the goal is to have a real optimum source noise reflection coefficient $\Gamma_{S_{opt}}$ and therefore the imaginary part of $\widetilde{\rho_{n_{tot}}}$ is to be cancelled out by an input inductance L_g: (4.9) sets the required value to:

$$L_g = \frac{\Im m\left[\rho_n \sqrt{R_n\, g_n}\right]}{2\,\pi\, f_o\, g_n} = \frac{1}{2\,\pi\, f_o}\,\Im m\left[\rho_n \sqrt{\frac{R_n}{g_n}}\right] = \frac{1}{2\,\pi\, f_o}\,\Im m\left[Z_c\right] \qquad (4.11)$$

The correlation impedance Z_c [18] is defined as the impedance which makes the equivalent noise resistance R_n and conductance g_n uncorrelated.

For the HP ATF21186, $L_g \approx 21$ nH is obtained. After back–substituting the value of L_g into (4.7), (4.8) and (4.9) and converting the noise parameters to the set R_n, F_{min} and $\Gamma_{S_{opt}}$,

$$R_n = 1.105\ \Omega$$
$$F_{min} = 0.55 \text{ dB}$$
$$\Gamma_{S_{opt}} = -0.271$$

are found. The signal performance at f_o with $L_g \approx 21$ nH is

$$\begin{aligned} S_{11} &= 0.845 \quad \angle\, 92.058 \quad \text{deg} \\ S_{12} &= 0.126 \quad \angle - 40.797 \quad \text{deg} \\ S_{21} &= 4.664 \quad \angle\, 38.203 \quad \text{deg} \\ S_{22} &= 0.522 \quad \angle - 142.781 \quad \text{deg} \end{aligned}$$

which corresponds to an available gain of 14.8 dB when the source is 50 Ω or an associated gain of 15.1 dB. The required loads Γ_L at the output port are respectively $\Gamma_L = S_{22}^*$ and $\Gamma_L = 0.629 \angle - 154.168$ deg. The value $\Gamma_{S_{opt}} = -0.271$ corresponds to 28.67 Ω and is equal to $\Re e\left[Z_{S_{opt}}\right]$ of the device.

Table 4.1 Comparison between $R_{n_{min}}$ obtained with the series inductance $L_{S_{opt}}$ and R_n obtained from (4.11) with L_g.

Device	f_o GHz	$R_{n_{min}}$ Ω	$L_{S_{opt}}$ nH	$R_n\,(L_g)$ Ω	L_g nH	$\frac{L_{S_{opt}}-L_g}{L_g}$ %	$\frac{R_{n_{min}}-R_n(L_g)}{R_n(L_g)}$ %
ATF21186	0.5	1.29	71.15	1.11	55.65	27.85	16.74
ATF21186	1.0	1.18	26.95	1.10	20.99	28.39	6.96
ATF21186	2.0	1.61	7.88	1.62	6.11	28.94	-0.12
AT41486	0.1	8.50	1.34	8.50	1.29	3.63	0.00
AT41486	0.5	8.48	1.10	8.47	1.07	2.50	-0.01
AT41486	1.0	7.97	0.48	7.98	0.46	3.80	-0.01
ATF10136	1.0	4.94	36.45	4.85	32.47	12.26	1.75
ATF10136	2.0	4.65	8.83	4.57	7.61	16.01	1.71
ATF10136	4.0	12.17	0.88	11.59	0.78	12.62	5.07
ATF35176	2.0	2.40	17.24	2.38	15.66	10.04	0.91
ATF35176	4.0	1.59	4.87	1.59	4.32	12.81	-0.02
ATF35176	6.0	1.43	1.82	1.43	1.63	11.36	-0.36
ATF35176	8.0	1.31	0.96	1.30	0.87	10.29	0.89

Some comments are worthwhile at this point:

1. L_g makes R_n decrease;

2. chapter 3 showed that the optimum series reactance $X_{s_{min}} = \omega\, L_{S_{opt}}$ makes $R_n = R_{n_{min}}$ for any 2–port device. The input series inductor L_g calculated with (4.11) and applied to the same device (without series feedback), provides $R_n\,(L_g) \approx R_{n_{min}}$ as Table 4.1 shows numerically with different transistors;

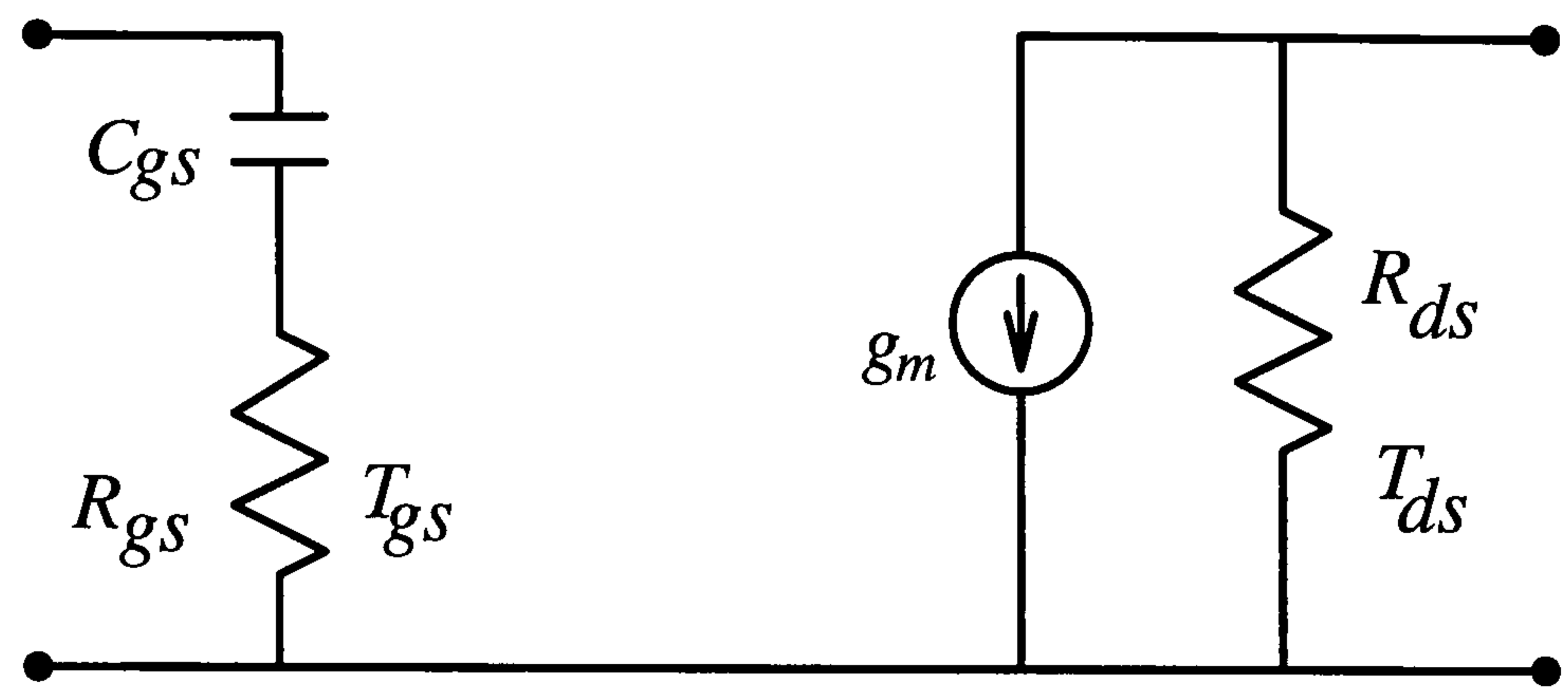

Figure 4.2 Pospieszalski noise model for intrinsic MESFETs and HEMTs.

3. the minimum noise figure F_{min} does not change because L_g is ideal and lossless: it does not feed the amplifier with any noise power. F_{min} is another quantity along with $R_{S_{opt}}$ (4.10.a) and $g_{n_{tot}}$ (4.8) that is not affected by L_g;

4. (4.11) tacitly assumes that $\Im m\,[\rho_n] > 0$ in order to get an acceptable value for L_g. If $\Im m\,[\rho_n] < 0$, a series capacitor can still provide a real correlation coefficient for the final network;

5. the previous point may make one wonder whether it is by chance that a MESFET like the ATF21186 has $\Im m\,[\rho_n] > 0$. A simple reasoning based on an intrinsic FET noise model, proves that this condition is likely to be achieved by any FET. Consider Figure 4.2, the Pospieszalski noise model [7] for intrinsic devices. The imaginary part of the optimum noise source impedance $Z_{S_{opt}}$ is $1/\omega\, C_{gs}$ and it is linearly related to $\Im m\,[\widetilde{\rho_{n_{tot}}}]$ (4.10.b). For intrinsic FETs, L_g at the input port must be inductive as (4.9) demonstrates; this reasoning may lose strength for extrinsic and packaged devices because parasitics make the noise parameters change in a complex fashion. However, the capacitive MESFET input, the Pospieszalski noise model and the small values associated with parasitic elements give a certain confidence in stating that the input element generally works out to be an inductor;

6. a LNA should provide good return losses associated with S_{11} and S_{22}. The input inductor cannot be expected to satisfy these requirements on its own. However,

   - a series feedback impedance increases the value of $\Re e\left[Z_{S_{opt}}\right]$ [109];
   - L_g modifies $\Gamma_{S_{opt}}$ but does not affect $\Re e\left[Z_{S_{opt}}\right]$;

- the condition $\Gamma_{in} = \Gamma_{S_{opt}}{}^*$ can be achieved independently by properly choosing $\Gamma_L = \Gamma_L^{SSNM}$ according to (3.44), chapter 3.

These facts suggest a reason for using an input inductance and a series feedback for LNA design: the series feedback increases the real part of the optimum noise source impedance of the LNA; then, the input inductance cancels out the imaginary part of the optimum noise source impedance (4.10.b) since the real part (4.10.a) is not affected. Series feedback L_s and input series inductance L_g have been used to produce LNAs [133]; however, those LNA designs have been kept confidential.

Hughes [75] made use of an input (parallel) reactance in order to cancel out the imaginary part of $Z_{S_{opt}}$ of a MMIC LNA at 12 GHz; however, no study of the influence of an input element on the noise parameters of the following stage is reported.

The previous results can be applied to any type of device (extrinsic or packaged) because the active stage has been described by matrices in a general fashion. The use of L_g and series inductance L_s should be coupled with optimisation software in order to look into the frequency behaviour of both noise and scattering parameters.

Finally, (4.11) relates an external component to Z_c and therefore explains how a reactive element can make the internal noise sources of the second stage uncorrelated. It is difficult to find in the literature suggestions on how to realise Z_c. The quality factor Q_g [134] of the input inductor L_g should be as high as possible for this analysis to model real applications.

4.2 The Modified Pospieszalski Noise Model

Here, series feedback impedance is applied to the Pospieszalski noise model for intrinsic MESFETs and HEMTs [7] in order to investigate its noise parameters. The R_n analysis of chapter 3 is the mathematical tool required for this exercise. The interesting result is to point out the importance of both L_g and the parasitic components surrounding the intrinsic transistor when extending the Pospieszalski noise model to extrinsic devices.

4.2.1 The Intrinsic Noise Model

Figure 4.2 shows the intrinsic device [7]: four elements (R_{gs}, C_{gs}, R_{ds} and g_m) are required to model any intrinsic MESFET or HEMT. The noise performance is completely defined by associating the temperatures T_{gs} and T_{ds} with the resistors R_{gs} and R_{ds}, respectively. The following features apply to the Pospieszalski network:

- Pospieszalski states that the noise sources:

$$\overline{| v_{gs} |^2} = 4kT_o\nu_{gs}\, R_{gs}\Delta f \qquad (4.12)$$

$$\overline{| i_{ds} |^2} = 4kT_o\nu_{ds}\, \frac{1}{R_{ds}}\Delta f \qquad (4.13)$$

  are uncorrelated. The terms:

$$\nu_{gs} = \frac{T_{gs}}{T_o} \qquad (4.14)$$

$$\nu_{ds} = \frac{T_{ds}}{T_o} \qquad (4.15)$$

  allows gate and source temperatures to be accounted for by (4.12) and (4.13), respectively.

- any intrinsic MESFET or HEMT can be modelled if the condition:

$$1 \leq 4\,\Re e\left[Z_{S_{opt}}\right]\, g_n\, \frac{T_o}{T_{min}} \leq 2$$

  is satisfied; standard temperature T_o is 290 K [131]. This condition is not affected by an input series inductor L_g;

- the value of T_{gs} is close to the room temperature, $T_{gs} \approx 290$ K;

- the value of T_{ds} is in the order of thousands of Kelvin [58], $T_{ds} \approx 2000$ K.

- T_{gs} is highly dependant on the precision related to the determination of R_{gs} [7];

- the input impedance $Z_{in} = R_{gs} + \frac{1}{j\,\omega\, C_{gs}}$ is independent of the load impedance, since the model is unilateral ($S_{12} = 0$);

- the source that power–matches the input port for maximum available gain is $Z_s^G = Z_{in}{}^{\star} = R_{gs} - \frac{1}{j\,\omega\,C_{gs}}$;

- the optimum noise source impedance for minimum noise figure at frequency f_o is [7]:

$$Z_{S_{opt}} = \left(\frac{f_t}{f_o}\right)\sqrt{R_{ds}\, R_{gs}\left[\frac{\nu_{gs}}{\nu ds} + \frac{R_{gs}}{R_{ds}}\left(\frac{f_o}{f_t}\right)^2\right]} + j\,\frac{1}{\omega\, C_{gs}},$$

  where $\omega = 2\,\pi\, f_o$ and:

$$f_t = \frac{g_m}{2\,\pi\, C_{gs}} \qquad (4.16)$$

- the imaginary parts of $Z_{S_{opt}}$ and Z_s^G have equal magnitudes and signs; the real part of $Z_{S_{opt}}$ is frequency dependent; on the contrary, the real part of Z_s^G is not.

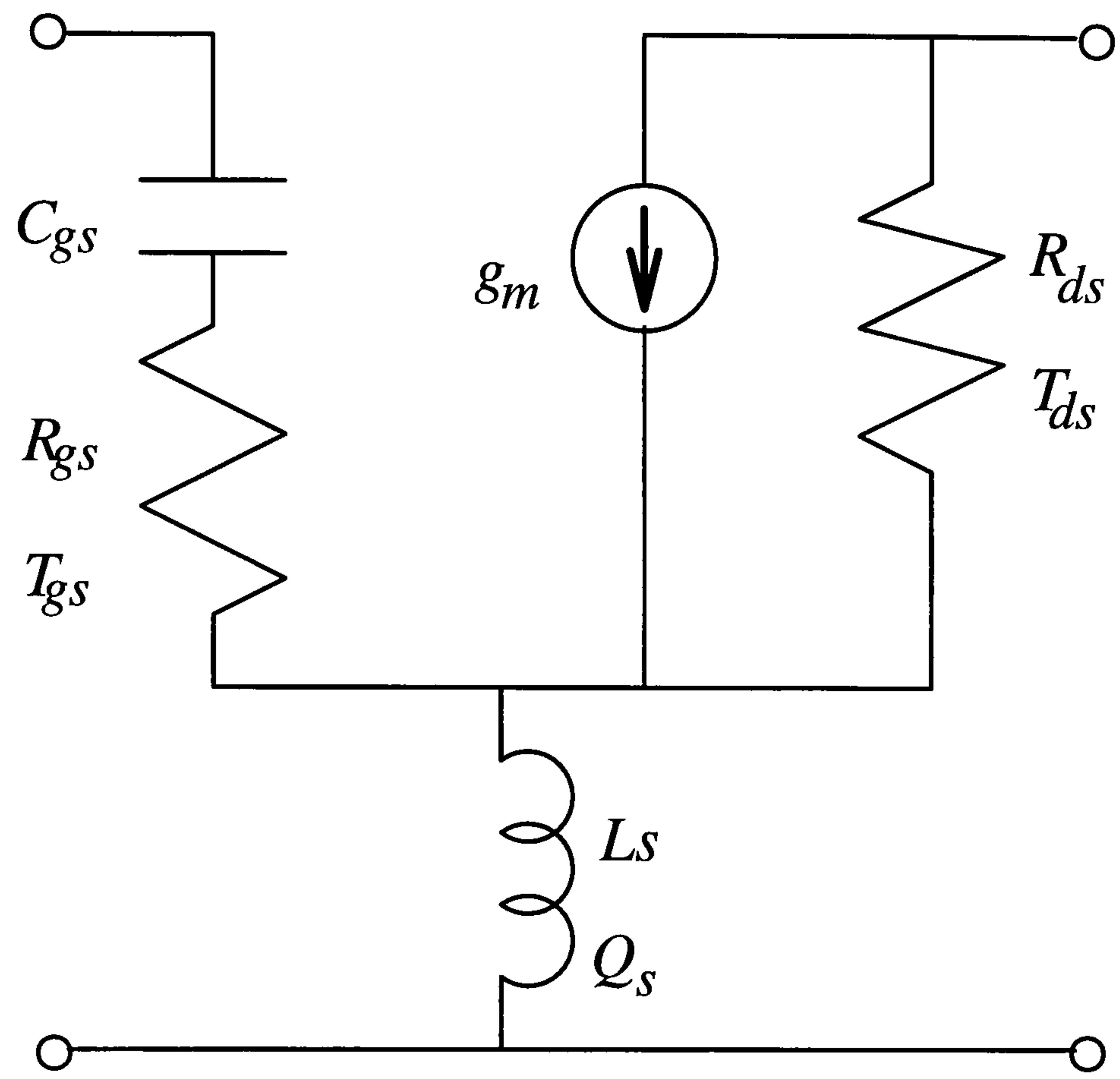

Figure 4.3 Modified Pospieszalski noise model with lossy series feedback inductor.

4.2.2 Extension of the Intrinsic Noise Model

The Pospieszalski noise model can be extended to extrinsic or packaged transistors if a lossy series inductance L_s is located between the reference and source terminals of the active device (Figure 4.3). Two independent causes can make the series feedback impedance Z_s lossy: a finite quality factor Q_s of L_s; or a resistive series component $R_s = \Re e\,[Z_s]$. Any combinations of these two cases can be dealt with by the noise analysis of chapter 3 at the given frequency f_o.

The initial known quantities for the noise analysis of Figure 4.3 are:

1. the signal parameters in hybrid matrix representation:

$$\mathbf{H}_t = \begin{bmatrix} \frac{1+j\,\omega\,C_{gs}\,R_{gs}}{j\,\omega\,C_{gs}} & 0 \\ \frac{g_m}{j\,\omega\,C_{gs}} & \frac{1}{R_{ds}} \end{bmatrix} \tag{4.17}$$

At the frequency f_t (4.16), the magnitude of the current gain $\mid H_{t_{21}} \mid$ is 1;

2. the noise parameters in the same representation [7]:

$$\mathbf{C}_t^{(H)} = 4kT_o\Delta f \begin{bmatrix} \nu_{gs}\, R_{gs} & 0 \\ 0 & \frac{\nu_{ds}}{R_{ds}} \end{bmatrix} \tag{4.18}$$

3. the lossy series feedback element $z_s = Z_s/Z_o$ normalised to $Z_o = 50\ \Omega$ is:

$$z_s = \left(\frac{1}{Q_s} + j\right) x_s \tag{4.19}$$

$$x_s = \frac{\omega\, L_s}{Z_o} \tag{4.20}$$

$$Q_s = \frac{\Im m\,[z_s]}{\Re e\,[z_s]} \tag{4.21}$$

Q_s is the quality factor associated with the series impedance Z_s and may model the quality factor of the inductor as well as allow for a resistance R_s in series with the lossy (or lossless) inductance L_s;

4. the parallel admittance $Y_p = G_p + j\, B_p$ is set to zero.

Some considerations about the sign of Q_s are made [86]. The quality factor Q of any electric component is defined by:

$$Q = \frac{\omega\ \cdot\ \text{Average Stored Electric and Magnetic Energy}}{\text{Power Loss}},$$

and is a measure of the energy stored by the component at the pace determined by the angular frequency ω, relative to the dissipated power. Therefore, from a circuit point–of–view:

$$Q = \frac{\Im m\,[V\, I^\star]}{\Re e\,[V\, I^\star]} \tag{4.22}$$

is an equivalent expression. V and I denote voltage and current phasors at the angular frequency ω. (4.22) can describe both inductors and capacitors:

1. *Inductors:* the relationship between V and I with the convention that the current I flows into the node at the highest potential, is $V = Z\, I$ where $Z = R + j\,\omega\, L$. The quality factor is

$$Q = \frac{\Im m\,[Z\ \mid I \mid^2]}{\Re e\,[Z\ \mid I \mid^2]} = \frac{\Im m\,[Z]}{\Re e\,[Z]} = \frac{\omega\, L}{R}.$$

2. *Capacitor:* in this case, $I = Y\,V$ where $Y = G + j\,\omega\,C$ and the quality factor is

$$Q = \frac{\Im m\left[Y^{\star}\ |\ V\ |^{2}\right]}{\Re e\left[Y^{\star}\ |\ V\ |^{2}\right]} = \frac{-\omega\,C}{G}.$$

In conclusion, the quality factor is positive if referred to an inductance and negative if referred to a capacitance.

The noise analysis at frequency f_o can make use of the expressions of chapter 3 once the hybrid matrix representation $\left(\mathbf{H}_t; \mathbf{C}_t^{(H)}\right)$ is converted into a transmission matrix representation $(\mathbf{T}_t; \mathbf{C}_t)$:

$$\begin{aligned}
\mathbf{T}_t &= \begin{bmatrix} -\frac{1}{g_m\,R_{ds}} - j\,\frac{R_{gs}}{R_{ds}}\,\xi & -\frac{1}{g_m} - j\,R_{gs}\,\xi \\ -j\,\frac{1}{R_{ds}}\,\xi & -j\,\xi \end{bmatrix} && (4.23)\\
\mathbf{C}_t &= 4kT_o\Delta f \begin{bmatrix} \nu_{gs}\,R_{gs} + \frac{|H_{11}|^2}{|H_{21}|^2}\,\frac{\nu_{ds}}{R_{ds}} & \frac{H_{11}}{|H_{21}|^2}\,\frac{\nu_{ds}}{R_{ds}} \\ \frac{H_{11}{}^{\star}}{|H_{21}|^2}\,\frac{\nu_{ds}}{R_{ds}} & \frac{\nu_{ds}}{|H_{21}|^2\,R_{ds}} \end{bmatrix} && (4.24)\\
\xi &= \frac{f_o}{f_t} && (4.25)
\end{aligned}$$

The expansion of (4.24) provides the noise parameters R_t, g_t and ρ_{t_o} for intrinsic devices:

$$\begin{aligned}
R_t &= R_{gs}\left[\nu_{gs} + \nu_{ds}\,\frac{1}{g_m^2\,R_{gs}\,R_{ds}} + \nu_{ds}\,\frac{R_{gs}}{R_{ds}}\,\xi^2\right] && (4.26)\\
g_t &= \frac{\nu_{ds}}{R_{ds}}\,\xi^2 && (4.27)\\
\rho_{t_o} &= \frac{\nu_{ds}}{R_{ds}}\,\xi\left[R_{gs}\,\xi + j\,\frac{1}{g_m}\right] && (4.28)
\end{aligned}$$

These expressions are equal to the ones found by Hughes [73] if $f_{max} = 2\,f_{max}^{Hughes}$, where f_{max} is the maximum frequency of oscillation, i.e. the frequency that makes the available gain G_{av} unity. For the network of Figure 4.2, f_{max} is obtained by solving:

$$G_{av}\left(f_{max}\right) = \frac{g_m^2\,R_{ds}\,R_{gs}}{1 + \left(2\,\pi\,f_{max}\,C_{gs}\,R_{gs}\right)^2} = 1.$$

The noise parameters for Figure 4.3 are worked out from (3.31), (3.32) and (3.33), chapter 3, as functions of the series feedback impedance (4.19). The optimum noise source impedance $Z_{S_{opt}}$ for the modified Pospieszalski noise model is:

$$Z_{S_{opt}} = R_{S_{opt}} + j\,X_{S_{opt}} = \frac{\sqrt{R_n\,g_n - \Im m\left[\rho_{n_o}\right]^2} + j\,\Im m\left[\rho_{n_o}\right]}{g_n} \qquad (4.29)$$

where real and imaginary parts are:

$$
\begin{aligned}
R^2_{S_{opt}} \mid \Delta_A \mid^4 &= \xi^4\, x_s^2\, c_1 + \xi^3\, x_s\, c_2 + \xi^2 \left(\frac{x_s}{Q_s}\right) c_3 + \xi^3\, x_s \left(\frac{x_s}{Q_s}\right) c_4 \\
&+ \xi^2\, c_5 + \xi^4 \left(\frac{x_s}{Q_s}\right)^2 c_6 + \xi^4 \left(\frac{x_s}{Q_s}\right)^3 c_7 \\
&+ \xi^4\, x_s^2 \frac{x_s}{Q_s}\, c_8 + \xi^4 \frac{x_s}{Q_s}\, c_9 + \xi^4\, c_{10}
\end{aligned}
\tag{4.30}
$$

$$
\begin{aligned}
c_1 &= \frac{r_{gs}\, \nu_{ds}}{r_{ds}^3} && (4.30.a) \\
c_2 &= 2\,\frac{r_{gs}\, \nu_{gs}\, \nu_{ds}}{r_{ds}^2} && (4.30.b) \\
c_3 &= \frac{\nu_{ds}}{r_{ds}} \left(1 + \frac{r_{gs}\, \nu_{gs}}{r_{ds}\, \nu_{ds}}\right) \approx \frac{\nu_{ds}}{r_{ds}} && (4.30.c) \\
c_4 &= 2\,\frac{\nu_{ds}}{r_{ds}^2} \left(1 + \frac{r_{gs}\, \nu_{gs}}{r_{ds}\, \nu_{ds}}\right) \approx 2\,\frac{\nu_{ds}}{r_{ds}^2} && (4.30.d) \\
c_5 &= \frac{r_{gs}\, \nu_{gs}\, \nu_{ds}}{r_{ds}} && (4.30.e) \\
c_6 &= \left(\frac{\nu_{ds}}{r_{ds}}\right)^2 \left[\left(1 + \frac{r_{gs}}{r_{ds}\, \nu_{ds}}\right)^2 + \frac{r_{gs}}{r_{ds}\, \nu_{ds}}\right] \approx \left(\frac{\nu_{ds}}{r_{ds}}\right)^2 && (4.30.f) \\
c_7 &= \frac{\nu_{ds}}{r_{ds}^3} \left(1 + \frac{r_{gs}}{r_{ds}\, \nu_{ds}}\right) \approx \frac{\nu_{ds}}{r_{ds}^3} && (4.30.g) \\
c_8 &= \frac{\nu_{ds}}{r_{ds}^3} \left(1 + \frac{r_{gs}}{r_{ds}\, \nu_{ds}}\right) \approx \frac{\nu_{ds}}{r_{ds}^3} && (4.30.h) \\
c_9 &= 2\,\frac{\nu_{ds}}{r_{ds}}^2\, r_{gs} \left(1 + \frac{r_{gs}}{r_{ds}\, \nu_{ds}}\right) \approx \frac{2\, r_{gs}\, \nu_{ds}^2}{r_{ds}^2} && (4.30.i) \\
c_{10} &= \left(\frac{r_{gs}\, \nu_{ds}}{r_{ds}}\right)^2 && (4.30.j)
\end{aligned}
$$

$$
x_{S_{opt}} = \frac{X_{S_{opt}}}{Z_o} = \frac{1}{\xi}\, \frac{\left[\frac{1}{g_m\, Z_o} - \xi\, x_s\right] + \Delta_u}{1 + \Delta_d} \tag{4.31}
$$

$$
\begin{aligned}
\Delta_u &= \frac{1}{\nu_{ds}} \left(1 + \frac{1}{g_m\, Z_o\, r_{ds}}\right) \frac{x_s}{Q_s} && (4.31.a) \\
\Delta_d &= \frac{1}{r_{ds}\, \nu_{ds}}\, \frac{x_s}{Q_s} && (4.31.b)
\end{aligned}
$$

and the equivalent noise source conductance g_n is:

$$g_n\, Z_o \mid \Delta_A \mid^2 \;=\; \xi^2 \frac{x_s}{Q_s} \frac{1}{r_{ds}^2} + \xi^2 \frac{\nu_{ds}}{r_{ds}} \tag{4.32}$$

The term $\mid \Delta_A \mid^2$ is the common denominator of the noise parameters for the feedback network (chapter 3, section 3.1.3); r_{gs} and r_{ds} are equal to R_{gs}/Z_o and R_{ds}/Z_o, respectively. Coefficients (4.30.c), (4.30.d), (4.30.f), (4.30.g), (4.30.h) and (4.30.i) have been approximated after noticing that:

$$\frac{\nu_{ds}}{r_{ds}} \gg 1$$
$$1 + \frac{r_{gs}}{r_{ds}\, \nu_{ds}} \approx 1$$

for any intrinsic model [58].

4.3 Applications of the Modified Pospieszalski Noise Model

The optimum noise source impedance $Z_{S_{opt}}$ (4.29), shown in Figure 4.4 vs. frequency for a typical FET with 0.3×250 μm gate [135], is investigated. A summary from the new results described by the author in [59] for the imaginary part $X_{S_{opt}}$ is reported before looking into the real part $R_{S_{opt}}$. Changes in the scattering parameters are not studied, which constitutes a limitation. The results of this section are devoted to suggest and improve the understanding of FET noise behaviour as modelled by Pospieszalski and extended in [59]. A great deal of further investigation could originate from here.

4.3.1 The Imaginary Part of $Z_{S_{opt}}$

An approximated expression for the optimum noise source reactance $\Im m\left[Z_{S_{opt}}\right] = X_{S_{opt}}$ stems from (4.31) after back–substituting ξ (4.25), f_t (4.16) and x_s (4.20):

$$X_{S_{opt}} \;\approx\; \xi \frac{1}{g_m} - x_s\, Z_o = \frac{1}{\omega\, C_{gs}} - \omega\, L_s \tag{4.33}$$

(4.33) is valid if the conditions:

$$\Delta_u \;\ll\; \left[\frac{1}{g_m\, Z_o} - \xi\, x_s\right] \tag{4.33.a}$$

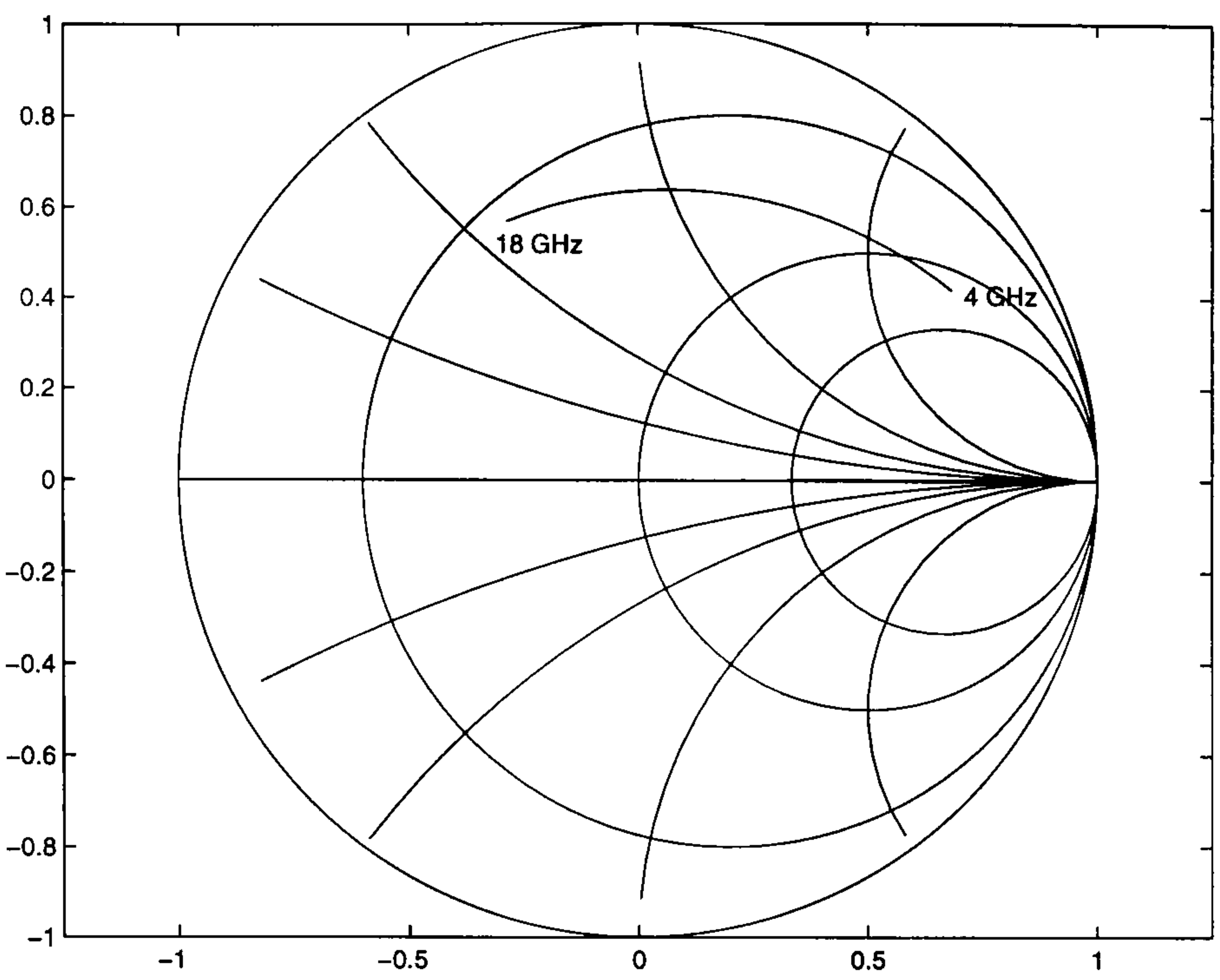

Figure 4.4 Typical $Z_{S_{opt}}$ vs frequency for a FET model.

$$\Delta_d \ll 1 \tag{4.33.b}$$

are verified. (4.31.a) and (4.31.b) show that (4.33) is likely to be acceptable as long as $\nu_{ds} = T_{ds}/T_o \gg 1$: this has been proven experimentally [58]. The modified Pospieszalski model has been used to model the imaginary part of $Z_{S_{opt}}$ successfully [59] and provide a better insight on the influence of the parasitic inductances L_g and L_s on the noise performance of field effect transistors. In fact, the main achievement of [59] is to prove that:

$$X_{S_{opt}} \approx \frac{1}{\omega\, C_{gs}} - \omega\,(L_s + L_g) \tag{4.34}$$

is well–suited to describe the optimum noise source reactance when the modified Pospieszalski noise model is extended to extrinsic and packaged devices.

4.3.2 Analysis of $R_{S_{opt}}$ with L_s when $R_s = 0$

Consider an extrinsic MESFET or HEMT characterised as a 2–port device and use a modified Pospieszalski model (Figure 4.3) to describe it. Assume that there is no resistive component in the series feedback impedance ($R_s = 0$); however, $\Re e\left[Z_{S_{opt}}\right] \neq 0$ because the series inductance L_s may be lossy ($Q_s < \infty$). The frequency at which $R_{S_{opt}} = Z_o$ (50 Ω

for instance) can be calculated from (4.30) if the frequency behaviour of $Q_s(f)$ is known. Initially, for an approximated solution,

$$\lim_{Q_s \to \infty} \frac{x_s}{Q_s} = 0 \tag{4.35}$$

and the coefficients in (4.30) are modified accordingly.

Imposing $R_{S_{opt}} = Z_o$ makes (4.29) read:

$$\frac{g_n Z_o}{|\Delta_A|^2} = \frac{\sqrt{R_n g_n - \Im m\left[\rho_{n_o}\right]^2}}{|\Delta_A|^2} \tag{4.36}$$

which can be written in the unknown ξ (4.25) after considering (4.30) and (4.32):

$$\xi^4 d_2 + \xi^2 d_1 + d_0 = 0 \tag{4.37}$$

The coefficients are found to be:

$$d_2 = \frac{x_t^2 r_{gs}}{r_{ds}^2} \tag{4.37.a}$$

$$d_1 = -\frac{\nu_{ds}}{r_{ds}} \left(1 - 2 x_t r_{gs} - r_{gs}^2\right) \tag{4.37.b}$$

$$d_0 = r_{gs} \nu_{gs} \tag{4.37.c}$$

$$x_t = \frac{2 \pi f_t L_s}{Z_o} \tag{4.37.d}$$

x_t is the normalised reactance associated with L_s at the frequency f_t (4.16).

(4.37) is readily solved. In particular:

1. the coefficient (4.37.a) is negligible;
2. the coefficient (4.37.b) is the only one dependent on T_{ds} and the main contribution to it comes from $(-\nu_{ds}/r_{ds})$;
3. the solution of (4.37) provides up to 2 positive solutions for ξ: only the one within or closest to the given frequency range of the model is considered.

(4.37) is applied to many published networks [59] and Table 4.2 collects the numerical results.

The frequency ξf_t which solves (4.37) and f_{Z_o} at which $R_{S_{opt}} = Z_o$ as obtained after frequency simulation of the same network, are compared. Some f_{Z_o} values fall outside the frequency range specified by each reference. The error between f_{Z_o} and ξf_t is within $\pm 10\%$ for the device in [135] (the different values for T_{gs} and T_{ds} correspond to different bias conditions). The equivalent circuits described in [136], [137] and [138] are not noise models based on T_{gs} and T_{ds}; nevertheless, the coefficients of Table 4.2 are comparable to each other because they are based on R_{gs} and R_{ds} which are similar for every referenced device.

Table 4.2 Coefficients of (4.36), the frequency $\xi\, f_t$ at which the equation is satisfied, the frequency f_{Z_o} at which $R_{S_{opt}} = Z_o$ as worked out by a frequency simulator for a number of published results. $T_{ds} = 2000$ K and $T_{gs} = 290$ K have been assumed for networks not directly based on the Pospieszalski noise model.

Ref.	Range GHz	T_{gs} K	T_{ds} K	d_2 $\times 10^6$	$-d_1$	$-\frac{\nu_{ds}}{r_{ds}}$	$\xi\, f_t$ GHz	f_{Z_o} GHz	$\frac{\xi f_t - f_{Z_o}}{f_{Z_o}}$ %
[7]	1–23	304	5514	67.13	2.37	2.38	4.82	1.30	270.87
[7]	1–23	210	5468	93.99	2.34	2.36	4.77	1.30	266.68
[135]	4–18	220	1234	5.14	1.37	1.37	6.30	6.98	-9.60
[135]	4–18	447	7529	5.14	8.37	8.39	3.64	3.40	7.81
[135]	4–18	389	5696	5.14	6.33	6.34	3.90	3.75	4.06
[135]	4–18	295	2550	5.14	2.83	2.84	5.08	5.20	-2.32
[82]	6–18	295	2547	16.11	1.68	1.69	3.67	3.00	22.28
[136]	2–18	290	2000	113.46	1.63	1.65	12.01	13.90	-13.59
[137]	2–18	290	2000	21.78	1.02	1.03	8.15	11.70	-30.33
[138]	12–25	290	2000	2.64	0.37	0.37	10.26	15.50	-33.83

The largest errors are associated with the transistor described by Pospieszalski in [7]; however, two conditions are not met by the device:

1. the noise temperatures T_{gs} and T_{ds} result out of a fitting procedure over the frequency range. In the region around f_{Z_o} shown in Table 4.2, Pospieszalski warns that the model is not as accurate as it is at higher frequencies;
2. T_{gs} and T_{ds} do not satisfy the empirical relationship by Byzery [81]:

$$\frac{T_{ds}\,(T_{room})}{T_{ds}\,(T_o)} \quad = \quad \frac{T_{gs}\,(T_{room})}{T_{gs}\,(T_o)} \tag{4.38}$$

   where T_{room} is the temperature at which the noise measurement is carried out and $T_o = 293$ K [82].

On the basis of Table 4.2, d_2 (4.37.a) can be neglected and (4.36) can be solved:

$$\xi \;\approx\; \sqrt{\frac{r_{gs}\, r_{ds}\, \nu_{gs}}{\nu_{ds}}} \tag{4.39}$$

Some confidence on this analysis is given by noting that (4.39) is found in [7][1] for intrinsic

[1] Eqn. (25), page 1343

device, if $R_{S_{opt}}/Z_o = 1$ is imposed. Noteworthy is the fact that (4.39) supports Byzery's empirical expression (4.38) since (4.39) can be rewritten as

$$\frac{\nu_{gs}}{\nu_{ds}} = \frac{T_{gs}}{T_{ds}} \approx \frac{\xi}{r_{gs}\, r_{ds}} = \text{const}$$

for a given frequency f_o and temperature T_{room} of measurement.

(4.39) could be used to have an indication of what value should be associated with T_{ds} by measuring the frequency f_{Z_o} at which $R_{S_{opt}} = Z_o$. This proposed method can also be applied to intrinsic devices [7]. If the component values C_{gs}, R_{ds} and R_{gs} of the intrinsic model are known, then f_t (4.16) can be computed and finally:

$$\widehat{T}_{ds} = \nu_{ds}\, T_o = \left(\frac{1}{\xi}\right)^2 (r_{ds}\, r_{gs}\, \nu_{gs})\, T_o \tag{4.40}$$

T_{gs} can be set to the value of the temperature at which the measurement of $R_{S_{opt}}$ has been carried out [58]; if measured data are available, the use of the product $R_{gs}T_{gs}$ may help to reduce the uncertainties associated with the Pospieszalski noise model [7]. If measured data are not available, $T_{gs} = 295$ K can be assumed [58] in order to calculate $\widehat{T}_{ds}$ from (4.40). This has been done with the references of Table 4.2 and the resulting $\widehat{T}_{ds}$ are collected in Table 4.3. The best results in comparison with Table 4.2 correspond to [135] with T_{ds} equal

Table 4.3 Comparison between T_{ds} as given in each reference and $\widehat{T}_{ds}$ for the Pospieszalski based models if $T_{gs} = 295$ K is assumed.

Reference	T_{ds} K	$\widehat{T}_{ds}$ K	$\frac{\widehat{T}_{ds}-T_{ds}}{T_{ds}}$ %
[7]	5514	73294	1229
[7]	5468	102611	1776
[135]	1234	1350	9.38
[135]	7529	5680	-24.55
[135]	5696	4669	-18.02
[135]	2550	2428	-4.77
[82]	2547	3829	50.35
[136]	2000	1500	-24.99
[137]	2000	978	-51.07
[138]	2000	886	-55.71

to 1234 K and 2550 K, which are the ones with T_{gs} closer to 295 K.

4.3.3 Analysis of $R_{S_{opt}}$ with L_s when $R_s \neq 0$

Figure 4.3 assumes that the series feedback branch at the source consists of a lossy inductor L_s only and no resistance R_s is present. This resistance can readily be taken into account by modifying the quality factor Q_s in (4.19):

$$Z_s^{tot} = R_s + Z_s = R_s + \frac{X_s}{Q_s} + j\,X_s = \left(\frac{1}{Q_s^{tot}} + j\right) X_s \tag{4.41}$$

$$Q_s^{tot} = \frac{X_s}{R_s + \frac{X_s}{Q_s}} = \frac{1}{\frac{1}{Q_s^{'}} + \frac{1}{Q_s}} \tag{4.42}$$

$$Q_s^{'} = \frac{X_s}{R_s} \tag{4.43}$$

The new quality factor Q_s^{tot} should be used in (4.19) if a resistance R_s is considered in the model of Figure 4.3. Notice that if the inductance L_s is lossless and R_s is ideal, then Q_s^{tot} at any frequency f_o is known: $Q_s^{tot} = (2\,\pi\,f_o\,L_s)\,/R_s$. This is the case for any device equivalent circuit: the components of the model are ideal. Therefore, (4.41) is modified accordingly.

The following assumptions are made:

1. the series inductor L_s is ideal: $Q_s \to \infty$;
2. the normalised series reactance is defined with (4.20) and (4.37.d):
$$x_s = \frac{2\,\pi\,f_o\,L_s}{Z_o} = \frac{2\,\pi\,f_t\,L_s}{Z_o}\,\xi = x_t\,\xi;$$
3. the quality factor Q_s^{tot} (4.42) of the series feedback impedance accounts for R_s:
$$r_s = \frac{R_s}{Z_o} = \frac{x_s}{Q_s^{tot}} = \frac{x_s}{Q_s^{'}}$$

Then, $R_{S_{opt}} = Z_o$ is solved in the unknown ξ (4.25):

$$\xi^4\,\delta_2 + \xi^2\,\delta_1 + \delta_0 = 0 \tag{4.44}$$

The coefficients are:

$$\delta_2 = x_t^2\,c_1 + x_t^2\,r_s\,c_8 \tag{4.44.a}$$

$$\begin{aligned}\delta_1 = {} & x_t\,c_2 + x_t\,r_s\,c_4 + r_s\,c_6 \\ & + r_s^3\,c_7 + r_s\,c_9 + c_{10} - \left(\frac{r_s}{r_{ds}^2} + \frac{\nu_{ds}}{r_{ds}}\right)^2\end{aligned} \tag{4.44.b}$$

$$\delta_0 = r_s\,c_3 + c_5 \tag{4.44.c}$$

Again, the frequency $\xi\, f_t$ which solves (4.44) is calculated and compared to f_{Z_o} in Table 4.4.

Table 4.4 Coefficients of (4.45) for the same models of Table 4.2, the quality factor $Q_s^{'}$ associated with the series feedback impedance, the frequency $\xi\, f_t$ at which the equation is satisfied and the frequency f_{Z_o} at which $R_{S_{opt}} = Z_o$ as worked out by a frequency simulator.

Ref.	Range GHz	T_{gs} K	T_{ds} K	$Q_s^{'}$ @ f_{Z_o}	d_2 $\times 10^6$	$-d_1$	$-\frac{\nu_{ds}}{r_{ds}}$	$\xi\, f_t$ GHz	f_{Z_o} GHz	$\frac{\xi f_t - f_{Z_o}}{f_{Z_o}}$ %
[7]	1–23	304	5514	1.18	550.51	2.35	2.38	4.82	1.30	306.50
[7]	1–23	210	5468	1.18	765.34	2.33	2.36	5.23	1.30	302.61
[135]	4–18	220	1234	0.41	17.81	1.35	1.37	7.72	6.98	10.70
[135]	4–18	447	7529	0.20	17.80	8.26	8.39	4.07	3.40	19.80
[135]	4–18	389	5696	0.22	17.80	6.25	6.34	4.43	3.75	18.15
[135]	4–18	295	2550	0.31	17.80	2.80	2.84	5.96	5.20	14.60
[82]	6–18	295	2547	2.24	151.04	2.82	1.69	3.67	4.28	42.57
[136]	2–18	290	2000	0.57	558.98	1.51	1.65	16.56	13.90	19.14
[137]	2–18	290	2000	0.69	162.65	0.95	1.03	11.33	11.70	-3.14
[138]	12–25	290	2000	1.26	51.77	0.34	0.37	15.09	15.50	-2.64

In order to have an expression equivalent to (4.40), (4.44) is solved for $\tilde{T}_{ds} = \nu_{ds}\, T_o$:

$$\frac{\tilde{T}_{ds}}{T_o} = \nu_{ds} = \frac{r_{ds}}{\xi^2}\,\frac{\delta_A\,\xi^4 + \delta_B\,\xi^2 + \delta_C}{1 - (r_s + r_{gs})^2} \tag{4.45}$$

where:

$$\delta_A = \frac{(r_{gs} + r_s)\, x_t^2}{r_{ds}^2} \tag{4.45.a}$$

$$\delta_B = 2\,\frac{r_{gs}\,\nu_{gs}\,x_t}{r_{ds}} + 2\,\frac{x_t\, r_s}{r_{ds}} + \left(\frac{r_s}{r_{ds}}\right)^3 \tag{4.45.b}$$

$$\delta_C = r_s + r_{gs}\,\nu_{gs} \tag{4.45.c}$$

The normalised frequency ξ in (4.45) corresponds to the frequency where $R_{S_{opt}} = Z_o$ (either measured or simulated). Some results for $T_{gs} = 295$ K are collected in Table 4.5.

4.4 Discussion on the Influence of the Inductor L_g on the Network Performance

It has been stated in chapter 3, section 3.4 that input matching circuits should not be used when designing LNAs. There, an analysis of input matching circuit is developed where

Table 4.5 Comparison between T_{ds} and the approximated temperature $\tilde{T}_{ds}$ (4.45) for the Pospieszalski based models after assuming $R_s \neq 0$ and $T_{gs} = 295$ K.

Reference	T_{ds}	$\tilde{T}_{ds}$	$\frac{\tilde{T}_{ds}-T_{ds}}{T_{ds}}$
	K	K	%
[7]	5514	88032	1496.51
[7]	5468	117790	2054.17
[135]	1234	1840	49.08
[135]	7529	7739	2.78
[135]	5696	6362	11.69
[135]	2550	3309	29.76
[82]	2547	5161	102.64
[136]	2000	2702	35.13
[137]	2000	1794	-10.27
[138]	2000	1811	-9.43

precise boundary conditions are assumed. The main assumption which is of interest now, is (3.49.c):

$$\Gamma^{I}_{out} = \Gamma^{A}_{S_{opt}}{}^{\star}$$

which is the SSNM condition at the plane between the output port of the matching circuit and the input port of the second (active) stage. Γ^{I}_{out} is the output reflection coefficient of the matching circuit and $\Gamma^{A}_{S_{opt}}{}^{\star}$ is the conjugate of the optimum noise reflection coefficient of the amplifier. It is assumed that the second stage is simultaneously matched, i.e.

$$\Gamma^{A}_{in} = \Gamma^{A}_{S_{opt}}{}^{\star}$$

where Γ^{A}_{in} is its input reflection coefficient.

When studying the input series inductance L_g in section 4.1, the only assumption made is linearity; since (3.49) is not satisfied, the conclusions of section 3.4 do not apply.

This result is quite obvious but its implications are nevertheless important. A matching circuit as simple as L_g may achieve remarkable results in designing LNAs if paired with other components, such as the series feedback impedance applied to the second stage. Series feedback can be optimised in order to achieve good noise and signal performances and the input inductance L_g obtained with (4.11) can tune out the reactive part of $Z_{S_{opt}}$. Ideally, L_g affects neither the minimum noise figure nor the real part of the optimum source impedance $Z_{S_{opt}}$ of the overall network. This fact explains why a really lossy L_g can produce remarkable low noise performances.

This procedure is quite general and can be applied to any black box as long as a set of noise parameters is available. It allows the SSNM condition to be achieved at the input plane, not at the plane between L_g and second stage (Figure 4.1): it is very important to know where the SSNM condition is required. Conclusions in section 3.4 suggest that an input matching circuit is to be avoided if SSNM conditions and small $| \Gamma_{S_{opt}} |$ are required. This stems from the fact that noise parameters of cascaded stages combine non–linearly (3.46) and the design of the overall network becomes difficult. However, a simple input network such as L_g can still be manageable for design purposes.

Low noise designs should not be split into single steps because noise contributions from each stage do not combine linearly. Therefore, the challenge for the LNA designer is to find a suitable and useful approach to the whole network to be designed and consider it as one single item.

4.5 Conclusion

This chapter has studied the influence of an input series inductance L_g on the noise performance of the amplifier to which it is applied. Similarities with the results of the analysis of series feedback networks have been highlighted. A lossy series inductor has been applied to the well–known Pospieszalski noise model. A discussion has highlighted the influence of L_g on $Z_{S_{opt}}$. Suggestions for determining parameters of this model have been made. The use of both L_g and series feedback has been discussed in order to design for SSNM condition. The L_g analysis improves significantly the understanding of the different impact of L_s and L_g on the intrinsic device performance. It also allows for the first time the imaginary part of the correlation impedance Z_c to be linked to an external component controllable by the designer. The extension of the Pospieszalski noise model provides new and original insights on the transistor noise performance and supports an empirical expression introduced by Byzery. Future experimental work should verify the suggestions of this chapter.

Chapter 5

Design for Simultaneous Signal and Noise Match

An analytical approach to the solution of the simultaneous signal and noise matched (SSNM) requirement with feedback amplifiers is presented. The discussion that follows leads to the development of original techniques for optimum noise reflection coefficient $\Gamma_{S_{opt}}$ design. To the author's knowledge, no procedures for noise parameter design have been devised previously. The new methods are described in detail and some case studies discussed. Finally, experimental results demonstrate the theory.

5.1 Design for Noise Performance

The analytical approach to SSNM feedback LNA design is based on the expressions developed for the noise parameters in chapter 3; full advantage is taken of having closed form expressions.

Consider the feedback amplifier in Figure 5.1. The noise parameters as functions of the feedback elements Z_s and Y_p are given in chapter 3, (3.31), (3.32) and (3.33). The signal behaviour can be described by different matrices [128]; the impedance representation $\mathbf{Z}_n$ is used, because it has already been worked out in chapter 3, section 3.1, (3.22). Its expression is rewritten here:

$$\mathbf{Z}_n = [\mathbf{Z}_t + \mathbf{Z}_s]\,[\mathbf{1} + \mathbf{Y}_p\,(\mathbf{Z}_t + \mathbf{Z}_s)]^{-1} \tag{5.1}$$

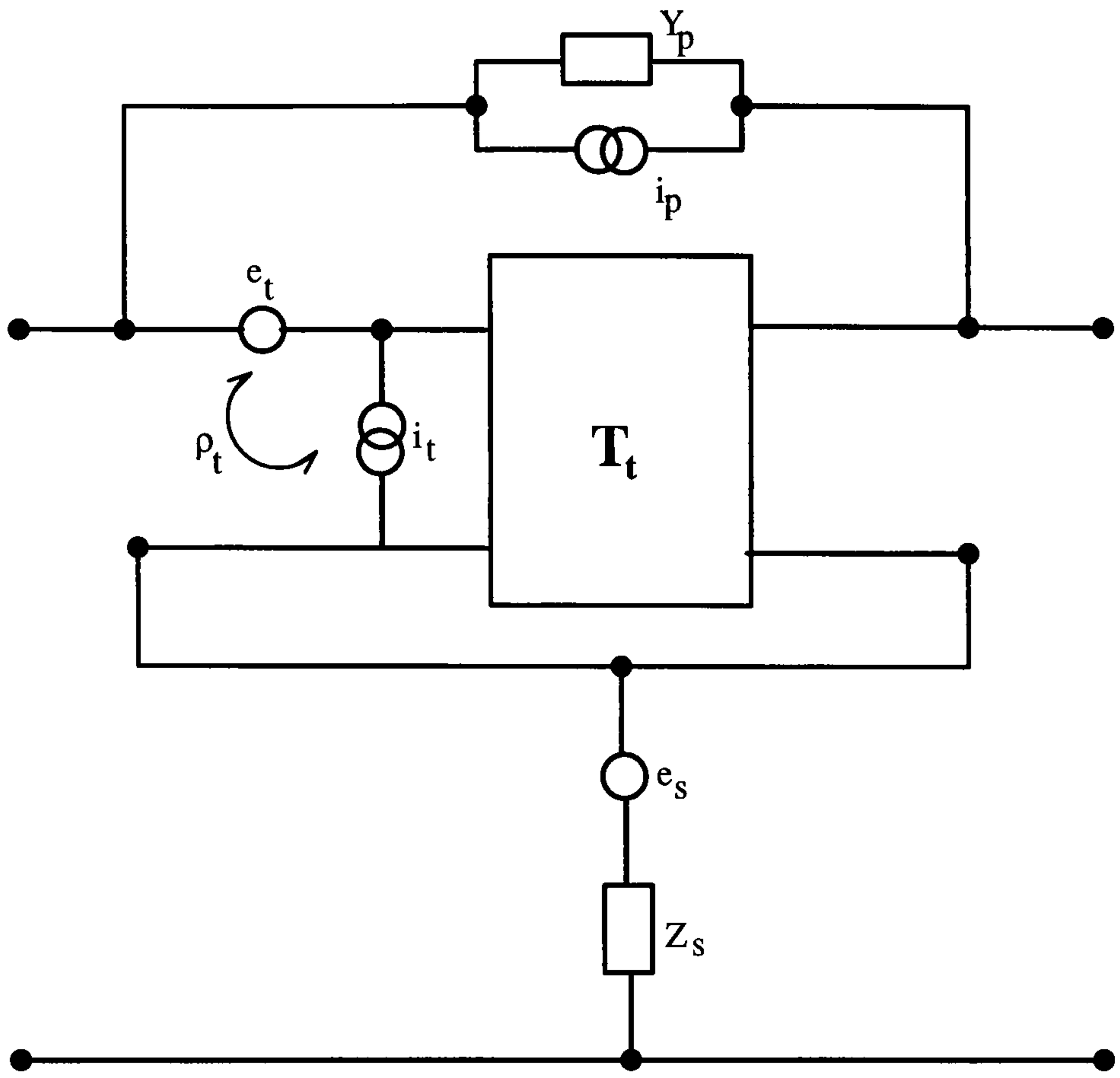

Figure 5.1 Feedback LNA for SSNM design

$\mathbf{Z}_n$ is a function of both series Z_s and parallel Y_p feedback immittances through $\mathbf{Z}_s$ (3.15) and $\mathbf{Y}_p$ (3.16) matrices. The elements of (5.1) can be expanded and the resulting expressions coupled with the noise parameter expressions. These equations form a non-linear system in the unknowns Z_s and Y_p. The solution – if any – is the set of feedback elements that can satisfy the required signal and noise performance. This simple idea is named *full system design* and it is developed and discussed. The full system design is one possible and straightforward approach to the solution of the SSNM requirement.

5.1.1 Full system Design

The full system design allows two (complex) specifications to be achieved simultaneously, since the feedback network of Figure 5.1 can provide two complex feedback elements. In order to focus on the SSNM design, the required conditions deal with the optimum noise source admittance $Y_{S_{opt}}$ and the input impedance Z_{in} at the design frequency f_o.

The input impedance depends on the load impedance Z_L at the output port; Z_L is a parameter that the designer may set separately. $Y_{S_{opt}}$ is independent of the load [51]. In fact, Z_L constitutes a third complex degree of freedom within the SSNM constraint. Once the solution has been worked out, a power mismatch at the plane between the load Z_L and the output port of the device is likely to occur, since the full system design as it is being described, does not set that quantity. It is important to be aware that the full system design deals with only two conditions simultaneously: nothing can be said about other quantities of the network such as gain, output return loss, etc.

The full system design unknowns are:

$$r_s = \Re e\left[\frac{Z_s}{Z_o}\right] \quad (5.2.a)$$

$$x_s = \Im m\left[\frac{Z_s}{Z_o}\right] \quad (5.2.b)$$

$$g_p = \Re e\left[\frac{Y_p}{Y_o}\right] \quad (5.2.c)$$

$$b_p = \Im m\left[\frac{Y_p}{Y_o}\right] \quad (5.2.d)$$

$Z_o = 1/Y_o$ is a normalising impedance. In order to take into account different load impedances, Z_o is assumed to be equal to the given load:

$$Z_o = \frac{1}{Y_o} = Z_L \quad (5.3)$$

Since the load impedance is, in general, a complex number at the design frequency f_o, attention must be paid to the definition of the set (5.2). In fact, the actual unknowns are the real and imaginary parts of the feedback elements Z_s and Y_p; the set (5.2) reduces to the actual unknowns if $\Im m\,[Z_o] = 0$. In case this condition does not hold, then (5.2.a), ..., (5.2.d) are linear combinations of the actual unknowns, whose coefficients are related to the real and imaginary parts of the load (5.3). From now on, the full system design is discussed with (5.2) normalised to a real load Z_o – for instance 50 Ω. The expressions for the noise parameters are not affected by the nature of Z_o because they have been obtained in terms of $\Re e\,[Z_s]$, $\Im m\,[Z_s]$, $\Re e\,[Y_p]$ and $\Im m\,[Y_p]$.

Condition on $Y_{S_{opt}}$

Any optimum noise admittance $Y_{S_{opt}} = G_{S_{opt}} + j\,B_{S_{opt}}$ can be rewritten as [18]:

$$G_c^2 + \frac{G_n}{R_n} = G_{S_{opt}}^2 \quad (5.4.a)$$

$$-B_c = B_{S_{opt}} \quad (5.4.b)$$

The correlation admittance $Y_c = G_c + j\, B_c$ can be expressed in terms of the elements of the correlation matrix (transmission form):

$$Y_c = \rho_n \sqrt{\frac{g_n}{R_n}} = \rho_n \, \frac{\sqrt{g_n\, R_n}}{R_n} = \frac{\rho_{n_o}}{R_n} \tag{5.5}$$

where $\rho_{n_o} = \rho_n \sqrt{g_n\, R_n}$.

The uncorrelated equivalent noise conductance G_n for the transmission representation of any noisy 2–port network is given in terms of the noise source powers proportional to R_n, g_n and the correlation admittance Y_c (5.5):

$$\begin{aligned} G_n &= g_n - \mid Y_c \mid^2 R_n && (5.6.a) \\ \frac{G_n}{R_n} &= \frac{g_n}{R_n} - \mid Y_c \mid^2 \\ &= \frac{g_n}{R_n} - \frac{\mid \rho_{n_o} \mid^2}{R_n^2} \\ &= \frac{g_n\, R_n - \mid \rho_{n_o} \mid^2}{R_n^2} && (5.6.b) \end{aligned}$$

If (5.5) and (5.6.b) are substituted into (5.4.a), a system equivalent to (5.4) is obtained:

$$\begin{aligned} g_n &= \mid Y_{S_{opt}} \mid^2 R_n && (5.7.a) \\ \Im m\, [\rho_{n_o}] &= -B_{S_{opt}}\, R_n && (5.7.b) \end{aligned}$$

The terms R_n, g_n and ρ_{n_o} as functions of the feedback elements Z_s and Y_p have been defined in (3.31), (3.32) and (3.33) respectively.

Condition on Z_{in}

The condition on the input impedance for a desired value of Z_{in} is straightforward. Once the load $Z_L = Z_o$ is defined by (5.3), simple circuit theory [15], [87] provides the required condition for the full system design:

$$\frac{Z_{n_{11}}\, Z_o + \Delta_Z}{Z_{n_{22}} + Z_o} = Z_{in} \tag{5.8}$$

where Δ_Z is the determinant of the impedance matrix (5.1).

5.1.2 Discussion of the Full System Design Approach

The full system approach for SSNM feedback amplifier design consists of the sets (5.7) and (5.8) to be solved simultaneously:

$$\Im m\left[\rho_{n_o}\right] = -\left(\Im m\left[Y_{S_{opt}}\right] Z_o\right)\left(R_n Y_o\right) \qquad (5.9.a)$$
$$\left(g_n Z_o\right) = \frac{|Y_{S_{opt}}|^2}{|Y_o|^2}\left(R_n Y_o\right) \qquad (5.9.b)$$
$$z_{11} + \Delta_{z_n} = z_{in}\left(z_{22}+1\right) \qquad (5.9.c)$$

where $z_{in} = Z_{in}/Z_o$, $z_{ij} = Z_{n_{ij}}/Z_o$ are the terms of (5.1) normalised to the (real) load Z_o (5.3) and Δ_{z_n} is its normalised determinant.

Once $Y_{S_{opt}}$ and Z_{in} have been set by the designer along with the load Z_L, (5.9) can be solved. For instance, typical SSNM requirements are:

$$Y_{S_{opt}} = 20 \text{ mS}$$
$$Z_{in} = 50\ \Omega$$

which make (5.9) equivalent to $\Gamma_{S_{opt}} = S_{11}{}^{\star} = 0$. A remarkable consequence is that no input matching circuit is required.

Even if the approach is strictly correct, it has not been developed further for the following reasons:

1. the goal is to achieve the SSNM condition along with some gain from the LNA. The numerical results from chapter 3 suggest that the SSNM condition can be accomplished with feedback amplifiers; however, the required series feedback value may be quite large and the gain is influenced dramatically;

2. if the network to be designed with the full system approach exists, every parameter such as the minimum noise figure is affected. Since a solution to (5.9) implies the presence of a conductance $G_p = \Re e\left[Y_p\right]$ in the parallel branch, F_{min} is likely to worsen with respect to the minimum noise figure of the device;

3. the choice of Z_L is an open issue. Since Z_L is a parameter, solutions should be found for different values of Z_L in order to check for the best solution which, for instance, corresponds to high gain and small minimum noise figure.

The full system design seems to require a very careful study, which is open to further investigation. Instead, a simplified approach has been devised.

5.2 $\Gamma_{S_{opt}}$ Design

The full system design (5.9) consists of 2 complex equations: the first one defines the optimum noise source admittance (or equivalently the optimum source reflection coefficient $\Gamma_{S_{opt}}$) and the second one, the input impedance Z_{in}. The influence of the load has been stressed throughout the definition of the full system design: it is a further degree of freedom [51] which can be set independently to achieve the SSNM condition:

$$\Gamma_{in}\left(\Gamma_L^{SSNM}\right) \;=\; \Gamma_{S_{opt}}{}^{\star} \tag{5.10}$$

Γ_L^{SSNM} is the value of the load which delivers the simultaneous match at the input port; it has been defined in (3.44), chapter 3. Assuming the value of $\Gamma_{S_{opt}}$ has been synthesised, (5.10) defines Γ_L^{SSNM} in order to achieve the SSNM condition; providing (5.10) is fulfilled, an input matching circuit transforms input and optimum noise source impedances in the same way; if $\mid \Gamma_{S_{opt}} \mid < 0.1$ in (5.10), an input matching circuit is not strictly necessary.

The full system design needs the boundary conditions to be set, in particular Z_L; under that constraint, the feedback immittances affect every element of the signal matrix (5.1). Disposing of (5.9.c) simplifies the SSNM design because it allows Z_L to be determined with (5.10) after the final feedback network has been obtained.

Two solutions to the SSNM problem which take full advantage of (5.9.a) and (5.9.b) coupled with (5.10) at the design frequency f_o are described.

5.2.1 Complex $\Gamma_{S_{opt}}$ Design

The solution of (5.9.a) and (5.9.b) for feedback amplifiers is outlined [139]. Substituting the expressions for R_n (3.31), g_n (3.32) and ρ_{n_o} (3.33) found in chapter 3 into (5.9.a) and (5.9.b) allows their expansion to be carried out. The final result is:

$$\begin{aligned}
& kA_{11}\, g_p x_s^2 + kA_{11}\, g_p r_s^2 \\
+ \quad & kA_{10}\, r_s^2 + kA_{10}\, x_s^2 + (kA_{21} + D_{rg})\; r_s g_p + (kA_{31} + D_{xg})\; g_p x_s + D_{xb}\, x_s b_p \\
+ \quad & D_{rb}\, r_s b_p + (kA_{20} + D_r)\; r_s + (kA_{30} + D_x)\; x_s + (kA_{41} + D_g)\; g_p + D_b\, b_p \\
+ \quad & (kr_{t_n} + D_o) = 0
\end{aligned} \tag{5.11.a}$$

$$\begin{aligned}
& qA_{11}\, g_p x_s^2 + qA_{11}\, g_p r_s^2 - B_{11}\, r_s b_p^2 - B_{11}\, r_s g_p^2 \\
+ \quad & qA_{10}\, r_s^2 - B_{10}\, g_p^2 + qA_{10}\, x_s^2 - B_{10}\, b_p^2 + (qA_{21} - B_{21})\; r_s g_p - B_{31}\, r_s b_p
\end{aligned}$$

$$+ \quad qA_{31}\, g_p x_s + (qA_{20} - B_{41})\, r_s + qA_{30}\, x_s + (qA_{41} - B_{20})\, g_p - B_{30}\, b_p$$
$$+ \quad (qr_{t_n} - g_{t_n}) = 0 \qquad (5.11.b)$$

The unknowns are r_s (5.2.a), x_s (5.2.b), g_p (5.2.c) and b_p (5.2.d), normalised to the real impedance Z_o. The coefficients have been published in [139]: they depend on the noise and signal parameters of the (active) network in Figure 5.1. The designer sets the desired value of complex $\Gamma_{S_{opt}}$ so that the coefficients:

$$\begin{aligned} k &= \Im m\left[Y_{S_{opt}}\right] Z_o \\ q &= \left(\mid Y_{S_{opt}} \mid Z_o\right)^2 \end{aligned}$$

are fixed.

Some features of (5.11) are pointed out;

1. the set of equations is valid for any linear 2–port network whose signal and noise performance is known at the frequency f_o;
2. a solution guarantees that the given $\Gamma_{S_{opt}}$ is achieved but nothing can be stated about other parameters of the circuit;
3. the system is nonlinear in the unknowns; and
4. there are more unknowns (four) than equations (two).

It is important to recognise that this procedure is not directly dependent on the frequency f_o and is independent of what the 2–port black box contains. These results can be applied to any type of device (e.g. BJTs or FETs), or even passive networks. It is up to the designer to assess the performance of the stage and to decide whether this technique can meet the required specifications. Apart from designer's considerations, (5.11) is, to the author's knowledge, the first and only analytical procedure available for the design of a noise parameter such as $\Gamma_{S_{opt}}$. Extensions to other noise parameters can be devised and is left for further investigation.

5.2.2 Case Studies for the Complex Design

(5.11) is solved after setting two of the four unknowns to zero and substituting one equation into the other one. Doing this yields a single polynomial in one unknown which can be easily solved. Table 5.1 tabulates the maximum number of solutions expected from (5.11).

Table 5.1 Maximum number N_s of solutions after setting a pair of unknowns to zero in (5.11); the symbol X shows the selected unknowns.

r_s	x_s	g_p	b_p	N_s
X	X	–	–	2
X	–	X	–	6
X	–	–	X	5
–	X	X	–	6
–	X	–	X	4
–	–	X	X	2

The normalised components r_s, x_s, g_p and b_p are ideal. For instance, the solution $(x_s; b_p)$ does not take into account the quality factor of the reactive elements, which is a limitation. However, it can be overcome as it will be shown later on.

Table 5.2 collects some of the available solutions with (5.11) when $\Gamma_{S_{opt}} = 0.1e^{j\,45\,deg}$ is required from a HP ATF21186 MESFET; no special reason is related to this choice, in particular as far as the phase of $\Gamma_{S_{opt}}$ is concerned.

Table 5.2 Some of the solutions achievable with ATF21186 at 1 GHz for $\Gamma_{S_{opt}} = 0.1e^{j\,45\,deg}$ ($Z_o = 50\ \Omega$) and corresponding minimum noise figure F_{min}, available gain G_{av} and noise measure M. The first row shows the device performance without feedback; a negative noise measure is related to $G_{av} < 1$.

R_s/Z_o	X_s/Z_o	$G_p \cdot Z_o$	$B_p \cdot Z_o$	F_{min} dB	G_{av} dB	M
0	0	0	0	0.55	15.1	0.16
0.0266	3.2737	0	0	0.46	4.9	0.26
0.5864	0	0.7551	0	17.5	-13.8	-14.17
$1.6505\ 10^3$	0	0	6.1704	0.01	0.0	∞
0	0.3492	0.2466	0	3.49	4.5	3.05
0	3.1565	0	-0.0890	0.50	9.4	0.18
0	0	0.3219	-0.2325	4.57	5.0	4.26

Some features, typical of feedback amplifiers, can be recognised: pure parallel feedback $(g_p; b_p)$ degrades both noise and gain performance; resistive parallel feedback G_p increases the minimum noise figure and decreases the gain. The solutions $(r_s; b_p)$ and $(r_s; g_p)$ are not acceptable in practice because of the gain drop. The most interesting case corresponds to the pair $(x_s; b_p)$ and $(r_s; x_s)$. The former delivers the highest gain in Table 5.2 and decreases the minimum noise figure; the latter decreases F_{min} in spite of a lossy component R_s in the feedback branch. This can be predicted with the R_n circles (chapter 3, section 3.3.1) and confirms that result.

The results of Table 5.2 are remarkable: they demonstrate that real feedback impedances do not always degrade the LNA noise performance. For the first time, a theory allows the designer to control real, lossy feedback components and to visualise them with the help of the R_n circles (chapter 3, section section 3.3.1). This should be a welcomed step forward in circuit theory because no ideal, lossless components exist.

The trade–offs between gain and noise performances are best described by the noise measure defined as:

$$M = \frac{F-1}{1-1/G_{av}} \tag{5.12}$$

where F is the noise figure and G_{av} the available gain. Table 5.2 reports the value for the noise measure. As expected [14], [52], when lossless elements such as $(x_s; b_p)$ embed the device, the noise measure is constant and equal to the value of the device without feedback; when the solution $(r_s; x_s)$ is used, the noise measure increases.

The HP ATF10136 and HP ATF35176 MESFETs are used to exemplify the design for two optimum reflection coefficients, $\Gamma_{S_{opt}} = \pm 0.1$. This magnitude ensures that the SSNM condition yields 20 dB input return loss. The phase of $\Gamma_{S_{opt}}$ (± 180 deg), the design frequency f_o and the solving pair of components are chosen arbitrarily.

HP ATF10136 MESFET

The design objectives at $f_o = 6$ GHz are $\Gamma_{S_{opt}} = 0.1\angle 0$ deg and $\Gamma_{S_{opt}} = 0.1\angle 180$ deg. A pure reactive solution $(x_s; b_p)$ is used to deliver the required optimum reflection coefficient. The results are tabulated in Table 5.3: they are the complete set of acceptable solutions out of the $N_s = 4$ available (Table 5.1) for the given goals; two of them are complex values and therefore unacceptable. Figure 5.2 shows some noise parameters associated with case B, Table 5.3.

Table 5.3 Design for complex $\Gamma_{S_{opt}} = \pm 0.1$ at 6 GHz with HP ATF10136 MESFET. The solutions make use of reactive series and parallel feedback elements; G_T is the transducer power gain when the load is Γ_L^{SSNM}.

Case	$\Gamma_{S_{opt}}$	L_s nH	or	C_s pF	C_p pF	F_{min} dB	R_n Ω	$\mid\Gamma_L^{SSNM}\mid$	G_T dB
A	+0.1	·		0.03	20.37	0.01	0.04	0.09	-0.01
B	+0.1	10.81		·	9.10	0.01	0.19	0.11	0.06
C	-0.1	·		0.04	23.15	0.01	0.03	0.11	-0.01
D	-0.1	4.97		·	6.34	0.04	0.39	0.12	0.17

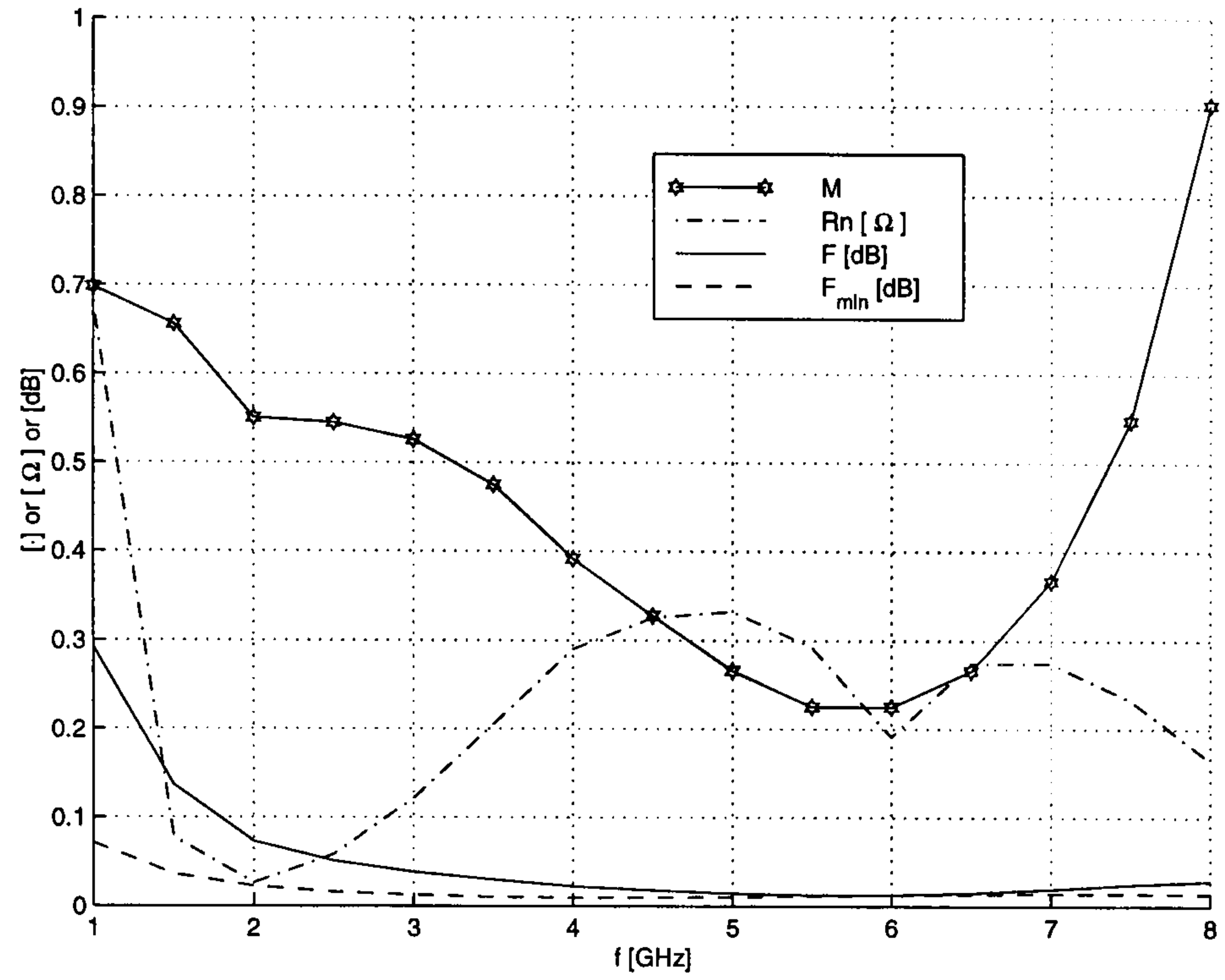

Figure 5.2 HP ATF10136 MESFET signal and noise parameters for Table 5.3, case B: $X_s = 2\pi f_o\, 10.81$ nH and $B_p = 2\pi f_o\, 9.10$ pF ($f_o = 6$ GHz). Notice that small values of noise measure M are associated with good LNAs.

HP ATF35176 MESFET

The design objectives at $f_o = 10$ GHz are again $\Gamma_{S_{opt}} = 0.1\angle 0$ deg and $\Gamma_{S_{opt}} = 0.1\angle 180$ deg. The solutions make use of the pair $(r_s; x_s)$; they are detailed in Table 5.4. Similar considerations as for the ATF10136 apply to the number of solutions N_s: in this case, one yields $R_s < 0$. Figure 5.3 shows some signal and noise parameters vs frequency for case B, Table 5.4.

Table 5.4 Series impedances for complex $\Gamma_{S_{opt}} = \pm 0.1$ with HP ATF35176 MESFET at 10 GHz. G_T is the transducer power gain (load impedance corresponding to Γ_L^{SSNM}).

Case	$\Gamma_{S_{opt}}$	R_s	L_s	F_{min}	R_n	$\mid\Gamma_L^{SSNM}\mid$	G_T
	–	Ω	nH	dB	Ω	–	dB
A	+0.1	10.67	0.58	1.27	9.52	0.89	0.17
B	-0.1	3.72	0.51	0.99	4.35	0.78	4.08

In order to show how different the final performance of the feedback network may be, the design for $\mid\Gamma_{S_{opt}}\mid = 0.1$ at 10 GHz with the HP ATF35176 MESFET is carried out for 8 different phases. The numerical results are tabulated in Table 5.5 and represented in

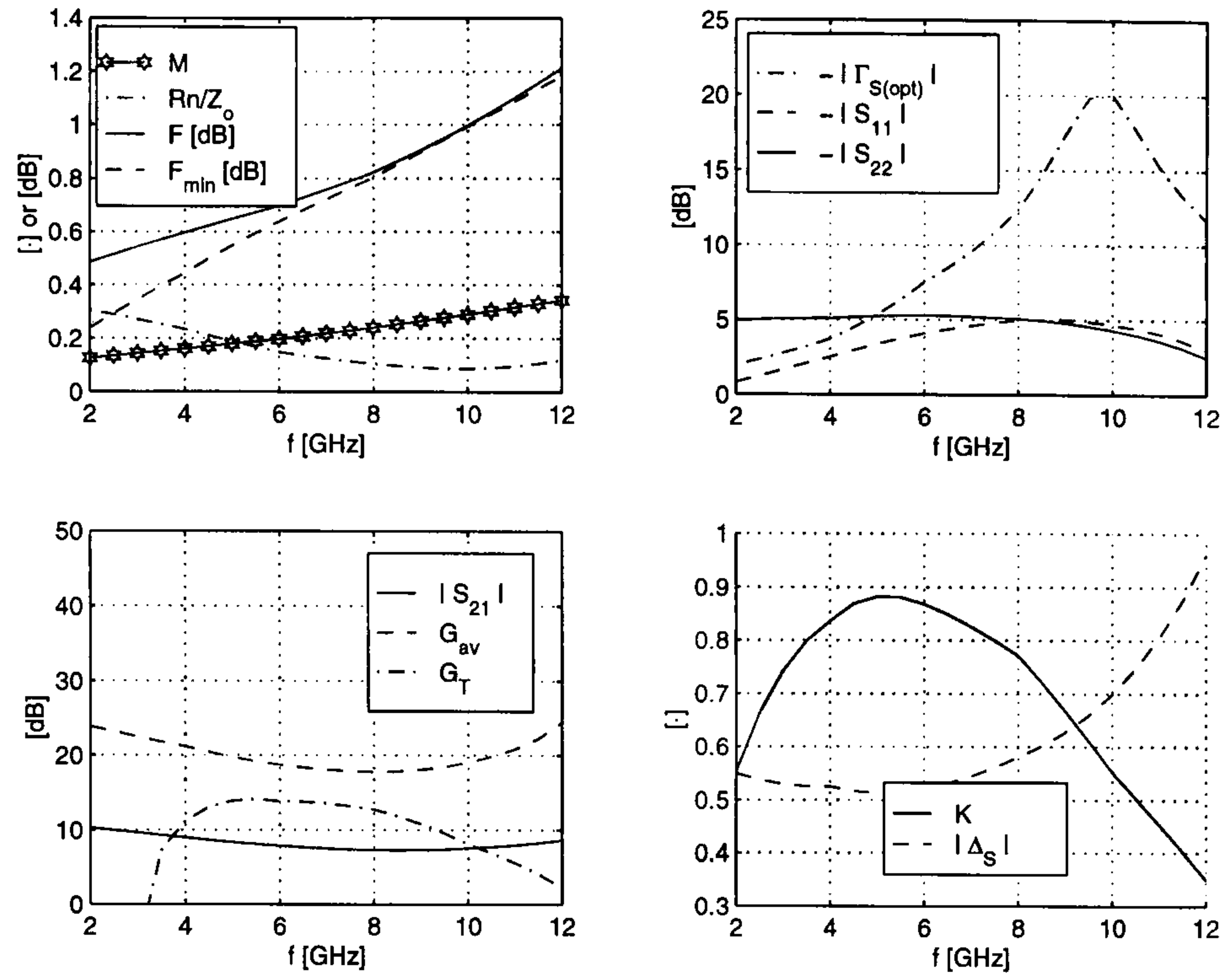

Figure 5.3 Signal and noise parameters for HP ATF35176 MESFET, case B in Table 5.4: $R_s = 3.72\ \Omega$ and $X_s = 2\,\pi\,f_o\,0.51$ nH ($f_o = 10$ GHz, $Z_o = 50\ \Omega$)

Figure 5.4. The figure demonstrates that a careful investigation should be carried out when choosing the optimum source reflection coefficient.

5.2.3 Discussion of the Case Studies

The previous examples show the wide range of possible results that the procedure can produce. The case studies have been carried out at 3 different frequencies since the design for $\Gamma_{S_{opt}}$ is not constrained by frequency. Results are reliable as long as linearity is verified and demonstrate that the SSNM condition can be achieved by feedback networks.

A common feature of Figure 5.2, Figure 5.3 and Figure 5.4 is that $\Gamma_{S_{opt}}$ magnitude as small as 0.1 is ensured. Consequently, the mismatch term:

$$\mid \Gamma_S - \Gamma_{S_{opt}} \mid^2$$

in the Friis formula [19] is very small (equal to 0.1^2 at f_o when $\Gamma_S = 0$) and the condition

$$F \approx F_{min}$$

Table 5.5 Minimum noise figure vs different phases for a constant optimum reflection coefficient $\mid \Gamma_{S_{opt}} \mid = 0.1$ design at $f_o = 10$ GHz with HP ATF35176 MESFET. The design is carried out with a series impedance $Z_s = R_s + j\,2\,\pi\,f_o\,L_s$.

$\mid \Gamma_{S_{opt}} \mid$	$\angle\,\Gamma_{S_{opt}}$	R_s	L_s	F_{min}
–	deg	Ω	nH	dB
0.1	0	10.67	0.58	1.27
0.1	45	9.33	0.41	1.24
0.1	90	6.43	0.36	1.13
0.1	135	4.44	0.41	1.04
0.1	180	3.72	0.51	0.99
0.1	-135	4.16	0.62	1.01
0.1	-90	5.84	0.71	1.08
0.1	-45	8.66	0.71	1.19

can be assumed. The final value of F_{min} is different as compared to the value of the single device: it increases when lossy parallel feedback elements are used (Table 5.2), it may decrease while the gain is not badly affected (Table 5.2), it may become very small (Table 5.3, case B: $F_{min} \approx 0.01$ dB with feedback elements compared to 0.80 dB for the device only) but without any gain left ($G_T \approx 0.06$ dB when $\Gamma_L = \Gamma_L^{SSNM}$).

Case A and B, Table 5.3, are very interesting. The attention is focused on case B because the available gain is larger than 1, while in case A is not. Although no transducer power gain is left after applying the feedback, some interesting numerical results can be pointed out. The noise measure of the device without any feedback elements is:

$$\begin{aligned} \mathrm{M} &= 0.70 \quad \text{when } \Gamma_S = 0; \\ \mathrm{M} &= 0.22 \quad \text{when } \Gamma_S = \Gamma_{S_{opt}}. \end{aligned}$$

Γ_S is the source reflection coefficient loading the input port of the device; its value affects both noise figure and available gain, which define the noise measure (5.12).

When the feedback reactive elements are applied, the scattering parameters of the stage at $f_o = 6$ GHz are:

$$\begin{aligned} S_{11} &= 0.03 \quad \angle\,97.10 \quad \text{deg} \\ S_{12} &= 0.99 \quad \angle\,5.19 \quad \text{deg} \\ S_{21} &= 1.01 \quad \angle\,5.09 \quad \text{deg} \\ S_{22} &= 0.03 \quad \angle\,93.80 \quad \text{deg} \end{aligned}$$

These numbers show that the stage is very close to a reciprocal ($S_{12} \approx S_{21}$) and symmetrical ($S_{11} = S_{22}$) network. Furthermore, the noise parameters are:

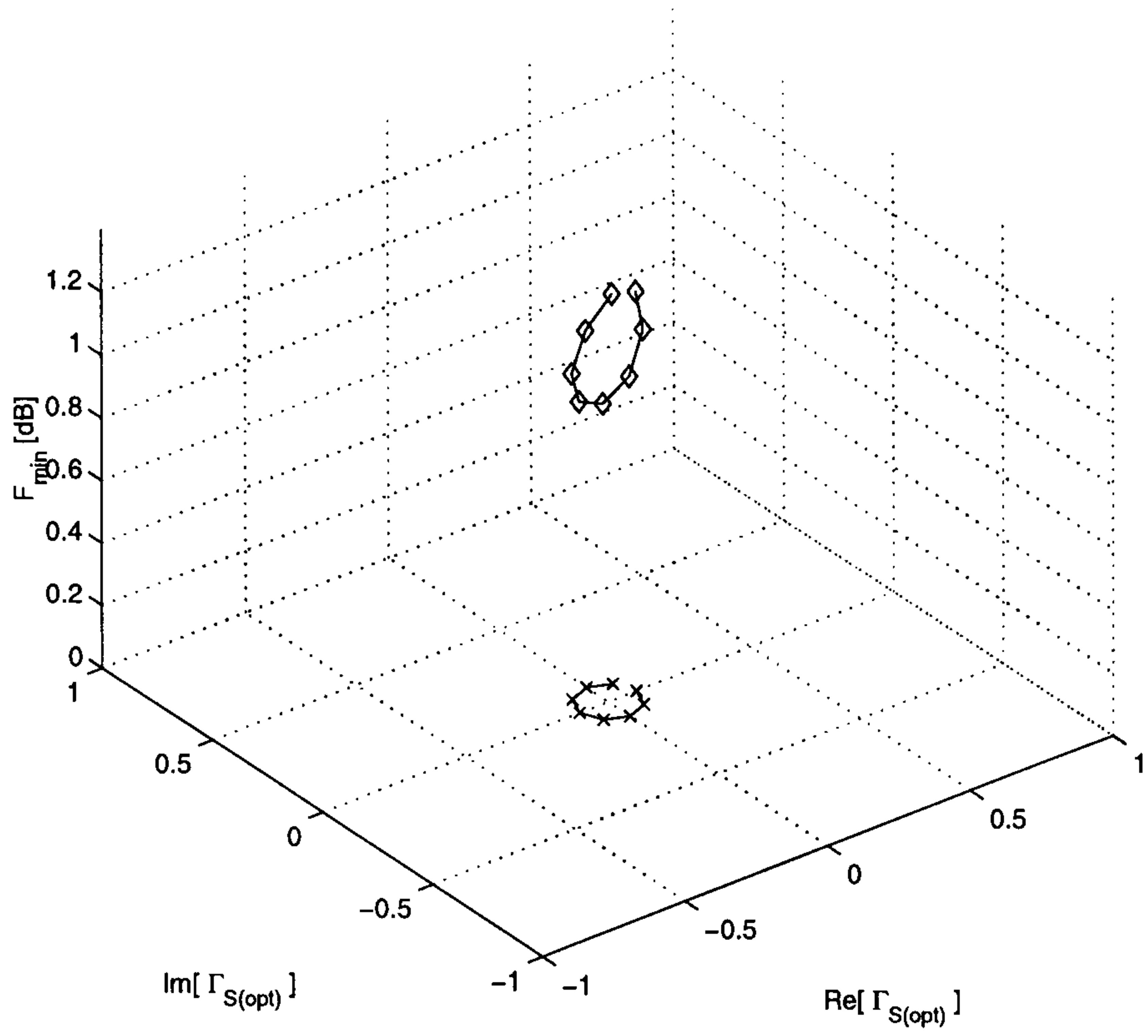

Figure 5.4 Graphic representation of Table 5.5 solutions. The X–marks represent the locus $|\ \Gamma_{S_{opt}} \ |= 0.1$ for 8 different phases; the diamonds are the corresponding minimum noise figure values.

$$\begin{aligned} F_{min} &= 0.01 \qquad\quad \text{dB} \\ \Gamma_{S_{opt}} &= 0.1 \quad \angle\, 0 \quad \text{deg} \\ R_n &= 0.19 \qquad\quad \Omega \end{aligned}$$

Since the stage has both S_{11}, S_{22} and $\Gamma_{S_{opt}}$ smaller or equal to 0.1 (or -20 dB), 50 Ω load at the output port guarantees that $|\ \Gamma_{in}\ |\approx|\ \Gamma_{S_{opt}}\ |\leq 0.1$. What is remarkable is that the stage is almost noiseless ($F_{min} \approx 1$ or 0 dB); and the noise measure is:

$$\begin{aligned} \text{M} = 0.2247 &\quad \text{when } \Gamma_S = 0; \\ \text{M} = 0.2240 &\quad \text{when } \Gamma_S = \Gamma_{S_{opt}}, \end{aligned}$$

which is nearly independent of the source reflection coefficients for either maximum gain or minimum noise figure since a SSNM stage has been designed. Given that the noise measure is constant when reactive elements embed a device [14], [52] and the available gain drops to 1 (0 dB), then the noise figure (or equivalently the minimum noise figure for SSNM stages) must tend to 1 (0 dB).

Case B, Table 5.3, demonstrates that the equivalent noise resistance R_n for the feedback network can achieve a value smaller than $R_{n_{min}}$, the minimum value when reactive series feedback impedance ($Z_s = j\,X_s$ and $Y_p = 0$) is used. $R_{n_{min}}$ for the ATF10136 MESFET is 5.87 Ω at 6 GHz with a series 5.81 pF capacitor; other parameters when this feedback is used are:

available gain	$\Rightarrow$	G_{av}	=	10.56			dB
load for SSNM condition	$\Rightarrow$	Γ_L^{SSNM}	=	0.42	$\angle$	-61.11	deg
transducer power gain with Γ_L^{SSNM}	$\Rightarrow$	G_T	=	9.42			dB
stability (Rollett) factor	$\Rightarrow$	K	=	0.96			
scattering matrix determinant	$\Rightarrow$	$\mid \Delta_S \mid$	=	0.61			
scattering matrix elements	$\Rightarrow$	S_{11}	=	0.51	$\angle$	154.01	deg
		S_{12}	=	0.19	$\angle$	-14.68	deg
		S_{21}	=	2.96	$\angle$	10.60	deg
		S_{22}	=	0.07	$\angle$	37.38	deg
minimum noise figure	$\Rightarrow$	F_{min}	=	0.80			dB
equivalent noise resistance	$\Rightarrow$	R_n	=	5.87			Ω
optimum noise source refl. coeff.	$\Rightarrow$	$\Gamma_{S_{opt}}$	=	0.36	$\angle$	179.54	deg

The point here is that two reactive elements are used instead of one. The analysis on $R_{n_{min}}$ deals with the reactive part of the series feedback element; R_n circles expand the analysis on the series impedance plane. A mix of reactive and susceptive immittances can modify the behaviour of the given 2–port network in order to achieve a desired condition (for instance, $S_{12} = 0$ [48]). Therefore, it is sensible to accept the fact that one parallel capacitance and one series reactance can make $F_{min} \approx 1$ or $S_{21} = S_{12}$ at the expense of other parameters. The absolute minimum for R_n could be found if:

$$dR_n = \sum_{q=1}^{4} \frac{\partial R_n}{\partial \chi_q}\, d\chi_q = 0 \tag{5.13}$$

is investigated; χ_q are the unknowns R_s, X_s, G_p and B_p when $q = 1, \ldots, 4$ respectively. Since the solution which corresponds to small F_{min} is preferred, the specific solution of (5.13) for $R_s = G_p = 0$ (no thermal noise added by the feedback elements) can be investigated. That solution makes use of reactive components only, namely $(X_{s_o}; B_{p_o})$; they satisfy:

$$\frac{\partial R_n}{\partial X_s}(X_{s_o}; B_{p_o}) = 0 \tag{5.14.a}$$

$$\frac{\partial R_n}{\partial B_p}(X_{s_o}; B_{p_o}) = 0 \tag{5.14.b}$$

Some of the acceptable solutions may correspond to maxima, some to points of inflection and some to minima in R_n. Since the expression of R_n as function of the feedback elements is known from chapter 3, (5.14) could be simplified by taking into account that R_n is a ratio of polynomials. The R_n circles (chapter 3, section 3.3.1) demonstrate that lossy feedback impedances can lower R_n as well as F_{min} (Table 5.2) at the expense of the noise measure. The system with either $(R_s; X_s)$ or $(R_s; X_s; B_p)$ as unknowns could be worthwhile investigating. However, the exact solution of (5.13) or (5.14) has not been attempted.

The experience based on the R_n analysis (chapter 3) and the design for $\Gamma_{S_{opt}}$ (Figure 5.2 and Figure 5.3) suggests that small magnitudes of $\Gamma_{S_{opt}}$ occur in the neighbourhood of $R_{n_{min}}$.

Figure 5.3 shows that the stability factor K [83] is smaller than 1 at the design frequency f_o, even if stability improves from the value relative to the single device. Reactive elements bring K very close to 1 but never above that threshold.

For a constant magnitude (Table 5.5), $\angle \Gamma_{S_{opt}} = 180$ deg seems to ensure higher gain to MESFETs and lower noise figure in comparison with the results obtained when other phases are selected.

5.2.4 Real $\Gamma_{S_{opt}}$ Design

The SSNM design aims to obtain the simultaneous match condition:

$$SSNM = \Gamma_{in} - \Gamma_{S_{opt}}{}^{\star} = 0,$$

with the further constraint that the magnitude of the optimum noise source reflection coefficient $\Gamma_{S_{opt}}$, or equivalently the input port reflection coefficient Γ_{in}, is smaller than 0.1. This condition on Γ_{in} corresponds to 20 dB return loss. The value associated with the phase of $\Gamma_{S_{opt}}$ is not paramount if its magnitude is kept small enough. Furthermore, the measurement of complex input reflection coefficients with small magnitudes is not trivial [22] and accuracy degrades as far as phases are concerned.

A procedure concerned with the design of small magnitudes of $\Gamma_{S_{opt}}$ has been devised during the course of this study [139]. Consider again Figure 5.1 and assume that the goal is:

$$\mid \Gamma_{S_{opt}} \mid \leq \epsilon \leq 1 \tag{5.15}$$

where ϵ ranges between 0 and 1andrepresents the required magnitude. Limitations on the value of ϵ will be pointed out later on.

(5.15) can be switched to the normalised admittance plane:

$$\Gamma_{S_{opt}} = \frac{Y_o - Y_{S_{opt}}}{Y_o + Y_{S_{opt}}} = \frac{1 - y_{S_{opt}}}{1 + y_{S_{opt}}} \tag{5.16}$$

where $y_{S_{opt}} = Y_{S_{opt}}/Y_o$ is the optimum source admittance corresponding to $\Gamma_{S_{opt}}$, normalised to the real admittance Y_o. If (5.16) is substituted into (5.15),

$$| \, y_{S_{opt}} - C_\epsilon \, | \;\; \leq \;\; R_\epsilon \tag{5.17}$$

is obtained. Centre and radius are respectively:

$$C_\epsilon = \frac{1+\epsilon^2}{1-\epsilon^2} \tag{5.17.a}$$

$$R_\epsilon = \frac{2\epsilon}{1-\epsilon^2} \tag{5.17.b}$$

and they are functions of the required magnitude ϵ.

The expression of $Y_{S_{opt}} = G_{S_{opt}} + j\, B_{S_{opt}}$ has been developed in (5.4); it can be normalised to Y_o and substituted into (5.17) with the help of (5.5). The final expression is:

$$(g_n Z_o)^2 + f_\epsilon^2 \, (R_n Y_o)^2 - 2h_\epsilon \, (g_n Z_o) \, (R_n Y_o) + 4C_\epsilon^2 \Im m \, [\rho_{n_o}]^2 = 0 \tag{5.18}$$

where $Z_o = 1/Y_o$ and the functions f_ϵ and h_ϵ are:

$$f_\epsilon = C_\epsilon^2 - \eta R_\epsilon^2 \tag{5.18.a}$$

$$h_\epsilon = C_\epsilon^2 + \eta R_\epsilon^2 \tag{5.18.b}$$

η is a parameter ranging from 0 and 1. It defines a new radius $\eta\, R_\epsilon^2$ to take the place of R_ϵ^2 in (5.17) in order to transform the inequality into equation. η is indispensable for computer implementation.

(5.18) is equivalent to (5.15). Its parameters are taken directly from the correlation matrix of the feedback network in transmission representation. Furthermore, the noise parameters R_n, g_n and ρ_{n_o} as functions of the feedback elements Z_s and Y_p have been defined in (3.31), (3.32) and (3.33) respectively and their expressions can be substituted into (5.18) in order to obtain the solution. The input reflection coefficient Γ_{in} is then set equal to $\Gamma_{S_{opt}}$ by properly choosing the load with (5.10): that makes the magnitude of Γ_{in}

as small as the magnitude of $\Gamma_{S_{opt}}$: the design for the magnitude of $\Gamma_{S_{opt}}$ also sets the value of input return loss.

Since there is only one equation to solve, one feedback element is sufficient to achieve the desired performance for $\Gamma_{S_{opt}}$. This can be carried out by setting three out of the four available feedback components to zero; the solution for the important case of pure reactive series feedback ($Z_s = j\,X_s$, $Y_p = 0$) is developed in [139]; here, the same case is described with the further condition that the series feedback is lossy [140].

The design for the magnitude of the optimum source reflection coefficient $\Gamma_{S_{opt}}$ has been verified experimentally at 1 GHz: a SSNM LNA has been designed, fabricated and tested. It is described in section 5.3.

Real $\Gamma_{S_{opt}}$ Design with Lossy Series Reactive Components

The main assumption is that the value of the quality factor Q_s of the series reactance X_s is known at the design frequency f_o. Therefore, the series impedance Z_s can be written as discussed in chapter 4,

$$Z_s \;=\; \left(\frac{1}{Q_s} + j\right) X_s \tag{5.19}$$

Having defined:

$$Q_s = \frac{\Im m\,[Z_s]}{\Re e\,[Z_s]}$$

in (4.21), chapter 4, (5.19) allows $R_s = \Re e\,[Z_s]$ to be written as:

$$R_s \;=\; \frac{X_s}{Q_s} \tag{5.20}$$

at the design frequency. (5.20) associates the real part of Z_s with X_s through a known constant Q_s; the noise parameters (3.31), (3.32) and (3.33) can be rewritten with the help of (5.20) before substitution into (5.18) for numerical solution.

It is important to stress that this procedure is based on the assumption that the quality factor Q_s of the reactive component is known before solving (5.20). This may be a problem if Q_s varies rapidly as a function of the reactance at the given frequency f_o. Unless a common feature between Q_s and X_s is known (such as the number of turns if X_s is inductive) and (5.18) is expressed as a function of that common term, results may be misleading.

Assume that the reactive element is an inductance L_s [14], [52], [113], [117]. A starting value for X_s can be found by considering an ideal element ($Q_s \to \infty$); Table 5.2 suggests that the real part of Z_s should be small. The solution for X_s depends on Q_s: if the relationship between Q_s and X_s is known, then the procedure to find X_s can be reiterated until the solution of (5.18) is such that the reactive element provides Q_s when its value is X_s. Taking into account the quality factor Q_s may make the actual solution of (5.18) more time–consuming but the model becomes closer to reality.

5.2.5 Minimum in $\mid \Gamma_{S_{opt}} \mid$

The design for the magnitude of the optimum source reflection coefficient $\Gamma_{S_{opt}}$ requires to specify the maximum value ϵ of the desired $\mid \Gamma_{S_{opt}} \mid$. This value may be subjected to some constraints which (5.18) does not highlight. As a matter of fact, it has been noticed [139] that the magnitude of $\Gamma_{S_{opt}}$ has a minimum at the design frequency when reactive series feedback impedance is applied ($Z_s = j X_s$ and $Y_p = 0$). The method to determine this minimum $\mid \Gamma_{S_{opt}} \mid_{min}$ is outlined with an example.

Consider a Mitsubishi MGF4918E HEMT at $f_o = 8$ GHz in common source configuration [141]. Its scattering parameters are:

$$\begin{array}{rclcrl} S_{11} & = & 0.743 & \angle & -132.00 & \text{deg} \\ S_{12} & = & 0.094 & \angle & +6.60 & \text{deg} \\ S_{21} & = & 3.248 & \angle & +58.80 & \text{deg} \\ S_{22} & = & 0.351 & \angle & -108.70 & \text{deg} \end{array}$$

and its noise parameters:

$$\begin{array}{rclcrl} F_{min} & = & 0.43 & & & \text{dB} \\ \Gamma_{S_{opt}} & = & 0.59 & \angle & +120 & \text{deg} \\ R_n & = & 4.50 & & & \Omega \end{array}$$

$R_{n_{min}}$ is 1.32 Ω when a 0.60 nH series inductance ($X_s = 30.227\ \Omega$) is applied between source and ground. Signal and noise parameters with that reactance are:

$$\begin{array}{rclcrl} S_{11} & = & 0.491 & \angle & -74.10 & \text{deg} \\ S_{12} & = & 0.282 & \angle & +101.61 & \text{deg} \\ S_{21} & = & 2.190 & \angle & +56.75 & \text{deg} \\ S_{22} & = & 0.543 & \angle & -43.50 & \text{deg} \\ F_{min} & = & 0.39 & & & \text{dB} \\ \Gamma_{S_{opt}} & = & 0.466 & \angle & +179.82 & \text{deg} \\ R_n & = & 1.32 & & & \Omega \end{array}$$

The feedback amplifier is unstable (Rollett stability factor $K \approx 0.71$); the available gain is 9.08 dB; a series feedback reactance ($Z_s = 0 + j\,X_s$) is used to solve (5.18) [139].

If there is a minimum $|\,\Gamma_{S_{opt}}\,|_{min}$ in the magnitude of the optimum noise source reflection coefficient for $Z_s = j\,X_{s_{min}}$, then:

$$|\,\Gamma_{S_{opt}}\,|_{min} = \epsilon_{min} \leq \epsilon < 1.$$

Therefore, as an initial guess, assume that ϵ is equal to the given value of $|\,\Gamma_{S_{opt}}\,|$ at the design frequency f_o when no feedback is applied: for the MGF4918E,

$$\epsilon = |\,\Gamma_{S_{opt}}\,|_{(Z_s=0)} = 0.59.$$

This value ensures that at least the solution $Z_s = 0$ exists. Then, (5.18) is solved with $\eta = 10$; there are 16 acceptable solutions out of $4 \times \eta = 40$ available, where 4 is the degree of the polynomial for pure series feedback [139]. The corresponding optimum noise reflection coefficient for each of those series feedback X_s is shown in Table 5.6; as expected, $X_s = 0$ provides an acceptable solution.

Table 5.6 Noise parameters and reactive series feedback X_s yielding $|\,\Gamma_{S_{opt}}\,| < 0.59$ for Mitsubishi MGF4918E HEMT at $f_o = 8$ GHz.

X_s Ω	$\|\,\Gamma_{S_{opt}}\,\|$	$\angle\Gamma_{S_{opt}}$ deg	F_{min} dB	R_n Ω
0.000	0.590	120.00	0.430	4.500
5.590	0.559	129.09	0.423	3.379
9.765	0.536	136.51	0.418	2.712
13.180	0.519	142.98	0.414	2.270
16.180	0.506	148.96	0.410	1.956
18.995	0.494	154.80	0.407	1.720
21.855	0.484	160.95	0.403	1.539
25.210	0.475	168.39	0.400	1.396
36.840	0.465	-165.01	0.386	1.446
40.635	0.469	-156.51	0.382	1.628
44.050	0.476	-149.11	0.378	1.854
47.580	0.486	-141.79	0.374	2.146
51.555	0.499	-134.00	0.370	2.542
56.360	0.518	-125.26	0.365	3.109
62.670	0.546	-114.95	0.358	3.985
71.985	0.590	-101.93	0.348	5.516

The trend in $|\,\Gamma_{S_{opt}}\,|$ is evident in Figure 5.5. In order to find the minimum in $|\,\Gamma_{S_{opt}}\,|$,

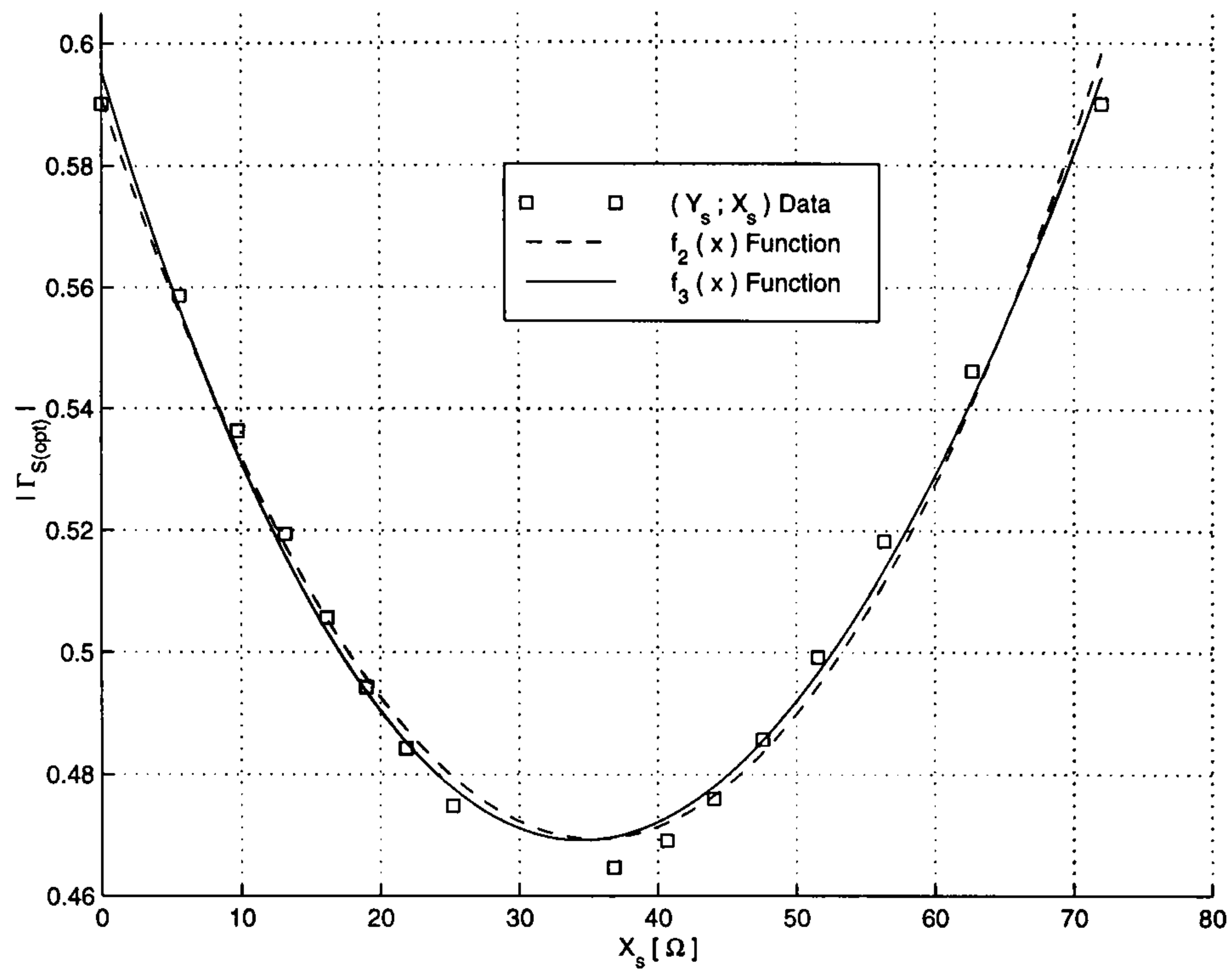

Figure 5.5 Least squares approximations of $\mid \Gamma_{S_{opt}} \mid$ for Mitsubishi MGF4918E HEMT at $f_o = 8$ GHz.

consider Table 5.6 and name the column of feedback element values X_s as X_j and the column of magnitudes of $\Gamma_{S_{opt}}$ as Y_j where $j = 1, \ldots, 16$. Then, a least squares fit with a 2nd degree ($N = 2$) or a 3rd degree polynomial ($N = 3$):

$$f_N(x) = \sum_{i=0}^{N} c_i \, x^i \tag{5.21}$$

is used to minimise the error:

$$E^2 = \sum_{j=1}^{16} \mid Y_j - f_N(X_j) \mid^2$$

Once the coefficients c_i are obtained, the minimum $(x_{min}; f_N(x_{min}))$ is found by setting the first derivative df_N/dx of (5.21) to zero. Figure 5.5 shows two approximations, $f_2(x)$ and $f_3(x)$; their coefficients and the minimum in $\mid \Gamma_{S_{opt}} \mid$ for the Mitsubishi MGF4918E HEMT at $f_o = 8$ GHz are tabulated in Table 5.7 and Table 5.8, respectively.

The results demonstrate that, for the same frequency f_o, $\mid \Gamma_{S_{opt}} \mid_{min}$ occurs for a pure series feedback X_s similar in value to the one that yields the minimum equivalent noise resistance $R_{n_{min}}$: 0.60 nH inductance for $R_{n_{min}}$; 0.68 nH for $\mid \Gamma_{S_{opt}} \mid_{min} \approx 0.47$. The same

Table 5.7 c_i coefficients for the least squares fit polynomial (5.21) with $N = 2$ and corresponding $|\Gamma_{S_{opt}}|_{min}$ for Mitsubishi MGF4918E HEMT at $f_o = 8$ GHz.

c_2 $[\Omega]^{-2}$	c_1 $[\Omega]^{-1}$	c_0 $[\Omega]^0$	$X_{s_{min}}$ Ω	$f_2(X_{s_{min}})$
9.665×10^{-5}	-6.857×10^{-3}	0.591	35.475	0.4694

Table 5.8 c_i coefficients for the least squares fit polynomial (5.21) with $N = 3$ and corresponding $|\Gamma_{S_{opt}}|_{min}$ for Mitsubishi MGF4918E HEMT at $f_o = 8$ GHz.

c_3 $[\Omega]^{-3}$	c_2 $[\Omega]^{-2}$	c_1 $[\Omega]^{-1}$	c_0 $[\Omega]^0$	$X_{s_{min}}$ Ω	$f_3(X_{s_{min}})$
-2.436×10^{-7}	1.231×10^{-4}	-7.612×10^{-3}	0.595	34.447	0.4692

feature occurs at 1 GHz for HP ATF21186 MESFET, too [139]. The minimum noise figure F_{min} (Table 5.6) decreases because a lossless feedback is embedding an active device; since the noise measure is constant and the gain decreases as the feedback impedance increases, F_{min} is bound to decrease.

The least squares fit can be applied with non–polynomial functions. For instance, the function:

$$f(x) = a\,\frac{1}{(x+x_o)^2} + b\,\frac{1}{(x+x_o)} + c + d\,(x+x_o) + e\,(x+x_o)^2 \tag{5.22}$$

approximates the data of Table 5.6 and it is plotted in Figure 5.6. This function provides $1/x^i$ terms which characterise the expression of R_n vs series feedback $Z_s = j\,X_s$ in (3.34), chapter 3.

The $|\Gamma_{S_{opt}}|_{min}$ analysis is straightforward, easily implementable as software and allows the designer to select the best device for the application. For Mitsubishi MGF4918E HEMTs, the minimum in $|\Gamma_{S_{opt}}|$ is approximately 0.47 or -6.56 dB at 8 GHz. If a simultaneously matched LNA must yield an input return loss better than 6.56 dB at 8 GHz, this device is not suitable for the job. The designer must look into the performance of a different device if series feedback amplifier topology without an input matching circuit is to be used.

5.3 Experimental Validation

A simultaneously signal and noise matched LNA (SSNM LNA) has been fabricated [142] with the theory developed for optimum noise source reflection coefficient design. Centre frequency

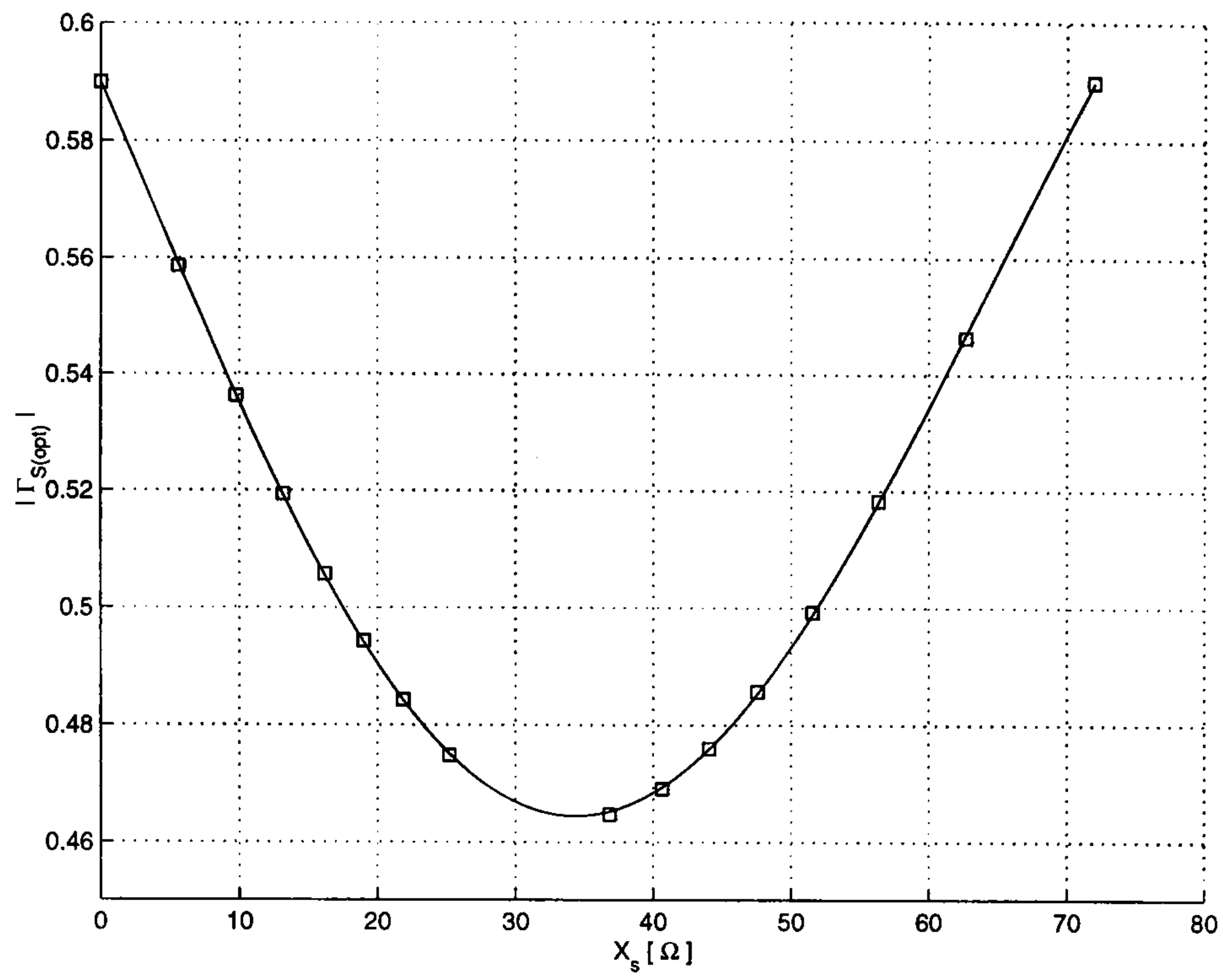

Figure 5.6 Least squares approximation of $\mid \Gamma_{S_{opt}} \mid$ with (5.22): $x_o/Z_o = 10$ and $Z_o = 50\ \Omega$ for Mitsubishi MGF4918E HEMT at $f_o = 8$ GHz (squares correspond to the $(X_s; \mid \Gamma_{S_{opt}} \mid)$ data in Table 5.6).

f_o is 1 GHz, which is close to typical mobile communication bands [8]. The circuit makes use of a packaged device and surface mount components on Duroid 5880 (Table 5.9). Both simulation and optimisation have been carried out with HP EEsof series IV[1]. A brass board provides for the common ground plane and houses input and output SMA connectors.

Table 5.9 Duroid 5880 substrate data.

Substrate thickness	h	0.7874	mm
Metal thickness	t	0.017018	mm
Metal conductivity (copper)	σ	5.80×10^{7}	$\mathrm{S{\cdot}m^{-1}}$
Dielectric constant	ϵ	2.2	
Dielectric loss tangent	$\tan\delta$	0.0006	

[1]HP EEsof series IV requires the metal resistivity ρ of the metal conductor to be normalised to the resistivity of gold: $\rho = \rho_{rel} \cdot \rho_{Au}$ where $\rho_{Au} = 2.44\times10^{-6}$ [Ω·cm]

5.3.1 SSNM LNA Design

The SSNM LNA main specification is $|\Gamma_{S_{opt}}| = |S_{11}| \leq -20$ dB, where S_{11} is measured at the input SMA connector of the stage. It is also required that the noise figure is as small as possible and the gain $|S_{21}|$ as large as possible. These goals should be verified over a bandwidth spanning at least 70 MHz around f_o.

Selection of the device

A correlation between series reactances $X_{S_{opt}}$ for $R_{n_{min}}$ and $|\Gamma_{S_{opt}}|_{min}$ has been highlighted in section 5.2.5. Furthermore, it has been pointed out that R_n behaves similarly in both frequency (for constant feedback components) and X_s (for constant frequency f_o) domains, if the device parameters do not vary significantly as a function of frequency. Therefore, the selection of the device can start from the investigation of R_n vs frequency as given in the transistor data book. Then, (5.18) is solved and its results are investigated.

Mobile communication receivers [133] usually take advantage of the superior noise performance of majority carrier devices such as MESFETs or HEMTs. However, if the $R_{n_{min}}$ analysis vs series feedback reactance (chapter 3, section 3.2.2) is applied to such devices [85], it is found that:

1. $R_{n_{min}} \ll R_t$, the minimum noise resistance is far smaller than the value of the noise resistance of the device without feedback;
2. the value of the series reactance for $R_{n_{min}}$ is usually quite large at the given frequency.

This has been demonstrated in Table 3.7 (chapter 3, section 3.2.2) for HP ATF21186 MESFETs; another example is shown in Table 5.10.

Table 5.10 Equivalent noise resistance R_n extremes for HP ATF10136 MESFET.

f GHz	$R_{n_{min}}$ Ω	$X_{s_{min}}$ Ω	$R_{n_{max}}$ kΩ	$X_{s_{max}}$ kΩ	$R_{n_{sat}}$ Ω	$-\left(\frac{R_{n_{min}}-R_t}{R_t}\right)$ %
1.0	4.94	229.01	106.37	-0.98	550.07	85.88
2.0	4.65	110.97	7.06	-0.50	365.66	79.78
4.0	12.17	22.06	4.77	-0.42	1466.40	32.38
6.0	5.87	-4.56	1.04	-0.79	825.81	2.21
8.0	8.75	-45.23	0.76	3.82	756.08	53.97

The R_n performance vs series feedback for HP AT41486 BJTs is different. Table 5.11 (equal to Table 3.12, chapter 3, section 3.2.2) shows that the variation in R_n when the feedback is applied, is quite small. Therefore the device is already tuned around $R_{n_{min}}$.

Table 5.11 Equivalent noise resistance R_n extremes for HP AT41486 BJT.

f GHz	$R_{n_{min}}$ Ω	$X_{s_{min}}$ Ω	$R_{n_{max}}$ kΩ	$X_{s_{max}}$ kΩ	$R_{n_{sat}}$ $k\Omega$	$-\left(\frac{R_{n_{min}}-R_t}{R_t}\right)$ %
0.1	8.499	0.840	23030	-7.34	113.08	0.02
0.5	8.473	3.455	118.82	-1.32	3.91	0.32
1.0	7.976	3.003	12.64	-0.68	1.18	0.31
2.0	7.843	-6.021	1.31	-0.38	0.44	1.97
4.0	8.792	-32.560	0.23	-0.44	0.21	56.04

Table 3.14 (chapter 3, section 3.2.2) shows that for the AT41486 at 1 GHz, the value of the magnitude of $\Gamma_{S_{opt}}$ at $R_{n_{min}}$ is 0.031 or -30 dB. This corresponds to a 30 dB input return loss when the SSNM condition is achieved, 10 dB better than the required 20 dB. The available gain when the source is 50 Ω is about 16.9 dB (Table 3.13, chapter 3, section 3.2.2). The conclusion is that the HP AT41486 BJT is a good candidate for SSNM design at 1 GHz.

Selection of the Feedback Impedance

Table 5.11 shows that the required lossless reactive feedback for $R_{n_{min}}$ at $f_o = 1$ GHz is inductive (3 Ω or 0.48 nH at f_o). The BJT scattering and noise parameters in common emitter configuration are simulated in frequency domain around f_o when a 0.48 nH inductor is placed between emitter and ground. Figure 5.7 shows the result in the range $(f_{min} - f_{max}) = 0.1$ – 4.0 GHz, where the Hewlett Packard catalogue [85] provides signal and noise data. Outside this band, the simulation is less meaningful: HP EEsof series IV warns the user when the simulation frequency f is outside the range of available data ($f > f_{max}$ or $f < f_{min}$) and assumes that scattering and noise parameters of the device remain constant to the values at the extremes of the frequency range – for instance, $S_{11}(f) = S_{11}(f_{max})$ for $f > f_{max}$.

If (5.18) is solved for the design goal $|\Gamma_{S_{opt}}| \leq 0.1$ at f_o [139] with a lossless series feedback $Z_s = j\,X_s$ and $\eta = 10$, the acceptable solutions out of $4 \times \eta$ available are tabulated in Table 5.12. $X_s = 0$ (device with no feedback) is a solution since the data book value for $|\Gamma_{S_{opt}}|$ is $0.04 < 0.1$. Some of the series feedback values are negative: in those cases, the instability of the device is enhanced (the Rollett factor K becomes negative and the determinant of the scattering matrix Δ_S becomes larger than 1 in magnitude). The minimum noise figure increases as the lossless feedback becomes increasingly negative because the gain increases and the noise measure remains constant.

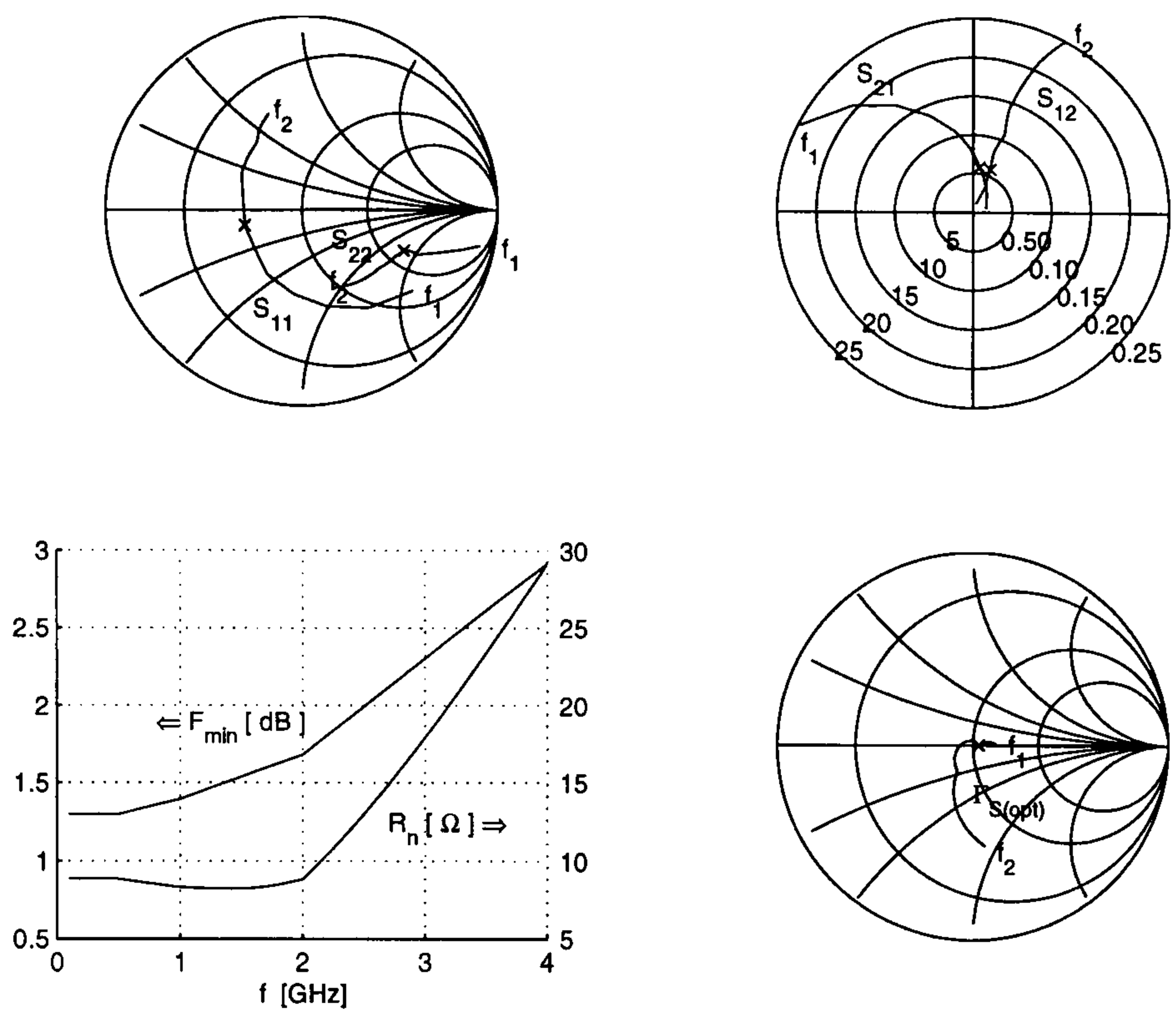

Figure 5.7 Magnitude and phase of scattering and noise parameters from $f_1 = 0.1$ GHz to $f_2 = 4$ GHz with series inductance for $R_{n_{min}}$ at $f_o = 1$ GHz. The cross x represents the data at f_o.

One of the possible solution is $L_s = 0.87$ nH or $X_s = 5.44\ \Omega$ and the corresponding parameters are shown in Table 5.13.

The frequency behaviour over the band 0.1 – 4.0 GHz is demonstrated in Figure 5.8. No output matching circuit has been included, yet. In comparison with the behaviour obtained with $X_s = 3.00\,\Omega$ for $R_{n_{min}}$, the input reflection coefficient is smaller: $\mid S_{11}\,(X_s = 3.00\ \Omega) \mid = 0.301$, $\mid S_{11}\,(X_s = 5.44\ \Omega) \mid = 0.150$. The advantage of the design for $\mid \Gamma_{S_{opt}} \mid$ is to have a set of solutions from which the solution which best meets every specification can be selected.

Another solution in Table 5.12 is $X_s = 9.54\ \Omega = 2\,\pi\,f_o\,1.52$ nH and the corresponding signal and noise parameters are detailed in Table 5.14. Some important remarks can be highlighted when comparing Table 5.13 and Table 5.14, i.e as the feedback element changes from 0.87 to 1.52 nH:

- the input reflection coefficient S_{11} decreases in magnitude (about -47%) and drops below 0.1 at $L_s = 1.52$ nH;
- the output reflection coefficient S_{22} increases in magnitude by about 10%;
- the forward transmission coefficient S_{21} decreases (about -16%). However the trans-

Table 5.12 Hewlett–Packard AT41486 BJT vs reactive series feedback X_s for $|\Gamma_{S_{opt}}| < 0.1$ at $f_o = 1$ GHz: optimum noise source reflection coefficient $\Gamma_{S_{opt}}$, minimum noise figure F_{min}, equivalent noise source impedance R_n, stability factors K and $|\Delta_S|$, noise measure M.

X_s Ω	$\mid\Gamma_{S_{opt}}\mid$	$\angle\Gamma_{S_{opt}}$ deg	F_{min} dB	R_n Ω	K	$\mid\Delta_S\mid$	M
-7.240	0.100	71.04	1.413	8.270	-0.612	1.108	0.415
-6.555	0.094	70.19	1.412	8.231	-0.556	0.946	0.418
-5.820	0.087	69.08	1.411	8.193	-0.478	0.796	0.421
-5.020	0.080	67.59	1.409	8.155	-0.365	0.657	0.423
-4.130	0.072	65.49	1.408	8.117	-0.191	0.525	0.426
-3.115	0.064	62.33	1.406	8.079	0.075	0.401	0.429
-1.875	0.053	56.86	1.403	8.041	0.445	0.279	0.432
-0.140	0.041	44.36	1.400	8.002	0.813	0.165	0.436
0.000	0.040	43.00	1.400	8.000	0.831	0.159	0.437
5.445	0.040	-34.94	1.390	7.991	1.016	0.256	0.448
7.215	0.053	-48.01	1.387	8.023	1.016	0.314	0.451
8.485	0.063	-53.68	1.385	8.056	1.015	0.352	0.453
9.540	0.072	-56.98	1.383	8.090	1.013	0.381	0.455
10.460	0.080	-59.14	1.381	8.124	1.011	0.405	0.456
11.295	0.087	-60.67	1.379	8.158	1.009	0.425	0.457
12.065	0.094	-61.81	1.378	8.193	1.008	0.442	0.459
12.785	0.100	-62.69	1.377	8.229	1.006	0.458	0.460

ducer power gain G_T when the load Γ_L^{SSNM} as defined by (5.10), increases from 7.24 dB to 12.80 dB;

- the reverse transmission coefficient S_{12} increases by about 25% even if its magnitude remains well below 0.1;
- the load Γ_L^{SSNM} decreases its magnitude from 0.79 to 0.33;
- the minimum noise figure F_{min} decreases because the series reactance is lossless; and the equivalent noise resistance R_n is slightly larger than $R_{n_{min}}$. However both F_{min} and R_n variations are within $\pm 1.5\%$;
- in both cases, series feedback makes the unstable device stable at f_o (Rollett factor $K > 1$ and magnitude of the scattering matrix determinant $|\Delta_S| < 1$).

It should be noticed that $L_s = 1.52$ nH makes the AT41486 device a SSNM LNA, since the input return loss is better than 20 dB and $|\Gamma_{S_{opt}}|$ is better than -20 dB. Moreover, no input matching circuit is required. As long as the feedback is lossless, the minimum noise figure (or equivalently, the noise figure under SSNM condition) is lowered as well. The equivalent

Table 5.13 AT41486 BJT performance with $X_s = 5.44\ \Omega$ at $f_o = 1$ GHz. G_T is the transducer power gain gain when Γ_L^{SSNM} loads the output port.

S_{11}	0.150	-154.31 deg
S_{12}	0.064	+75.89 deg
S_{21}	5.133	+81.01 deg
S_{22}	0.609	-18.54 deg
F_{min}	1.39 dB	
$\Gamma_{S_{opt}}$	0.040	-34.92 deg
R_n	7.99 Ω	
Γ_L^{SSNM}	0.789	-114.45 deg
G_T	7.238 dB	

Table 5.14 AT41486 BJT performance with $X_s = 9.54\ \Omega$ at $f_o = 1$ GHz. G_T is the transducer power gain gain when Γ_L^{SSNM} loads the output port.

S_{11}	0.080	-45.46 deg
S_{12}	0.080	+81.94 deg
S_{21}	4.303	+79.66 deg
S_{22}	0.671	-15.45 deg
F_{min}	1.38 dB	
$\Gamma_{S_{opt}}$	0.072	-56.97 deg
R_n	8.09 Ω	
Γ_L^{SSNM}	0.325	-51.04 deg
G_T	12.799 dB	

noise resistance R_n close to its minimum value guarantees that the dependence of the noise figure on the input mismatch $\mid \Gamma_{in} - \Gamma_{S_{opt}} \mid$ is almost as little as possible.

The conclusion is that 1 nH at f_o is a good starting value for the series inductance.

Layout and Optimisation in the Frequency Domain

The topology of the circuit is shown in Figure 5.9. Some components required to bias the transistor at $V_{CE} = 8.0$ V and $I_C = 10$ mA [85] are not included.

The SSNM LNA is fabricated with surface mount components on Duroid substrate. Therefore, the availability of a component suitable for the design is a further constraint to be considered. 120 pF capacitors (C_h) are used wherever either paths to ground or RF short circuits are necessary (at $f_o = 1$ GHz, $Z = 1/(j\,2\,\pi\,f_o\,C_h) \approx -j\,1.33\ \Omega$); 22 pF capacitors are available, as well. 82 nH inductors (L_h) are extensively employed where DC paths and RF open circuits are required at the same time ($Z = j\,2\,\pi\,f_o\,L_h \approx j\,515.22\ \Omega$); 150 nH inductors are available but at higher cost. 10, 50 and 68 Ω resistors are also used.

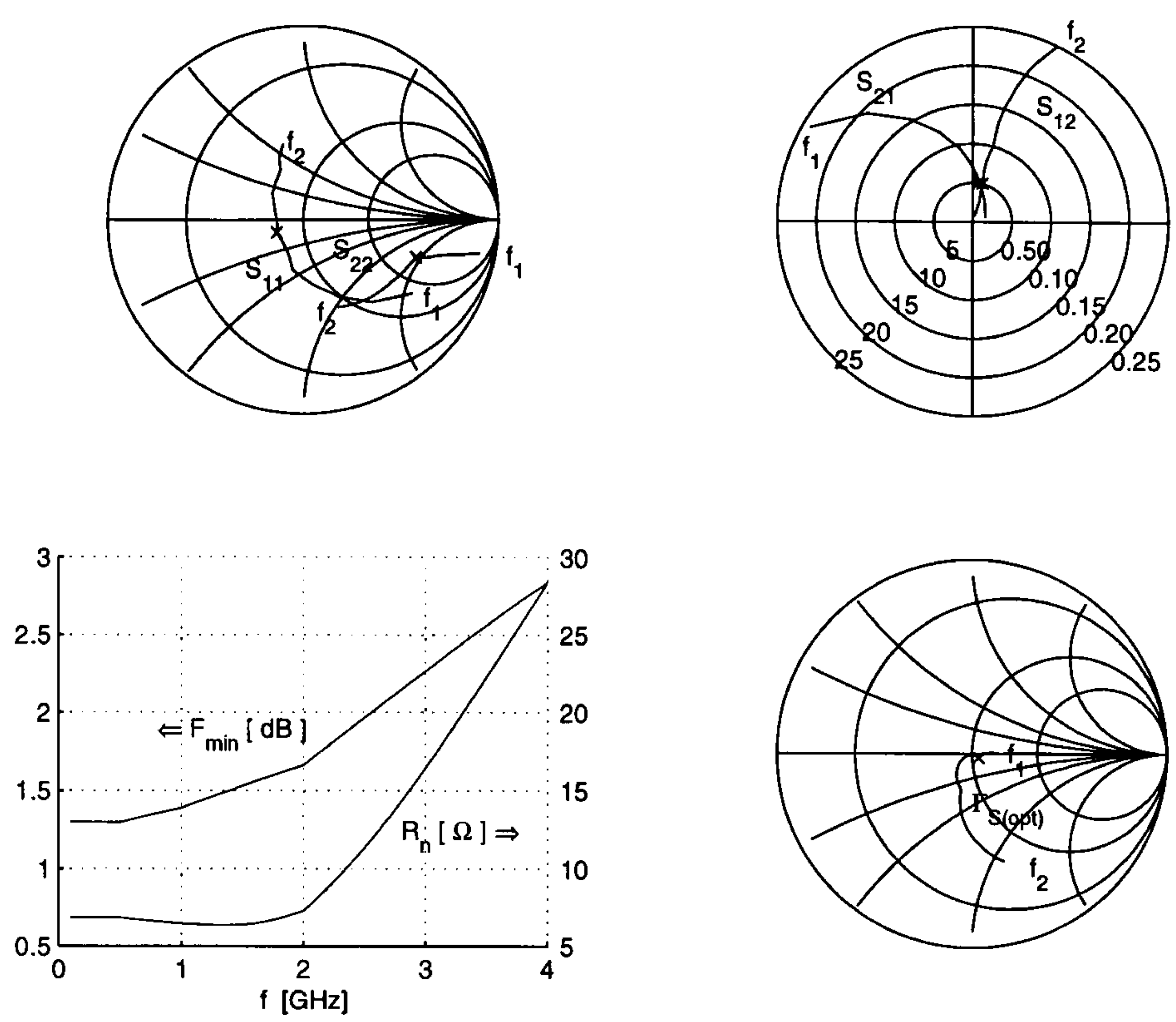

Figure 5.8 Magnitude and phase of the scattering and noise parameters from $f_1 =$ 0.1 GHz to $f_2 = 4$ GHz with a 0.87 nH series inductance delivering $\mid \Gamma_{S_{opt}} \mid < 0.1$ at $f_o = 1$ GHz. The cross x represents the data at f_o.

The SSNM LNA (Figure 5.9) receives the input radio frequency from the 3.5 mm SMA connector on the left, typical for applications around 1 GHz. C_h prevents the DC current from flowing to the previous stage but does not block the incoming signal. A copper pad (not shown) connects the SMA connector and C_h. However, it has not been included in the simulation because its length has been kept as short as physically possible – the capacitor could be soldered directly on the connector. The short pad PAD_I houses the other terminal of the input capacitor C_h, the lead of the transistor and the input resistor[2] R_{in}. PAD_I seems to heavily affect the SSNM condition [34], [35], [123]. For instance, with the components obtained after optimisation, the input return loss associated with S_{11} is 19.34 dB and $\mid \Gamma_{S_{opt}} \mid$ is -25.58 dB; if the capacitor C_h, the transistor base and the resistor R_{in} are connected together and PAD_I is taken off the circuit, S_{11} and $\mid \Gamma_{S_{opt}} \mid$ are respectively 24.96 dB and -20.45 dB. As a matter of fact, the pad is indispensable and therefore has been included in the optimisation of the circuit.

[2]Figure 5.9 shows that the resistor R_{in} is connected at the right end of PAD_I; that means that given the physical dimensions of the three components, the surface mount resistor R_{in} is to be kept as close as possible to the right end of the pad.

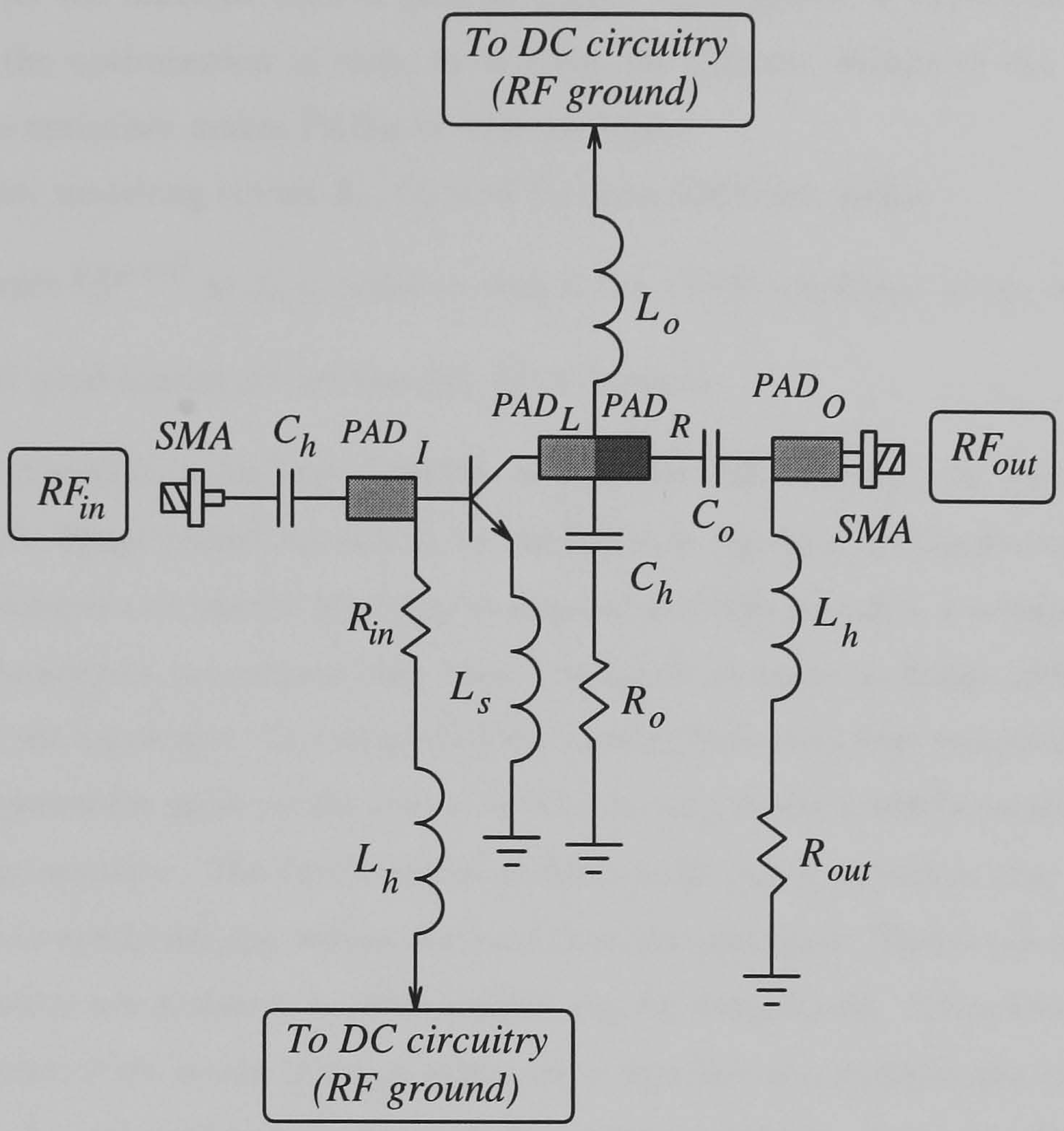

Figure 5.9 Designed AT41486 BJT SSNM LNA at $f_o = 1$ GHz.

The resistor R_{in} provides a path for the DC current and helps to damp low frequency oscillations. It may also stop high frequency oscillations ($f \gg 4.0$ GHz) through a capacitive coupling to ground of its floating terminal – the inductor L_h disconnects the resistor from the ground as frequency increases.

The AT41486 BJT comes with a plastic package and four leads. The leads are about 0.85 mm wide: this dimension imposes a constraint on the width of the pads. Two of the four leads are the BJT emitter: one of them has been cut off in order to decrease the reactance already associated with the emitter leads. Base and collector terminals overlap the pads as much as possible; when a lead is soldered on a pad, a perfect connection is assumed for simulation purposes. The feedback inductance consists of a short wire: it provides the required amount of RF feedback inductance and connects the emitter to ground as far as the DC current is concerned.

The collector is connected to a pad. Figure 5.9 denotes it as PAD_R (right) and PAD_L (left) with respect to the point where the output matching circuit (L_o, C_o and R_o) is ideally connected. As the different tone of grey in Figure 5.9 suggests, a discontinuity has been included in the optimisation in order to account for different widths of the components. However, the optimiser makes PAD_R as wide as PAD_L.

The output matching circuit L_o, C_o and R_o must fulfill two tasks:

1. to provide Γ_L^{SSNM} at f_o in order to ensure the SSNM condition at the input port;
2. to yield good output return loss (20 dB or better).

The first requirement is an indispensable step of the LNA design; the second one is a practical need. Those conditions should be verified over the required band of the LNA. The output matching circuit should also help to improve stability, which is a requirement at any frequency. Analytical procedures have been developed in order to design different output matching circuit topologies. The analytical expressions have been kept simple and therefore, they do not guarantee good return loss, even if they can provide a reliable starting point for successive optimisation. The fundamental problem with this approach is that the designer must be able to synthesise any values obtained from the optimiser. This is not possible when only fixed values are available as with surface mount components. Therefore, the output matching circuit is the result of many attempts to find the best compromise for the design.

Capacitor C_o, immediately in front of the output connector, decouples the LNA from the next stage. Capacitor C_h between PAD_L and resistor R_o disconnects the latter from the DC ground but it acts like a short circuit at f_o. The values for C_o and R_o have been kept constant for the optimiser; inductor L_o has been left free to vary within the range 0 – 150 nH.

Finally, PAD_O houses the output SMA connector as well as a pair of components (L_h and R_{out}) which comply to a task similar to R_{in} and L_h as far as stability is concerned.

Pads have been modelled as transmission lines. Since the design seems very sensitive to changes in pad dimensions, 3 main contraints have been imposed on the optimiser:

1. the length L_{pad} of any pad must be larger than its width W_{pad} ($L_{pad} > W_{pad}$);
2. the ratio L_{pad}/W_{pad} must meet the constraints for fabrication on Duroid 5880;
3. width must be larger than minimum width $W_{pad_{min}}$ imposed by the dimensions of any component terminal: 0.85 mm by the BJT leads in this case.

The relationship between length and width is defined by:

$$W_{pad} = W_{pad_{min}} + m\,(L_{pad} - L_{min}) \tag{5.23.a}$$

$$L_{min} \leq L_{pad} \leq L_{max} \tag{5.23.b}$$

where $W_{pad_{min}}$ and L_{min} are the minimum width and length of the pad. The constant of proportionality m has been expressed as $m = m_n/m_d$ where the numerator $m_n = 2.15$ mm is the same for every pad of Figure 5.9; the denominator m_d is set equal to $L_{max} - L_{min}$, the difference between the maximum and minimum length of a given pad. It follows that the maximum width of any pad is $W_{pad_{min}} + m_n = 3$ mm, which is slightly more than the maximum dimension of the components of the circuit.

The goals of the optimiser over the 70 MHz bandwidth are:

1. $\Gamma_{S_{opt}}$ magnitude smaller than 0.1;
2. each real and imaginary part of S_{11} smaller than $\sqrt{0.1^2/2} \approx 0.07$;
3. each real and imaginary part of S_{22} smaller than $\sqrt{0.1^2/2} \approx 0.07$.

The final performance of the circuit after optimisation is shown in Figure 5.10. Some

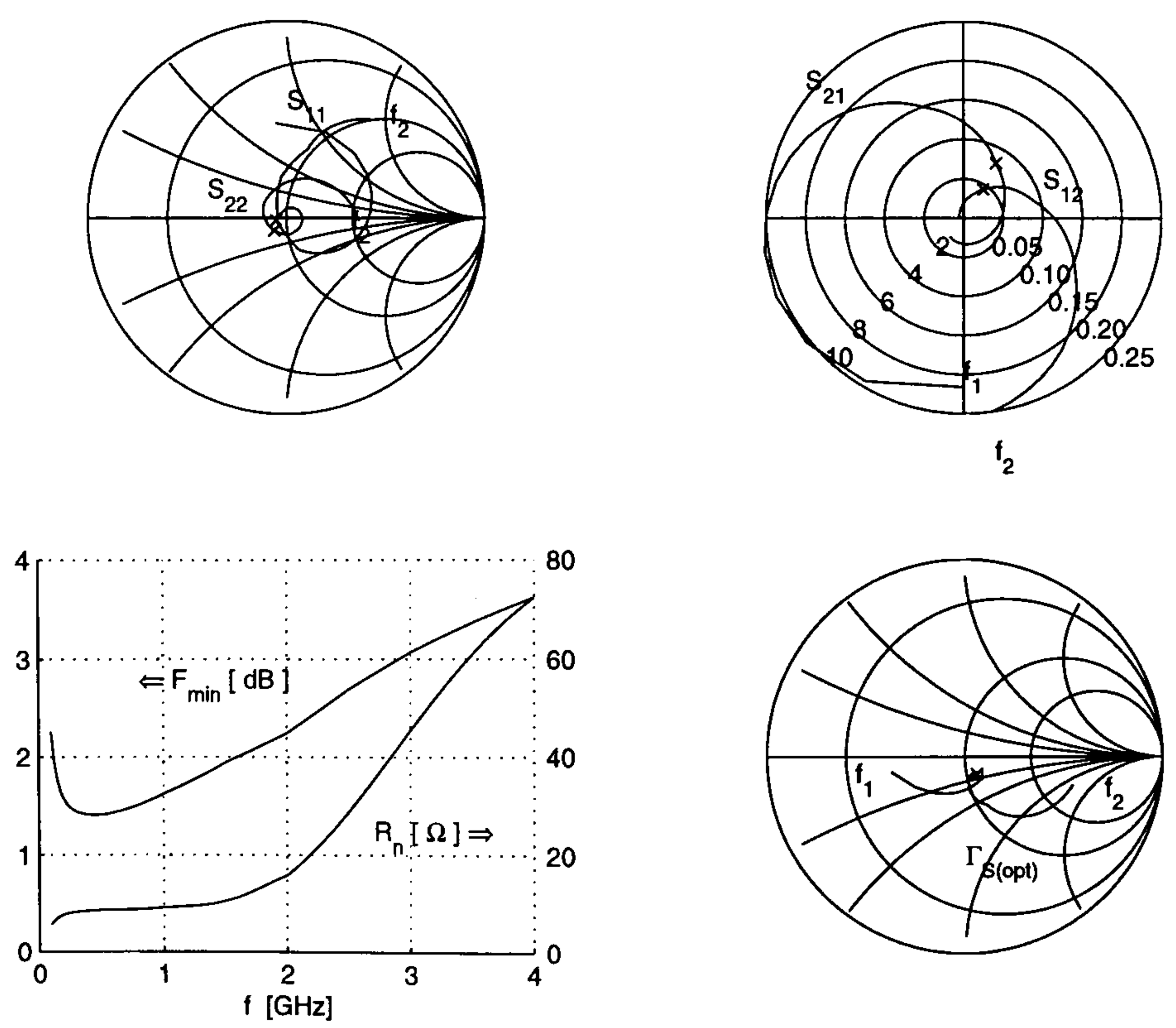

Figure 5.10 Magnitude and phase of scattering and noise parameters from $f_1 = 0.1$ GHz to $f_2 = 4$ GHz of the optimised SSNM LNA. The cross x represents the data at f_o.

numerical values for scattering and noise parameters as well as noise figure F are tabulated

Table 5.15 AT41486 SSNM BJT parameters around f_o = 1 GHz.

f_o	0.965	1.000	1.035	GHz
$\mid S_{11} \mid$	-26.00	-25.58	-25.92	dB
$\mid S_{12} \mid$	-27.73	-27.36	-27.09	dB
$\mid S_{21} \mid$	10.57	10.16	9.95	dB
$\mid S_{22} \mid$	-21.27	-21.15	-21.06	dB
F_{min}	1.60	1.62	1.64	dB
$\mid \Gamma_{S_{opt}} \mid$	-19.49	-19.34	-19.56	dB
R_n	9.64	9.73	9.77	Ω
F	1.62	1.65	1.66	dB

in Table 5.15. The value of the feedback element after optimisation is L_s = 0.95 nH. A picture of the circuit on Duroid is shown in Figure 5.11.

5.3.2 Signal Performance

Standard measurement of the scattering parameters S_{ij} has been carried out with a network analyser [143]; particular attention has been paid to verifying the correctness of its calibration. Some details about both calibration and verification are outlined before presenting the measured S_{ij} parameters. Since the theory on network analysers is a vast field of microwave engineering [78], [144], [145], [146], only the details which are important to the BJT SSNM LNA test are discussed.

Calibration and Verification

Automatic network analysers (ANA) require that the user accomplishes two preliminary tasks in order to ensure that estimated data are referred to the desired measurement planes [143], [147]: calibration and verification. The first step as well as any other test involving the ANA, has been carried out according to the instrument manual [143] at a power level of -10 dBm for both port 1 and 2.

Verifying the correctness of the ANA calibration is very important in order to test the LNA performance. It is very possible that the network analyser may measure input reflection coefficients of passive networks larger than 1, in particular with very reflective circuits. Verification kits are available in order to check out calibration over the required band; since the ANA is to measure a 2–port device, kits provide a transmission line of known length in order to verify the scattering parameters. A careful investigation of the data shown by the ANA when a transmission line is connected between the reference planes, should be carried

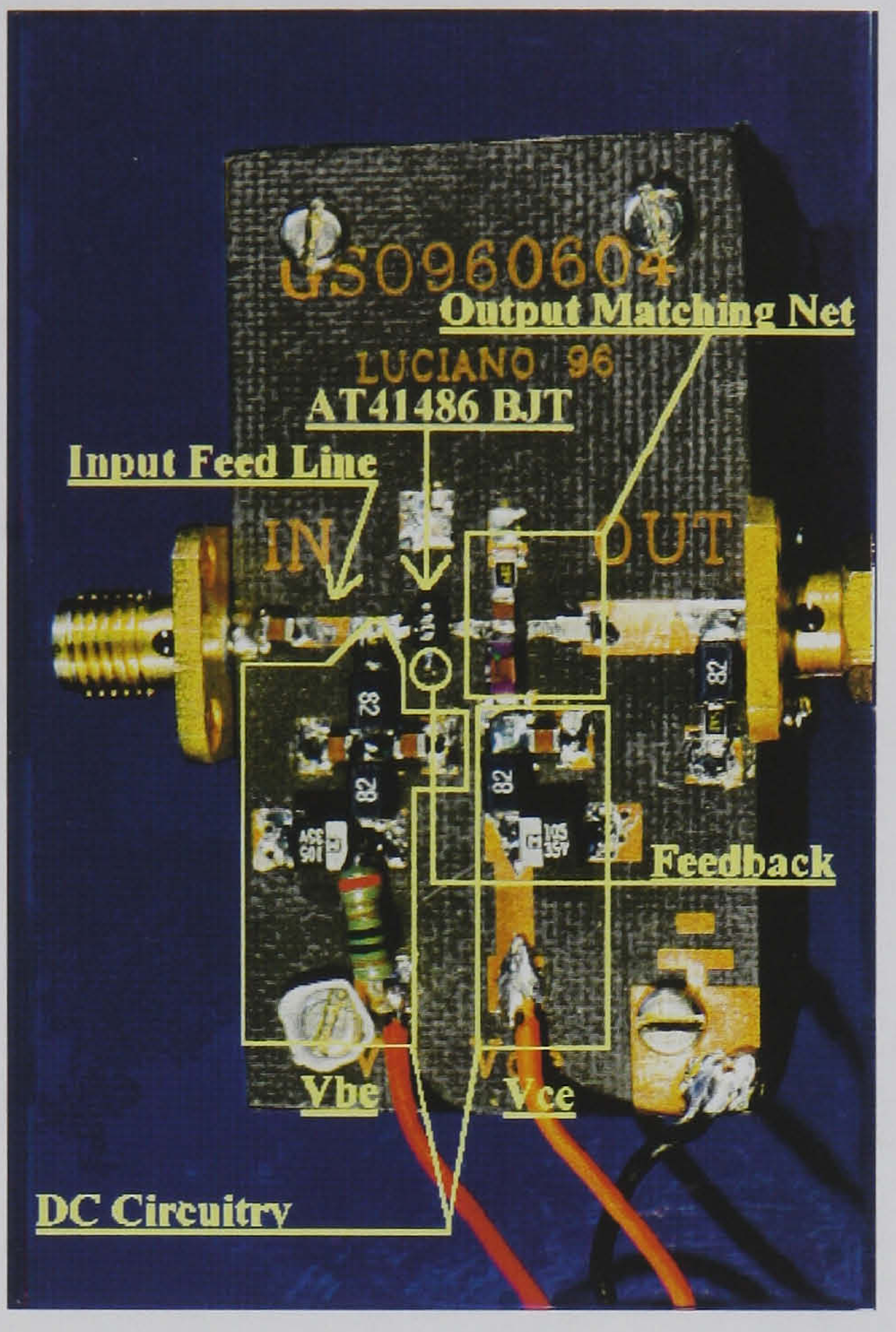

Figure 5.11 The final SSNM LNA circuit along with the DC circuitry; board dimension: 28×52 mm^2

out.

A more user–friendly, less time–consuming approach has been devised. Any passive 2–port network dissipates some of the incoming power P_{in} before delivering back the remaining power P_{out} at its ports. In terms of scattering parameters, $P_{out} \leq P_{in}$ is equivalent to:

$$| b_1 |^2 + | b_2 |^2 \quad \leq \quad | a_1 |^2 + | a_2 |^2 \tag{5.24}$$

where b_1 (a_1) is the outgoing (incoming) power at the input reference plane (port 1) and b_2 (a_2) is the outgoing (incoming) power at the output reference plane (port 2). For any symmetrical and reciprocal network, (5.24) is equivalent to require that:

$$A_{11} \quad \geq \quad 0 \tag{5.25.a}$$

$$| \mathbf{A} | \quad \geq \quad 0 \tag{5.25.b}$$

are satisfied simultaneously. A_{11} is an element of matrix $\mathbf{A} = \mathbf{1} - \mathbf{S}\,\mathbf{S}^{+}$, whose determinant is

$\mid \mathbf{A} \mid$ and $\mathbf{S}$ is the scattering matrix of the passive 2–port network. The equivalence between (5.24) and (5.25) for a passive 2–port network is described in appendix C.1.

When the verification kit transmission line is connected between the reference planes, (5.25) must be satisfied at every frequency at which the test is executed. (5.25) ensures that the noise parameters of any passive device can be calculated from its scattering parameters [123]. In fact, checking that $\mid S_{11} \mid < 1$ or $\mid S_{21} \mid \approx 1$ on the network analyser display is not sufficient for the calibration to be deemed acceptable.

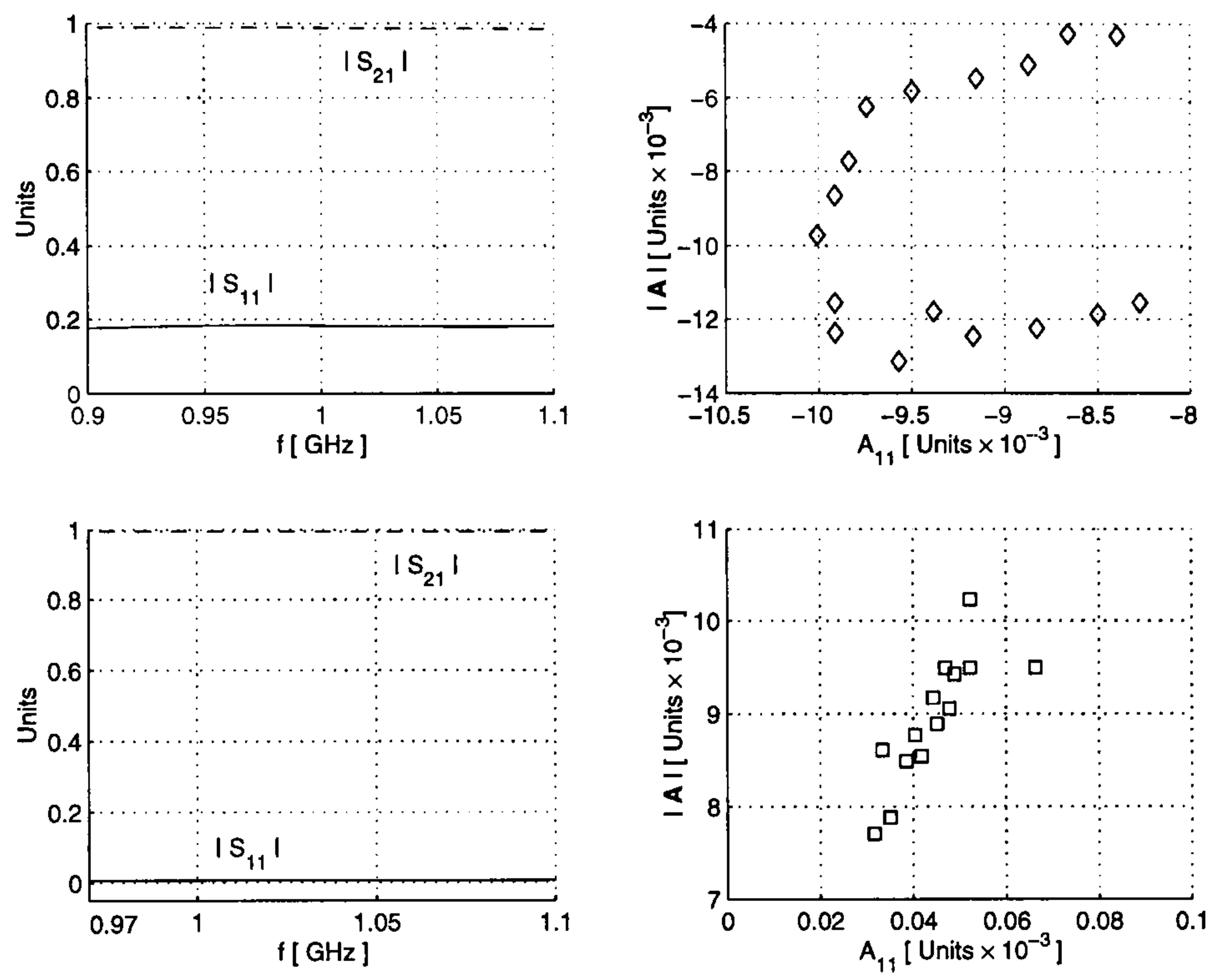

Figure 5.12 Comparison between two different verifications with a 7.5 cm long transmission line: top figures show a bad calibration; bottom figures, a good one.

(5.25) is a quick and simple approach to verify the calibration with lossy and reciprocal circuits, as Figure 5.12 shows: the first quadrant of plane $(A_{11}(f); \mid \mathbf{A}(f) \mid)$ at the frequency f, is identified by (5.25) as the only acceptable region of the whole plane. For a passive device, every point at any frequency must lie in the first quadrant (on the axes if the 2–port network is lossless); if one point has at least one negative coordinate, the calibration should be carried out again[3]. For this reason, the frequency at which each point on the $(A_{11}; \mid \mathbf{A} \mid)$ plane occurs, has not been indicated in Figure 5.12. Numerical values for both axes relative to the correct calibration plot in Figure 5.12 are very small. This is due to the fact that the

[3]This statement is based on the fact that modern ANAs do not let the user carry out the calibration at one single frequency point within the defined frequency band.

transmission line has an exceedingly low loss.

Measurement

The SSNM LNA scattering parameters have been measured after calibrating the network analyser at the planes identified by the SMA connectors and verifying the calibration procedure; they are displayed in Figure 5.13.

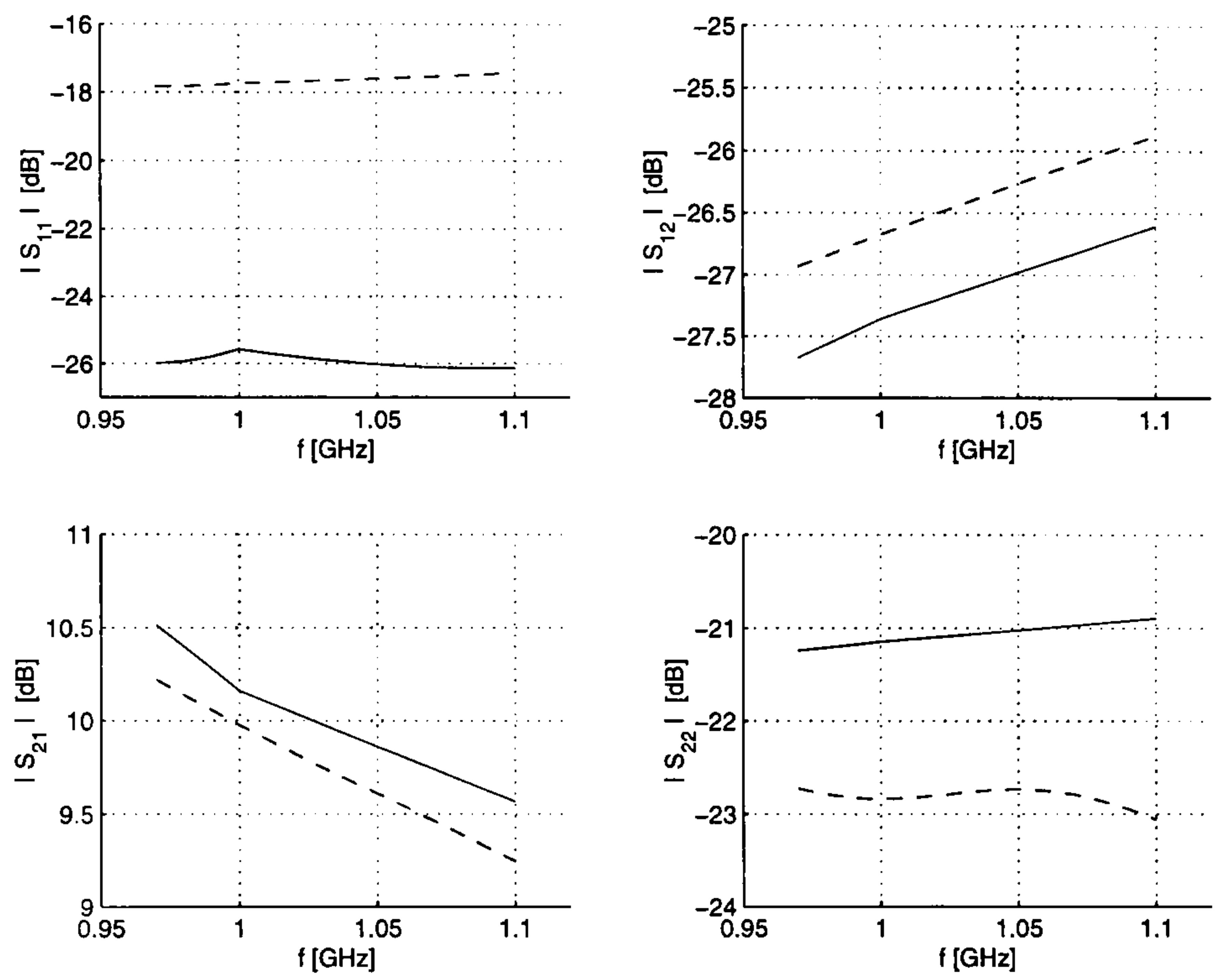

Figure 5.13 Measured (dashed line) and simulated (solid line) scattering parameters (DC biasing point: $V_{CE} = 8.0$ V, $I_C = 10$ mA).

The overall performance is remarkable. The input return loss is not as good as predicted; the output return loss is better than expected; forward and reverse transmissions are about 0.5 dB apart from the simulated curve. The reason for the tested S_{11} and S_{22} curves to be so far from the simulated curves is not known. A great deal of uncertainty is due to the lumped components as well as to the fact that the actual device has not been characterised before the design. Random variations of the values of C_o and R_o (Figure 5.9) may explain the upward change in slope of $\mid S_{11} \mid$ over 1 GHz. However, the uncertainties are so many that a thorough investigation seems too complex to carry out. The fact that $\mid S_{22} \mid$ is better than the simulated curve may suggest that the $SSNM = 0$ condition has not been achieved; therefore S_{11} is affected. Nevertheless, -18 dB input return loss is quite a good result – the use of dB rather than units may be misleading. Table 5.16 collects the measured points of

Figure 5.13 at $f_o = 1$ GHz.

Table 5.16 AT41486 BJT SSNM LNA measured scattering parameters at $f_o = 1$ GHz.

S_{11}	-17.73	dB	+138.72	deg
S_{12}	-26.67	dB	+5.21	deg
S_{21}	+9.98	dB	+12.78	deg
S_{22}	-22.84	dB	+171.46	deg

The 3rd order intercept point and the output power at the 1 dB compression point have also been measured and they have been found to be 17 dBm and 3.4 dBm respectively.

5.3.3 Noise Measurement Procedure

The discussion of the measurement of the noise parameters F_{min}, R_n and $\Gamma_{S_{opt}}$ is the objective of this section. This goal is achieved in 2 distinct steps at each frequency f_o of interest [37], [39]: the noise figure is measured for different source reflection coefficients; and the noise parameters are determined. A method[4] recently developed, has been tailored [40], [148] for the measurement of the BJT SSNM LNA noise figure. Then, a standard least squares fit [37], [42], [41], calculates the noise parameters. An outline of the noise figure measurement precedes the description of the noise parameter determination.

The noise figure measurement relies on a procedure which accounts for mismatches existing between:

1. the noise source and the receiver during calibration;

2. the noise source and the device under test (DUT) and

3. the DUT and the receiver during the test.

The method is not new [46] and it has been applied recently [40] at 94 GHz.

Consider Figure 5.14. A noise source at temperature T_s feeds the DUT with noise power, which is amplified and detected by a receiver. Both DUT and receiver contribute to the total noise power budget N_{meas} measured by the detector:

[4] I would like to acknowledge the help of Tariq Alam who gave me the opportunity to look into the interesting subject of noise measurement techniques and kindly made available for me a modified version of his software based on his work [40].

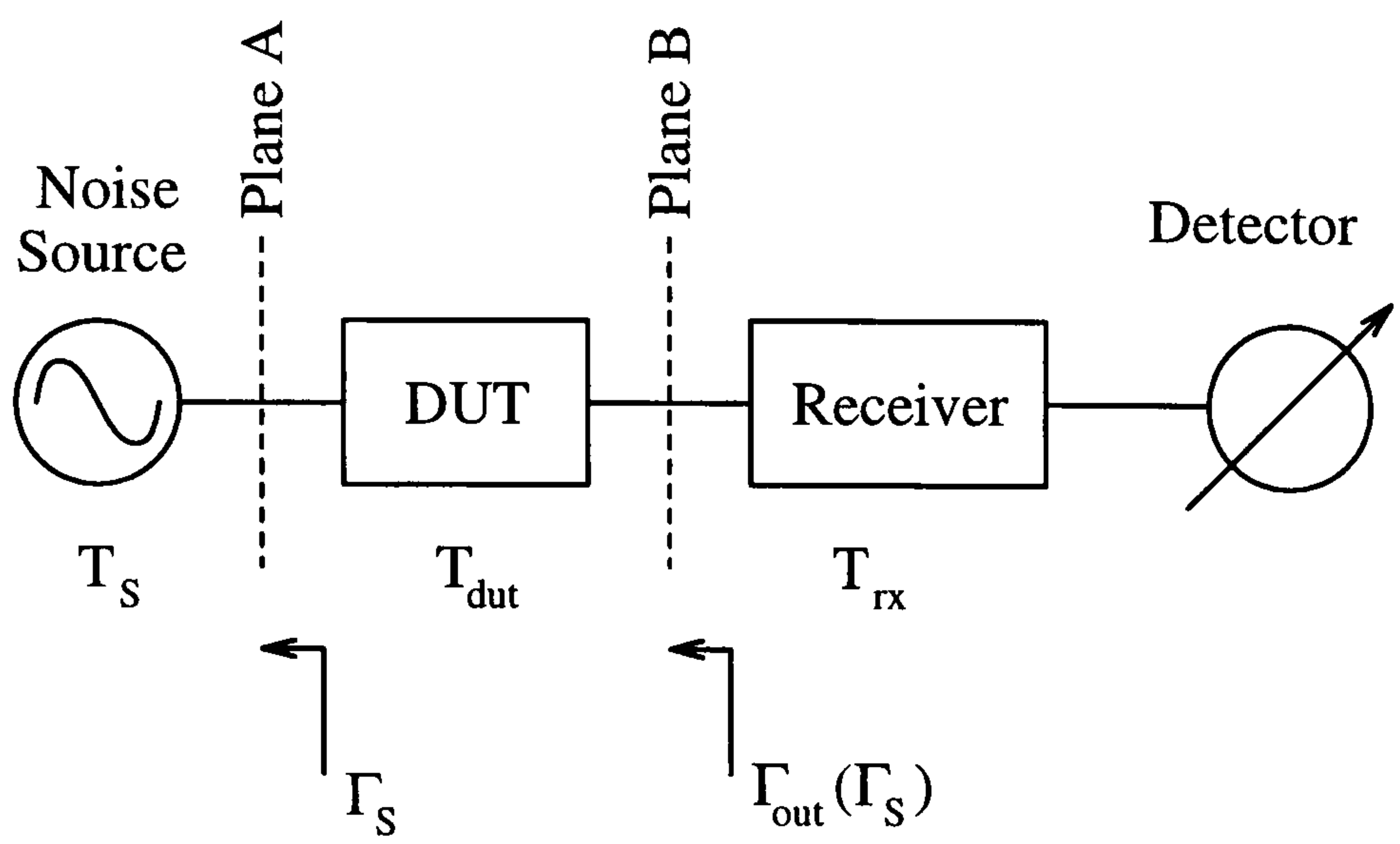

Figure 5.14 Noise measurement setup.

Noise source contribution	+	$k\,B\,T_s \cdot G_{dut}\,G_{rx}$
DUT contribution	+	$k\,B\,T_{dut} \cdot G_{dut}\,G_{rx}$
Receiver contribution	+	$k\,B\,T_{rx} \cdot G_{rx}$
Total detected noise power	=	N_{meas}

where k is the Boltzmann constant and B is the bandwidth of the receiver. Equivalent noise temperatures T_{dut} and T_{rx} depend on the value of the reflection coefficient Γ_S connected at the input port of the DUT; the dependence of T_{rx} on Γ_S occurs through Γ_{out}, the output reflection coefficient of the DUT seen from the input port of the receiver. The available gains G_{dut} of the DUT and G_{rx} of the receiver also depend on the reflection coefficient loading their respective input ports. It is possible to eliminate the dependence of T_{rx} on $\Gamma_{out}(\Gamma_S)$ by inserting an isolator between the reference plane B of Figure 5.14 and the receiver.

Commercially available receivers (noise figure meters) [22] are affected by one crucial drawback: the available gain of the DUT, G_{dut}, is substituted by the insertion gain[5] G_{ins}. If the DUT is perfectly matched, then the insertion gain is numerically equal to the available gain; if there is mismatch, a measurement error occurs.

The procedure in use copes with these problems. At any given frequency f_o, it consists of:

1. *Calibration*: the determination of the gain–bandwidth product $B\,G_{rx}$ and the equivalent noise temperature T_{rx} of the receiver;

[5] The insertion gain is defined as the ratio of the power delivered to the load by the source when the DUT is inserted between source and load to the power delivered to the load by the source when the DUT is not inserted.

2. *Measurement*: the determination of the equivalent noise temperature T_{dut} of the DUT.

Calibration

The calibration is accomplished by making 2 measurements after removing the DUT from the setup (planes A and B in Figure 5.14 are coincident):

- detect the noise power N_h when the noise source is at the equivalent temperature $T_s = T_h$ (hot source);
- detect the noise power N_c when $T_s = T_c < T_h$ (cold source).

The measurement of N_h and N_c lets system (5.26) be laid out and solved for the two unknowns $B\,G_{rx}$ and T_{rx}:

$$k\,B\,T_h\,G_{rx} + k\,B\,T_{rx}\,G_{rx} = N_h \tag{5.26.a}$$

$$k\,B\,T_c\,G_{rx} + k\,B\,T_{rx}\,G_{rx} = N_c \tag{5.26.b}$$

The little dependence[6] of G_{rx} on the source Γ_S when $T_s = T_h$ or $T_s = T_c$ is ideally removed by an isolator between plane B and receiver input port.

Measurement

The actual measurement considers the total noise power budget equation:

$$k\,B\,T_c\,G_{rx}\,G_{dut} + k\,B\,T_{dut}\,G_{rx}\,G_{dut} + k\,B\,G_{rx}\,T_{rx} = N_{meas} \tag{5.27}$$

N_{meas} is the noise power detected by the receiver when the noise source is cold ($T_s = T_c$). The only unknown, the DUT equivalent noise temperature T_{dut}, can be obtained. However, the procedure makes some assumptions which constitute a limitation:

1. the receiver's equivalent noise temperature T_{rx} is independent of the reflection coefficient Γ_{out} at plane B of Figure 5.14 because a (perfect) isolator is connected in front of the receiver;
2. the mismatch at planes A and B is not taken into account in (5.27). If it is considered [40], the noise figure F_{dut} of the DUT is found to be

$$F_{dut} = \frac{1}{G_{dut}}\left[1 + \frac{(N_{meas} - N_c)\,M_h\,(T_h - T_o)}{(N_h - N_c)\,T_o\,M_{dut}}\right] \tag{5.28}$$

[6] Figure 5.16 shows that Γ_S of the noise source varies between hot and cold states.

where N_c, T_c, N_h and T_c are evaluated during calibration; M_h is the mismatch factor [86] between the source and the receiver during calibration (plane A and B coincident); M_{dut} is the mismatch factor at plane B between DUT and receiver during measurement;

3. the cold noise source temperature T_c in (5.28) is equal to the external (room) temperature $T_o = 290$ K.

As a matter of fact, the noise figure F_{dut} can be determined with (5.28) only if source reflection coefficient Γ_S and scattering parameters of the DUT have been previously measured with a network analyser. This is easily carried out and every element of the noise setup (Figure 5.14) is characterised. The scattering parameters are measured and stored on disk for successive computation with noise data.

This methodology for measuring the DUT noise figure has been applied to calculate the SSNM LNA noise parameters.

A direct measurement of the noise parameters is possible [21], [29], [43]. However, skillful operators are necessary in order to guarantee a successful and reliable outcome. A different approach (called here *the Lane method*) has been proposed [37], [39] and it is widely accepted. During the years, the Lane method has been improved and different versions of this technique [41] have been published as discussed in chapter 2. All of them are affected by the difficult task of determining the correct value of the noise equivalent resistance R_n, because it is very sensitive to measurement errors.

The Lane method is based on the collection of a number N_{Lane} of DUT noise figure values F_{dut} for different input source reflection coefficients Γ_S connected at the input port of the DUT itself. The procedure is repeated at each frequency f_o of interest. A value $N_{Lane} = 7$ is usually considered the minimum requirement for a reliable computation of the noise parameters; there is evidence [40], though, that a larger number of samples should be taken. A least squares fit is applied to the measured pairs $(\Gamma_S; F_{dut}(\Gamma_S))$ to minimise the error between the tested noise figure F_{dut} and the calculated noise figure:

$$F = F_{min} + \frac{R_n/Z_o}{\mid 1 + \Gamma_{S_{opt}} \mid^2} \frac{\mid \Gamma_S - \Gamma_{S_{opt}} \mid^2}{1 - \mid \Gamma_{S_{opt}} \mid^2}$$

for the same Γ_S.

The selection of the optimum number N_{Lane} has been addressed for a number of reasons related to the particular case under investigation. When measuring LNAs with small equivalent noise resistances R_n, the surface described by the noise figure is very flat around $\Gamma_{S_{opt}}$

and may be quite spread out around the centre of the Smith chart if $\Gamma_{S_{opt}} \approx 0$ is expected. Figure 5.15 shows that this is the case with the SSNM BJT LNA under discussion. The mismatch $\mid \Gamma_S - \Gamma_{S_{opt}} \mid$ must become very large before causing the noise figure to sensibly increase from F_{min}; this feature is enhanced by small R_n values. The minimum value of the noise figure may be difficult to identify if only a small number of data points are available. These considerations suggest the use of a large N_{Lane} value.

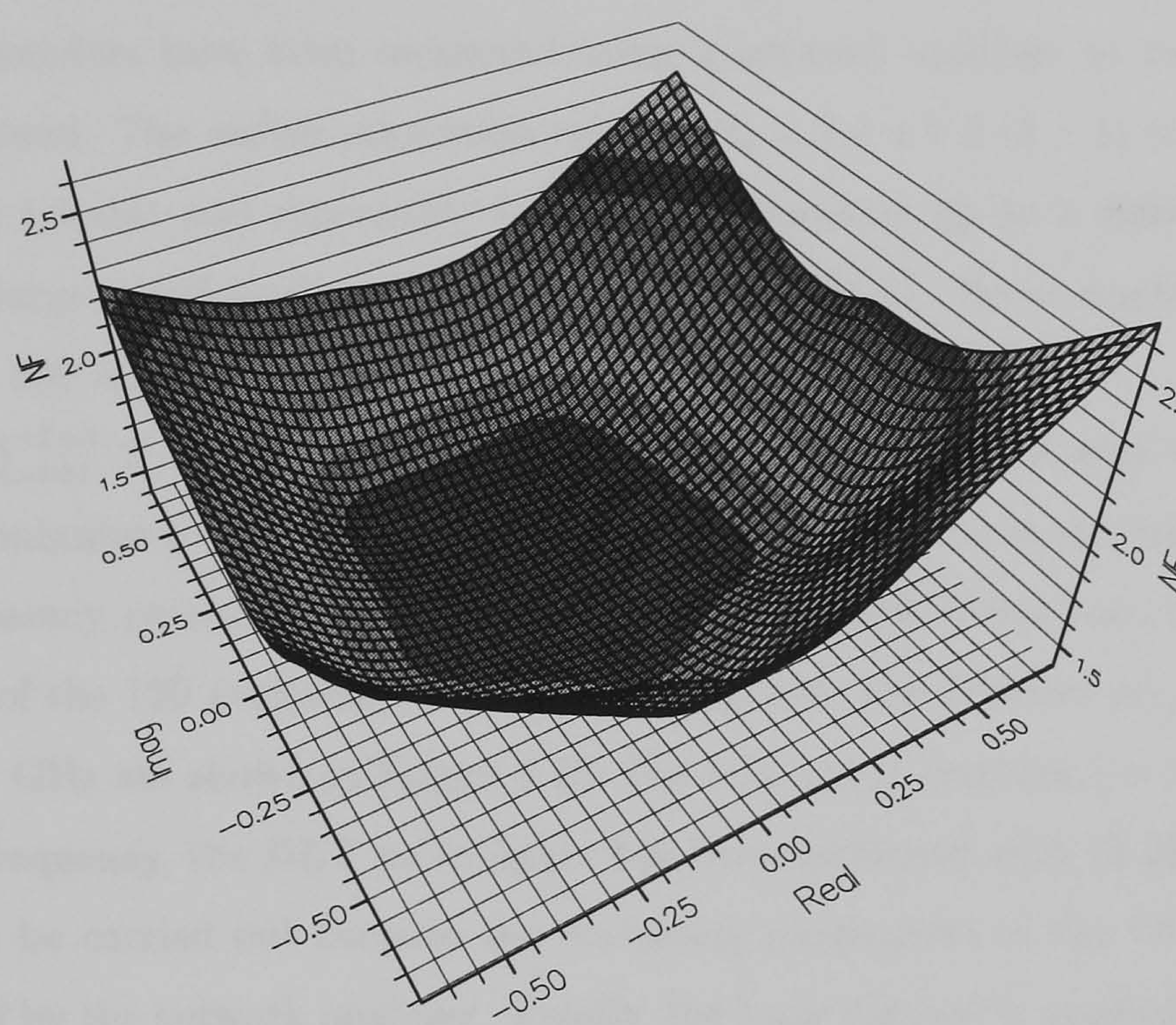

Figure 5.15 Tested noise figure F (NF on the z axis) vs measured source reflection coefficients Γ_S at 1 GHz (DC biasing point: $V_{CE} = 8.0$ V, $I_C = 10$ mA).

5.3.4 Noise Performance

The procedure for the measurement of the noise parameters makes use of the mismatch correction technique (5.28) in order to determine the DUT noise figure vs Γ_S and the Lane method in order to calculate the DUT noise parameters.

$N_{Lane} = 100$ source reflection coefficients Γ_S have been defined on the Smith chart according to the following rules:

1. any point lies on $I = 4$ possible circles; each circle $i = 1, \ldots, I$ is centred in $\Gamma_S = 0$ and its radius is $R_i = 0.1 + 0.2\ (i - 1)$;
2. the number of points N_i on each circle increases as they lie on more and more external

circumferences. On the i^{th} circle, there are 2^i points in each quadrant and the total number of points is $N_i = 4 \times 2^i$; any pair of points are $\Delta\phi_i = 360/N_i$ degree apart, starting at $\varphi_i = \Delta\phi_i/2$.

These rules locate the q^{th} point ($q = 1, \ldots, N_i$) on the i^{th} circle in $\Gamma_S = R_i\, e^{j\,\psi_{iq}}$ where $\psi_{iq} = \varphi_i + \Delta\phi_i\ (q-1)$; and guarantee that there is a constant number of points per unit length of any circumference with radius R_i.

Each value Γ_S has been implemented with a computer controlled tuner [149] whose scattering parameters have been measured using a network analyser at each frequency of interest and stored. The radius maximum value is $R_4 = 0.1 + 0.2\ (4-1) = 0.7$ because the tuner provides reliable and repeatable scattering parameters up to a reflection coefficient magnitude as large as 0.8 (voltage standing wave ratio >10:1). Tuner resetability[7] is better than 50 dB at 800 MHz.

There are $\sum_{i=1}^{I=4} 2^i = 30$ points each quadrant, 120 in total. The semi-automatic setup takes about 4 minutes to acquire data for each tuner position within the required frequency range (14 frequency points from 970 to 1100 MHz); therefore, it has been decided to select 99 points out of the 120 available, plus the point $\Gamma_S = 0$. The selected $N_{Lane} = 100$ points measured at 1 GHz are shown in Figure 5.16. For each tuner position $i = 1, \ldots, N_{Lane}$ and for each test frequency, the DUT noise figure has been measured with (5.28); the mismatch correction can be carried out because the scattering parameters of the DUT have already been measured by the network analyser. Finally, the Lane method is applied to data subsets: $N_{Lane}^{sub} = 25$ point subsets have been used. The resulting measured noise parameters are shown in Figure 5.17 and the values at $f_o = 1$ GHz in Table 5.17.

Table 5.17 SSNM AT41486 BJT LNA measured noise performance at $f_o = 1$ GHz.

F_{min}	1.44	dB
R_n	7.83	Ω
$\mid \Gamma_{S_{opt}} \mid$	-28.44	dB
$\angle\Gamma_{S_{opt}}$	172.42	deg

The results are reliable because they satisfy the Pospieszalski inequality $T_{min} \leq 4\, N\, T_o$ (chapter 2, section 2.3.1).

The measurement band 970 MHz – 1100 MHz cannot be extended toward smaller fre-

[7] The Producer [149] defines the resetability as the *S–parameter dispersion when the tuner is moved 10 times to the same set of positions corresponding to concentric circles on the Smith chart.*

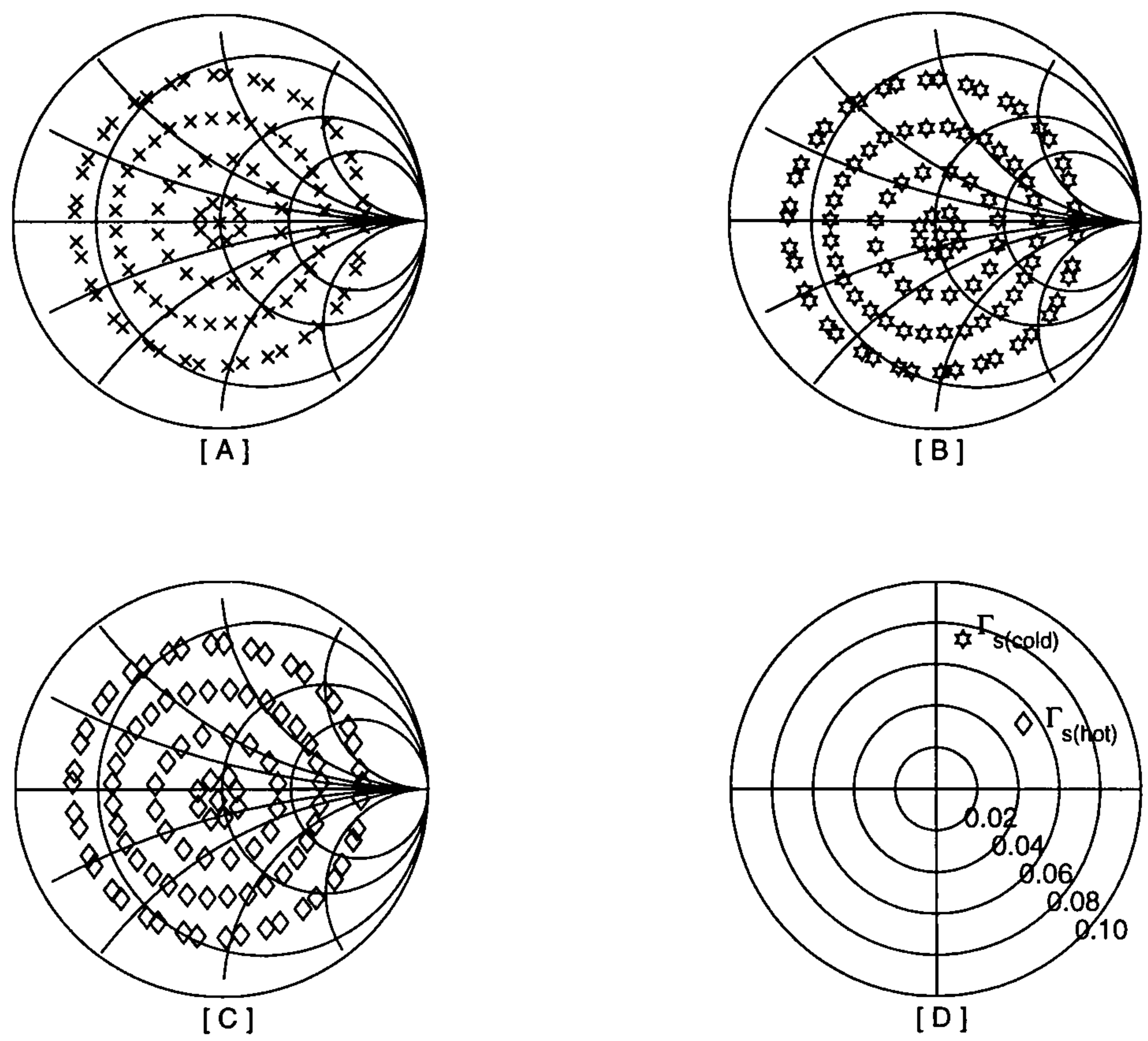

Figure 5.16 100 tuner positions at $f_o = 1$ GHz: plot A shows S_{11} of the tuner at the DUT input plane; plot B and C show the input reflection coefficient of the tuner seen by the DUT when the other port is connected respectively with a hot noise source $\Gamma_{s(hot)}$ and with a cold noise source $\Gamma_{s(cold)}$; plot D shows the position of $\Gamma_{s(cold)}$ and $\Gamma_{s(hot)}$ at f_o. The noise source is a HP346B noise source.

quencies because the noise figure meter suffers from strong interferences due to mobile communication transceivers located in the area around the laboratory. However, the good performance of the LNA is demonstrated.

The optimum noise source coefficient $\Gamma_{S_{opt}}$ in Figure 5.17 is smaller than 0.1 or -20 dB at 1 GHz; the SSNM condition is very good (input return loss is 17.73 dB, Table 5.16; $\mid SSNM \mid = -19.27$ dB as defined in (3.42), chapter 3, section 3.3.2). The shape of $\mid \Gamma_{S_{opt}} \mid$ is similar to the the shape demonstrated numerically for $\mid \Gamma_{S_{opt}} \mid_{min}$ in Figure 5.5 and Figure 5.6; its measured value -28.44 dB (Table 5.17) corresponds to 0.038, which is close to 0.04, the data book value for $\Gamma_{S_{opt}}$. The actual value is affected by both the Lane method fitting procedure and the subset of Γ_S points in use. Despite numerical changes, the resulting values are always consistent with the published results [142]. Figure 5.17 shows that the condition $F \approx F_{min}$ is achieved, within the measurement uncertainty, in the 970–1100 MHz range.

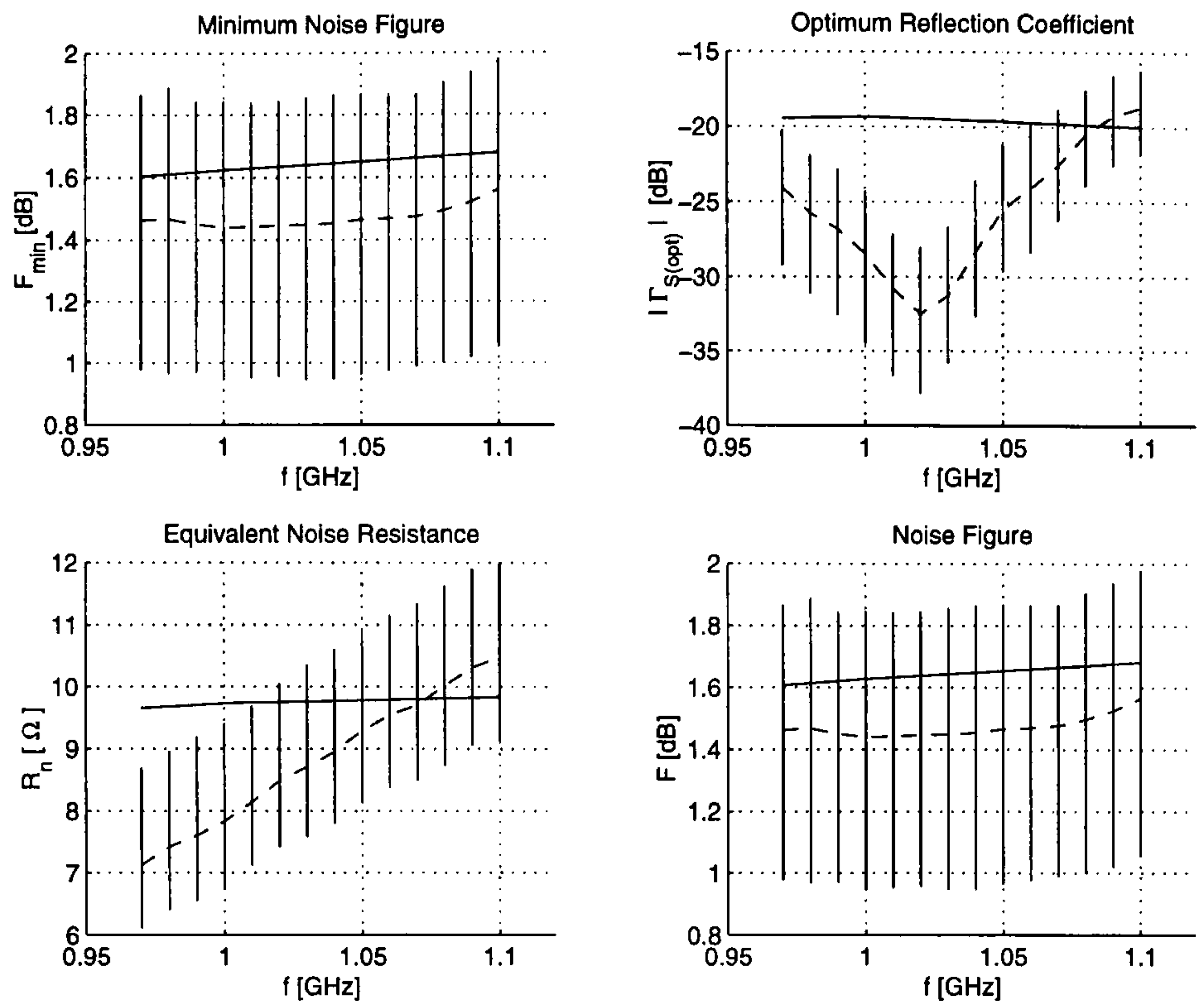

Figure 5.17 Measured (dashed line) and simulated (solid line) noise parameters and noise figure with associated uncertainty at each frequency (DC biasing point: $V_{CE} = 8.0$ V, $I_C = 10$ mA).

5.3.5 Error Analysis

The uncertainty associated with the noise parameter measurement has been evaluated. The core of the procedure consists of:

1. assigning a random variation around the nominal (measured) values of the tested quantities within a fixed range;

2. applying the Lane method to the error–affected values and working out the noise parameters. Repeat this step $N_{err} = 1000$ times; and

3. determining the statistical averages of the error–affected noise parameters.

Assignment

The quantities to which random variations have been assigned in order to simulate measurement uncertainty are:

- magnitude and phase of any parameter measured with the network analyser;

- noise powers measured by the receiver;

- noise power generated by the noise source.

Errors are assigned in terms of maximum span ΔX_o from the measured value X_o ($X_o \pm \Delta X_o$). Magnitude of scattering parameters and noise source excess noise ratio ENR[8] are expressed in dB and so is their uncertainty ΔX_o. It has been assumed that ΔX_o dB around X_o corresponds to a relative error:

$$\frac{dx_o}{x_o} = \frac{\delta x_o - 1}{\delta x_o + 1} \tag{5.29}$$

where:

$$\delta x_o = 10^{\Delta X_o/10}$$

dx_o and x_o are, respectively, the quantities ΔX_o and X_o in units. Table 5.18 shows the values of errors expressed in dB and units with (5.29). As a rule of thumb, 1% error corresponds to 0.1 dB, 10% to 1 dB.

Table 5.18 Transformation table between dB and relative errors.

ΔX_o dB	$\frac{dx_o}{x_o}$ %
0.00	0.00
0.10	1.15
0.25	2.88
0.50	5.75
0.75	8.61
1.00	11.46
1.50	17.10
2.00	22.63

Scattering parameters measured by the network analyser are affected by an error which is function of the magnitude of the quantity under test [143]. This fact has not been accounted for, even though it could be easily implemented.

- Hot noise source input reflection coefficient $\Gamma_S = \Gamma_{Sh}$;
- cold noise source input reflection coefficient $\Gamma_S = \Gamma_{Sc}$;
- receiver input reflection coefficient Γ_L;
- tuner scattering parameters $S_{ij}^{(Tuner)}$; and

[8] The excess noise ratio represents the increment of the equivalent noise temperature T_h of a (hot) noise source from the standard temperature $T_o = 290$ K relative to T_o and it is given in dB.

- SSNM LNA scattering parameters $S_{ij}^{(LNA)}$.

are affected by measurement errors. Magnitude and phase may vary within, respectively, $\pm\ \Delta M$ dB and $\pm\ \Delta P$ % of their measured value.

The receiver introduces another error in the measurement process. Detected power is allowed to vary within $\pm\ \Delta W$ dB of the tested value. Noise powers affected by this error are:

- the power from the noise source measured during the calibration; and
- the output power delivered by the chain *noise source – tuner – DUT* during measurement.

Noise source ENR is also affected by an uncertainty ranging within $\pm\ \Delta S$ dB; it may heavily affect the measurement because it concerns the calibration step. However, during calibration, the noise source is connected directly to the receiver and the error produced can be associated with it. As a matter of fact, a relative error can be interpreted as if an error–free power level is supplied by the noise source but the detector in Figure 5.14 shows a value which is within the range $\pm\ \Delta W$ around the real value. Furthermore, (5.28) shows that noise source power during measurement is accounted for by the equivalent temperature $T_s = T_c$. As long as the available gain of the DUT, which depends on the scattering parameter measurement, is large, the uncertainty associated with T_c is not significant.

Calculation

Evaluation of the error–affected noise parameters has been carried out with:

$$\begin{aligned}
\Delta M &= 0.5 \quad \text{dB} \\
\Delta P &= 2.5 \quad \text{deg} \\
\Delta W &= 0.5 \quad \text{dB} \\
\Delta S &= 0.5 \quad \text{dB}
\end{aligned}$$

assigned to any of the 14 frequency points in the range 970–1100 MHz. The errors associated with the scattering parameter measurement are much larger than typical ANA errors [143], typically ± 0.1 dB and ± 1 deg for magnitude and phase, respectively. The error procedure has been repeated $N_{err} = 1000$ times on the entire set of data points: $N_{Lane}^{sub} = N_{Lane} = 100$.

Statistic

A simple study of the main sources of error for each noise parameter has been carried out. The influence of the uncertainty associated with the noise source has been neglected because it has been associated with the error of the receiver and the gain of the LNA is quite large ($\approx$10 dB, Table 5.16).

The main cause of error for minimum noise figure is the uncertainty ΔW related to the measurement of the detected noise power. Equivalent noise resistance R_n has little dependence on ΔP associated with scattering parameter phases; both ΔM and ΔW affect R_n in a similar fashion. The magnitude of the optimum noise source reflection coefficient $\Gamma_{S_{opt}}$ depends on ΔM and ΔW as in the R_n case. These results are collected in Table 5.19; the σ value[9] of each parameter is shown.

Table 5.19 Noise parameter standard deviation σ at $f_o = 1$ GHz.

	$\Delta M = 1.0$ dB $\Delta P = 0.0$ deg $\Delta W = 0.0$ dB	$\Delta M = 0.0$ dB $\Delta P = 2.0$ deg $\Delta W = 0.0$ dB	$\Delta M = 0.0$ dB $\Delta P = 0.0$ deg $\Delta W = 1.0$ dB
$F_{min}^{(\sigma)}$	± 0.09 dB	≈ 0 dB	± 0.28 dB
$R_n^{(\sigma)}$	$\pm 0.76\ \Omega$	$\approx 0\ \Omega$	$\pm 0.83\ \Omega$
$\mid \Gamma_{S_{opt}} \mid^{(\sigma)}$	± 4.85 dB	± 0.004 dB	± 3.77 dB

Error bars are shown in Figure 5.17 along with their respective noise parameters. Numerical values vs frequency are collected in Table 5.20. Standard deviations tend to increase as the frequency increases. Only for the optimum noise source reflection coefficient case, it tends to decrease as expected; it should be noticed that $\mid \Gamma_{S_{opt}} \mid$ is very small where $\mid \Gamma_{S_{opt}} \mid^{(\sigma)}$ is the largest (see Figure 5.13).

5.4 Conclusion

Original and unique techniques for the design of the optimum noise source reflection coefficient $\Gamma_{S_{opt}}$ have been presented. They permit the designer to determine the feedback elements in order to deliver the desired $\Gamma_{S_{opt}}$ at the design frequency f_o. The procedures allow the design of complex optimum noise source reflection coefficient or its magnitude. A by–product of the design for $\mid \Gamma_{S_{opt}} \mid$ is the discovery that the magnitude of $\Gamma_{S_{opt}}$ has a minimum; a simple procedure has been described for its determination. Finally, the fabrication of a simultaneously signal and noise matched low noise amplifier has demonstrated that the technique can achieve remarkable results with simple surface mount components at 1 GHz.

[9] The standard deviation σ determines the range $\pm\sigma$ around x_o where there are 63 out of 100 chances to find the expected $\hat{x}_o$.

Table 5.20 Noise parameter standard deviations vs frequency. The uncertainties ΔM, ΔW and ΔS ranges between ± 0.5 dB and ΔP between ± 2.5 deg.

f GHz	$\pm F_{min}^{(\sigma)}$ dB	$\pm R_n^{(\sigma)}$ Ω	$\pm \mid \Gamma_{S_{opt}} \mid^{(\sigma)}$ dB
0.97	0.44	1.29	4.51
0.98	0.46	1.28	4.61
0.99	0.44	1.32	4.88
1.00	0.45	1.32	5.09
1.01	0.44	1.28	4.76
1.02	0.44	1.31	4.93
1.03	0.45	1.38	4.58
1.04	0.46	1.40	4.56
1.05	0.45	1.39	4.25
1.06	0.45	1.39	4.28
1.07	0.44	1.41	3.67
1.08	0.45	1.44	3.17
1.09	0.46	1.42	2.98
1.10	0.46	1.53	2.78

Chapter 6

Conclusions

6.1 Contributions to LNA Design

There are at least six crucial and significant contributions produced by this research on the topic of:

1. input matching network design;
2. analysis of feedback amplifier noise parameters;
3. the Pospieszalski noise model;
4. noise parameter design with feedback amplifier;
5. experimental validation of the noise parameter design; and
6. noise parameter design with lossy elements.

All of them are original and they constitute an important step forward in the design of low noise amplifiers; noteworthy implications are pointed out for the design of active devices such as HEMTs or MESFETs tuned for best simultaneous signal and noise match performance.

6.1.1 Input Matching Networks

Input matching networks have been analysed under the constraint that the SSNM condition is required at the input plane of the matching network; the results of that analysis have been presented in this work and published in [123].

Input matching circuits can transfer the SSNM match from their output to input port only if it has already been achieved at their output terminals. This point suggests that if the SSNM condition is required, the design of LNAs should concentrate on avoiding the use of input matching circuits.

The analysis concludes that an input matching network capable of satisfying the SSNM requirement must include lossy elements if it is to be reciprocal. Therefore, when considering the remaining noise parameters, the minimum noise figure and the equivalent noise resistance are likely to deteriorate. The issue that input matching circuits can badly affect the overall noise performance had already been reported in the literature [34]; however, the fact that the design of input matching circuits is carried out without accounting for its noise contribution is hardly mentioned in the literature and rarely formalised.

6.1.2 Analysis of Feedback Amplifiers

Analytical expressions for the noise parameters R_n, g_n and ρ_{n_o} of feedback amplifiers with noisy series and parallel immittances have been worked out in the course of the present study [127]. These expressions are functions of the real and imaginary parts of the feedback elements; they can be studied analytically at the given frequency f_o based on the assumptions that:

- the given device is a 2–port network. No radio frequency path must exist when the common lead is connected to ground through the series impedance Z_s; and
- the network to which feedback elements are applied, is linear at the given frequency f_o and its signal and noise correlation matrices are available.

The analysis is applicable to any type of passive or active, distributed or lumped network, as long as the previous hypotheses are verified. It also provides a model for published experimental results [111] as well as demonstrating that:

- a duality principle holds; and
- for series reactance feedback amplifiers, any equivalent noise resistance R_n value lies between $R_{n_{max}}$ and $R_{n_{min}}$ and approaches $R_{n_{sat}}$ for $X_s = \Im m\,[Z_s] \rightarrow \pm\infty$.

The duality principle brings up the intimate link between series and parallel feedback amplifiers. The series reactance $X_{S_{opt}}$ for minimum equivalent noise resistance $R_{n_{min}}$ may lead to the definition of an optimum value for noise figure design: $R_{n_{min}}$ minimises the dependence of the noise figure on the input mismatch $\mid \Gamma_S - \Gamma_{S_{opt}} \mid$. Therefore, larger mismatch and $SSNM \rightarrow 0$ can be achieved for the same noise figure with series feedback LNAs.

6.1.3 Extension of the Pospieszalski Noise Model

The analysis of feedback amplifiers has been applied to a well–known noise model for intrinsic MESFETs, extending it to extrinsic and packaged devices; the results have been generated from this investigation of the author and made available in refereed literature [59]. The new analysis shows that the reactive part of the optimum source impedance $Z_{S_{opt}}$ for extrinsic or packaged MESFETs depends on C_{gs} as well as on the series source inductance L_s and gate inductance L_g; a simple approximation of $X_{S_{opt}} = \Im m\left[Z_{S_{opt}}\right]$ has been validated. Finally, the present study furnishes a theoretical model for an empirical expression experimentally supported by researchers and broadens the investigation of the behaviour of $Z_{S_{opt}}$ to its real part $R_{S_{opt}}$ when a lossy feedback impedance is applied.

6.1.4 Optimum Noise Source Reflection Coefficient Design

A further new and original result of this work is the design of a noise parameter such as $\Gamma_{S_{opt}}$ with feedback amplifiers [139]: this is a genuine step forward in circuit analysis and design techniques because, to the author's knowledge, no previous procedures were available. They are based on the closed form expressions for feedback LNA noise parameters and they allow the optimum noise source reflection coefficient $\Gamma_{S_{opt}}$ or its magnitude to be analytically determined with feedback immittances.

Since the techniques stem from the noise parameters analysis which has been part of this study [127], the same assumptions apply and the results are valid for the same wide range of 2–port active or passive, distributed or lumped networks. The proper choice of the load ensures that the SSNM condition is met at the design frequency f_o. As a consequence, input matching circuits are not strictly necessary.

By–products of the new technique in [139] are:

- $\Gamma_{S_{opt}}$ vs series reactance X_s shows a minimum in magnitude, which can be approximated with standard least squares fit. Consequently, the input return loss cannot be improved from the threshold value $\mid \Gamma_{S_{opt}} \mid_{min}$ under the SSNM constraint; and
- the minimum noise figure of the given 2–port network can be lowered by feedback immittances.

6.1.5 Validation of the Design Technique

The original techniques for optimum noise source reflection coefficient design described in this thesis [139] have been applied to the design of a 1 GHz single stage LNA which has been published in [142] and thoroughly discussed in this study. The measurements show that the noise figure F is convincingly demonstrated to be equal to the minimum noise figure F_{min} of the device within the measurement uncertainty. The SSNM BJT LNA presented in [142] is the first analytically–designed amplifier to achieve the SSNM condition.

6.1.6 Design with Lossy Series Feedback Elements

The technique for $\mid \Gamma_{S_{opt}} \mid$ design does not allow the use of lossy reactive elements; for instance, the series inductance quality factor Q_s is assumed to be infinity. An innovative and novel extension to lossy reactive elements has been devised for the first time by the author of the present work and made available to everyone in [140]. The minimum in $\mid \Gamma_{S_{opt}} \mid$ and the decrease of F_{min} can still be obtained if the inductor quality factor is large enough; the threshold value for Q_s can also be evaluated. Different behaviours between BJTs and FETs have been highlighted.

6.2 Future Works

The results this research has pointed out are based on an analytical approach which is often left aside in favour of CAD and optimisation programs or direct experiments. Far from diminishing the indispensable help CAD software provides, the analytical approach gives valuable insights and starting design points which do not depend on the designer's experience.

Many suggestions for further investigations are spread throughout the dissertation. They may have been pointed out as limitations based on the assumed hypotheses or as work which could be worthwhile developing.

In particular, some specific indications for further developments of this present study are:

- the analysis of the noise parameters is valid for any 2–port networks and therefore it can be applied to a wide class of devices. The importance of the parasitics in microwave devices is a well–known fact; the expressions for the noise parameters allows further study to be undertaken;
- the formulæ for the noise parameters give the transistor designer a tool to tune the design of the transistor for optimum SSNM performance. As a matter of fact, the 2–port device to which the feedback elements are connected, can be intrinsic or extrinsic.

In the first case, the transistor SSNM performance itself can be optimised; in the second case, the package can be designed accordingly;

- the characterisation of both the real and imaginary parts of inductors in terms of a common parameter (such as the number of turns) would allow optimum $| \Gamma_{S_{opt}} |$ design of the series feedback impedance. Numerical or even analytical solutions could be worked out since the equations for $| \Gamma_{S_{opt}} |$ design are already available;

- most of the results of this research have been assessed and made available in IEEE journals and refereed literature. The design technique for optimum noise source reflection coefficient has also been demonstrated experimentally. However, further experiments should be carried out at different frequencies and with different devices and technologies in order to fully validate the original procedure. Some work along these lines is in progress;

- the way the linear range of operation [150] is affected by the series feedback impedance for SSNM condition has not been the main target of this research and therefore constitutes another open field of research;

- a new direction of investigation is to apply the results collected in this dissertation to distributed amplifiers. Little is available on their noise performance; having a better understanding of the noise parameters versus feedback elements, should permit the designer to investigate how to reduce the noise contribution of the amplifier to the output signal–to–noise ratio.

Among many underlying problems of modern microwave engineering that have been faced during this research, two would be worthwhile of more investigation:

1. a method to characterise the transition due to the use of SMA connectors has been looked into and analytical expressions for calculating scattering parameter through a series of measurements with transmission lines have been obtained; software has been written to obtain the numerical solution. The problem is not new and resembles very closely a calibration procedure [144], [145], [146], [151]. Some network analyser software [143] allows the connectors to be automatically removed from the measured data; others have implemented time domain techniques aiming at solving this problem. However, the approach has some interesting by–products such as the determination over the measurement bandwidth of the transmission line characteristic impedance

and it is applicable to any linear transition. The drawback is an extreme sensitivity to the starting measured values;

2. it is quite well accepted that the measurement of the noise parameters with the Lane method may be troublesome, in particular as far as R_n is concerned. Furthermore, the equipment required and the operator's skills still are two basic limitations of the practical measurement. A simplified method would be highly desirable. Recently, neural networks have drawn microwave engineers' attention (see for instance, *IEEE Transactions on Microwave Theory and Techniques*, Vol. 45, Part II, May 1997 or *IEEE MTT–S International Microwave Symposium*, Workshop WFE, *Application of Artificial Neural Networks to Microwave Design*, Denver, 13 June 1997). A brand new line of research is to apply neural networks to the determination of the noise parameters. The training of the neural network could be carried out with sets of data easily obtainable from existing simulators for different values of input source reflection coefficients [37] and/or different noise temperature of the source [40], [46]. Once the neural network has been determined, one single measurement could determine the noise performance of the DUT.

Appendix A

Chapter 2 Appendix

A.1 The Pospieszalski Inequality

An independent demonstration of (2.8), chapter 2, section 2.3.1:

$$\frac{T_{min}}{T_o} \leq 4\,N \tag{A.1}$$

is provided. (A.1) is cited by Pospieszalski [7], [47] from a PhD thesis in Polish without repeating the demonstration.

Consider the transmission matrix representation of 2–port noisy networks when a noisy source admittance $Y_s = G_s + j\,B_s$ is connected at its input port. The correlation matrix:

$$\mathbf{C}_n = \begin{bmatrix} R_n & {\rho_{n_o}}^{\star} \\ \rho_{n_o} & g_n \end{bmatrix} \tag{A.2.a}$$

is semi–definite positive (see appendix C.1):

$$\begin{aligned} \Delta_n &= R_n\,g_n - \mid \rho_{n_o} \mid^2 = R_n\,g_n\,(1 - \mid \rho_n \mid^2) \geq 0 && \text{(A.3.a)} \\ R_n &\geq 0 && \text{(A.3.b)} \\ g_n &\geq 0 && \text{(A.3.c)} \end{aligned}$$

The terms R_n, g_n and $\rho_{n_o} = \rho_n\,\sqrt{R_n\,g_n}$ are the 2–port noise parameters in transmission matrix representation; the term $4kT_o\Delta f$ in (A.2.a) has been dropped for simplicity.

The new set of noise parameters $Y_{S_{opt}} = G_{S_{opt}} + j\,B_{S_{opt}}$, F_{min} and R_n for the noise figure expression can be calculated in terms of R_n, g_n and ρ_{n_o}:

$$\begin{aligned}
G_{S_{opt}} &= \frac{\sqrt{R_n\, g_n - (\Im m\,[\rho_{n_o}])^2}}{R_n} && \text{(A.4.a)}\\
B_{S_{opt}} &= \frac{\Im m\,[\rho_{n_o}]}{R_n} && \text{(A.4.b)}\\
F_{min} - 1 &= 2\left[\sqrt{R_n\, g_n - (\Im m\,[\rho_{n_o}])^2} - \Re e\,[\rho_{n_o}]\right] && \text{(A.4.c)}
\end{aligned}$$

From (A.4.a), the Lange invariant $N = R_n\, G_{S_{opt}}$ is found to be:

$$N = \sqrt{R_n\, g_n - (\Im m\,[\rho_{n_o}])^2} \tag{A.5}$$

which can be rewritten as:

$$\begin{aligned}
N &= \sqrt{R_n\, g_n - \mid \rho_{n_o} \mid^2 + (\Re e\,[\rho_{n_o}])^2}\\
&= \sqrt{\Delta_n + (\Re e\,[\rho_{n_o}])^2} && \text{(A.6)}
\end{aligned}$$

after adding $\pm\ (\Re e\,[\rho_{n_o}])^2$ and substituting (A.3.a) into (A.5); (A.6) shows that $N \geq 0$. Furthermore, since $\Delta_n \geq 0$ (A.3.a),

$$\mid \Re e\,[\rho_{n_o}] \mid \ \leq\ N \tag{A.7}$$

can be obtained after squaring (A.6), omitting Δ_n and taking the square root.

Since equivalent temperature T and noise figure F are related by:

$$\frac{T}{T_o} = F - 1$$

where $T_o = 290$ K, (A.4.c) becomes:

$$\begin{aligned}
\frac{T_{min}}{T_o} = 2\ (N - \Re e\,[\rho_{n_o}]) &\leq 2\ (N + \mid \Re e\,[\rho_{n_o}] \mid) && \text{(A.8.a)}\\
&\leq 4\,N && \text{(A.8.b)}
\end{aligned}$$

by applying (A.7) in (A.8.a). (A.8.b) is equivalent to (A.1).

Appendix B

Chapter 4 Appendices

B.1 Solution of the noise analysis system

The system to be solved is laid out in (3.25), chapter 3, section 3.1.3 and here rewritten:

$$
\begin{aligned}
I_1 + I_{22} &= I_3 && \text{(B.1.a)}\\
I_3 &= I_{11} + i_t && \text{(B.1.b)}\\
V_{11} &= A_t V_{22} + B_t I_{22} && \text{(B.1.c)}\\
I_{11} &= C_t V_{22} + D_t I_{22} && \text{(B.1.d)}\\
-Y_p V_1 &= I_{22} + i_p && \text{(B.1.e)}\\
V_{22} + V_4 &= 0 && \text{(B.1.f)}\\
V_4 &= e_s + Z_s I_4 && \text{(B.1.g)}\\
I_3 &= I_4 + I_{22} && \text{(B.1.h)}\\
V_1 &= e_t + V_{11} + V_4 && \text{(B.1.i)}
\end{aligned}
$$

Define:

$$
\begin{aligned}
X &= [I_1 \quad I_{11} \quad I_{22} \quad I_3 \quad I_4 \quad V_1 \quad V_{11} \quad V_{22} \quad V_4]^T && \text{(B.2)}\\
Y &= [0 \quad i_t \quad 0 \quad 0 \quad i_p \quad 0 \quad e_s \quad 0 \quad e_t]^T && \text{(B.3)}
\end{aligned}
$$

to collect unknowns and given noise sources, respectively. In X, only V_1 and I_1 are of interest because they correspond to voltage and current at the input port of the final feedback circuit

(Figure 3.3). The formal solution of (B.1) is $X = \mathbf{D}^{-1}Y$ where $\mathbf{D}$ is the proper matrix of coefficients. Here, the unknowns of interest V_1 and I_1 are found by substitutions:

1. rewrite the system without (B.1.f) after having V_4 substituted with $-V_{22}$:

$$\begin{aligned}
I_1 + I_{22} &= I_3 && \text{(B.4.a)}\\
I_3 &= I_{11} + i_t && \text{(B.4.b)}\\
V_{11} &= A_t V_{22} + B_t I_{22} && \text{(B.4.c)}\\
I_{11} &= C_t V_{22} + D_t I_{22} && \text{(B.4.d)}\\
-Y_p V_1 &= I_{22} + i_p && \text{(B.4.e)}\\
-V_{22} &= e_s + Z_s\, I_4 && \text{(B.4.f)}\\
I_3 &= I_4 + I_{22} && \text{(B.4.g)}\\
V_1 &= e_t + V_{11} - V_{22} && \text{(B.4.h)}
\end{aligned}$$

2. substitute (B.4.a) and (B.4.g) into (B.4.b) and (B.4.h) respectively:

$$\begin{aligned}
I_1 + I_{22} &= I_3 && \text{(B.5.a)}\\
I_{11} - I_{22} &= I_1 - i_t && \text{(B.5.b)}\\
V_{11} &= A_t V_{22} + B_t I_{22} && \text{(B.5.c)}\\
I_{11} &= C_t V_{22} + D_t I_{22} && \text{(B.5.d)}\\
I_{22} &= -Y_p V_1 - i_p && \text{(B.5.e)}\\
-V_{22} &= e_s + Z_s\, I_4 && \text{(B.5.f)}\\
e_s &= -V_{22} - Z_s\, I_3 + Z_s\, I_2 && \text{(B.5.g)}\\
V_1 &= e_t + V_{11} - V_{22} && \text{(B.5.h)}
\end{aligned}$$

3. substitute (B.5.a) into (B.5.g) along with (B.5.e) and (B.5.e) into (B.5.b):

$$\begin{aligned}
I_1 + I_{22} &= I_3 && \text{(B.6.a)}\\
I_{11} &= I_1 - i_t - Y_p\, V_1 - i_p && \text{(B.6.b)}\\
V_{11} &= A_t V_{22} + B_t I_{22} && \text{(B.6.c)}\\
I_{11} &= C_t V_{22} + D_t I_{22} && \text{(B.6.d)}\\
I_{22} &= -Y_p V_1 - i_p && \text{(B.6.e)}
\end{aligned}$$

$$
\begin{aligned}
-V_{22} &= e_s + Z_s\, I_4 && \text{(B.6.f)}\\
e_s &= -V_{22} - Z_s\, I_1 && \text{(B.6.g)}\\
V_1 &= e_t + V_{11} - V_{22} && \text{(B.6.h)}
\end{aligned}
$$

4. substitute (B.6.g) into (B.6.h):

$$
\begin{aligned}
I_1 + I_{22} &= I_3 && \text{(B.7.a)}\\
I_{11} &= I_1 - i_t - Y_p\, V_1 - i_p && \text{(B.7.b)}\\
V_{11} &= A_t V_{22} + B_t I_{22} && \text{(B.7.c)}\\
I_{11} &= C_t V_{22} + D_t I_{22} && \text{(B.7.d)}\\
I_{22} &= -Y_p\, V_1 - i_p && \text{(B.7.e)}\\
-V_{22} &= e_s + Z_s\, I_4 && \text{(B.7.f)}\\
e_s &= -V_{22} - Z_s\, I_1 && \text{(B.7.g)}\\
V_1 &= e_t + V_{11} + Z_s\, I_1 + e_s && \text{(B.7.h)}
\end{aligned}
$$

5. the unknowns V_{11}, I_{11}, V_{22} and I_{22} appear respectively in (B.7.h), (B.7.b), (B.7.g) and (B.7.e) as functions of V_1, I_1 and the known noise sources. In order to solve the system, two more equations, (B.7.c) and (B.7.d), are necessary:

$$
\begin{aligned}
V_1 &= e_t + V_{11} + Z_s\, I_1 + e_s && \text{(B.8.a)}\\
I_{11} &= I_1 - i_t - Y_p\, V_1 - i_p && \text{(B.8.b)}\\
V_{22} &= -e_s - Z_s\, I_1 && \text{(B.8.c)}\\
I_{22} &= -Y_p V_1 - i_p && \text{(B.8.d)}\\
V_{11} &= A_t V_{22} + B_t I_{22} && \text{(B.8.e)}\\
I_{11} &= C_t V_{22} + D_t I_{22} && \text{(B.8.f)}
\end{aligned}
$$

6. substitute (B.8.a), (B.8.b), (B.8.c) and (B.8.d) into (B.8.e) and (B.8.f) and take every noise source to the right hand side of the equal sign:

$$
\begin{aligned}
V_1 + B_t\, Y_p\, V_1 - Z_s\, I_1 + A_t\, Z_s\, I_1 &= e_t + e_s - B_t\, i_p - A_t\, e_s && \text{(B.9.a)}\\
-Y_p\, V_1 + D_t\, Y_p\, V_1 + I_1 + C_t\, Z_s\, I_1 &= i_t - C_t\, e_s + i_p - D_t\, i_p && \text{(B.9.b)}
\end{aligned}
$$

(B.9) can be arranged in matrix form:

$$\begin{bmatrix} 1+B_tY_p & -(1-A_t)\ Z_s \\ -(1-D_t)\ Y_p & 1+C_tZ_s \end{bmatrix} \begin{bmatrix} V_1 \\ I_1 \end{bmatrix} = \begin{bmatrix} 0 & 1 & -B_t & 1-A_t \\ 1 & 0 & 1-D_t & -C_t \end{bmatrix} \begin{bmatrix} e_t \\ e_s \\ i_p \\ e_s \end{bmatrix}$$

Left and right hand side matrices are respectively defined as **A** in (3.26.b) and **N** in (3.26.c):

$$\mathbf{A} \begin{bmatrix} V_1 \\ I_1 \end{bmatrix} = \mathbf{N} \begin{bmatrix} e_t \\ e_s \\ i_p \\ e_s \end{bmatrix}.$$

B.2 Property of Matrices A and $\mathbf{T}_n$

For any feedback amplifier, the four elements of transmission matrix $\mathbf{T}_n$ are proven to have denominator equal to matrix **A** determinant (3.26.b), as obtained by chapter 3, section 3.1.3 noise analysis.

The determinant of **A** (3.26.b) is:

$$\begin{aligned} |\,\mathbf{A}\,| &= (1+B_tY_p)(1+C_tZ_s) - [-(1-A_t)\ Z_s][-(1-D_t)\ Y_p] \\ &= 1+B_t\,Y_p + C_t\,Z_s + B_t\,C_t\,Z_s\,Y_p - adZ_s\,Y_p \\ &= 1+B_t\,Y_p + C_t\,Z_s - \Delta_{t_o} \end{aligned} \quad \text{(B.10.a)}$$

where:

$$\mathbf{Z}_s = \begin{bmatrix} Z_s & Z_s \\ Z_s & Z_s \end{bmatrix} \quad \text{(B.10.b)}$$

$$\mathbf{Y}_p = \begin{bmatrix} Y_p & -Y_p \\ -Y_p & Y_p \end{bmatrix} \quad \text{(B.10.c)}$$

$$\begin{aligned} a &= 1-A_t \\ d &= 1-D_t \\ \Delta_{t_o} &= a\,d - B_t\,C_t \end{aligned}$$

Consider now (3.22) which is restated here for convenience:

$$\mathbf{Z}_n = [\mathbf{Z}_t + \mathbf{Z}_s]\,[\mathbf{1} + \mathbf{Y}_p\,(\mathbf{Z}_t + \mathbf{Z}_s)]^{-1} \tag{B.11}$$

$\mathbf{Z}_s$ and $\mathbf{Y}_p$ are defined by (B.10.b) and (B.10.c) respectively. Instead of dealing with (B.11),

$$\mathbf{Y}_n = \mathbf{Z}_n^{-1} = \mathbf{Y}_p + [\mathbf{Z}_t + \mathbf{Z}_s]^{-1} \tag{B.12}$$

is considered for simplicity. $\mathbf{Z}_t$ is the impedance matrix of the 2–port device in Figure 3.2. The demonstration makes use of the following steps:

1. expressing the elements of the device impedance matrix $\mathbf{Z}_t$ in terms of transmission matrix elements [87]:

$$\mathbf{Z}_t = \begin{bmatrix} \frac{A_t}{C_t} & \frac{\Delta_t}{C_t} \\ \frac{1}{C_t} & \frac{D_t}{C_t} \end{bmatrix} \tag{B.13}$$

Here, $\Delta_t = A_t\,D_t - B_t\,C_t = A_t + D_t + \Delta_{t_o} - 1$ is the determinant of $\mathbf{Z}_t$;

2. expanding (B.12) in terms of (B.10.b), (B.10.c) and the elements of $\mathbf{Z}_t$. This step requires:

   - to add the series feedback to the device matrix:

$$\begin{aligned} \mathbf{Z}_t + \mathbf{Z}_s &= \begin{bmatrix} \frac{A_t}{C_t} + Z_s & \frac{\Delta_t}{C_t} + Z_s \\ \frac{1}{C_t} + Z_s & \frac{D_t}{C_t} + Z_s \end{bmatrix} \\ &= \frac{1}{C_t} \begin{bmatrix} A_t + C_t\,Z_s & \Delta_t + C_t\,Z_s \\ 1 + C_t\,Z_s & D_t + C_t\,Z_s \end{bmatrix} \end{aligned}$$

   - to sum the parallel feedback admittance matrix $\mathbf{Y}_p$ to the inverse of $\mathbf{Z}_t + \mathbf{Z}_s$:

$$\begin{aligned} \mathbf{Y}_n &= (\mathbf{Z}_t + \mathbf{Z}_s)^{-1} + \mathbf{Y_p} \\ &= \frac{1}{\Delta_z} \begin{bmatrix} D_t + C_t\,Z_s & -(\Delta_t + C_t\,Z_s) \\ -(1 + C_t\,Z_s) & A_t + C_t\,Z_s \end{bmatrix} + \begin{bmatrix} Y_p & -Y_p \\ -Y_p & Y_p \end{bmatrix} \\ \Delta_z &= \mid \mathbf{Z}_t + \mathbf{Z}_s \mid = B_t + Z_s\,(A_t + D_t - \Delta_t - 1) \end{aligned}$$

3. transforming the result from admittance to transmission representation [87]:

$$\mathbf{T} = -\frac{1}{Y_{21}} \begin{bmatrix} Y_{22} & 1 \\ Y_{11}\,Y_{22} - Y_{21}\,Y_{22} & Y_{11} \end{bmatrix}$$

Therefore, the denominator of the $\mathbf{T}$ elements is the numerator of Y_{21} after swapping its sign. The numerator is called $N_{Y_{21}}$:

$$\begin{aligned}
N_{Y_{21}} &= 1 + C_t\, Z_s + Y_p\, \Delta_z \\
&= 1 + C_t\, Z_s + Y_p\, [B_t + Z_s\, (A_t + D_t - \Delta_t - 1)] \\
&= 1 + C_t\, Z_s + Y_p\, [B_t - Z_s\, \Delta_{t_o}] \\
&= 1 + C_t\, Z_s + Y_p\, B_t - Z_s\, Y_p\, \Delta_{t_o}
\end{aligned}$$

Comparing $N_{Y_{21}}$ and (B.10.a) proves that $N_{Y_{21}} =\mid \mathbf{A} \mid$.

B.3 Scattering Parameter Circles on the Feedback Element Plane

The analysis by Narhi for series feedback amplifiers [96] is detailed here; [95] develops similar results for parallel feedback amplifiers.

Consider any two–port network; describe its linear behaviour in terms of impedance matrix $\mathbf{Z} = \begin{bmatrix} Z_{11} & Z_{12} \\ Z_{21} & Z_{22} \end{bmatrix}$ and apply a series feedback element Z_f. The overall network impedance matrix $\mathbf{z}_T$ normalized to a given Z_o is:

$$\mathbf{z}_T = \frac{\mathbf{Z}}{Z_o} = \begin{bmatrix} z_{11} + z_f & z_{12} + z_f \\ z_{21} + z_f & z_{22} + z_f \end{bmatrix}$$

Transform $\mathbf{z}_T$ into scattering matrix $\mathbf{S}$ representation relative to Z_o. The dependance of each S_{ij} on the impedance $z_f = (1 + \Gamma_f)/(1 - \Gamma_f)$ can be written as:

$$S_{ij} = \frac{A_{ij}\, \Gamma_f + B_{ij}}{C\, \Gamma_f + D}$$

where C and D are common to every S_{ij}:

$$\begin{aligned}
C &= 1 - z_{12} - z_{21} - (z_{11}\, z_{22} - z_{12}\, z_{21}) \\
D &= 3 + 2\, z_{11} + 2\, z_{22} - z_{12} - z_{21} + (z_{11}\, z_{22} - z_{12}\, z_{21})
\end{aligned}$$

while A_{ij} and B_{ij} depend on the indeces i and j:

$$A_{11} = 1 + 2\, z_{22} - z_{12} - z_{21} - (z_{11}\, z_{22} - z_{12}\, z_{21})$$

$$B_{11} = -1 + 2\,z_{11} - z_{12} - z_{21} + (z_{11}\,z_{22} - z_{12}\,z_{21})$$

$$\begin{aligned} A_{12} &= 2 - 2\,z_{12} \\ B_{12} &= 2 + 2\,z_{12} \end{aligned}$$

$$\begin{aligned} A_{21} &= 2 - 2\,z_{21} \\ B_{21} &= 2 + 2\,z_{21} \end{aligned}$$

$$\begin{aligned} A_{22} &= 1 - 2\,z_{11} - z_{12} - z_{21} - (z_{11}\,z_{22} - z_{12}\,z_{21}) \\ B_{22} &= -1 + 2\,z_{22} - z_{12} - z_{21} + (z_{11}\,z_{22} - z_{12}\,z_{21}) \end{aligned}$$

If constant $\mid S_{ij} \mid = K$ is imposed, the locus of z_f on the Γ_f plane is

$$\mid \Gamma - \Gamma_o \mid^2 = r^2$$

where

$$\begin{aligned} \Gamma_o &= -\frac{A_{ij}{}^{\star}\,B_{ij} - K^2\,C^{\star}\,D}{\mid A_{ij} \mid^2 - K^2 \mid C \mid^2} \\ r^2 &= \mid \Gamma_o \mid^2 - \frac{\mid B_{ij} \mid^2 - K^2 \mid D \mid^2}{\mid A_{ij} \mid^2 - K^2 \mid C \mid^2} \end{aligned}$$

The region of interest is usually inside for constant $\mid S_{11} \mid$, $\mid S_{12} \mid$ and $\mid S_{22} \mid$ circles, outside for constant $\mid S_{21} \mid$ circle; in doubt, direct substitution of any known value, e.g. $\Gamma_f = 0$, sorts this point out.

Appendix C

Chapter 5 Appendix

C.1 Conditions for 2–Port Networks not to be Active

Consider the linear 2–port network in Figure 3.1, chapter 3, section 3.1 and use the scattering parameters to represent its signal performance at frequency f_o. Define $a = [\,a_1 \quad a_2\,]^T$ and $b = [\,b_1 \quad b_2\,]^T$ as incident and reflected voltage wave vectors, respectively. The subscript 1 (2) refers to port 1 (2); and the superscript ^{T} is the transpose operator. Incident and reflected waves are linked by 2×2 scattering matrix **S**:

$$b \;=\; \mathbf{S}\,a \tag{C.1}$$

Assume that the 2–port circuit is not active. The net power flowing into port i ($i = 1, 2$) is $P_{in}^{(i)} = \mid a_i \mid^2 - \mid b_i \mid^2$; the sum of these powers gives the total power flowing into the network. Because of the principle of energy conservation, the net power is equal to the power dissipated P_d by the network:

$$\begin{aligned} P_d &= P_{in}^{(1)} + P_{in}^{(2)} \\ P_d &= \mid a_1 \mid^2 - \mid b_1 \mid^2 + \mid a_2 \mid^2 - \mid b_2 \mid^2 \end{aligned}$$

and, after rearranging:

$$P_d + \mid b_1 \mid^2 + \mid b_2 \mid^2 \;=\; \mid a_1 \mid^2 + \mid a_2 \mid^2 \tag{C.2}$$

If the network is lossless, then $P_d = 0$ and (C.2) states that the power flowing in is equal to the power flowing out of the network, as expected. Therefore, (C.2) can be extended to lossy networks by dropping P_d:

$$| b_1 |^2 + | b_2 |^2 \;\; \leq \;\; | a_1 |^2 + | a_2 |^2 \tag{C.3}$$

The next task is to find out what conditions the elements of the network scattering matrix $\mathbf{S}$ must satisfy in order to represent non–active 2–port circuits. Rewrite (C.3) in terms of $\mathbf{S}$:

$$\begin{aligned} b^+ b &\leq a^+ a \\ (\mathbf{S}\, a)^+ (\mathbf{S}\, a) &\leq a^+ a \\ a^+ \mathbf{S}^+ \mathbf{S}\, a &\leq a^+ a \\ 0 &\leq a^+ \left[\mathbf{1} - \mathbf{S}^+ \mathbf{S}\right] a \end{aligned} \tag{C.3.a}$$

where $\mathbf{1} = \begin{bmatrix} 1 & 0 \\ 0 & 1 \end{bmatrix}$ and $^+$ is the Hermitian conjugate operator.

For any excitation $a = [a_1 \quad a_2]^T$,

$$\mathbf{A} = \begin{bmatrix} A_{11} & A_{12} \\ A_{21} & A_{22} \end{bmatrix} = \mathbf{1} - \mathbf{S}^+ \mathbf{S} \tag{C.4}$$

must be such that (C.3.a) is verified. (C.4) prooves that $\mathbf{A}$ is Hermitian: $\mathbf{A} = \mathbf{A}^+$.

If (C.3.a) is written in terms of the matrix elements A_{ij},

$$A_{11} \; | a_1 |^2 + A_{22} \; | a_2 |^2 + A_{12}\, a_1^\star\, a_2 + A_{12}^\star\, a_1\, a_2^\star \;\; \geq \;\; 0 \tag{C.5}$$

is obtained and valid for any excitation. Two particular cases are important:

$$a = [a_1 \quad 0]^T \;\; \Rightarrow \;\; A_{11} \; | a_1 |^2 \geq 0 \tag{C.6}$$

$$a = [0 \quad a_2]^T \;\; \Rightarrow \;\; A_{22} \; | a_2 |^2 \geq 0 \tag{C.7}$$

They state that both A_{11} and A_{22} must be positive.

Consider the general case that both a_1 and a_2 are not zero. The cross term products in (C.5) can be rewritten as:

$$\begin{aligned} A_{12}\, a_1^\star\, a_2 + A_{12}^\star\, a_1\, a_2^\star &= 2\, \Re e \left[A_{12}\, a_1^\star\, a_2\right] \\ &= 2 \; | A_{12} || a_1 || a_2 | \; \cos\left(\angle A_{11} + \angle a_1^\star + \angle a_2\right) \end{aligned}$$

$$= \quad 2 \mid A_{12} \mid \mid a_1 \mid \mid a_2 \mid \cos\alpha \tag{C.8}$$

When $\cos\alpha = \cos(\angle A_{11} + \angle a_1{}^{\star} + \angle a_2) = -1$, (C.8) is the only negative term in (C.5); and it is also the worst case possible because -1 is the cosine minimum value. When this condition occurs, (C.5) is equivalent to:

$$A_{11} \mid a_1 \mid^2 + A_{22} \mid a_2 \mid^2 - 2 \mid A_{12} \mid \mid a_1 \mid \mid a_2 \mid \quad \geq \quad 0 \tag{C.9}$$

The cases $a_1 = 0$ and $a_2 = 0$ have already been analysed; therefore, the new variable $x = \mid a_1 \mid / \mid a_2 \mid$ can be defined without affecting the generality of the analysis. Simple manipulations can transform (C.9) into:

$$A_{11}\, x^2 - 2 \mid A_{12} \mid x + A_{22} \quad \geq \quad 0 \tag{C.10}$$

in terms of x and A_{ij} only. (C.10) is a parabola, whose coefficients A_{11} and A_{22} satisfy (C.6) and (C.7) respectively. In order for (C.10) to be positive for any x,

$$\mid A_{12} \mid^2 - A_{11}\, A_{22} \quad \leq \quad 0 \tag{C.11}$$

must be verified. Since $A_{12} = A_{21}{}^{\star}$, (C.11) is a condition on the determinant of $\mathbf{A}$:

$$\mid \mathbf{A} \mid \quad = \quad A_{11}\, A_{22} - A_{12}\, A_{21}{}^{\star} \geq 0 \tag{C.12}$$

If (C.6), (C.7) and (C.12) are true, the network is not active. In particular, if a transmission line is considered (chapter 5, section 5.3.2), only (C.6) and (C.12) are to be taken into account because $A_{11} = A_{22}$ for symmetrical and reciprocal networks.

References

[1] George R. Kay, *The Penguin Book of Italian Verse*, Penguin Books, 1958.

[2] D. J. Withers, *Radio Spectrum Management*, Peter Peregrinus Ltd., London, UK, 1991, Published on behalf of the Institution of Electrical Engineers.

[3] Sander Weinreb, "Low noise cooled GaAs FET amplifiers", *IEEE Trans. on Microwave Theory and Techniques*, vol. 28, pp. 1041–1054, October 1980.

[4] John Pierro, "Cryogenically cooled GaAs FET amplifier with a noise temperature under 70K at 5. 0 GHz", *IEEE Trans. on Microwave Theory and Techniques*, vol. 24, pp. 972–975, December 1976.

[5] Marian W. Pospieszalski, Sander Weinreb, Roger D. Norrod, and Ronald Harris, "FET's and HEMT's at cryogenic temperatures – their properties and use in low–noise amplifiers", *IEEE Trans. on Microwave Theory and Techniques*, vol. 36, No. 3, pp. 552–560, March 1988.

[6] K. H. George Duh, Marian W. Pospieszalski, William F. Kopp, Pin Ho, Amani A. Jabra, Pane-Chane Chao, Phillip M. Smith, Luke F. Lester, James M. Balligall, and Sander Weinreb, "Ultra–low–noise cryogenic high–electron–mobility transistors", *IEEE Trans. on Electron Devices*, vol. 35, No. 3, pp. 249–254, March 1988.

[7] Marian W. Pospieszalski, "Modelling of noise parameters of MESFET's and MODFET's and their frequency and temperature dependence", *IEEE Trans. on Microwave Theory and Techniques*, vol. 37, No. 9, pp. 1340–1350, September 1989.

[8] J. D. Rhodes, *RF Receivers for Cellular Telephone Base Stations - Circuit and System Tutorials*, LTP Electronics Ltd., Oxford UK, 1994, On behalf of IEEE ISCAS 1994.

[9] Langis Roy, "30 GHz GaAs monolithic low noise amplifier–antennas", *IEEE MTT–S International Microwave Symposium Digest*, pp. 967–970, Denver, 1997.

[10] Roger L. Freeman, *Telecommunication Transmission Handbook*, John Wiley & Sons, USA, 1991.

[11] David Pozar, *Microwave Engineering*, Addison Wesley, 1990.

[12] Kevin W. Kobayashi, D. K. Umemoto, T. R. Block, A. K. Oki, and D. C. Streit, "A wideband HEMT cascode low noise amplifier with HBT bias regulation", *IEEE Microwave and Guided Wave Letters*, vol. 5, No. 12, pp. 457–459, December 1995.

[13] Kevin W. Kobayashi, D. K. Umemoto, T. R. Block, A. K. Oki, and D. C. Streit, "A novel monolithic LNA integrating a common source HEMT with an HBT darlington amplifier", *IEEE Microwave and Guided Wave Letters*, vol. 5, No. 12, pp. 442–444, December 1995.

[14] Randall E. Lehmann and David D. Heston, "X band monolithic series feedback LNA", *IEEE Trans. on Microwave Theory and Techniques*, vol. 33, No. 12, pp. 1560–1566, December 1985.

[15] George D. Vendelin, Anthony M. Pavio, and Ulrich L. Rohde, *Microwave Circuit Design Using Linear and Nonlinear Techniques*, John Wiley & Sons, USA, 1990.

[16] Juin J. Liou, *Principles and Analysis of AlGaAs/GaAs Heterojunction Bipolar Transistors*, Artech House, London, 1996.

[17] Aldert Van der Ziel, *Noise: Source, Characterisation, Measurement*, John Wiley & Sons, 1986.

[18] H. Rothe and W. Dalke, "Theory of noisy four poles", *Proc. IRE*, vol. 44–I, pp. 811–818, June 1956.

[19] H. T. Friis, "Noise figure of radio receivers", *Proc. IRE*, vol. 32, pp. 419–422, July 1944.

[20] H. Nyquist, "Thermal agitation of electric charge in conductors", *Physical Review*, vol. 32, pp. 110–113, July 1928.

[21] Hermann A. Haus, "Representation of noise in linear two ports", *Proc. IRE*, vol. 48–I, January 1960, IRE Subcommittee 7. 9 on Noise.

[22] Hewlett Packard Application Note 57-1, *Fundamentals of RF and Microwave Noise Figure Measurements*, Hewlett Packard Company, Palo Alto, CA, Jul 1983.

[23] Hewlett Packard Application Note 57-2, *Noise Figure Measurement Accuracy*, Hewlett Packard Company, Palo Alto, CA, Nov 1988.

[24] Hermann A. Haus and Rirchard B. Adler, "Optimum noise performance of linear amplifiers", *Proc. IRE*, vol. 46, August 1958.

[25] Hermann A. Haus and Richard B. Adler, *Circuit Theory of Linear Noisy Networks*, The Technology Press of The Massachusetts Institute of Technology, 1959.

[26] Hatsuaki Fukui, "Available power gain, noise figure and noise measure of two ports and their graphical representation", *IEEE Trans. on Circuit Theory*, vol. CT–13, No. 2, pp. 137–142, June 1966.

[27] R. S. Tucker, "Low noise design of microwave transistor amplifiers", *IEEE Trans. on Microwave Theory and Techniques*, pp. 697–700, August 1975.

[28] C. R. Poole and D. K. Paul, "Optimum noise measure terminations for microwave transistor amplifiers", *IEEE Trans. on Microwave Theory and Techniques*, vol. 33, No. 11, pp. 1254–1257, November 1985.

[29] IRE, "IRE standards on methods of measuring noise in linear two ports - 1959", *Proc. IRE*, vol. 48–I, pp. 60–68, January 1960.

[30] Herbert Hillbrand and Peter H. Russer, "An efficient method for computer aided noise analysis of linear amplifier networks", *IEEE Trans. on Circuits and Systems*, vol. CAS–23, No. 4, pp. 235–238, April 1976.

[31] P. Penfield, "Wave representation of amplifier noise", *IRE Trans. on Circuit Theory*, vol. CT–9, pp. 84–86, March 1962.

[32] K. Kurokawa, "Power waves and the scattering matrix", *IEEE Trans. on Microwave Theory and Techniques*, vol. 13, pp. 194–202, March 1965.

[33] R. P. Meys, "A wave approach to the noise properties of linear microwave devices", *IEEE Trans. on Microwave Theory and Techniques*, vol. 26, No. 1, pp. 34–37, January 1978.

[34] Rudolf P. Hecken, "Analysis of linear noisy two ports using scattering parameters", *IEEE Trans. on Microwave Theory and Techniques*, vol. 29, No. 10, pp. 997–1003, October 1981.

[35] Jackob Engberg and Torben Larsen, *Noise Theory of Linear and Nonlinear Circuits*, John Wiley & Sons, 1995.

[36] Giovanni Caruso and Mario Sannino, "Computer aided determination of microwave two port noise parameters", *IEEE Trans. on Microwave Theory and Techniques*, vol. 26, No. 9, pp. 639–642, September 1978.

[37] Richard Q. Lane, "The determination of device noise parameters", *Proc. IEEE*, vol. 57, pp. 1461–1462, August 1969.

[38] Hatsuaki Fukui, "The noise performance of microwave noise transistors", *IEEE Trans. on Electron Devices*, vol. ED-13, No. 3, pp. 229–241, March 1966.

[39] Mario Sannino, "On the determination of device noise and gain parameters", *Proc. IEEE*, vol. 67, pp. 1364–1366, September 1979.

[40] Tariq Alam, Roger D. Pollard, and Christopher M. Snowden, "The determination of on–wafer noise parameters at W–band", *27th European Microwave Conference Proc.*, pp. 687–691, Jerusalem, Israel, 8–12 September 1997.

[41] Laurent Escotte, Robert Plana, and Jacques Graffeuil, "Evaluation of noise parameter extraction methods", *IEEE Trans. on Microwave Theory and Techniques*, vol. 41, No. 3, pp. 382–387, March 1993.

[42] Masataka Mitama and Hidehiko Katoh, "An improved computational method for noise parameter measurement", *IEEE Trans. on Microwave Theory and Techniques*, vol. 27, No. 6, pp. 612–615, June 1979.

[43] Scott W. Wedge and David B. Rutledge, "Wave techniques for noise modelling and measurement", *IEEE Trans. on Microwave Theory and Techniques*, vol. 40, No. 11, pp. 2004–2011, November 1992.

[44] G. I. Vasilescu, G. Alquie, and M. Krim, "Exact computation of 2–port noise parameters", *Electronics Letters*, vol. 25, No. 4, pp. 292–293, February 1989.

[45] Giovanni Martines and Mario Sannino, "The determination of the noise, gain and scattering parameters of microwave transistors (HEMT's) using only an automatic noise figure test–set", *IEEE Trans. on Microwave Theory and Techniques*, vol. 42, No. 7, pp. 1105–1113, July 1994.

[46] Vahev Adamian and Arthur Uhlir, "A novel procedure for receiver noise characterisation", *IEEE Trans. on Instrumentation and Measurements*, vol. IM-6, pp. 181–182, June 1973.

[47] Marian W. Pospieszalski, "On the measurement of noise parameters of microwave two–ports", *IEEE Trans. on Microwave Theory and Techniques*, vol. -34, No. 4, pp. 456–458, April 1986.

[48] Madhu S. Gupta, "Power gain in feedback amplifiers, a classic revisited", *IEEE Trans. on Microwave Theory and Techniques*, vol. 40, No. 5, pp. 864–879, May 1992.

[49] J. Lange, "Noise characterization of linear two ports in term of invariant parameters", *IEEE Journal of Solid State Circuits*, vol. SC-2, No. 2, pp. 37–40, June 1967.

[50] Karl Hartmann and Max J. O. Strutt, "Changes of the four noise parameters due to general changes of linear two port circuit", *IEEE Trans. on Electron Devices*, vol. ED-20, No. 10, pp. 874–877, October 1973.

[51] Jackob Engberg, "Simultaneous input power match and noise optimisation using feedback", *4th European Microwave Conference Proc.*, pp. 385–389, Montreux, Switzerland, 1974.

[52] Nobuo Shiga, Shigeru Nakajima, Kenji Otobe, Takeshi Sekiguchi, Nobuhiro Kuwata, Ken-ichiro Matsuzaki, and Hideki Hayashi, "X band MMIC amplifier with pulsed doped GaAs MESFETs", *IEEE Trans. on Microwave Theory and Techniques*, vol. 39, No. 12, pp. 1987–1993, December 1991.

[53] Vittorio Rizzoli and Alessandro Lipparini, "Computer aided noise analysis of linear multiport networks of arbitrary topology", *IEEE Trans. on Microwave Theory and Techniques*, vol. 33, No. 12, pp. 1507–1512, December 1985.

[54] Janusz A. Dobrowolski, "Noise power sensitivities and noise figure minimisation of two-ports with any internal topology", *IEEE Trans. on Microwave Theory and Techniques*, vol. 39, No. 1, pp. 136–140, January 1991.

[55] Niranjan G. Kanaglekar, Robert E. McIntosh, and William E. Bryant, "Wave analysis of noise in interconnected multiport networks", *IEEE Trans. on Microwave Theory and Techniques*, vol. 35, No. 2, pp. 112–115, February 1987.

[56] Janusz A. Dobrowolski, "CAD oriented method for noise analysis of microwave circuits described by the nodal admittance matrix", *IEE Proceedings-H*, vol. 140, No. 4, pp. 321–325, August 1993.

[57] Pertti K. Ikalainen, "Extraction of device noise sources from measured data using circuit simulator software", *IEEE Trans. on Microwave Theory and Techniques*, vol. 41, No. 2, pp. 340–343, February 1993.

[58] Brian Hughes, "A temperature noise model for extrinsic FET's", *IEEE Trans. on Microwave Theory and Techniques*, vol. 40, No. 9, pp. 1821–1831, September 1992.

[59] Luciano Boglione, Roger D. Pollard, and Vasil Postoyalko, "The pospieszalski noise model and the imaginary part of the optimum noise source impedance of extrinsic or packaged FETs", *IEEE Microwave and Guided Wave Letters*, vol. 7, No. 9, pp. 270–272, September 1997.

[60] Jackob Millman and Arvin Grabel, *Microelectronics*, McGraw Hill Inc., 1987, Second Edition.

[61] Robert A. Pucel et al., "A general noise de-embedding procedure for packaged two port linear active devices", *IEEE Trans. on Microwave Theory and Techniques*, vol. 40, No. 11, pp. 2013–2023, November 1992.

[62] W. Shockley, "Unipolar field effect transistor", *Proc. IRE*, vol. 40, pp. 1365–1376, November 1952.

[63] A. Van der Ziel, "Thermal noise in field effect transistor", *Proc. IRE*, vol. 50, pp. 1808–1812, August 1962.

[64] A. Van der Ziel, "Gate noise in field effect transistor at moderately high frequencies", *Proc. IRE*, vol. 51, pp. 461–467, March 1963.

[65] W. C. Bruncke and A. Van der Ziel, "Thermal noise in junction gate field effect transistors", *IEEE Trans. on Electron Devices*, vol. ED-13, pp. 323–329, March 1966.

[66] Robert A. Pucel, Hermann Haus, and H. Statz, "Signal and noise properties of gallium arsenide microwave field effect transistors", *Advances in Electronics and Electron Physics*, vol. 38, pp. 194–265, 1975.

[67] S. Sze, *Semiconductor Devices: Physics and Technology*, John Wiley & Sons, USA, 1985.

[68] W. Baechtold, "Noise behaviour of GaAs FET with short gate lengths", *IEEE Trans. on Electron Devices*, vol. ED-19, No. 5, pp. 674–680, May 1972.

[69] Hatsuaki Fukui, "Determination of the basic device parameters of a GaAs MESFET", *Bell System Tech. Journal*, vol. 58, pp. 771–797, March 1979.

[70] Hatsuaki Fukui, "Optimal noise figure of microwave GaAs MESFETs", *IEEE Trans. on Electron Devices*, vol. ED-26, pp. 1032–1037, July 1979.

[71] Francois Danneville, Henri Happy, Gilles Dambrine, Jean-Maxence Belquin, and Alain Cappy, "Microscope noise modelling and macroscopic noise models: How good a connection?", *IEEE Trans. on Electron Devices*, vol. ED-41, No. 5, pp. 779–786, May 1994.

[72] Paul J. Tasker, W. Reinert, Brian Hughes, J. Braunstein, and M. Schlechtweg, "Transistor noise parameter extraction using a 50 ohm measurement system", *IEEE MTT-S International Microwave Symposium Digest*, pp. 1251–1254, Atlanta, 1993.

[73] Brian Hughes, "Designing FET's for broad band circles", *IEEE Trans. on Microwave Theory and Techniques*, vol. 41, No. 2, pp. 190–198, February 1993.

[74] Brian Hughes, "A linear dependence of f_{min} of frequency for FET's", *IEEE Trans. on Microwave Theory and Techniques*, vol. 41, No. 6/7, pp. 979–981, June/July 1993.

[75] Brian Hughes, Julio Perdomo, and Hiroshi Kondoh, "12 GHz low-noise MMIC amplifier designed with a noise model that scales with MODFET size and bias", *IEEE Trans. on Microwave Theory and Techniques*, vol. 41, No. 12, pp. 2311–2316, December 1993.

[76] Jong-Hee Hau and Kwyro Lee, "A new extraction method for noise sources and correlation coefficient in MESFET", *IEEE Trans. on Microwave Theory and Techniques*, vol. 44, No. 3, pp. 487–490, March 1996.

[77] Madhu S. Gupta, Octavious Pitzalis Jr., Steven E. Rosenbaum, and Paul T. Greiling, "Microwave noise characterization of GaAs MESFET's: Evaluation by on-wafer low frequency output noise current measurement", *IEEE Trans. on Microwave Theory and Techniques*, vol. 35, No. 12, pp. 1208–1217, December 1987.

[78] Roman Meierer and Christos Tsironis, "On wafer noise parameter measurement technique with automatic receiver calibration", *Microwave Journal*, vol. 38, No. 3, pp. 22–37, March 1995.

[79] Gilles Dambrine, Henri Happy, Frederic Heliodore, and Edouard Playez, "A new method for determining the FET small signal equivalent circuit", *IEEE Trans. on Microwave Theory and Techniques*, vol. 36, No. 7, pp. 1151–1159, July 1988.

[80] Alfy Riddle, "Extraction of FET model noise parameters from measurements", *IEEE MTT-S International Microwave Symposium Digest*, pp. 1113–1116, Boston, MA, June 10–14, 1991.

[81] B. Byzery, "Direct extraction of noise sources for MESFETs and HEMTs", *23th European Microwave Conference Proc.*, pp. 508–510, Madrid, Spain, 8–12 September 1993.

[82] Alina Caddemi, A. Di Paola, and Mario Sannino, "Microwave noise parameters of HEMTs vs. temperature by a simplified measurement procedure", *Proceedings of the 1996 Workshop on High Performance Electron Devices for Microwave and Optoelectronic Applications – EDMO*, pp. 153–157, Leeds, United Kingdom, 25–26 November 1996.

[83] J. M. Rollett, "Stability and power gain invariants of linear two ports", *Trans. of IRE on Circuit Theory*, vol. CT–9, pp. 29–32, March 1962.

[84] D. Woods, "Reappraisal of the unconditionally stability criteria for active two port networks in terms of S parameters", *IEEE Trans. on Circuits and Systems*, vol. CAS-23, No. 2, pp. 73–81, February 1976.

[85] Hewlett Packard Company, *Communication Components, Designer's Catalogue, GaAs and Silicon Products*, Hewlett Packard Company, Palo Alto, CA, 1993.

[86] Robert Collin, *Foundation for Microwave Engineering*, McGraw Hill Inc., second edition, 1992.

[87] Guillermo Gonzalez, *Microwave Transistor Amplifiers: Analysis and Design*, Prentice Hall, 1984.

[88] W. K. Chen, "Distributed amplifiers: Survey of the effects of lumped transmission line design on performance", *Proc IEE*, vol. 114, No. 8, August 1967.

[89] James B. Beyer, S. N. Prasad, Robert C. Becker, James E. Nordman, and Gert K. Hohenwarter, "MESFET distributed amplifier design guidelines", *IEEE Trans. on Microwave Theory and Techniques*, vol. 32, pp. 268–275, March 1984.

[90] Hans L. Hartnagel, "Achievements and prospects of microwave distribute amplifiers", *19th European Microwave Conference Proc.*, pp. 17–28, 1989.

[91] Karl B. Niclas, Walter T. Wilser, Thomas R. Kritzer, and Ramon R. Pereira, "On theory and performance of solid state microwave distributed amplifiers", *IEEE Trans. on Microwave Theory and Techniques*, vol. 31, No. 6, pp. 447–456, June 1983.

[92] Karl B. Niclas and Brett A. Tucker, "On noise in distributed amplifiers at microwave frequencies", *IEEE Trans. on Microwave Theory and Techniques*, vol. 31, No. 8, pp. 661–668, August 1983.

[93] Yalcin Ayasli, Leonard D. Reynolds, Robert L. Mozzi, and Larry K. Hanes, "2-20 GHz GaAs travelling wave power amplifiers", *IEEE Trans. on Microwave Theory and Techniques*, vol. 32, No. 3, pp. 290–294, March 1984.

[94] Eric Ulrich, "Use negative feedback to slash wideband VSWR", *Microwaves*, vol. 17, pp. 66–70, October 1978.

[95] Tapani Narhi, "Smith charts speed design of feedback amps", *Microwaves & RF*, vol. 23, No. 11, pp. 99–106, November 1984.

[96] Tapani Narhi, "Series feedback design is easier on a Smith chart", *Microwaves & RF*, vol. 23, No. 12, pp. 113–114, December 1984.

[97] Felix Perez and Vincent Ortega, "A graphical method for the design of feedback networks for microwave transistor amplifiers: Theory and applications", *IEEE Trans. on Microwave Theory and Techniques*, vol. 29, No. 10, pp. 1019–1026, October 1981.

[98] Karl B. Niclas, "The exact noise figure of amplifiers with parallel feedback and lossy matching circuits", *IEEE Trans. on Microwave Theory and Techniques*, vol. 30, No. 5, pp. 832–835, May 1982.

[99] Karl B. Niclas, "Noise in broad band GaAs MESFET amplifiers with parallel feedback", *IEEE Trans. on Microwave Theory and Techniques*, vol. 30, No. 1, pp. 63–70, January 1982.

[100] Karl B. Niclas, Walter T. Wilser, Richard B. Gold, and William R. Hitchens, "The matched feedback amplifier: Ultrawide band-microwave amplification with GaAs MESFET's", *IEEE Trans. on Microwave Theory and Techniques*, vol. 28, No. 4, pp. 285–294, April 1980.

[101] Anthony M. Pavio Jr, "A network modelling and design method for a 2–18 GHz feedback amplifier", *IEEE Trans. on Microwave Theory and Techniques*, vol. 30, No. 12, pp. 2212–2216, December 1982.

[102] Kazuhiko Honjo, Tadahiko Sugiura, and Hitoshi Itoh, "Ultra broad band GaAs monolithic amplifier", *IEEE Trans. on Microwave Theory and Techniques*, vol. 30, No. 7, pp. 1027–1033, July 1982.

[103] Jun Tajima, Yasushi Yamao, Takayuki Sugeta, and Masahiro Hirayama, "GaAs monolithic low–power amplifiers with RC parallel feedback", *IEEE Trans. on Microwave Theory and Techniques*, vol. 32, No. 5, pp. 542–544, May 1984.

[104] Manuel Sierra, "Matching, gain and noise limits on linear amplifier four–poles", *Microwave and Optical Technology Letters*, vol. 2, No. 1, pp. 29–34, January 1989.

[105] Bjoern M. Albinsson, "A graphic design method for matched low noise amplifier", *IEEE Trans. on Microwave Theory and Techniques*, vol. 38, No. 2, pp. 118–122, February 1990.

[106] Sheau-Shong Bor, Ji-Chyun Liu, and Po-Chiang Lu, "Plots with matching circles for optimising the performance of a low noise amplifier", *Microwave and Optical Technology Letters*, vol. 6, No. 2, pp. 141–148, February 1993.

[107] Ji-Chyun Liu, Sheau-Shong Bor, C. C. Chang, and Po-Chiang Lu, "Modified determinations of stability criteria for accurate designing the linear two port amplifiers", *IEE Proceedings–H*, vol. 141, No. 3, pp. 238–240, June 1994.

[108] Marion L. Edwards, Sheng Cheng, and Jeffrey H. Sinsky, "A deterministic approach for designing conditionally stable amplifiers", *IEEE Trans. on Microwave Theory and Techniques*, vol. 43, No. 7, pp. 1567–1575, July 1995.

[109] A. Anastassiou and M. J. O. Strutt, "Effect of the source lead impedance on the noise figure of a GaAs FET", *Proc. IEEE*, vol. 62, pp. 406–408, March 1974.

[110] Svein Iversen, "Comments on 'Effect of the source lead impedance on the noise figure of a GaAs FET'", *Proc. IEEE*, vol. 63, No. 6, pp. 983–984, June 1975.

[111] George Vendelin, "Feedback effects on the noise performance of GaAs MESFETs", *IEEE MTT–S International Microwave Symposium Digest*, pp. 324–326, Palo Alto, CA, May 12–14, 1975.

[112] Garry N. Link and V. S. Rao Giudimetla, "Analytical expressions for simplifying the design of broadband low noise microwave transistor amplifiers", *IEEE Trans. on Microwave Theory and Techniques*, vol. 43, No. 10, pp. 2498–2501, October 1995.

[113] Les Besser, "Stability considerations of low noise transistor amplifiers with simultaneous noise and power match", *IEEE MTT-S International Microwave Symposium Digest*, pp. 327–329, Palo Alto, CA, May 12–14, 1975.

[114] Beom Kyu Ko and Kwyro Lee, "A new simultaneous noise and input power matching technique for monlithic lna's using cascode feedback", *IEEE Trans. on Microwave Theory and Techniques*, vol. 45, No. 9, pp. 1627–1630, September 1997.

[115] Kevin W. Kobayashi and A. O. Oki, "A low noise baseband 5 GHz direct coupled HBT amplifier with common base active input match", *IEEE Microwave and Guided Wave Letters*, vol. 4, No. 11, pp. 373–375, November 1994.

[116] Kevin W. Kobayashi, D. C. Streit, D. K. Umemoto, and T. R. Block, "A novel monolithic HEMT LNA integrating HBT–tunable active–feedback linearization by selective MBE", *IEEE Trans. on Microwave Theory and Techniques*, vol. 44, No. 12, pp. 2384–2391, December 1996.

[117] Y. Tsukahara, S. Chaki, Y. Sasaki, K. Nakahara, N. Andoh, H. Mastubayasi, N. Tanino, and O. Ishihara, "A C–band 4–stage low noise miniaturised amplifier using lumped elements", *IEEE MTT–S International Microwave Symposium Digest*, vol. 3, pp. 1125–1128, Orlando, FL, 1995.

[118] N. Camilleri, P. Chye, A. Lee, and P. Gregory, "Monolithic 40 to 60 GHz LNA", *IEEE MTT–S International Microwave Symposium Digest*, pp. 599–602, Dallas, TX, May 8–10, 1990.

[119] D. P. Lunden, M. Sipila, and M. Jenn, "60 GHz LNAs using commercially available PM HEMTs", *Microwave Journal*, vol. 38, No. 3, pp. 80–88, March 1995.

[120] H. Wang, R. Lai, D. C. W. Lo, D. C. Streit P. H. Liu, R. M. Dia, Marian W. Pospieszalski, and J. Berenz, "A 140–GHz monolithic low noise amplifier", *IEEE Microwave and Guided Wave Letters*, vol. 5, No. 5, pp. 150–152, May 1995.

[121] Robert Collin, *Foundation for Microwave Engineering*, McGraw Hill Inc., first edition, 1966.

[122] R. S. Pengelly, *Microwave FET – Theory, Design and Applications*, Research Study Press, second edition, 1986.

[123] Luciano Boglione, Roger D. Pollard, Vasil Postoyalko, and Tariq Alam, "Specifications for a linear network simultaneously noise and available–power matched", *IEEE Microwave and Guided Wave Letters*, vol. 6, No. 11, pp. 407–409, November 1996.

[124] Karl B. Niclas, "On design and performance of lossy match GaAs MESFET amplifiers", *IEEE Trans. on Microwave Theory and Techniques*, vol. 30, No. 11, pp. 1900–1906, November 1982.

[125] Karl B. Niclas, "Active matching with common gate MESFET's", *IEEE Trans. on Microwave Theory and Techniques*, vol. 33, No. 6, pp. 492–499, June 1985.

[126] Kevin W. Kobayashi, D. C. Streit, D. K. Umemoto, T. R. Block, and A. K. Oki, "A monolithic HEMT–HBT direct coupled amplifier with active input matching", *IEEE Microwave and Guided Wave Letters*, vol. 6, No. 1, pp. 55–57, January 1996.

[127] Luciano Boglione, Roger D. Pollard, and Vasil Postoyalko, "Analytical behaviour of the noise resistance and the noise conductance for a network with parallel and series feedback", *IEEE Trans. on Microwave Theory and Techniques*, vol. 45, No. 2, pp. 301–304, February 1997.

[128] Dean A. Frickey, "Conversion between S, Z, Y, h ABCD and T parameters which are valid for complex source and load impedances", *IEEE Trans. on Microwave Theory and Techniques*, vol. 42, pp. 205–211, February 1994.

[129] Alan Philip John Teale, *Low Noise Microwave Feedback Amplifiers*, Department of Electrical and Electronic Engineering, University of Leeds, 1987, PhD Thesis.

[130] NEC, *RF and Microwave Semiconductors Catalogue*, NEC, 1992–1993.

[131] W. W. Mumford and E. H. Scheibe, *Noise Performance Factors in Communication Systems*, Horizon House, 1968.

[132] Svein Iversen, "The effect of feedback on noise figure", *Proc. IEEE*, vol. 63, pp. 540–542, March 1975.

[133] Filtronic Component Ltd, *Filtronic Component Ltd Catalogue*, Filtronic Component Ltd, 1994.

[134] Frederick Emmons Terman, *Electronic and Radio Engineering*, McGraw Hill Inc., USA, 1955.

[135] Marian W. Pospieszalski and A. C. Niedzwiecki, "FET noise model and on-wafer measurement of noise parameters", *IEEE MTT–S International Microwave Symposium Digest*, pp. 1117–1120, Boston, MA, June 10–14, 1991.

[136] P. C. Chao, S. C. Palmateer, P. M. Smith, U. K. Mishra, K. H. G. Duh, and J. C. M. Hwang, "Millimeter–wave low–noise high electron mobility transistor", *IEEE Electron Device Letters*, vol. 6, No. 10, pp. 531–533, October 1985.

[137] Hikaru Hida, Keiichi Ohata, Yasuyuki Suzuki, and Hideo Toyoshima, "A new low–noise AlGaAs/GaAs 2DEG FET with a surface undoped layer", *IEEE Trans. on Electron Devices*, vol. ED–33, No. 5, pp. 601–607, May 1986.

[138] Paul R. Jay, Henri Derewonko, Didier Adam, Pierre Briere, Daniel Delagebeaudeuf, Philipe Delescluse, and Jean-Francois Rochette, "Design of TEGFET devices for optimum low–noise high–frequency operation", *IEEE Trans. on Electron Devices*, vol. ED–33, No. 5, pp. 590–594, May 1986.

[139] Luciano Boglione, Roger D. Pollard, and Vasil Postoyalko, "Optimum noise source reflection coefficient design with feedback amplifiers", *IEEE Trans. on Microwave Theory and Techniques*, vol. 45, No. 3, pp. 402–407, March 1997.

[140] Luciano Boglione, Roger D. Pollard, and Vasil Postoyalko, "Extension of the design of the optimum noise source reflection coefficient to lossy series feedback impedances", *The 3rd IEEE High Frequency Postgraduate Student Colloquium*, pp. 81–86, 19 September 1997, Institute of Microwaves and Photonics, School of Electronic and Electrical Engineering, The University of Leeds, UK.

[141] Mitsubishi Electric Corp., *Mitsubishi Semiconductors GaAs FET–MMIC Data Book*, Mitsubishi Electric Corp. – Semiconductor Marketing Division, 1996.

[142] Luciano Boglione, Roger D. Pollard, and Vasil Postoyalko, "BJT feedback LNA with input port simultaneously signal and noise matched", *27th European Microwave Conference Proc.*, pp. 1052–1057, Jerusalem, Israel, 8–12 September 1997.

[143] Hewlett Packard Company, *HP8510 Network Analyser – Operating and Device Manual*, Hewlett Packard Company, Palo Alto, CA, 1985.

[144] Kimmo J. Silvonen, "Calibration of test fixtures using at least two standards", *IEEE Trans. on Microwave Theory and Techniques*, vol. 39, No. 4, pp. 624–630, April 1991.

[145] John V. Butler, Douglas K. Rytting, Magdy F. Iskander, Roger D. Pollard, and Marc Vanden Bossche, "16–Term error model and calibration procedure for on–wafer network analysis measurements", *IEEE Trans. on Microwave Theory and Techniques*, vol. 39, pp. 2211–2217, December 1991.

[146] Don Metzger, "Improving TRL^* calibration of network analysers", *Microwave Journal*, vol. 38, No. 5, pp. 56–64, May 1995.

[147] G. H. Bryant, *Principles of Microwave Measurements*, Peter Peregrinus Ltd., London, 1993, Published on behalf of the Institution of Electrical Engineers, London, England.

[148] Caroline E. Collins, Roger D. Pollard, Robert E. Miles, and R. G. Dildine, "A new method for determination of single–side–band noise–figure", *IEEE Trans. on Microwave Theory and Techniques*, vol. 42, No. 12, Pt. 2, pp. 2435–2439, December 1994.

[149] Focus Microwave Inc., *Microwave Tuner System 800–3000 MHz*, Focus Microwave inc., 1996.

[150] M. Lang, "The intermodulation problem in mobile communications", *Microwave Journal*, vol. 38, No. 5, May 1995.

[151] Glenn F. Engen and Cletus A. Hoer, "Thru-Reflect-Line: An improved technique for calibrating the dual six port automatic network analyzer", *IEEE Trans. on Microwave Theory and Techniques*, vol. 27, No. 12, pp. 987–993, December 1979.

Annexe

Publications

The papers originated from this Ph.D. project are listed in cronological order of publication:

[123] **Specifications for a Linear Network Simultaneously Noise and Available–Power Matched**, by Luciano Boglione, Roger D. Pollard, Vasil Postoyalko, Tariq Alam, published on *IEEE Microwave and Guided Wave Letters*, vol. 6, No. 11, pp. 407–409, November 1996.

[127] **Analytical Behaviour of the Noise Resistance and the Noise Conductance for a Network with Parallel and Series Feedback**, by Luciano Boglione, Roger D. Pollard, Vasil Postoyalko, published on *IEEE Trans. on Microwave Theory and Techniques*, vol. 45, No. 2, pp. 301–304, February 1997.

[139] **Optimum Noise Source Reflection Coefficient Design with Feedback Amplifiers**, by Luciano Boglione, Roger D. Pollard, Vasil Postoyalko, published on *IEEE Trans. on Microwave Theory and Techniques*, vol. 45, No. 3, pp. 402–407, March 1997.

[142] **BJT Feedback LNA with Input Port Simultaneously Signal and Noise Matched**, by Luciano Boglione, Roger D. Pollard, Vasil Postoyalko, published on *27th European Microwave Conference Proc.*, pp. 1052–1057, Jerusalem, Israel, 8–12 September 1997.

[140] **Extension of the Design of the Optimum Noise Source Reflection Coefficient to Lossy Series Feedback Impedances**, by Luciano Boglione, Roger D. Pollard, Vasil Postoyalko, published on *The 3rd IEEE High Frequency Postgraduate Student*

Colloquium, 19 September 1997, Institute of Microwaves and Photonics, School of Electronic and Electrical Engineering, The University of Leeds, UK.

[59] **The Pospieszalski Noise Model and the Imaginary Part of the Optimum Noise Source Impedance of Extrinsic or Packaged FETs**, by Luciano Boglione, Roger D. Pollard, Vasil Postoyalko, published on *IEEE Microwave and Guided Wave Letters*, vol. 7, No. 9, pp. 270–272, September 1997.

A copy of each of them is attached.

Specifications for a Linear Network Simultaneously Noise and Available-Power Matched

Luciano Boglione, *Student Member, IEEE*, Roger D. Pollard, *Senior Member, IEEE*, Vasil Postoyalko, *Member, IEEE*, and Tariq Alam, *Student Member, IEEE*

***Abstract*— This letter addresses the problem of designing a linear lossy input matching network for low-noise amplifiers so that the source impedance can deliver its available power and correspond to the minimum noise figure of the driven stages. The differences between lossless and lossy networks are highlighted because matching circuits are usually considered to be lossless when designing an amplifier. After stating the assumptions, a solution to the problem of the minimum number of elements fulfilling the requirements is developed. The result explains why the standard distributed approach often fails to cope with minimum noise specifications when practical elements are considered.**

I. Introduction

THE MOST desirable input matching circuit for a microwave active device should allow the source to deliver all its available power and simultaneously be the impedance corresponding to the minimum noise figure of the cascaded stages (Fig. 1). This letter addresses this issue and presents some theoretical results about the design of a real lossy input matching circuit. It is noticeable that the device $F_{\min}$ can still be achieved if a series feedback is applied to the transistor: the lossy input matching stage will increase the overall $F_{\min}^{ov}$, but a proper choice of the series feedback element can decrease the device $F_{\min}$ [1], [2] so that $F_{\min}^{ov} \simeq F_{\min}$. The chained stages are described by

$$C^{IA} = \begin{bmatrix} R_n^{IA} & \widetilde{\rho_n^{IA*}} \\ \widetilde{\rho_n^{IA}} & g_n^{IA} \end{bmatrix} = C^I + T^I C^A T^{I^+} \qquad (1)$$

$$T^{IA} = \begin{bmatrix} A^{IA} & B^{IA} \\ C^{IA} & D^{IA} \end{bmatrix} = T^I T^A. \qquad (2)$$

C's are correlation matrices [3], $\widetilde{\rho_n^{IA}} = \rho_n^{IA}\sqrt{R_n^{IA} g_n^{IA}}$ where ρ_n^{IA} is the correlation coefficient of the stage, T's are transmission matrices, and the superscripts refer to the input matching circuit (I), to the following active network (A), and to the cascade of the two (IA). * and $^+$ are, respectively, the conjugate and the Hermitian conjugate operation. Thus, noise parameters change nonlinearly as functions of the input stage (1), while the signal matrix T^{IA} is linearly dependent on the input matching network (2), once the active stage T^A is defined. Further stages are neglected in (1) because they follow the active device [4].

Manuscript received June 4, 1996.

The authors are with the Microwave Terahertz and Technology Group, Department of Electronic and Electrical Engineering, The University of Leeds, Leeds LS2 9JT, U.K.

Publisher Item Identifier S 1051-8207(96)07883-X.

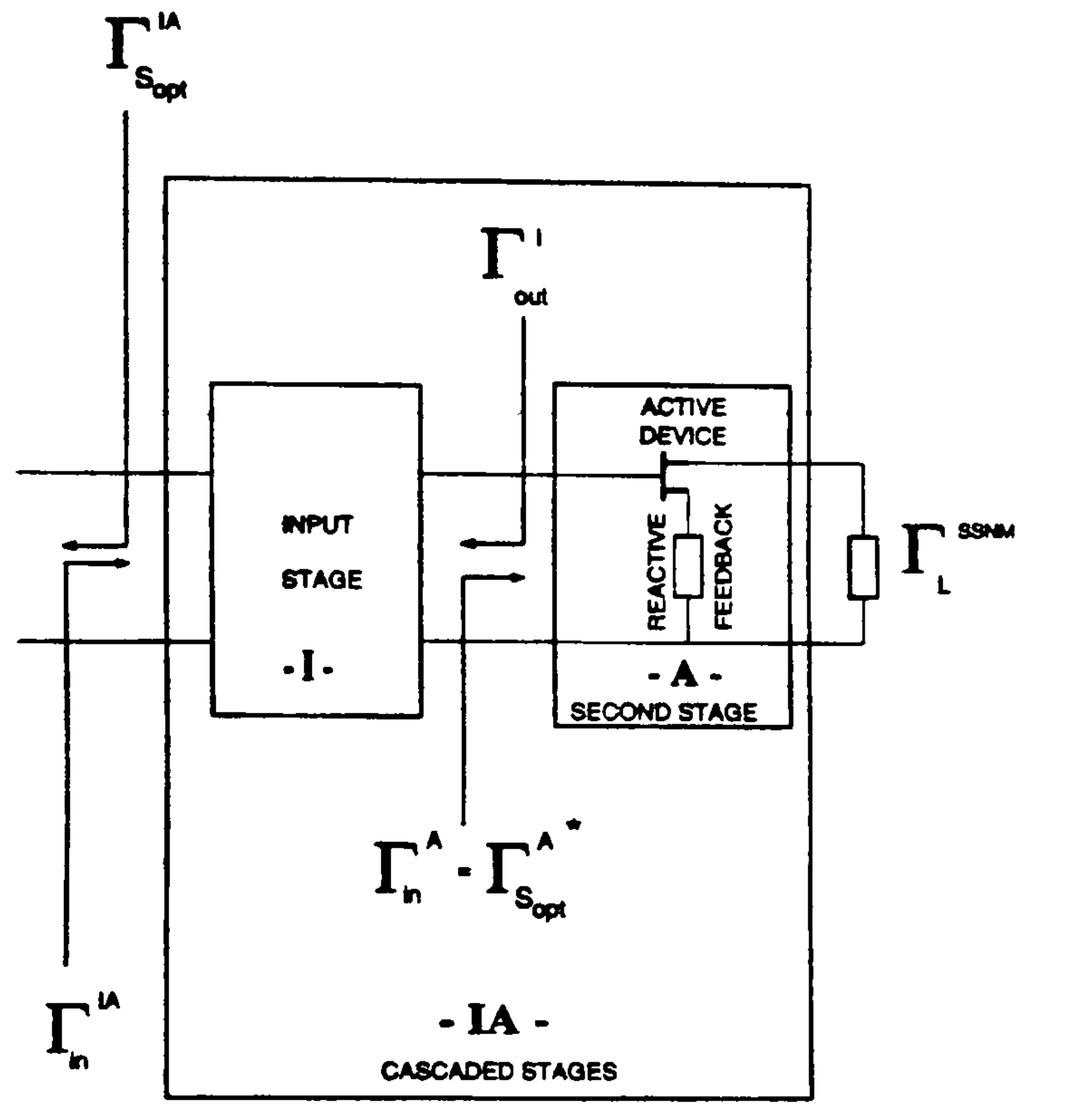

Fig. 1. Input-matching stage cascaded with a microwave amplifier and the assumptions for the design.

II. Assumptions

Consider Fig. 1. The following assumptions are made.

1) The stages are linear.
2) The source impedance is Z_o and the scattering parameters are normalized to Z_o.
3) The amplifier is assumed to be simultaneously signal and noise matched, i.e., $\mathrm{SSNM}^A = \Gamma_{\mathrm{in}}^A - \Gamma_{S_{\mathrm{opt}}}^{A^*} = 0$.

SSNM defines a measure of how close the power match is to the condition for minimum noise figure. The condition $\mathrm{SSNM}^A = 0$ is achievable in microwave low-noise amplifiers by a proper choice of the load $\Gamma_L = \Gamma_L^{\mathrm{SSNM}}$ [5], usually after making use of a feedback element [1].

A proper choice of the load is necessary in order to get a SSNM condition at the input port of the device; this technique usually fails if applied to a device without feedback. If this condition is not achieved, the input matching network cannot simultaneously provide two different values—i.e., $\Gamma_{\mathrm{in}}^{A^*}$ and $\Gamma_{S_{\mathrm{opt}}}^A$—at the design frequency. The SSNM condition of the amplifier allows for the matching circuit to deliver its available power and a simultaneous noise and input match to be transferred to the input port of the cascaded stages, i.e., $\mathrm{SSNM}^{IA} = 0$. The underlying assumption is that the overall design is carried out in two steps, the design of the amplifier and the design of the input matching circuit. If the amplifier's matrices $\boldsymbol{C}^A$ and $\boldsymbol{T}^A$ are known, the analysis can be focused on the input matching stage and simplifies the design problem. Different results might be expected if both the matching network and the amplifier had to be designed at the same time, e.g., by letting the feedback element vary. A full analytical approach as the following Sections, however, describe seems too complicated due to the inherent nonlinear nature of (1).

III. Requirements

At the design frequency, the input matching circuit must satisfy the following requirements:

$$\Gamma^{IA}_{S_{\rm opt}} = 0 \tag{3a}$$
$$\Gamma^{IA}_{\rm in} = 0 \tag{3b}$$
$$\Gamma^{I}_{\rm out} = \Gamma^{A}_{S_{\rm opt}}. \tag{3c}$$

The system of equations (3) implies:

a) the source impedance to correspond to the optimum source reflection coefficient of the driven stages, so that the minimum noise figure of the cascaded stages is achieved;
b) the source to deliver all its available power to the driven stages;
c) the output port of the matching circuit to deliver all its available power to the next active stage.

Notice that (3a) implies a noise requirement that is usually neglected at the early stage of the design. Equations (3b) and (3c) are equivalent in the case of lossless reciprocal networks, but not for practical lossy networks.

IV. Discussion

As described in Appendix A, system (3) can be restated as

$$\begin{aligned}0 = {} & Z_o(g^I_n + R^A_n|C^I|^2 + 2\Re e[\widetilde{\rho^A_n} C^{I^*} D^I] + g^A_n|D^I|^2) \\ & - Y_o(R^I_n + R^A_n|A^I|^2 + 2\Re e[\widetilde{\rho^A_n} A^{I^*} B^I] + g^A_n|B^I|^2)\end{aligned} \tag{4a}$$

$$\begin{aligned}0 = {} & \Im m[\widetilde{\rho^I_n} + R^A_n A^{I^*} C^I \\ & + \widetilde{\rho^A_n}^* B^{I^*} C^I + \widetilde{\rho^A_n} A^{I^*} D^I + g^A_n B^{I^*} D^I]\end{aligned} \tag{4b}$$

$$\begin{aligned}0 = {} & [1 + (\Gamma^A_{S_{\rm opt}})^*]A^I + [1 - (\Gamma^A_{S_{\rm opt}})^*](B^I Y_o) \\ & - [1 + (\Gamma^A_{S_{\rm opt}})^*](C^I Z_o) - [1 - (\Gamma^A_{S_{\rm opt}})^*]D^I\end{aligned} \tag{4c}$$

$$\begin{aligned}0 = {} & [1 + \Gamma^A_{S_{\rm opt}}]A^I - [1 - \Gamma^A_{S_{\rm opt}}](B^I Y_o) \\ & + [1 + \Gamma^A_{S_{\rm opt}}](C^I Z_o) - [1 - \Gamma^A_{S_{\rm opt}}]D^I.\end{aligned} \tag{4d}$$

The system (4) is a compact set of nonlinear equations at a fixed frequency; there are seven unknown input stage parameters: four of them refer to its transmission matrix, A^I, B^I, C^I, and D^I; three refer to its noise behavior, R^I_n, g^I_n, and $\widetilde{\rho^I_n}$. These seven unknowns are not independent.

1) If the input matching circuit is passive, then a plain expression between noise and signal parameters is obtainable as Appendix B demonstrates.
2) Suppose the input stage is an ordinary distributed matching circuit—a transmission line and a stub. Once the substrate has been chosen, the length and width of the transmission line and of the stub are the only independent variables. These four variables set up both the signal (the transmission $\boldsymbol{T}^I$ matrix) and the noise (the correlation $\boldsymbol{C}^I$ matrix) performance of the stage [6].
3) Assume the input stage is made of lumped RLC components: then, it is possible to work out the signal and noise parameters of the input stage as functions of these components.

There is no assumption about the passive or active, distributed or lumped nature of the input stage in writing (3). The relation between the noise and signal parameters of the input stage, however, has to be known, so that the expansion (4) may be restated as a function of the unknown circuit elements.

The input stage noise parameters may be expressed as functions of the complex unknowns A^I, B^I, C^I, and D^I. Three complex equations form system (3): there are more unknowns than equations. If the circuit has to be reciprocal, however, the determinant of $\boldsymbol{T}^I$ must be one. A reciprocal matching circuit must provide four degrees of freedom for its $\boldsymbol{T}^I$ matrix; each is responsible for a complex matrix term. A lumped circuit must contain resistors in order to get complex elements in $\boldsymbol{T}^I$. Therefore, either a simple stub plus transmission-line matching circuit or a lossless network cannot fulfill the goals (3).

For instance, if a single lossy transmission line is considered as input matching circuit, the only unknown is its length l. Its correlation matrix is [6]

$$\boldsymbol{C}^I = \begin{bmatrix} \frac{1}{2} Z_o \sinh(2\alpha l) & \sinh^2(\alpha l) \\ \sinh^2(\alpha l) & \frac{1}{2} Y_o \sinh(2\alpha l) \end{bmatrix}$$

where α is the attenuation in Np/m. Its transmission matrix satisfies $|\boldsymbol{T}^I| = \cosh^2(\gamma l) - \sinh^2(\gamma l) = 1$ where $\gamma = \alpha + j\beta$ and β is the phase constant in rad/m. After substituting the transmission line parameters into (4a) the condition $(g^A_n Z_o - R^A_n Y_o)\cos(2\beta l) = 2\Re e[j\widetilde{\rho^A_n}]\sin(2\beta l)$ is obtained; (4b) is satisfied if $(g^A_n Z_o - R^A_n Y_o)\sin(2\beta l) = 2\Im m[\widetilde{\rho^A_n}]\cos(2\beta l)$; (4c) and (4d) are solved only if $\Gamma^A_{S_{\rm opt}} = 0$. This last condition on the amplifier is equivalent to $g^A_n Z_o = R^A_n Y_o$ and $\Im m[\widetilde{\rho^A_n}] = 0$, as it can easily be demonstrated by applying the expressions developed for $Y^{IA}_{S_{\rm opt}}$ in Appendix A to $Y^A_{S_{\rm opt}}$ when a real characteristic impedance Z_o is considered. Therefore, (4) is valid $\forall l$ only if $\Gamma^A_{S_{\rm opt}} = 0$. This result is quite obvious: the amplifier is already signal and noise matched at its input port $\Gamma^A_{\rm in} = \Gamma^{A^*}_{S_{\rm opt}} = 0$ and a lossy transmission line will transfer the SSNM condition to its input port while affecting the noise figure only.

V. Conclusion

Noise and signal requirements for a distributed or lumped, active or passive matching network set up a system of nonlinear equations. A reciprocal matching circuit must provide four independent complex terms for its signal matrix. Therefore, a microstrip network comprising only two transmission line elements cannot satisfy the requirements. Nonreciprocal networks can satisfy the system. The matching network must comprise resistive elements in order to have complex elements in its T^I matrix. The active network after the matching stage must satisfy the condition $\Gamma_{in}^A = (\Gamma_{S_{opt}}^A)^*$ if the source has to deliver its available power and to assure $F^{IA} = F_{min}^{IA}$ simultaneously. This letter assumes that the second stage (Fig. 1) is designed before defining (3) on the input-matching circuit. A simultaneous design may lead to different results. The SSNM requirements (3a) and (3b) may be relaxed in order to investigate those applications where an extremely low input return loss is not required.

APPENDIX A

The system of equations is given as (3). Consider equation (3a), which corresponds to $Y_{S_{opt}}^{IA} = Y_o$. According to [7], after taking real and imaginary parts, the equation can be rewritten as

$$\frac{G_n^{IA}}{R_n^{IA}} + G_{cor}^{IA^2} = Y_o^2 \tag{5a}$$

$$B_{cor}^{IA} = 0 \tag{5b}$$

where $Y_{cor} = G_{cor}^{IA} + jB_{cor}^{IA}$ is the correlation admittance of the cascaded network. Since $Y_{cor}^{IA} = \rho_n^{IA}\sqrt{g_n^{IA}/R_n^{IA}} = \widetilde{\rho_n^{IA}}/R_n^{IA}$, it is possible to write

$$G_n^{IA} = g_n^{IA} - |Y_{cor}^{IA}|^2 R_n^{IA} = g_n^{IA} - \frac{|\widetilde{\rho_n^{IA}}|^2}{R_n^{IA}} \tag{6}$$

$$G_{cor}^{IA} = \Re e[Y_{cor}^{IA}] = \frac{\Re e[\widetilde{\rho_n^{IA}}]}{R_n^{IA}} \tag{7}$$

$$B_{cor}^{IA} = \Im m[Y_{cor}^{IA}] = \frac{\Im m[\widetilde{\rho_n^{IA}}]}{R_n^{IA}}. \tag{8}$$

After substituting (6)–(8), system (5) is equivalent to

$$4g_n^{IA}R_n^{IA} + (\widetilde{\rho_n^{IA}} - \widetilde{\rho_n^{IA*}})^2 = (2R_n^{IA}Y_o)^2 \tag{9a}$$

$$\widetilde{\rho_n^{IA}} - \widetilde{\rho_n^{IA*}} = 0. \tag{9b}$$

After expanding R_n^{IA}, g_n^{IA}, and $\widetilde{\rho_n^{IA}}$ from (1), (4a) and (4b) are obtained from (9a) and (9b).

Now consider (3b). $\Gamma_{in}^{IA} = 0$ is equivalent to $Z_{in}^{IA} = Z_o$ or in terms of the T^I matrix elements

$$Z_{in}^{IA} = \frac{B^I + A^I Z_{in}^A}{D^I + C^I Z_{in}^A} = Z_o$$

which gives

$$Z_{in}^A A^I + B^I - Z_o Z_{in}^A C^I = Z_o D^I - 0. \tag{10}$$

Using $\Gamma_{in}^A = \Gamma_{S_{opt}}^{A^*}$ and $Z_{in}^A = Z_o(1+\Gamma_{in}^A)/(1-\Gamma_{in}^A)$, (10) reduces to

$$[1 + (\Gamma_{S_{opt}}^A)^*]A^I + [1 - (\Gamma_{S_{opt}}^A)^*]B^I Y_o - [1 + (\Gamma_{S_{opt}}^A)^*]C^I Z_o - [1 - (\Gamma_{S_{opt}}^A)^*]D^I = 0.$$

Finally, consider (3c). Since the source reflection coefficient is zero, $\Gamma_{out}^I = S_{22}^I$, which can be rewritten in terms of the T^I elements [8] as

$$S_{22}^I = \frac{-A^I + Y_o B^I - C^I Z_o + D^I}{A^I + Y_o B^I + C^I Z_o + D^I} = \Gamma_{S_{opt}}^A.$$

The final equation is therefore

$$[1 + \Gamma_{S_{opt}}^A]A^I - [1 - \Gamma_{S_{opt}}^A]B^I Y_o + [1 + \Gamma_{S_{opt}}^A]C^I Z_o - [1 - \Gamma_{S_{opt}}^A]D^i = 0$$

APPENDIX B

The noise figure can be expressed as

$$F = F_{min} + \beta\frac{|\Gamma_S - \Gamma_{S_{opt}}|^2}{1 - |\Gamma_S|^2} \tag{11}$$

where $\beta = R_n/Z_o/|1 + \Gamma_{S_{opt}}|^2$, while the available gain as

$$G_{av} = \frac{1 - |\Gamma_S|^2}{|1 - S_{11}\Gamma_S|^2}|S_{21}|^2\frac{1}{1 - |\Gamma_{out}|^2} \tag{12}$$

both as functions of the scattering parameters of the stage. Here $\Gamma_{out} = (S_{22} - \Delta\Gamma_S)/(1 - S_{11}\Gamma_S)$ and $\Delta = S_{11}S_{22} - S_{12}S_{21}$. For a passive noisy network $F = 1/G_{av}$ holds so that (11) and (12) can be equated. The result is

$$F_{min} = \frac{1 - |S_{11}|^2 - |S_{22}|^2 + |\Delta|^2 \pm \alpha}{2|S_{21}|^2}$$

$$\Gamma_{S_{opt}} = \frac{(S_{11} - S_{22}^*\Delta)^*}{\beta|S_{21}|^2}$$

$$\beta = \frac{1 + |S_{11}|^2 - |S_{22}|^2 - |\Delta|^2 \pm \alpha}{2|S_{21}|^2}$$

$$\alpha = \sqrt{(1 + |S_{11}|^2 - |S_{22}|^2 - |\Delta|^2)^2 - 4|S_{11} - S_{22}^*\Delta|^2}.$$

The sign providing $|\Gamma_{S_{opt}}| < 1$ and $F_{min} > 1$ should be chosen.

REFERENCES

[1] R. E. Lehmann and D. D. Heston, "X band monolithic series feedback LNA," *IEEE Trans. Microwave Theory Tech.*, vol. MTT-33, no. 12, pp. 1560–1566, Dec. 1985.

[2] N. Shiga, S. Nakajima, K. Otobe, T. Sekiguchi, N. Kuwata, K.-i. Matsuzaki, and H. Hayashi, "X band MMIC amplifier with pulsed doped GaAs MESFETs," *IEEE Trans. Microwave Theory Tech.*, vol. 39, no. 12, pp. 1987–1993, Dec. 1991.

[3] H. Hillbrand and P. H. Russer, "An efficient method for computer aided noise analysis of linear amplifier networks," *IEEE Trans. Circuits Syst.*, vol. CAS-23, no. 4, pp. 235–238, Apr 1976.

[4] H. T. Friis, "Noise figure of radio receivers," *Proc. IRE*, vol. 32, pp. 419–422, July 1944.

[5] J. Engberg, "Simultaneous input power match and noise optimization using feedback," in *Proc. 4th European Microwave Conf.*, 1974, pp. 385–389.

[6] J. Engberg and T. Larsen, *Noise Theory of Linear and Nonlinear Circuits*. New York: Wiley, 1995.

[7] H. Rothe and W. Dalke, "Theory of noise four poles," *Proc. IRE*, vol. 44-I, pp. 811–818, June 1956.

[8] G. Gonzalez, *Microwave Transistor Amplifiers: Analysis and Design*. Englewood Cliffs, NJ: Prentice-Hall, 1984.

with

$$\alpha r_n = \begin{cases} 0.088\,969, & \text{if n=1} \\ 0.011\,57, & \text{if n=2} \\ 0.019\,70, & \text{if n=3} \end{cases}$$

$$\beta r_n = \begin{cases} 0.4450, & \text{if n=1} \\ 0.3985, & \text{if n=2} \\ 0.4277, & \text{if n=3} \end{cases}$$

$$\gamma r_n = \begin{cases} 0.6189, & \text{if n=1} \\ 0.6039, & \text{if n=2} \\ 0.5178, & \text{if n=3.} \end{cases}$$

The values of the parameters αr_n, βr_n, and γr_n were determined numerically, in order to minimize the average error of the approximate roots.

The exact values of the roots can now be calculated by the method of [4] using as interval for the search of the roots xr_{nm}: $[xr_{1m}^{ap} - .4(xr_{2m}^{ap} - xr_{1m}^{ap}),\ xr_{1m}^{ap} + .4(xr_{2m}^{ap} - xr_{1m}^{ap})]$, for $n = 1$, $[xr_{nm}^{ap} - .4(xr_{nm}^{ap} - xr_{n-1,m}),\ xr_{nm}^{ap} + .4(xr_{nm}^{ap} - xr_{n-1,m})]$, for $n = 2$ and $n = 3$, and $[xr_{n-1,m} + .4(xr_{n-1,m} - xr_{n-2,m}),\ xr_{n-1,m} + 1.4(xr_{n-1,m} - xr_{n-2,m})]$ for $n \geq 4$.

The roots of the denominator of the function S are the solution of:

$$J_m(\delta x)Y_m'(x) - J_m(x)Y_m'(\delta x) = 0. \tag{A3}$$

It should be observed that this equation is the same as the characteristic equation for TM modes in a coaxial circular waveguide.

The procedure to determine the roots xs_{nm} is the same as applied to the function R. The method of [4] is again used, with the same intervals defined above for R, but replacing xr_{nm}^{ap} and xr_{nm} by xs_{nm}^{ap} and xs_{nm}, respectively. The values of xs_{nm}^{ap} are given by:

$$xs_{nm}^{ap} = \sqrt{(c_3 xs_{nm}^{<})^2 + (c_4 xs_{nm}^{>})^2}, \quad n = 1, 2, 3, \quad 0 \leq m \leq 50 \tag{A4}$$

with

$$c_3 = (1. - \delta)^{\alpha s_n} \quad c_4 = \left(\frac{2\delta}{1+\delta}\right)^{\beta s_n (m+1)^{\gamma s_n}}$$

$$xs_{nm}^{<} = p_{nm} \qquad xs_{nm}^{>} = \frac{n\pi}{1+\delta}$$

$$\alpha s_n = \begin{cases} -0.002\,591, & \text{if n=1} \\ 0.015\,33, & \text{if n=2} \\ 0.024\,62, & \text{if n=3} \end{cases}$$

$$\beta s_n = \begin{cases} 0.2853, & \text{if n=1} \\ 0.4413, & \text{if n=2} \\ 0.4068, & \text{if n=3} \end{cases}$$

$$\gamma s_n = \begin{cases} 0.8402, & \text{if n=1} \\ 0.5396, & \text{if n=2} \\ 0.5014, & \text{if n=3.} \end{cases}$$

References

[1] P. J. B. Clarricoats, and P. K. Saha, "Propagation and radiation behavior of corrugated feeds, Part I–Corrugated-waveguide feed," *Proc. Inst. Elect. Eng.*, vol. 118, pp. 1167–1176, Sept. 1971.

[2] I. Pincherle, "Electromagnetic waves in metal tubes filled longitudinally with two dielectrics," *Phys. Rev.*, vol. 66, pp. 118–130, Sept. 1944.

[3] P. J. B. Clarricoats, "Propagation along unbounded and bounded dielectric rods, Part II–Propagation along a dielectric rod contained in a circular waveguide," *Proc. Inst. Elect. Eng.*, vol. 108c, pp. 177–186, 1961.

[4] R. P. Brent, "An algorithm with guaranteed convergence for finding a zero of a function," *Comput. J.*, vol. 14, pp. 422–425, 1971.

[5] D. E. Muller, "A method for solving algebraic equations using an automatic computer," *Math. Tables and Aids to Computation*, vol. 10, pp. 208–215, 1956.

[6] K. A. Zaki and C. Chunning, "Intensity and distribution of hybrid-mode fields in dielectric-loaded waveguides," *IEEE Trans. Microwave Theory Tech.*, vol. MTT-33, pp. 1442–1447, Dec. 1985.

Analytical Behavior of the Noise Resistance and the Noise Conductance for a Network with Parallel and Series Feedback

Luciano Boglione, Roger D. Pollard, and Vasil Postoyalko

An analysis is presented of the changes of the noise parameters of a two-port network when noisy series and parallel feedback immittances are applied. Exact formulas for the noise parameters R_n, g_n, and ρ_n are given as functions of the feedback for a given network. It is proved that R_n always reaches a minimum when a reactive series feedback is considered. The same results are demonstrated for g_n since a duality principle is pointed out. The results are valid for a wide range of linear microwave two-port networks, either passive or active, and they are used to confirm the data from previously published work.

Index Terms—**Amplifier noise, feedback amplifiers, feedback circuits, microwave amplifiers, noise.**

I. Introduction

In [1], some guidelines are outlined for feedback amplifier design. The resistive parallel feedback has been investigated by [2] and [3]. The change of the noise figure in the case of either parallel or series feedback was worked out by [4]. In [5], series and parallel feedback are analyzed in order to get simultaneously optimum noise and good input/output standing-wave ratio (SWR). In [6], monolithic technology to fabricate a series feedback amplifier in order to get good repeatability during fabrication and the simultaneous noise match and optimum input SWR is applied. Both simulation and experimental validation of an X-band monolithic four-stage low-noise amplifier with series feedback is carried out in [7]; however, the paper does not detail how the simulation has been carried out.

This paper generalizes the results of [6] and [7] using a procedure similar to [1], provides a mathematical tool to investigate the signal

Manuscript received December 1, 1995; revised October 18, 1996. This work was supported by Filtronic Comtek plc.

The authors are with Microwave Terahertz and Technology Group, Department of Electronic and Electrical Engineering, The University of Leeds, Leeds LS2 9JT, U.K.

Publisher Item Identifier S 0018-9480(97)00842-9.

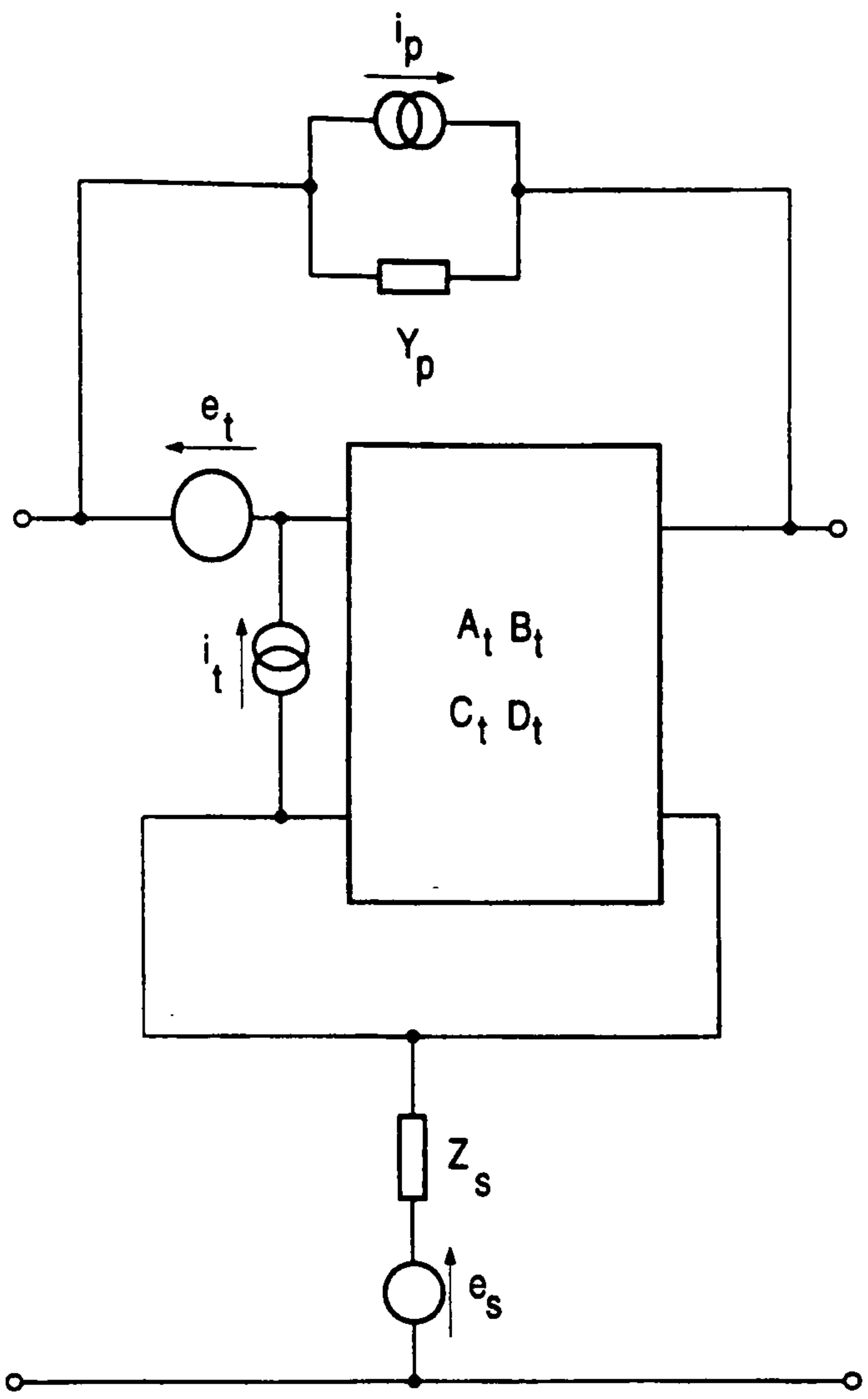

Fig. 1. Schematic of a noisy two-port with series and parallel feedback.

and noise behavior of a feedback network, and presents exact and explicit formulas of the noise parameters for a network with both parallel and series noisy feedback at a given frequency. The approach is not related to any particular technology; the only requirement is a knowledge of the signal matrix and the noise parameters at a given frequency.

II. The Signal and Noise Linear Analysis

Consider the linear circuit in Fig. 1 at a constant frequency f_o whose elements are as follows:

1) black box (typically an active device) characterized by its noise parameters R_t, g_t, ρ_t [8], and a signal matrix (as the scattering or the transmission $A_tB_tC_tD_t$ matrix);
2) parallel admittance $Y_p = G_p + jB_p$;
3) series impedance $Z_s = R_s + jX_s$.

Z_s and Y_p are uncorrelated noise sources, modeled by e_s and i_p, respectively [9].

The subscript t refers to the active network, s to the series feedback, p to the parallel feedback, and n to the overall network. Assume the active network is represented by its impedance matrix $\mathbf{Z_t}$. The series feedback element can be added directly: $\mathbf{Z_t} + \mathbf{Z_s}$ where $\mathbf{Z_s} = Z_s\mathbf{U_s}$, $\mathbf{U_s} = \begin{bmatrix} 1 & 1 \\ 1 & 1 \end{bmatrix}$. Then, the sum matrix is inverted and the parallel feedback matrix is added:

$$\mathbf{Y_n} = \mathbf{Y_p} + (\mathbf{Z_t} + \mathbf{Z_s})^{-1} \tag{1}$$

where $\mathbf{Y_p} = Y_p\mathbf{U_p}$ and $\mathbf{U_p} = \begin{bmatrix} 1 & -1 \\ -1 & 1 \end{bmatrix}$. $\mathbf{Y_n}$ is the admittance matrix of the overall circuit.

A similar procedure can be followed in order to obtain the noise parameters [10] and [11]. Let the following matrices be defined:

$$\mathbf{C_t} = \begin{bmatrix} \overline{e_t e_t^*} & \overline{e_t i_t^*} \\ \overline{i_t e_t^*} & \overline{i_t i_t^*} \end{bmatrix} \tag{2}$$

$$\mathbf{C_s} = \begin{bmatrix} \overline{e_s e_s^*} & \overline{e_s e_s^*} \\ \overline{e_s e_s^*} & \overline{e_s e_s^*} \end{bmatrix} = \Re e[\mathbf{Z_s}] \tag{3}$$

$$\mathbf{C_p} = \begin{bmatrix} \overline{i_p i_p^*} & -\overline{i_p i_p^*} \\ -\overline{i_p i_p^*} & \overline{i_p i_p^*} \end{bmatrix} = \Re e[\mathbf{Y_p}] \tag{4}$$

where * denotes the complex conjugate and the overbar the statistical average. It is tacitly assumed that all noise powers, hence the matrices, are normalized to $4kT_o\Delta f$. The impedance form [10] of the noise matrix of the active circuit is obtained:

$$\mathbf{C_t^{(z)}} = \mathbf{T}_{(t-Z)}\mathbf{C_t}\mathbf{T}_{(t-Z)}{}^+ \quad \text{where: } \mathbf{T}_{(t-Z)} = \begin{bmatrix} 1 & -\frac{A_t}{C_t} \\ 0 & -\frac{1}{C_t} \end{bmatrix}.$$

A_t and C_t are elements of the transmission matrix of the active circuit and $^+$ indicates the Hermitian conjugation. $\mathbf{T}_{(P-Q)}$ is the transformation matrix from the P to the Q network representation [10].

The noise matrix (3) of the series feedback impedance is added:

$$\mathbf{C_z} = \mathbf{C_t^{(z)}} + \mathbf{C_s}.$$

Converting this to admittance form and adding to it the noise matrix of the parallel feedback (4) we obtain the admittance form of the noise matrix for the complete circuit. Thus:

$$\mathbf{C_y} = \mathbf{T}_{(Z-Y)}\mathbf{C_z}\mathbf{T}_{(Z-Y)}{}^+ + \mathbf{C_p} \quad \text{where: } \mathbf{T}_{(Z-Y)} = (\mathbf{Z_t} + \mathbf{Z_s})^{-1}.$$

Converting the admittance form to the $ABCD$ matrix form:

$$\begin{aligned} \mathbf{C_n} =& \mathbf{T}_{(Y-T)}\mathbf{C_y}\mathbf{T}_{(Y-T)}{}^+ \\ =& \mathbf{T}_{(Y-T)}\mathbf{C_p}\mathbf{T}_{(Y-T)}{}^+ + \mathbf{T}_{(Z-T)}\mathbf{C_s}\mathbf{T}_{(Z-T)}{}^+ \\ &+ \mathbf{T}_{(t-T)}\mathbf{C_t}\mathbf{T}_{(t-T)}{}^+. \end{aligned}$$

$\mathbf{C_n}$ is formed by the sum of the contributions from the parallel feedback (first term), from the series feedback (second term), and from the active network (third term). Here,

$$\mathbf{T}_{(Y-T)} = \begin{bmatrix} 0 & -\frac{1}{Y_{n21}} \\ 1 & -\frac{Y_{n11}}{Y_{n21}} \end{bmatrix}$$

$$\mathbf{T}_{(Z-T)} = \mathbf{T}_{(Y-T)}\mathbf{T}_{(Z-Y)}$$

$$\mathbf{T}_{(t-T)} = \mathbf{T}_{(Z-T)}\mathbf{T}_{(t-Z)}$$

and $Y_{n_{ij}}$ are terms of (1).

The four noise parameters can be expressed in terms of the matrix elements of $\mathbf{C_n}$ [10]:

$$\mathbf{C_n} = \begin{bmatrix} \overline{e_n e_n^*} & \overline{e_n i_n^*} \\ \overline{i_n e_n^*} & \overline{i_n i_n^*} \end{bmatrix} = \begin{bmatrix} R_n & \rho_n^*\sqrt{R_n g_n} \\ \rho_n\sqrt{R_n g_n} & g_n \end{bmatrix}. \tag{5}$$

The expansion of (5) gives (see (6)–(8) at the bottom of the next page), where

$$\begin{aligned} r_1 =& \ g_t \mid a \mid^2 + R_t \mid C_t \mid^2 + 2\,\Re e[a\rho_o C_t{}^*] + \mid \Delta_o \mid^2 G_p \\ r_2 =& \ \mid a \mid^2 + 2\,\Re e[a\rho_o] + 2R_t\,\Re e[C_t] + 2\,\Re e[\Delta_o B_t{}^*]\,G_p \\ r_3 =& \ -2\,(\Im m[C_t R_t + a\rho_o] + \Im m[\Delta_o B_t{}^*]\,G_p) \\ r_4 =& \ \mid B_t \mid^2 \\ g_1 =& \ R_t \mid d \mid^2 + g_t \mid B_t \mid^2 + 2\,\Re e[d\rho_o{}^* B_t{}^*] + \mid \Delta_o \mid^2 R_s \\ g_2 =& \ \mid d \mid^2 + 2\,\Re e[d\rho_o{}^*] + 2g_t\,\Re e[B_t] + 2\,\Re e[\Delta_o C_t{}^*]\,R_s \\ g_3 =& \ -2\,(\Im m[B_t g_t + d\rho_o{}^*] + \Im m[\Delta_o C_t{}^*]\,R_s) \\ g_4 =& \ \mid C_t \mid^2 \\ c_1 =& \ g_t a^* + \rho_o C_t{}^* \end{aligned}$$

TABLE I
DUALITY RULES

I	R_n	ρ_n	Z_s	R_s	X_s	A_t	C_t	R_t	ρ_o
II	g_n	$\rho_n{}^\star$	Y_p	G_p	B_p	D_t	B_t	g_t	$\rho_o{}^\star$

$$\begin{aligned}
c_2 &= g_t a^\star B_t + \rho_o C_t{}^\star B_t + \rho_o{}^\star a^\star d + R_t d C_t{}^\star \\
c_3 &= \rho_o B_t + R_t d \\
c_4 &= -d\Delta_o{}^\star \\
c_5 &= -\Delta_o a^\star \\
c_6 &= -B_t{}^\star d \\
c_7 &= -C_t a^\star \\
a &= 1 - A_t \\
d &= 1 - D_t \\
\Delta &= 1 + C_t Z_s + B_t Y_p + \Delta_o Y_p Z_s \\
\Delta_o &= 1 - a - d - (A_t D_t - B_t C_t) \\
\rho_o &= \rho_t \sqrt{R_t g_t}.
\end{aligned}$$

III. THE DUALITY IN THE NOISE PARAMETERS

Equations (6)–(8) are ratios of polynomials where the common denominator is $|\Delta|^2$. Notice that the coefficients r_i of (6) depend on G_p, the real part of Y_p, but not on B_p, its imaginary part. Since R_n depends on B_p only through the denominator $|\Delta|^2$, it follows that a large value of susceptive feedback (at constant frequency) will decrease R_n. This dependence on B_p will make R_n close to zero for large values of $|Z_s|$ and different from zero for small values of $|Z_s|$ at constant Y_p.

Also notable is that the noise parameters transform into each other according to the rules of Table I. This set of duality rules is to be read as follows: if R_n is determined as in (6) but g_n has not yet been determined, then (7) can be worked out by substituting every symbol of (6) found in Table I, line I, with the corresponding one in line II. On this basis, if a particular behavior is found in R_n (g_n), a similar behavior will be expected in g_n (R_n).

IV. MINIMA IN R_n AND g_n

The noise parameters (6), (7), and (8) can be studied analytically. This aims to design $F_n \simeq F_{n_{\min}}$, an overall noise figure F_n as insensitive as possible to the mismatch $|Y_S - Y_{S\text{opt}}|$ [12] or equivalently to $|\Gamma_S - \Gamma_{S\text{opt}}|$. This goal can be achieved when R_n is as small as possible at the design frequency. Thus, the feedback element values which provide minima in R_n are sought. On the basis of the duality principle, equivalent results can be expected from g_n.

This analysis is easily carried out when one single reactive feedback element is considered. Thus, assume $Z_s = jX_s, Y_p = 0$; the dual task concerning g_n would require $Z_s = 0, Y_p = jB_p$.

In order to proceed, R_n is rewritten as

$$R_n = \frac{A X_s{}^2 + B X_s + C}{D X_s{}^2 + E X_s + 1}. \tag{9}$$

$A, \cdots, E$ are derived from (6). Since R_n cannot be negative, the following statements are satisfied.

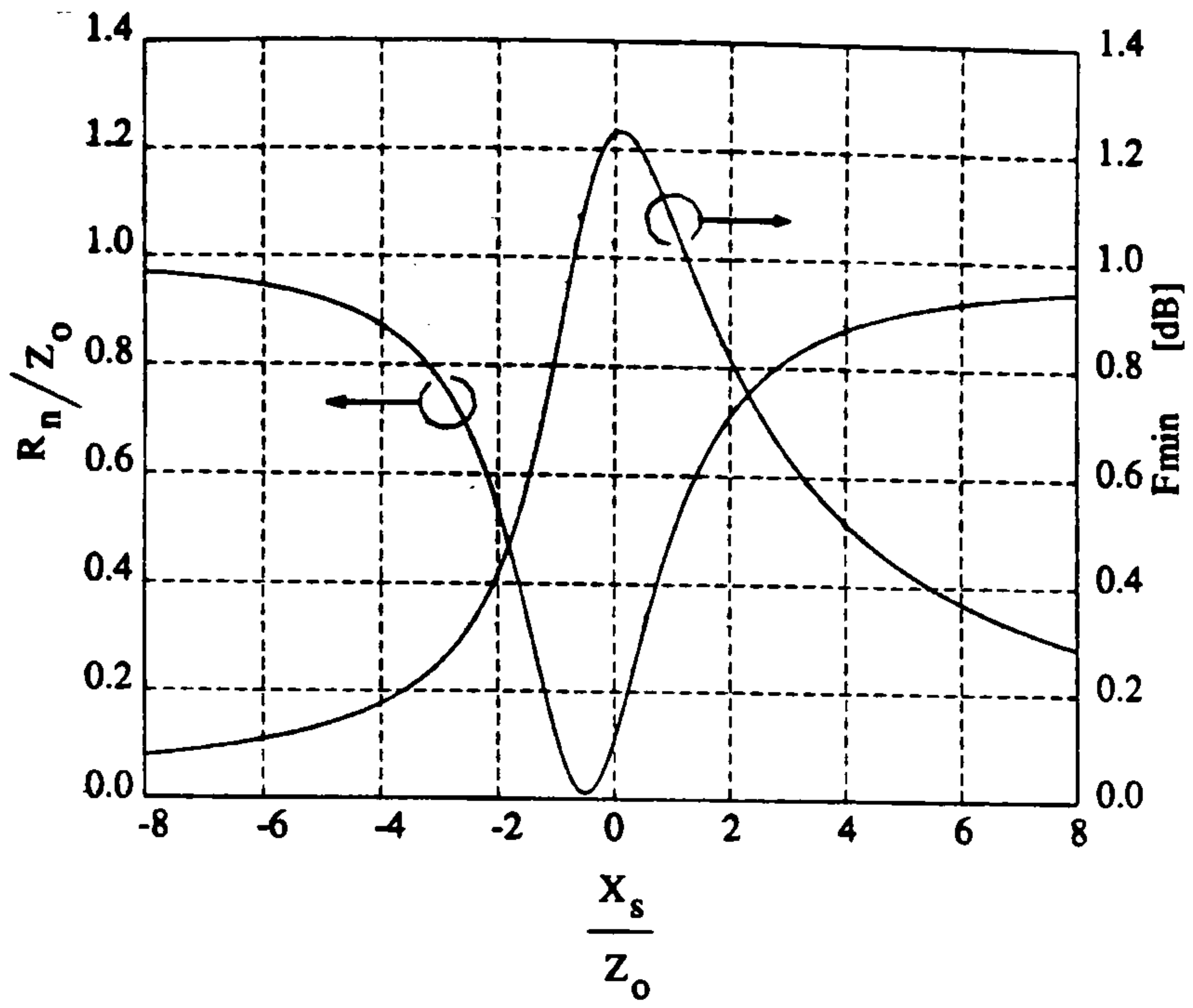

Fig. 2. Equivalent noise resistance R_n and minimum noise figure F_{min} versus feedback for Hewlett Packard ATF21186 MESFET at 8 GHz: $R_{n_{\max}} = 49.53\ \Omega$ at $C_s = 0.01$ pF (not shown); $R_{n_{\min}} = 0.57\ \Omega$ at $C_s = 0.80$ pF; $R_{n_{sat}} = 49.42\ \Omega$; $Z_o = 50\ \Omega$.

1) The coefficient A is always positive:

$$A = |\, a\sqrt{g_t} + C_t \rho_t{}^\star \sqrt{R_t}\,|^2 + R_t\,|C_t|^2\,(1 - |\rho_t|^2);$$

2) $B^2 - 4AC \leq 0$. Thus, a particular black box along with the proper feedback might provide $R_n = 0$.

The limit $R_{n_{sat}} = \lim_{X_s \to \pm\infty} R_n$ is finite and positive because (9) is a ratio of second-degree polynomials.

By setting the first derivative to zero, it is found that the minima X_{s_o} satisfy

$$(AE - BD)X_{s_o}^2 + 2(A - DC)X_{s_o} + (B - EC) = 0.$$

Two solutions are expected: a minimum $R_{n_{\min}}$ for $X_{s_o} = X_{s_m}$ and a maximum $R_{n_{\max}}$ for $X_{s_o} = X_{s_M}$.

V. DISCUSSION OF THE RESULTS

Microwave-active devices such as MESFET's, JFET's, and HEMT's with a reactive-series feedback have been analyzed in order to work out the value of X_{s_m} and the corresponding $R_{n_{\min}}$. The simulation shows that where $R_{n_{\min}}$ occurs, the minimum noise figure $F_{n_{\min}}$ of the overall network is smaller than the minimum noise figure $F_{t_{\min}}$ of the black box. It is also noticeable that $R_{n_{\min}}$ may be achieved by a capacitive-series feedback (Fig. 2).

This analysis shows that if the signal matrix is comprised of real numbers, no minimum will occur. Thus, a microwave active device will exhibit a minimum, while a simple resistive attenuator will not. However, a minimum in the noise parameters will occur when feedback is applied to a passive L, C, R network.

$$R_n = \frac{r_1\,|Z_s|^2 + r_2 R_s + r_3 X_s + r_4 G_p + R_t}{|\Delta|^2} \tag{6}$$

$$g_n = \frac{g_1\,|Y_p|^2 + g_2 G_p + g_3 B_p + g_4 R_s + g_t}{|\Delta|^2} \tag{7}$$

$$\rho_n \sqrt{R_n g_n} = \frac{c_1 Z_s{}^\star + c_2 Z_s{}^\star Y_p + c_3 Y_p + c_4 Z_s{}^\star G_p + c_5 Y_p R_s + c_6 G_p + c_7 R_s + \rho_o}{|\Delta|^2} \tag{8}$$

TABLE II
CALCULATED RESULTS FOR THE DEVICE IN [13].

f	[GHz]	4	8
X_{s_m}	[Ω]	73.76	18.96
$R_{n_{min}}$	[Ω]	13.25	27.21
X_{s_M}	[Ω]	−116.51	−358.19
$R_{n_{max}}$	[Ω]	218.54	56.17
$R_{n_{sat}}$	[Ω]	145.89	55.96

To demonstrate experimental evidence for the validity of the analysis presented above, the results in [13] are considered, which show a minimum in R_n [13, Fig. 4]. If device parameters [13, page 324] are entered into (6), (7), and (8), the values of Table II are obtained in agreement with those results. The maximum in R_n is missing in [13, Fig. 4], since it occurs for a very large value of $(-X_s)$, where $R_n \simeq R_{n_{max}} \simeq R_{n_{sat}}$.

VI. CONCLUSION

Closed-form expressions have been presented for the noise parameters with parallel and series feedback. It has been demonstrated that R_n always reaches a maximum and minimum, and the possibility of $R_n = 0$ has been pointed out. The same conclusions can be applied to g_n, since a duality principle exists. The theory shows that a minimum in the noise parameter R_n or g_n of either an active or passive black box may exist as long as its signal matrix is not purely real. A previous paper and its results have been used in order to demonstrate experimental evidence for the correctness of the formulas presented. This theory may help to design very low noise-feedback microwave amplifiers.

ACKNOWLEDGMENT

The authors acknowledge the recommendations made by one of the reviewers concerning the transformations in Section II.

REFERENCES

[1] J. Engberg, "Simultaneous input power match and noise optimization using feedback," in *Proc. 4th European Microwave Conf.*, Montreaux, Switzerland, pp. 385–389, 1974.
[2] K. B. Niclas, "Noise in broad band GaAs MESFET amplifiers with parallel feedback," *IEEE Trans. Microwave Theory Tech.*, vol. MTT-30, pp. 63–70, Jan 1982.
[3] ——, "The exact noise figure of amplifiers with parallel feedback and lossy matching circuits," *IEEE Trans. Microwave Theory Tech.*, vol. MTT-30, pp. 832–835, May 1982.
[4] S. Iversen, "The effect of feedback on noise figure," *Proc. IEEE*, vol. 63, pp. 540–542, Mar. 1975.
[5] L. Besser, "Stability considerations of low noise transistor amplifiers with simultaneous noise and power match," in *IEEE MTT-S Int. Symp. Dig.*, Palo Alto, CA, pp. 327–329, May 12–14, 1975.
[6] R. E. Lehmann and D. D. Heston, "X band monolithic series feedback LNA," *IEEE Trans. Microwave Theory Tech.*, vol. MTT-33, pp. 1560–1566, Dec. 1985.
[7] N. Shiga, S. Nakajima, K. Otobe, T. Sekiguchi, N. Kuwata, K.-I. Matsuzaki, and H. Hayashi, "X band MMIC amplifier with pulsed doped GaAs MESFETs," *IEEE Trans. Microwave Theory Tech.*, vol. 39, pp. 1987–1993, Dec. 1991.
[8] H. Rothe and W. Dalke, "Theory of noise four poles," *Proc. IRE*, vol. 44 1, pp. 811–818, June 1956.
[9] H. Nyquist, "Thermal agitation of electric charge in conductors," *Phys. Rev.*, vol. 32, pp. 110–113, July 1928.
[10] H. Hillbrand and P. H. Russer, "An efficient method for computer aided noise analysis of linear amplifier networks," *IEEE Trans. Circuits Syst.*, vol. CAS-23, pp. 235–238, Apr. 1976.
[11] K. Hartmann and M. J. O. Strutt, "Changes of the four noise parameters due to general changes of linear two-port circuit," *IEEE Trans. Electron Devices*, vol. ED-20, pp. 874–877, Oct. 1973.
[12] H. Fukui, "Available power gain, noise figure and noise measure of two ports and their graphical representation," *IEEE Trans. Circuit Theory*, vol. CT-13, pp. 137–142, June 1966.
[13] G. Vendelin, "Feedback effects on the noise performance of GaAs MESFETs," in *IEEE MTT-S Int. Symp. Dig.*, Palo Alto, CA, pp. 324–326, May 12–14, 1975.

Investigating Nonlinear Propagation in Dielectric Slab Waveguides

Jian-Guo Ma

Abstract—**A numerical method is employed to analyze the TE-wave propagation in Kerr-like nonlinear dielectric waveguides in which a nonlinear film is sandwiched between two linear media. The dispersion curves dependent on the magnitude of the electric field are obtained. All the results can be used in future investigations of devices composed of nonlinear dielectric slab structures.**

Index Terms—**Dispersion, Kerr-like, nonlinearity, waveguide.**

I. INTRODUCTION

It has been apparent for a long time that nonlinear propagation in optical and millimetric waveguides holds promise in the context of integrated signal processing [1]. In recent years, with the development of technology, guided waves in nonlinear dielectric slab waveguides received considerable attention owing to their potential applications to optical communications and optical computing.

For the nonlinear core waveguide, a general dispersion equation was developed in [2], using the modulus of a Jacobian elliptic function; however, spurious roots then appear in the dispersion equations [4]. The phase-plane approach was recently used in [1] to discuss the problem, which provides a physical interpretation of the results. This method can be applied to arbitrary nonlinearities. In all other cases, numerical methods such as in [3], [7], and [8], along with many others, have been employed.

In this paper, another numerical method is used to solve the nonlinear propagation in slab guides with a nonlinear core. The method transmits the values of the field from one boundary to another, therefore, it is called the transfer matrix method (TMM). In [9], the same idea was successfully used to numerically analyze the nonlinear planar waveguide with a linear core—a linear film is supported by a linear medium and covered by a nonlinear medium. In this paper, global coordinates are used to simplify the problem.

Manuscript received December 14, 1995; revised October 18, 1996.
The author was with the Department of Electrical Engineering, Gerhard-Mercator University, 47057 Duisburg, Germany. He is now with the Department of Electrical Engineering, Technical University of Nova Scotia, Halifax, NS, Canada B3J 2X4.
Publisher Item Identifier S 0018-9480(97)00843-0.

Optimum Noise-Source Reflection-Coefficient Design with Feedback Amplifiers

Luciano Boglione, *Student Member, IEEE*, Roger D. Pollard, *Fellow, IEEE*, and Vasil Postoyalko, *Member, IEEE*

***Abstract*—The issue of designing a low-noise microwave feedback amplifier for a given optimum noise-source coefficient $\Gamma_{S_{\rm opt}}$ is addressed and a set of original formulas is presented. These expressions define a new procedure which does not rely on computer optimization in order to get the required noise performance of the low-noise amplifier stage. The technique permits the design of a circuit which is simultaneously noise and power matched at its input port without an input matching circuit. This method can be used to screen devices for an optimum noise performance and it provides the essential mathematical tool for designing the core of a feedback amplifier.**

***Index Terms*—Amplifier noise, circuit noise, feedback amplifiers, feedback circuits, microwave amplifiers, noise.**

I. Introduction

THE DESIGN of low-noise amplifiers has been investigated widely [1]–[3]; feedback is often cited as the method to move the optimum noise reflection coefficient $\Gamma_{S_{\rm opt}}$ on the Smith chart. Feedback amplifiers have been analyzed in the past [4]–[8]. Parallel feedback [9] has been shown to allow wider band response [10], [11] as well as to improve input $|\Gamma_{\rm in}|$ and output $|\Gamma_{\rm out}|$ return losses [12]; series feedback has been experimentally demonstrated to provide low input return loss and $\Gamma_{\rm in} \simeq (\Gamma_{S_{\rm opt}})^*$ simultaneously [13], [14]. Today, computer optimization is applied to low-noise amplifiers in order to determine the series feedback value [15].

This paper develops some expressions for the noise parameters of the feedback amplifier and then addresses the issue of designing for either a specified value of $\Gamma_{S_{\rm opt}}$ or $|\Gamma_{S_{\rm opt}}| < \epsilon$. The aim is to achieve $\Gamma_{\rm in} = (\Gamma_{S_{\rm opt}})^* = 0$ for a microwave amplifier without an input matching circuit. According to the correlation matrix noise theory [16], the transmission representation matrix $\mathbf{C}_n$ of the cascaded circuits is

$$\mathbf{C}_n = \mathbf{C}_M + \mathbf{T}_M \mathbf{C}_A \mathbf{T}_M{}^+ \tag{1}$$

where the subscript M refers to the input matching circuit, A to the following amplifier, $\mathbf{C}$'s are correlation matrices, $\mathbf{T}_M$ is the matching circuit transmission matrix, and $^+$ is the Hermitian conjugate operation. The stages driven by the amplifier are neglected in (1) on the basis that the amplifier gain can reduce their noise contribution [17].

Manuscript received May 22, 1996; revised November 21, 1996. This work was supported by Filtronic Comtek plc.

The authors are with the Department of Electronic and Electrical Engineering, Microwave Terahertz and Technology Group, The University of Leeds, Leeds LS2 9JT, U.K.

Publisher Item Identifier S 0018-9480(97)01728-6.

Equation (1) demonstrates that the elements of the matrix $\mathbf{C}_n$ are nonlinear combinations of the signal and the noise parameters of the cascaded stages. Direct control of $\mathbf{C}_n$ is therefore very difficult. The design is simplified by removing the input matching network: (1) then simply becomes $\mathbf{C}_n = \mathbf{C}_A$.

II. Expressions for the Design

The equations involving the noise parameters are written as functions of the elements of $\mathbf{C}_A$:

$$\mathbf{C}_A = \begin{bmatrix} R_n^A & \rho_o^{A*} \\ \rho_o^A & g_n^A \end{bmatrix}, \qquad \text{where } \rho_o^A = \rho_n^A \sqrt{g_n^A R_n^A}.$$

The term $4kT_o\Delta f$ has been dropped.

A. Expression for a Given $\Gamma_{S_{\rm opt}}^A$

Suppose that an optimum source reflection coefficient $\Gamma_{S_{\rm opt}}^A$ has to be achieved. According to [18]

$$\sqrt{(G_c^A)^2 + \frac{G_n^A}{R_N^A}} - jB_c^A = Y_{S_{\rm opt}}^A \tag{2}$$

where $Y_{S_{\rm opt}}^A = G_{S_{\rm opt}}^A + jB_{S_{\rm opt}}^A$ is the admittance which corresponds to $\Gamma_{S_{\rm opt}}^A$, $Y_c^A = G_c^A + jB_c^A$ is the correlation admittance of the stage, G_n^A and R_n^A are its uncorrelated noise conductance and resistance. After rewriting

$$\begin{aligned} Y_c^A &= \rho_n^A \sqrt{\frac{g_n^A}{R_n^A}} \\ &= \rho_n^A \frac{\sqrt{g_n^A R_n^A}}{R_n^A} \\ &= \frac{\rho_o^A}{R_n^A} \end{aligned} \tag{3}$$

$$G_n^A = g_n^A - |Y_c^A|^2 R_n^A \tag{4}$$

and substituting (3) and (4) into (2), the system

$$\Im m[\rho_o^A] = -B_{S_{\rm opt}}^A R_n^A \tag{5a}$$

$$g_n^A = |Y_{S_{\rm opt}}^A|^2 R_n^A \tag{5b}$$

is obtained.

System (5) can be solved for two unknowns. Equation (5a) states that real optimum source reflection coefficients (e.g., $\Gamma_{S_{\rm opt}}^A = 0$) require $\Im m[\rho_o^A] = 0$.

B. Expression for $|\Gamma^A_{S_{opt}}| \leq \epsilon$

Suppose the goal is

$$|\Gamma^A_{S_{opt}}| \leq \epsilon \leq 1. \tag{6}$$

Equation (6) defines a circle on the normalized admittance plane $y^A_{S_{opt}} = Y^A_{S_{opt}}/Y_o$:

$$|y^A_{S_{opt}} - C_\epsilon| \leq R_\epsilon \tag{7}$$

where

$$C_\epsilon = \frac{1+\epsilon^2}{1-\epsilon^2}$$

and

$$R_\epsilon = \frac{2\epsilon}{1-\epsilon^2}.$$

If (2) is substituted into (7), and (3) and (4) are used, the resulting general expression is

$$(g^A_n Z_o)^2 + f^2_\epsilon (R^A_n Y_o)^2 - 2h_\epsilon (g^A_n Z_o)(R^A_n Y_o) + 4C^2_\epsilon \Im m[\rho^A_o]^2 = 0 \tag{8}$$

where

$$f_\epsilon = C^2_\epsilon - \eta R^2_\epsilon$$

and

$$h_\epsilon = C^2_\epsilon + \eta R^2_\epsilon$$

η is a parameter, ranging from 0 to 1, which transforms the inequality (7) into an equation ($R^2_\epsilon \rightarrow \eta R^2_\epsilon$) and is useful for software implementation. One unknown can solve (8).

III. Expansion for the Feedback Amplifier

Expressions (5) and (8) will be expanded as functions of the noisy feedback elements $Z_s = R_s + jX_s$ and $Y_p = G_p + jB_p$ of a feedback amplifier (see Fig. 1). R^A_n, g^A_n, and $\rho^A_o = \rho^A_n \sqrt{g^A_n R^A_n}$ have been derived in [19] as functions of the feedback elements.

A. Expansion for a Given $\Gamma^A_{S_{opt}}$

Substituting R^A_n, g^A_n, and ρ^A_o into (5a) and (5b) results in the system:

$$\begin{aligned} &kA_{11}g_p x^2_s + kA_{11}g_p r^2_s \\ &\quad + kA_{10}r^2_s + kA_{10}x^2_s + (kA_{21} + D_{rg})r_s g_p \\ &\quad + (kA_{31} + D_{xg})g_p x_s + D_{xb}x_s b_p \\ &\quad + D_{rb}r_s b_p + (kA_{20} + D_r)r_s + (kA_{30} + D_x)x_s \\ &\quad + (kA_{41} + D_g)g_p + D_b b_p \\ &\quad + (kr_{t_n} + D_o) = 0 \end{aligned} \tag{9a}$$

$$\begin{aligned} &qA_{11}g_p x^2_s + qA_{11}g_p r^2_s - B_{11}r_s b^2_p - B_{11}r_s g^2_p \\ &\quad + qA_{10}r^2_s - B_{10}g^2_p + qA_{10}x^2_s - B_{10}b^2_p \\ &\quad + (qA_{21} - B_{21})r_s g_p - B_{31}r_s b_p \\ &\quad + qA_{31}g_p x_s + (qA_{20} - B_{41})r_s + qA_{30}x_s \\ &\quad + (qA_{41} - B_{20})g_p - B_{30}b_p \\ &\quad + (qr_{t_n} - g_{t_n}) = 0 \end{aligned} \tag{9b}$$

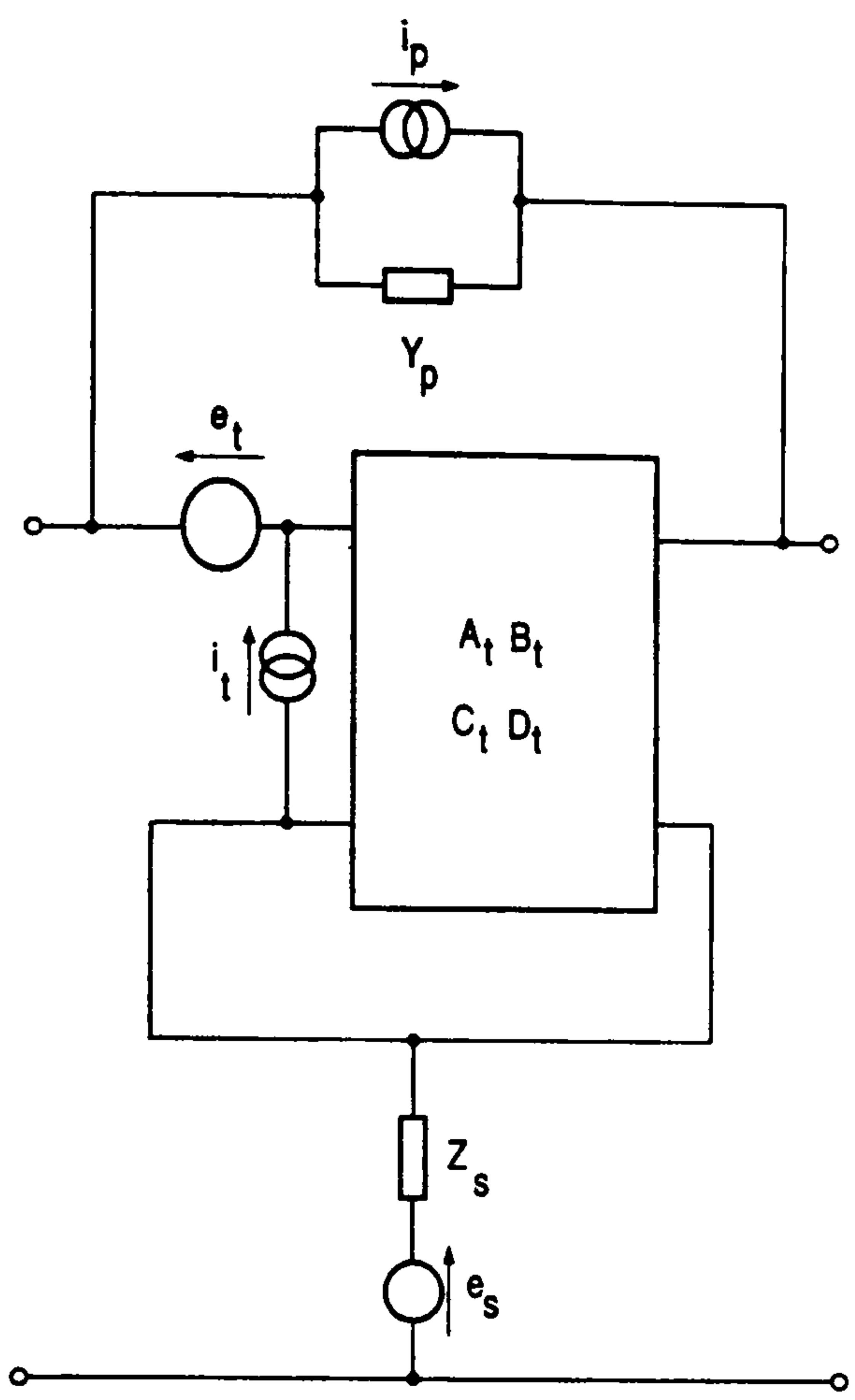

Fig. 1. Schematic of noisy two-port with series and parallel feedback.

The unknowns are $r_s = \Re e[Z_s/Z_o]$, $x_s = \Im m[Z_s/Z_o]$, $g_p = \Re e[Y_p/Y_o]$, and $b_p = \Im m[Y_p/Y_o]$. $Z_o = 1/Y_o$ is the characteristic impedance of the system. The coefficients of (9) are

$$\begin{aligned} k &= \Im m[Y^A_{S_{opt}}]Z_o \\ q &= \left(\frac{|Y^A_{S_{opt}}|}{Y_o}\right)^2 \\ \Delta &= 1 - a - d - (A_t D_t - B_t C_t) \\ a &= 1 - A_t \\ d &= 1 - D_t \\ \rho_{o_t} &= \rho_t \sqrt{R_t g_t} \\ A_{10} &= (g_t|a|^2 + R_t|C_t|^2 + 2\Re e[a\rho_{o_t} C^\star_t])Z_o \\ A_{11} &= |\Delta|^2 \\ A_{20} &= |a|^2 + 2\Re e[a\rho_{o_t}] + 2R_t \Re e[C_t] \\ A_{21} &= 2\Re e[\Delta B^\star_t]Y_o \\ A_{30} &= -2\Im m[C_t R_t + a\rho_{o_t}] \\ A_{31} &= -2\Im m[\Delta B^\star_t]Y_o \\ A_{41} &= (|B_t|Y_o)^2 \\ r_{t_n} &= \frac{R_t}{Z_o} \\ B_{10} &= R_t|d|^2 + g_t|B_t|^2 + 2\Re e[d\rho^\star_{o_t} B^\star_t]Y_o \\ B_{11} &= |\Delta|^2 \\ B_{20} &= |d|^2 + 2\Re e[d\rho^\star_{o_t}] + 2g_t \Re e[B_t] \\ B_{21} &= 2\Re e[\Delta C^\star_t]Z_o \\ B_{30} &= -2\Im m[B_t g_t + d\rho^\star_{o_t}] \end{aligned}$$

$$
\begin{aligned}
B_{31} &= -2\Im m[\Delta C_t^\star]Z_o \\
B_{41} &= (|C_t|Z_o)^2 \\
g_{t_n} &= \frac{g_t}{Y_o} \\
c_1 &= g_t a^\star + \rho_{o_t} C_t^\star \\
c_2 &= g_t a^\star B_t + \rho_{o_t} C_t^\star B_t + \rho_{o_t}^\star a^\star d + R_t\, d C_t^\star \\
c_3 &= \rho_{o_t} B_t + R_t\, d \\
c_4 &= -d\Delta^\star \\
c_5 &= -a^\star \Delta \\
c_6 &= -B_t^\star\, d \\
c_7 &= -C_t a^\star \\
D_{rg} &= \Im m[c_2 + c_5 + c_4] \\
D_{xb} &= \Im m[c_2] \\
D_{rb} &= \Re e[c_2 + c_5] \\
D_{xg} &= -\Re e[c_2 + c_4] \\
D_r &= \Im m[(c_1 + c_7)Z_o] \\
D_x &= -\Re e[c_1 Z_o] \\
D_g &= \Im m[(c_3 + c_6)Y_o] \\
D_b &= \Re e[c_3 Y_o] \\
D_o &= \Im m[\rho_{o_t}]
\end{aligned}
$$

k and q specify $\Gamma^A_{S_{\rm opt}}$ to be achieved; $A_t B_t C_t D_t$ is the transmission matrix of the transistor, R_t, g_t, and ρ_t its noise parameters. The subscript t refers to the transistor of the feedback amplifier stage.

B. Expansion for $|\Gamma^A_{S_{\rm opt}}| \le \epsilon$

The expansion is carried out for the particular case of a reactive feedback amplifier ($Z_s = jX_s$, $Y_p = 0$) because this configuration is widely used for achieving a simultaneous match between the input reflection coefficient $\Gamma^A_{\rm in}$ and the conjugate of the optimum source reflection coefficient $(\Gamma^A_{S_{\rm opt}})^\star$. Thus, (8) is expanded into

$$\sum_{i=0}^{4} \alpha_i x_s^i = 0 \tag{10}$$

where

$$
\begin{aligned}
\alpha_4 &= f_\epsilon^2 A_{10}^2 \\
\alpha_3 &= 2 f_\epsilon^2 A_{10} A_{30} \\
\alpha_2 &= f_\epsilon^2 A_{30}^2 + 2 f_\epsilon^2 A_{10} r_{t_n} + 4C_\epsilon^2 D_x^2 - 2h_\epsilon g_{t_n} A_{10} \\
\alpha_1 &= 2 f_\epsilon^2 A_{30} r_{t_n} - 8C_\epsilon^2 \rho_y D_x - 2h_\epsilon g_{t_n} A_{30} \\
\alpha_0 &= f_\epsilon^2 r_{t_n}^2 + 4C_\epsilon^2 \rho_y + g_{t_n}^2 - 2h_\epsilon g_{t_n} r_{t_n} \\
\rho_y &= \Im m[\rho_{o_t}].
\end{aligned}
$$

The unknown is $x_s = \Re e[Z_s/Z_o]$. The α_i's are defined in terms of the coefficients of (9).

IV. Discussion

Some observations about the system (9) are as follows.

- The set of (9a) and (9b) allows determination of the values of the feedback elements for a circuit to provide a given $\Gamma^A_{S_{\rm opt}}$ at the design frequency. No control on other stage parameters is exerted by (9).
- System (9) is nonlinear.
- System (9) has more unknowns than equations.

An exact solution of (9) can be formally derived by setting to zero two of the four variables r_s, x_s, g_p, and b_p and then substituting one equation into the other. Table I shows the number N_s of expected solutions as a function of the unknowns chosen. Some of them may be physically meaningless—for example, a solution (x_s; b_p) can be complex. The desired pair of feedback elements may not exist or may not be achievable at certain frequencies. However, the procedure applied to a number of different commercially available MESFET's has always found a numerical solution for a given $\Gamma^A_{S_{\rm opt}}$. The solution involving a resistive element is expected to correspond to a higher minimum noise figure than the one which makes use of reactive elements only; nonetheless, Table III demonstrates a decrease in $F_{\rm min}$ can result.

TABLE I
NUMBER N_s OF SOLUTIONS OBTAINABLE FROM (9) AFTER SETTING A PAIR OF UNKNOWNS TO ZERO: THE SYMBOL X SHOWS THE CHOSEN UNKNOWNS

r_s	x_s	g_p	b_p	N_s
X	X	-	-	2
X	-	X	-	6
X	-	-	X	5
-	X	X	-	6
-	X	-	X	4
-	-	X	X	2

TABLE II
EXPECTED MINIMUM IN $|\Gamma^A_{S_{\rm opt}}|$ FOR THREE HEWLETT PACKARD MESFET'S AND A THIRD-DEGREE POLYNOMIAL LEAST SQUARES APPROXIMATION (N.A.: DATA BOOK PARAMETERS NOT AVAILABLE)

GHz	ATF21186	ATF35376	ATF10136
0.5	0.024	N.A.	N.A.
1.0	0.057	N.A.	0.296
2.0	0.213	0.418	0.079
4.0	0.452	0.080	0.276
6.0	0.639	0.144	0.360
8.0	0.800	0.271	0.251

TABLE III
SOME OF THE SOLUTIONS ACHIEVABLE WITH ATF21186 @ 1 GHz FOR $\Gamma_{S_{\rm opt}} = 0.1e^{j45^\circ}$ (THE FIRST ROW SHOWS THE DEVICE PERFORMANCE WITHOUT FEEDBACK)

R_s/Z_o	X_s/Z_o	G_p/Y_o	B_p/Y_o	F_{min} [dB]	G_{av} [dB]
0	0	0	0	0.55	15.1
0.0266	3.2737	0	0	0.46	4.9
0.5864	0	0.7551	0	17.5	-13.8
$1.6505\ 10^3$	0	0	6.1704	0.01	0.0
0	0.3492	0.2466	0	3.49	4.5
0	3.1565	0	-0.0890	0.50	9.4
0	0	0.3219	-0.2325	4.57	5.0

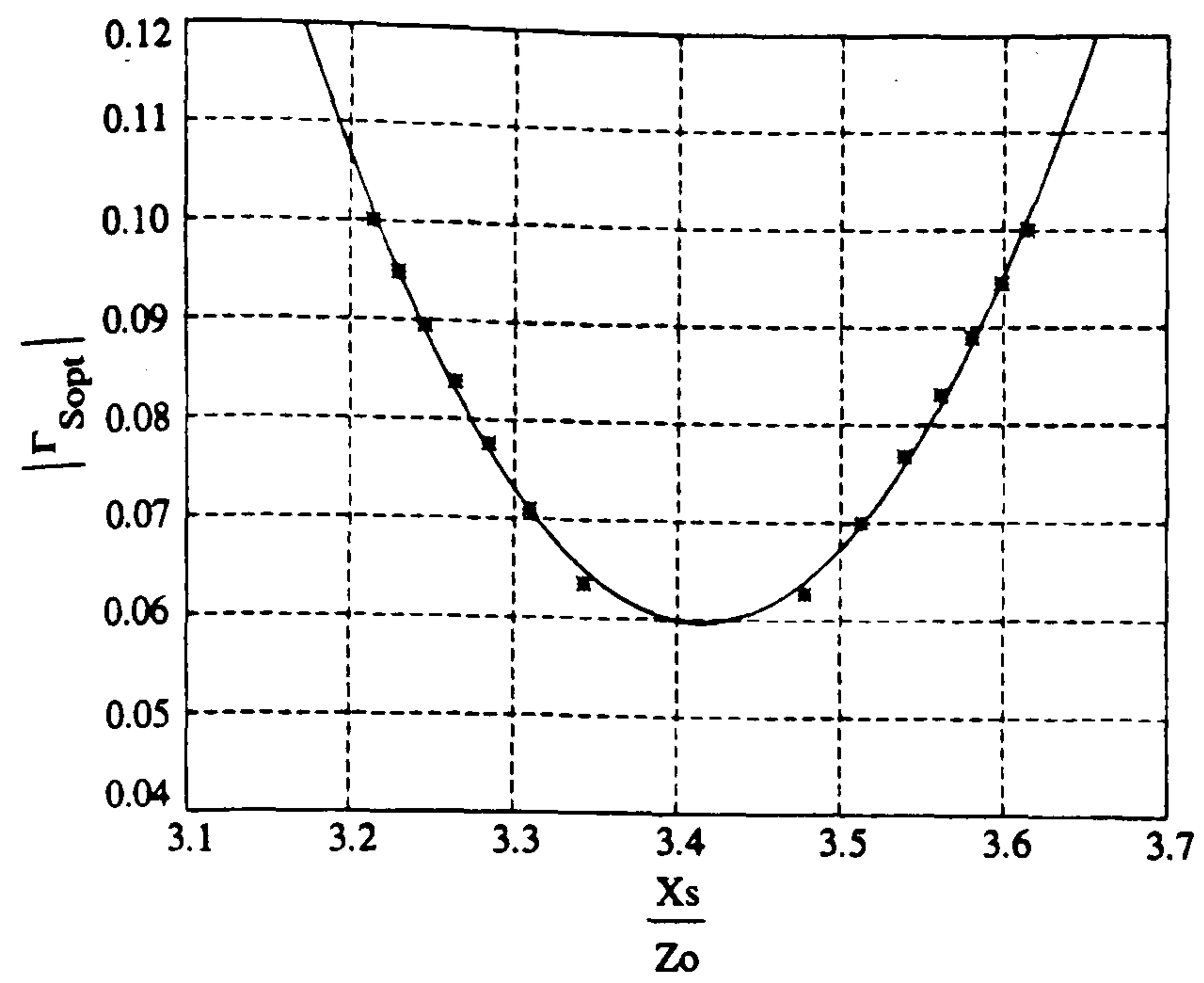

Fig. 2. Computed $\Gamma^A_{S_{opt}}$ (*) versus normalized series feedback x_s with $\epsilon = 0.1$ and $Y = ax_s^2 + bx_s + c$ (solid line; $a = 1.0303$, $b = -7.0350$, $c = 12.0685$) for a Hewlett Packard ATF21186 GaAs MESFET at 1 GHz: $|\Gamma^A_{S_{opt}}|_{\min} = 0.0596$ @ $x_s = -b/2a = 3.4141$.

TABLE IV
AMPLIFIER DESIGN VALUES FOR AN HP ATF21186 AT 1 GHz, $\epsilon = 0.1$

x_s	3.43	-
L_s	27.29	nH
$\lvert \Gamma^A_{S_{opt}} \rvert$	0.06	-
$\angle\Gamma^A_{S_{opt}}$	-164.81	deg
F^A_{min}	0.39	dB
R^A_n	1.18	Ω
$\lvert \Gamma^{SSNM}_L \rvert$	0.91	-
$\angle\Gamma^{SSNM}_L$	9.05	deg
G^A_{av}	4.80	dB
G^A_T	4.73	dB

The procedure for designing either $\Gamma^A_{S_{opt}}$ or $|\Gamma^A_{S_{opt}}| \le \epsilon$ is outlined below.

1) Choose a pair of unknowns and solve system (9) for the given $\Gamma^A_{S_{opt}}$ or solve (10) for the given ϵ.
2) For each acceptable solution work out the signal and noise parameters.
3) Calculate the value of the load which allows to get the input reflection coefficient $\Gamma^A_{in} = (\Gamma^A_{S_{opt}})^*$, where * is the conjugate operation; this particular load is

$$\Gamma_L^{SSNM} = \frac{S_{11} - \Gamma^*_{S_{opt}}}{\Delta - S_{22}\Gamma^*_{S_{opt}}}$$

where Δ is the determinant of the scattering matrix of the stage—transistor plus feedback elements. SSNM is the acronym for simultaneously signal and noise matched.
4) Find the transducer power gain G_T when Γ_L^{SSNM} loads the output along with other signal and noise parameters as desired.
5) If the required circuit performance is not satisfied, rerun this procedure with a different set of unknowns.

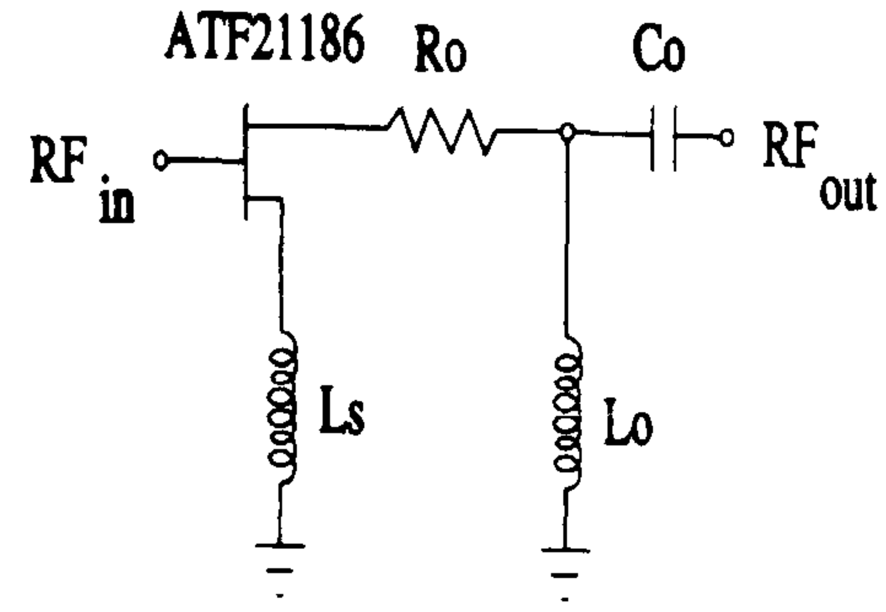

Fig. 3. Circuit layout for frequency domain simulation: $R_o = 10\ \Omega$, $L_o = 27.61$ nH, $C_o = 0.69$ pF for the output matching circuit.

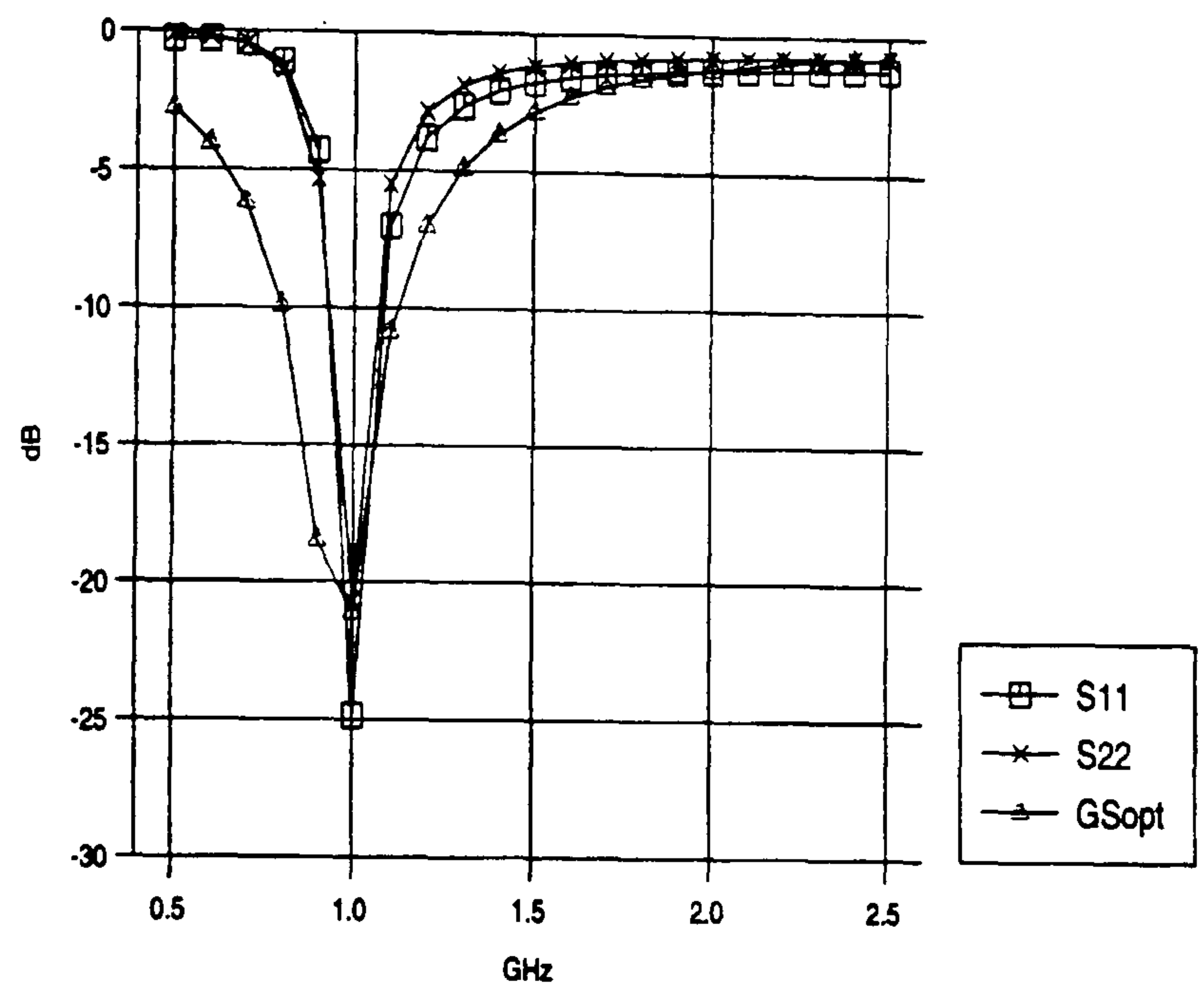

Fig. 4. Frequency dependence of the input return loss (S_{11}), the output return loss (S_{22}), and the optimum noise reflection coefficient (GS_{opt}) for the designed circuit.

When a series reactive feedback is considered, $\Gamma^A_{S_{opt}}$ has a minimum in magnitude. Equation (10) suggests a way to find this minimum. A least squares method may successfully be applied in order to evaluate this minimum (see Fig. 2). If $\epsilon < |\Gamma^A_{S_{opt}}|_{\min}$, a different device must be selected (see Table II); the input insertion loss when the simultaneous match $\Gamma_{in} = (\Gamma_{S_{opt}})^*$ is achieved cannot be better than $|\Gamma^A_{S_{opt}}|_{\min}$.

This procedure has been applied to a Hewlett Packard ATF21186 low-noise GaAs MESFET [20]. Table IV collects the design results for the circuit shown in Fig. 3. Finally, a simulation in the frequency domain has been carried out as shown in Figs. 4–6.

The simulation at the design frequency gives the same response as the calculations described above. The device is inherently unstable and this stability is usually further degraded by the calculated feedback elements. Both resistive and reactive components have to be properly added to the circuit in order to control the input and output return loss and restrain the amplifier from oscillating. Since this will affect $\Gamma^A_{S_{opt}}$, the number of circuit components should be kept as small as possible and should preferably be added after the transistor.

The output stage has the main task of providing the necessary Γ_L^{SSNM} at its input port when loaded at its output by 50

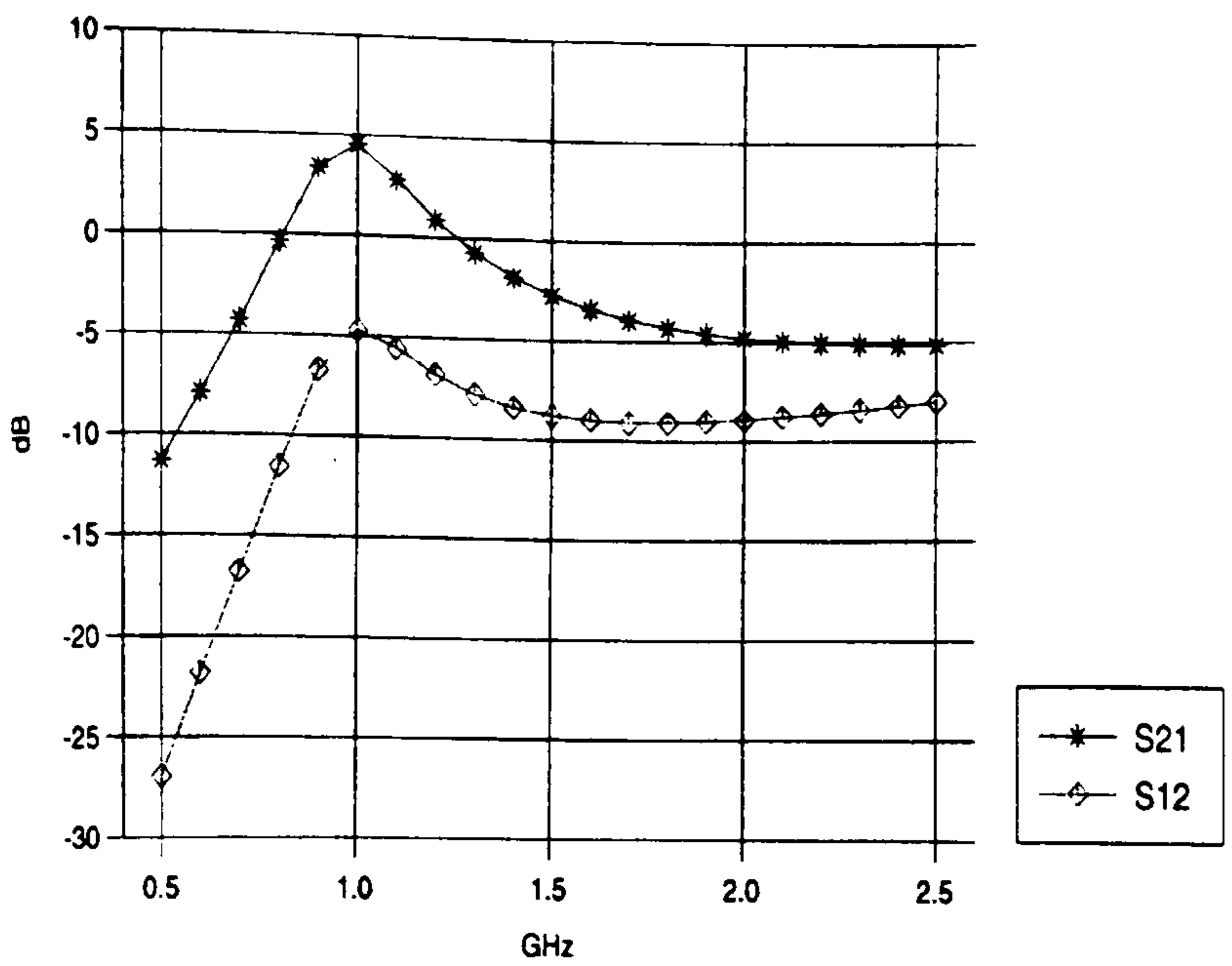

Fig. 5. Frequency dependence of the forward (S_{21}) and the inverse (S_{12}) transmission coefficients for the designed circuit.

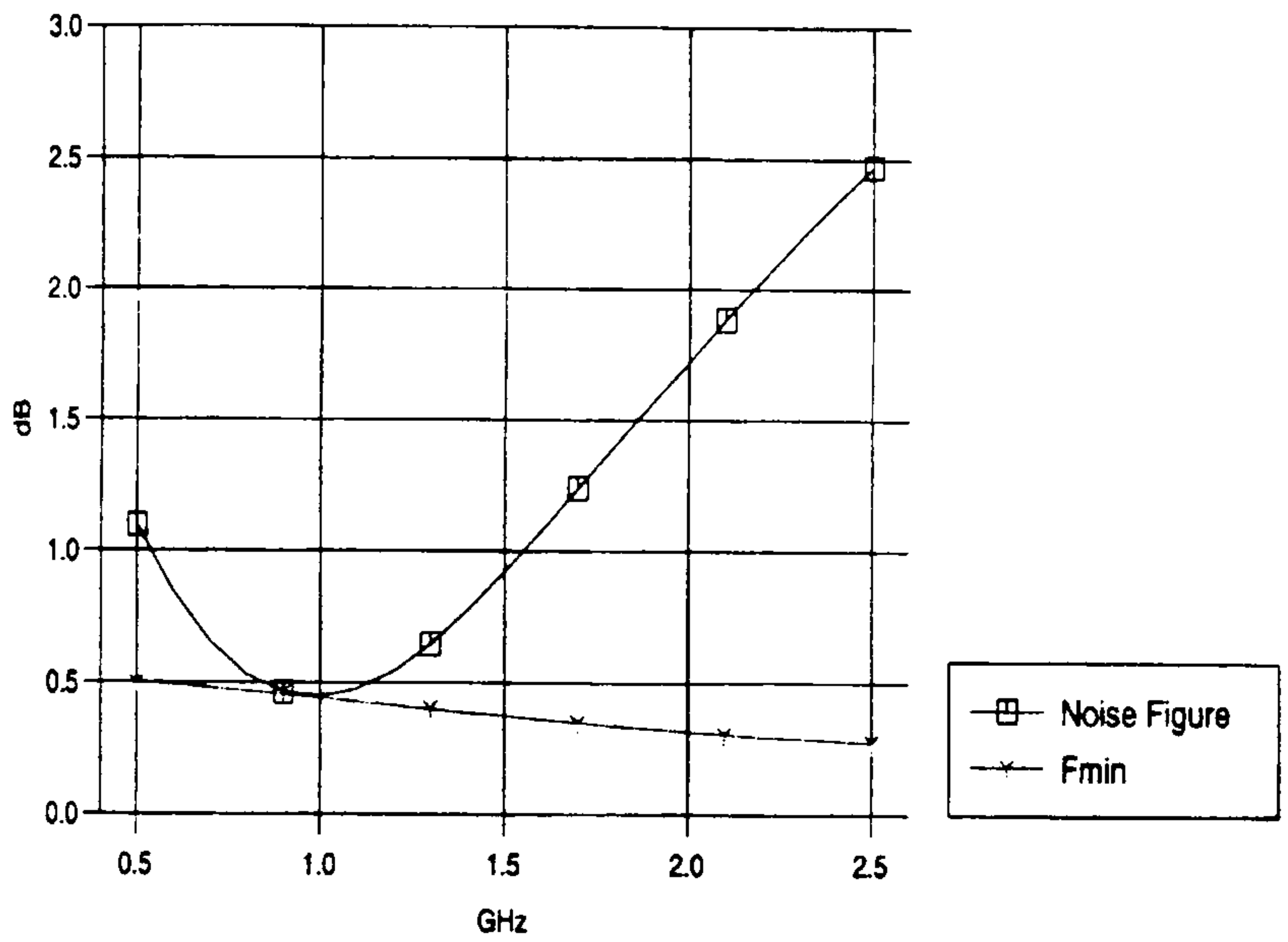

Fig. 6. Frequency dependence of the noise figure and the minimum noise figure ($F_{\min}$) for the designed circuit.

Ω. A resistor R_o can improve the stability without affecting the noise performance of the stage (see Fig. 3). Usually, the calculated Γ_L^{SSNM} is close to $\Gamma_L = (\Gamma_{\mathrm{out}})^{\star}$, the load at which the output port is power matched. Thus, the transducer power gain G_T^A of the feedback amplifier is close to its available power gain G_{av}^A.

The design must be considered as a starting point for a subsequent optimization. The optimization is required because this design does not take into account every physical component or the parasitic elements of the complete circuit. Frequency dependent elements have to be added to the network in order to improve its stability. Transmission lines to the active device input port are particularly important [21] because they have a large effect on the noise parameters. The design seems to be sensitive to these elements even if the input line is very short. However, the optimization at the design frequency is able to achieve the required $\Gamma_{S_{\mathrm{opt}}}$.

The authors are not aware of any other analytical technique to directly control $\Gamma_{S_{\mathrm{opt}}}$. These expressions are valid for either active and passive linear two-ports with feedback elements.

V. Conclusion

Original expressions for designing either a given $\Gamma_{S_{\mathrm{opt}}}$ or $|\Gamma_{S_{\mathrm{opt}}}| \leq \epsilon$ are derived and applied to a feedback amplifier. These formulas allow the design of a circuit simultaneously matched at its input port $\Gamma_{\mathrm{in}} = (\Gamma_{S_{\mathrm{opt}}})^{\star} = 0$ without the need of an input matching circuit. When a reactive series feedback is used, the procedure can select the most suitable device since a minimum value of $|\Gamma_{S_{\mathrm{opt}}}|$ as a function of the feedback exists. These equations apply to any linear noisy two-ports with feedback elements.

References

[1] M. Sierra, "Matching, gain and noise limits on linear amplifier four-poles," *Microwave Opt. Tech. Lett.*, vol. 2, no. 1, pp. 29–34, Jan. 1989.

[2] B. M. Albinsson, "A graphic design method for matched low noise amplifier," *IEEE Trans. Microwave Theory Tech.*, vol. 38, pp. 118–122, Feb. 1990.

[3] S.-S. Bor, J.-C. Liu, and P.-C. Lu, "Plots with matching circles for optimizing the performance of a low noise amplifier," *Microwave Opt. Tech. Lett.*, vol. 6, no. 2, pp. 141–148, Feb. 1993.

[4] J. Engberg, "Simultaneous input power match and noise optimization using feedback," in *Proc. 4th European Microwave Conf.*, Montreux, Switzerland, 1974, pp. 385–389.

[5] S. Iversen, "The effect of feedback on noise figure," *Proc. IEEE*, vol. 63, pp. 540–542, Mar. 1975.

[6] G. Vendelin, "Feedback effects on the noise performance of GaAs MESFET's," in *IEEE MTT-S Int. Symp. Dig.*, 1975, pp. 324–326.

[7] L. Besser, "Stability considerations of low noise transistor amplifiers with simultaneous noise and power match," in *IEEE MTT-S Int. Symp. Dig.*, Palo Alto, CA, 1975, pp. 327–329.

[8] F. Perez and V. Ortega, "A graphical method for the design of feedback networks for microwave transistor amplifiers: Theory and applications," *IEEE Trans. Microwave Theory Tech.*, vol. MTT-29, pp. 1019–1026, Oct. 1981.

[9] K. B. Niclas, "The exact noise figure of amplifiers with parallel feedback and lossy matching circuits," *IEEE Trans. Microwave Theory Tech.*, vol. MTT-30, pp. 832–835, May 1982.

[10] K. B. Niclas, W. T. Wilser, R. B. Gold, and W. R. Hitchens, "The matched feedback amplifier: Ultrawide band-microwave amplification with GaAs MESFET's," *IEEE Trans. Microwave Theory Tech.*, vol. MTT-28, pp. 285–294, Apr. 1980.

[11] K. B. Niclas, "Noise in broad band GaAs MESFET amplifiers with parallel feedback," *IEEE Trans. Microwave Theory Tech.*, vol. MTT-30, pp. 63–70, Jan. 1982.

[12] J. Tajima, Y. Yamao, T. Sugeta, and M. Hirayama, "GaAs monolithic low-power amplifiers with *RC* parallel feedback," *IEEE Trans. Microwave Theory Tech.*, vol. MTT-32, pp. 542–544, May 1984.

[13] R. E. Lehmann and D. D. Heston, "X band monolithic series feedback LNA," *IEEE Trans. Microwave Theory Tech.*, vol. MTT-33, pp. 1560–1566, Dec. 1985.

[14] N. Shiga, S. Nakajima, K. Otobe, T. Sekiguchi, N. Kuwata, K.-i. Matsuzaki, and H. Hayashi, "X band MMIC amplifier with pulsed doped GaAs MESFET's," *IEEE Trans. Microwave Theory Tech.*, vol. 39, pp. 1987–1993, Dec. 1991.

[15] Y. Tsukahara, S. Chaki, Y. Sasaki, K. Nakahara, N. Andoh, H. Mastubayasi, N. Tanino, and O. Ishihara, "A C-band 4-stage low noise miniaturized amplifier using lumped elements," *IEEE MTT-S Int. Symp. Dig.*, Orlando, FL, 1995, vol. 3, pp. 1125–1128.

[16] H. Hillbrand and P. H. Russer, "An efficient method for computer aided noise analysis of linear amplifier networks," *IEEE Trans. Circuits Syst.*, vol. CAS-23, pp. 235–238, Apr. 1976.

[17] H. T. Friis, "Noise figure of radio receivers," *Proc. IRE*, vol. 32, pp. 419–422, July 1944.

[18] H. Rothe and W. Dalke, "Theory of noise four poles," *Proc. IRE*, vol. 44-I, pp. 811–818, June 1956.

[19] L. Boglione, R. D. Pollard, and V. Postoyalko, "Analytical behavior of the noise resistance and the noise conductance for a network with parallel and series feedback," *IEEE Trans. Microwave Theory Tech.*, vol. 45, Feb. 1997.

[20] *Communication Components, Designer's Catalogue, GaAs and Silicon Products.* Palo Alto, CA: Hewlett Packard, 1993.

[21] J. Engberg and T. Larsen, *Noise Theory of Linear and Nonlinear Circuits*. New York: Wiley, 1995.

Luciano Boglione (S'96) was born in Turin, Italy. He received the Laurea degree in electronic engineering from the Politecnico di Torino, Turin, Italy, in 1991. He is currently pursuing his Ph.D. degree from The University of Leeds, Leeds, U.K.

In October 1990 he spent one year as a Visiting Researcher at The University of Leeds, Department of Electrical and Electronic Engineering, working on nonlinear device models. He was a Software Engineer for an Italian company from 1992 to 1994. His area of research includes low-noise amplifier lesign for microwave applications.

Roger D. Pollard (M'77–SM'91–F'97) was born in London, U.K., in 1946. He received the B.Sc. and Ph.D. degrees in electrical and electronic engineering from The University of Leeds, Leeds, U.K.

He holds the Chair in high-frequency measurements in the Department of Electronic and Electrical Engineering, The University of Leeds, where he has been a Faculty Member since 1974 as well as being a Consultant to the Hewlett-Packard Company, Santa Rosa, CA, since 1981. He is jointly responsible for the activities of the Microwave and erahertz Technology Research Group which has over 40 active researchers, strong graduate program, and has made contributions to microwave passive nd active device research. His personal research interests are in microwave etwork measurements, calibration and error correction, microwave and iillimeter-wave circuits, and large-signal and nonlinear characterization.

Dr. Pollard is a Chartered Engineer and a member of the Institution of lectrical Engineers (IEE), U.K. He is serving his second term as an elected iember of the IEEE MTT-S Administrative Committee, where he is 1997 ice President.

Vasil Postoyalko (S'82–M'82) was born in Leeds, U.K., in 1956. He received the B.Sc. degree in mathematics and Ph.D. degree in electronic engineering and applied mathematics from The University of Leeds, Leeds, U.K., in 1978 and 1985, respectively.

In 1983 he was appointed Research Engineer at The University of Leeds, Department of Electronic and Electrical Engineering. Since 1986, he has held the post of Hewlett-Packard Lecturer in the Department of Electronic and Electrical Engineering where he is a Member of the department's Microwave and Terahertz Technology Group. His present research interest is the design of microwave and millimeter-wave circuits.

BJT Feedback LNA with Input Port Simultaneously Signal and Noise Matched

Luciano Boglione, Roger D. Pollard, Vasil Postoyalko
Institute of Microwaves and Photonics
School of Electronic & Electrical Engineering
The University of Leeds
Leeds LS2 9JT
United Kingdom
Tel.: +44 113 2332084
Fax : +44 113 2332032
Email : eenlb@sun.leeds.ac.uk

ABSTRACT

This paper presents the first implementation of a novel technique for designing feedback low noise amplifiers (LNA) with Simultaneous Signal and Noise Matching (SSNM) at the input port. The design procedure relies on a new and original analytical approach that determines the exact value of the feedback element(s) in order to design either the complex value of the optimum noise source reflection coefficient $\Gamma_{S_{opt}}$ or its magnitude. The goal is to overcome the problem with a microwave amplifier that the maximum signal power transfer from the source to the active device cannot be achieved simultaneously with its minimum noise figure. The theoretical approach does not depend on a particular device, nor is it restricted to a given frequency. The LNA makes use of a BJT and commercially available surface mounted components. The good agreement between experimental and simulated results confirms that this new design technique can be applied successfully.

INTRODUCTION

The designer of low noise amplifiers (LNAs) faces the problem of achieving three main goals: high gain, low noise and stability at the same time. This is the typical case when mobile communication subsystems are considered. Standard approaches (Gonzalez [1]) split the design into two steps: 1) the LNA is designed at the desired frequency f_o for either signal or noise performance; 2) the designer takes advantage of computer optimisation programs in order to meet both signal and noise performance criteria according to specifications. Series feedback amplifiers (Lehman et al. [2], Shiga et al. [3], Tsukahara et al. [4]) have been proven to reach good Simultaneous Signal and Noise Match (SSNM) performances and are typical for LNA applications. What has not been available is an exact procedure applied to feedback amplifiers which provides the feedback element value independently of both the device in use and the design frequency. It is the purpose of this paper to apply and demonstrate the reliability of a novel design technique (Boglione et al. [5]) which addresses those very points. After a brief summary of the theory in [5], the design and the test results of a BJT LNA at 1 GHz are presented and discussed.

THEORY AND DESIGN

Our technique [5] describes an analytical procedure for the design of the optimum noise source reflection coefficient $\Gamma_{S_{opt}}$ or its magnitude. This procedure is based on an analysis of feedback amplifiers (Boglione et al. [6]) which proves that the minimum noise figure of the device under test can be lowered at the expense of the gain. This is particularly true when devices such as MESFETs are considered. However, stability problems may arise at higher frequency. BJTs are well behaved in this respect but their noise performance is not as good. The procedure described in [5] is applied to the design of a SSNM BJT LNA at $f_o = 1$ GHz. The low noise BJT is a HP AT41486 as described in the data sheet [7] which is capable of achieving the required design specification $|\Gamma_{S_{opt}}| < 0.1$ at the DC bias given in the same data sheet The gain of the LNA is to be as large as possible along with good output return loss (better than 20 dB)

The input return loss is related to $\Gamma_{S_{opt}}$ by (Engberg [8])

$$\Gamma_{in}(\Gamma_L^{SSNM}) = \Gamma_{S_{opt}}^* \tag{1}$$

where Γ_{in} is the input reflection coefficient of the feedback BJT when loaded by the reflection coefficient Γ_L^{SSNM}. Therefore, a requirement on $|\Gamma_{S_{opt}}|$ is equivalent to an input return loss requirement with the proper choice of the load at f_o. According to the theory [5], no input matching circuit is required. Once the analytical design at f_o is completed, a computer optimisation is carried out in order to look into the frequency response of the LNA.

SIMULATION AND OPTIMISATION

The simulation over the range of frequencies where both the scattering and noise parameters are available is paired with the desired optimisation goals for the required band around f_o. The circuit layout is shown in Fig. 1. Starting from the input SMA connector (on the left hand side), the important parts are

- the input DC blocking capacitor and the input DC circuitry; the latter provides the base current I_b to the BJT and acts as a *damper* against possible frequency instability
- the series feedback, which consists of a short length of wire between the transistor leg and the ground plane of the Duroid 5880 substrate
- the RF output matching circuit, which consists of the 3 components (R_o, C_o and L_o) and achieves several goals: it provides the required Γ_L^{SSNM} along with high output return loss; the capacitor C_o separates the output SMA connector; L_o provides the DC path for I_c to flow to the transistor. A 120 pF capacitor is used in order to stop I_c from reaching the ground through R_o
- another frequency dependent branch between the output SMA connector and ground, which improves stability and aids in achieving a good output return loss

Lumped commercially available surface mounted components are used. Copper pads have been included in the simulation in order to provide for the surface mounted components. In order to obtain best accuracy from the optimisation, the pads have been modelled as transmission lines; each width has been made dependent on its own length so that the optimiser fulfills 3 constraints: 1) satisfy the condition length > width; 2) limit the ratio length–width within the model requirements; 3) ensure that the width is larger than the minimum width achievable on the substrate in use.

RESULTS

The frequency range 970–1100 MHz has been divided in 14 points for testing; both noise and signal performances have been measured at $V_{ce} = 8$ V and $I_c = 10$ mA [7]. The scattering parameters are compared with the simulated results in Fig. 2. The gain $|S_{21}|$ of the LNA is in good agreement with the simulation as well as $|S_{12}|$; the output return loss does not show the correct slope. The reason is associated with the fact that the device scattering and noise parameters of the device and the nominal values of the components have been taken for granted and they have not been measured. A yield analisys has been carried out on the simulator after allowing a maximum 20% variation for R_o and C_o; the inductance L_o is large enough to assume that its actual value does not affect the output matching circuit performance significantly. The analyis shows that for some values of those components, $|S_{22}|$ may have a different slope; the large difference between simulation and test for $|S_{11}|$ is related to the variations of the circuit components from their nominal values.

The 3rd order intercept point and the output power have been measured at the 1 dB compression point and found to be 17 dBm and at 3.4 dBm respectively.

The noise parameters have been measured with a de–embedding technique (Adamian and Uhlir [9], Alam et al. [10]) paired with a standard least squares fit (Lane [11], Escotte et al. [12]): they are shown in ig. 3. A tuner has been used to define and collect a set of 100 pairs of source reflection coefficients $\Gamma_S^{(i)}$ loading the LNA input port and measured noise powers $N_{meas}^{(i)}$ at each test frequency $f_{(j)}$ within the measurement band. The de-embedding procedure has been carried out on sub-sets of the data. The mismatches at the input $M_h^{(i)}$ and the output ports $M_{DUT}^{(i)}$ are taken into account when working out the noise figure $F_{DUT}^{(i)}$ of the LNA

$$F_{DUT}^{(i)} = \frac{1}{G_{DUT}^{(j)}} \left[1 + \frac{\left(N_{meas}^{(i)} - N_c^{(j)}\right) M_h^{(i)} \left(T_h^{(j)} - T_o\right)}{\left(N_h^{(j)} - N_c^{(j)}\right) T_o M_{DUT}^{(i)}} \right] \quad (2)$$

$N_{meas}^{(i)}$ is the power measured when the LNA amplifies noise from a load at ambient temperature at its input port. $N_c^{(j)}$ and $N_h^{(j)}$ represent the powers measured when calibrating the measurement setup with the a cold (T_o) and a hot ($T_h^{(j)}$) noise source respectively at each $f_{(j)}$; $G_{DUT}^{(j)}$ is the LNA available gain and is worked out from scattering parameters.

The extracted value for $|\Gamma_{S_{opt}}|$ has been consistently much better than -20 dB. The LNA minimum noise figure and the equivalent noise resistance are very close, respectively, to the value of F_{min} of the BJT and to $R_{n_{min}}$ [6] within the measurement errors; a small value of R_n makes the noise figure insensitive to the input mismatch (Friis [13]). The noise figure is very nearly equal to F_{min} since $\Gamma_{S_{opt}} \simeq \Gamma_S \simeq 0$.

In order to asses the errors associated with the derivation of the noise parameters, a random variation of the tested scattering parameters (±1.0 dB and ±5 deg), the noise powers (±1.0 dB) and the excess noise ratio of the noise source (±1.0 dB) has been applied to the measured data. The averaged values are based on de-embedding the LNA with (2) 1000 times at each frequency point. The results are typical of this type of measurement. Good scattering parameter measurement and large available gain ensure that the uncertainty on $F_{DUT}^{(i)}$ in (2) is kept small.

CONCLUSIONS

A novel technique has been applied to the design of a feedback BJT low noise amplifier. It demonstrates that an analytical approach in order to determine the starting value of the feedback element is feasible and the results are comparable to the simulation within the measurement uncertainty. The LNA noise figure is equal to the minimum noise figure of the active device within the test errors and good input and output return losses are achieved at the same time in the band of interest.

ACKNOWLEDGEMENT

This work is part of a Ph.D. project funded by Filtronic Comtek plc, UK, through the University of Leeds. We thank Tariq Alam, for providing the software to collect the data for the noise parameter measurements and Dr. Neil Roddis and Bill Harrop for measurements of signal performances and noise figure at the Nuffield Radio Astronomy Labs, United Kingdom.

References

[1] Guillermo Gonzalez, *Microwave Transistor Amplifiers: Analysis and Design*, Prentice Hall, 1984.

[2] Randall E. Lehmann and David D. Heston, "X band monolithic series feedback LNA", *IEEE Trans. on Microwave Theory and Techniques*, vol. MTT-33, No. 12, pp. 1560–1566, December 1985.

[3] Nobuo Shiga, Shigeru Nakajima, Kenji Otobe, Takeshi Sekiguchi, Nobuhiro Kuwata, Ken-ichiro Matsuzaki, and Hideki Hayashi, "X band MMIC amplifier with pulsed doped GaAs MESFETs", *IEEE Trans. on Microwave Theory and Techniques*, vol. MTT-39, No. 12, pp. 1987–1993, December 1991.

[4] Y. Tsukahara, S. Chaki, Y. Sasaki, K. Nakahara, N. Andoh, H. Mastubayasi, N. Tanino, and O. Ishihara, "A C-band 4-stage low noise miniaturised amplifier using lumped elements", *IEEE MTT-s International Symposium Digest*, vol. 3, pp. 1125–1128, Orlando, FL, 1995.

[5] Luciano Boglione, Roger D. Pollard, and Vasil Postoyalko, "Optimum noise source reflection coefficient design with feedback amplifiers", *IEEE Trans. on Microwave Theory and Techniques*, vol. 45 No. 3, pp. 402–407, March 1997.

[6] Luciano Boglione, Roger D. Pollard, and Vasil Postoyalko, "Analytical behaviour of the noise resistance and the noise conductance for a network with parallel and series feedback", *IEEE Trans. on Microwave Theory and Techniques*, vol. 45, No. 2, pp. 301–304, February 1997.

[7] Hewlett Packard Company, *Communication Components, Designer's Catalogue, GaAs and Silicon Products*, Hewlett Packard Company, Palo Alto, CA, 1993.

[8] Jackob Engberg, "Simultaneous input power match and noise optimisation using feedback", *4th European Microwave Conference Proc.*, pp. 385–389, Montreux, Switzerland, 1974.

[9] Vahev Adamian and Arthur Uhlir, "A novel procedure for receiver noise characterisation", *IEEE Trans. on Instrumentation and Measurements*, vol. IM-6, pp. 181–182, June 1973.

[10] Tariq Alam, Roger D. Pollard, and Christopher M. Snowden, "The determination of on-wafer noise parameters at W-band", *27th European Microwave Conference Proc.*, pp. –, Jerusalem, Israel, 8–12 September 1997.

[11] Richard Q. Lane, "The determination of device noise parameters", *Proc. IEEE*, vol. 57, pp. 1461–1462, August 1969.

[12] L. Escotte, R. Plana, and J. Graffeuil, "Evaluation of noise parameter extraction methods", *IEEE Trans. on Microwave Theory and Techniques*, vol. MTT-41, No. 3, pp. 382–387, March 1993.

[13] H. T. Friis, "Noise figure of radio receivers", *Proc. IRE*, vol. 32, pp. 419–422, July 1944.

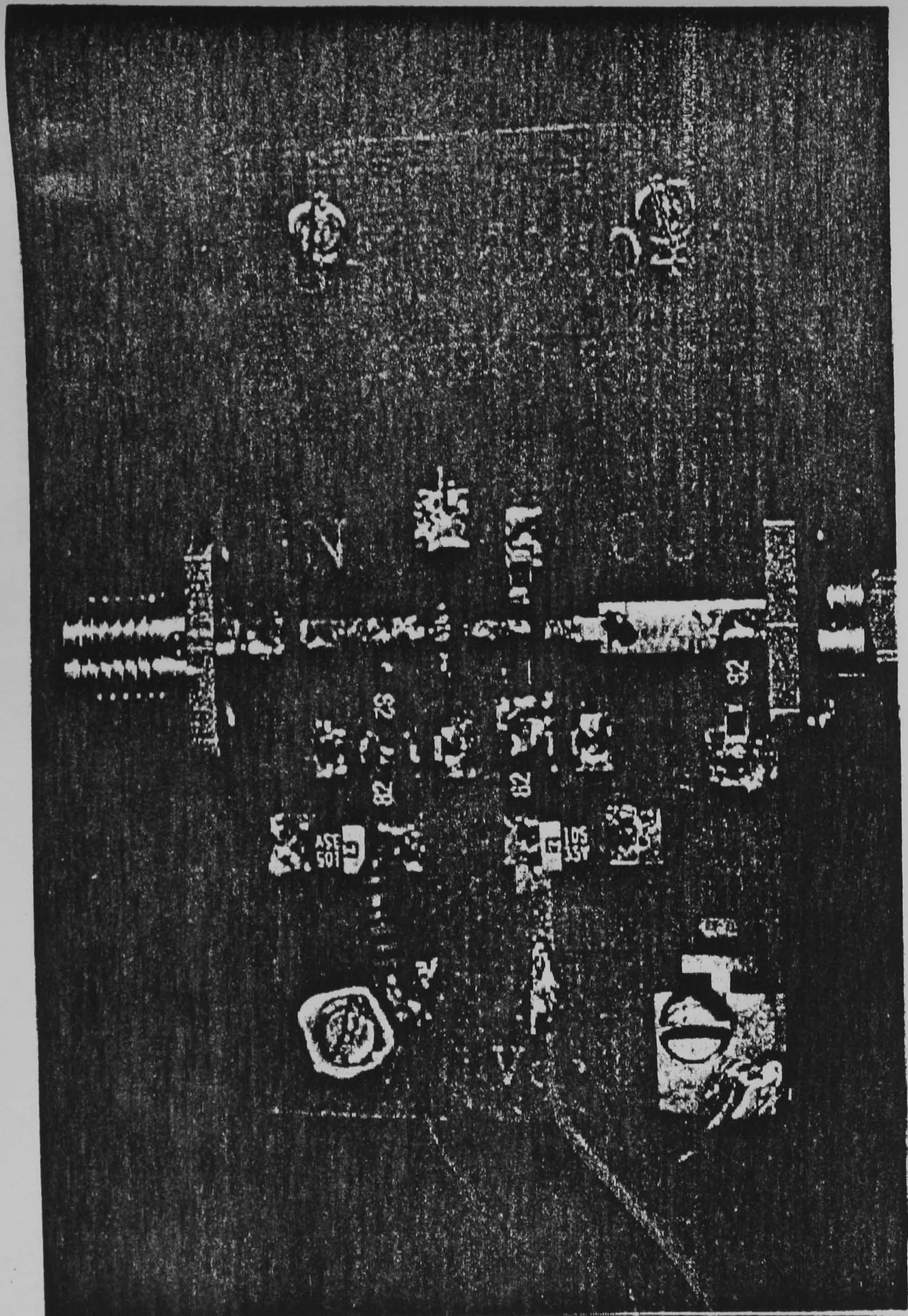

Figure 1: The final SSNM LNA circuit along with the DC circuitry; board dimension: 28×52 mm^2

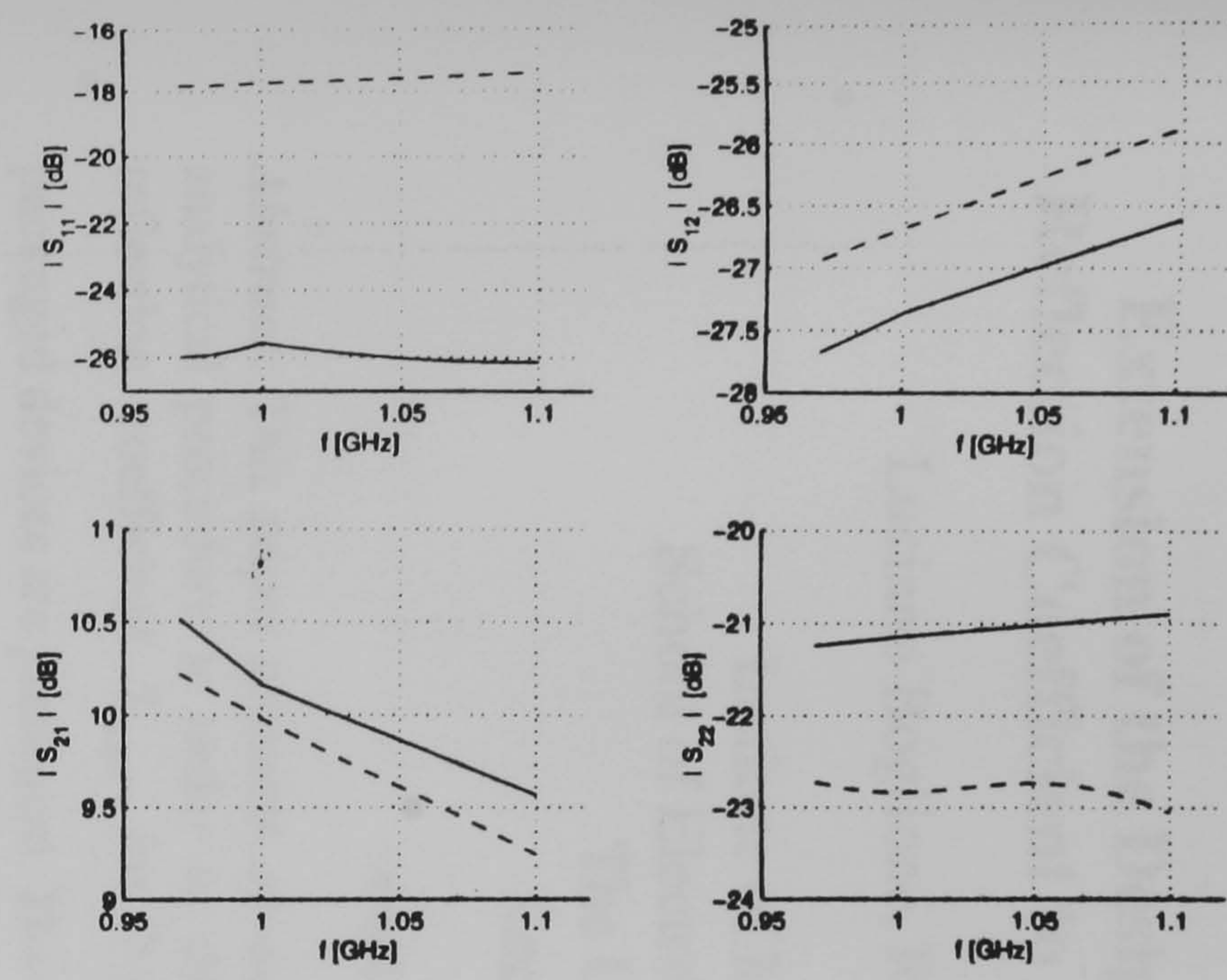

Figure 2: Measured (dashed line) and simulated (solid line) scattering parameters.

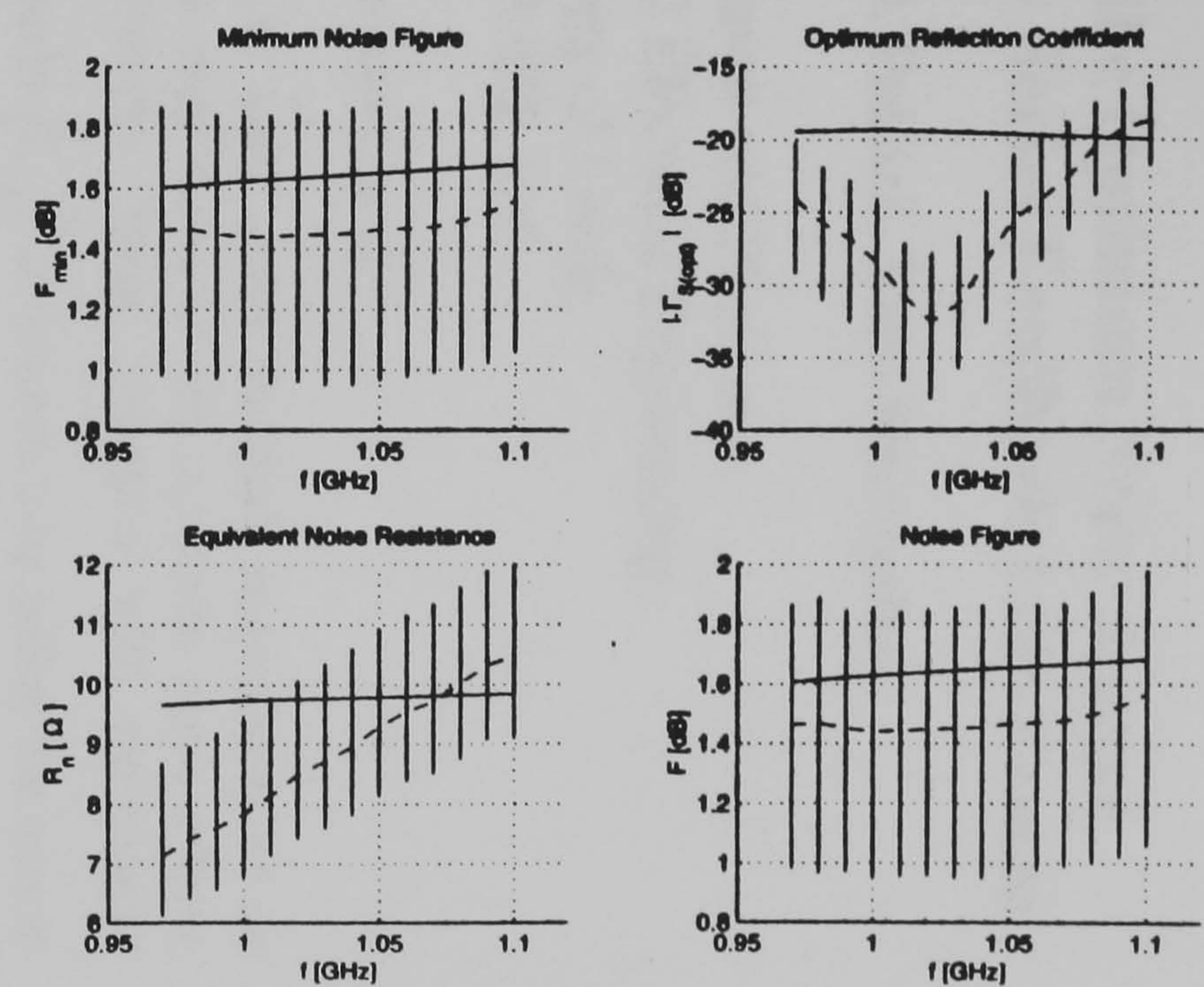

Figure 3: Measured (dashed line with associated error bars at each frequency) and simulated (solid line) noise performance; the goal is $|\Gamma_{S_{opt}}| < -20$ dB at $f_o = 1$ GHz.

1997 High Frequency Postgraduate Student Colloquium
19 September 1997, University of Leeds

Extension of the Design of the Optimum Noise Source Reflection Coefficient to Lossy Series Feedback Impedances

Luciano Boglione, Roger D. Pollard, Vasil Postoyalko

Institute of Microwaves and Photonics
School of Electronic and Electrical Engineering
The University of Leeds
Leeds LS2 9JT, UK

email: eenlb@sun.leeds.ac.uk

Abstract: This paper presents an extension to lossy series feedback impedances of an analytical procedure in order to design the magnitude of the optimum noise source reflection coefficient Γ_{Sopt} for 2-port networks. Some examples with microwave packaged devices are presented. The minimum in $|\Gamma_{Sopt}|$ is discussed by taking the loss of series feedback into account. Analytical design for $|\Gamma_{Sopt}|$ with a lossy series feedback impedance is still possible provided that the quality factor Q of the feedback is large enough. Q also affects the minimum noise figure $F_{\min}$ of the feedback network; however, a decrease in $F_{\min}$ relatively to the value of the active device in use, can still be achieved. The results improve the understanding of the feedback applied to microwave devices and they can be used to look into the noise performance of any type of microwave devices.

1. INTRODUCTION

Microwave series feedback amplifiers have been known to achieve very low noise performance [1], [2], [3]. Theoretical analysis has been carried out in the past [4], [5] but an analytical approach to series feedback is not used ordinarily [6], [7], [8]. More commonly, computer optimization is the main tool for the design of microwave networks.

Recently, a novel technique for the design of $|\Gamma_{Sopt}|$ for minimum noise figure using series impedance Z_S has been published [9]. There, it is shown that a lossless reactive impedance $Z_S = jX_S$ at the given frequency *f* satisfies the condition

$$|\Gamma_{Sopt}| \leq \varepsilon \tag{1}$$

if the required value ε is larger than the minimum value of $|\Gamma_{Sopt}|$; this minimum is a by-product of the design procedure itself.

0-7803-3151-6/97/$10.00©1997 IEEE

This paper extends the solution of (1) to lossy series feedback impedances $Z_S = R_S + jX_S$ and investigates the noise performance of the network by varying the loss of the feedback.

2. EXTENSION OF THE THEORY

The design for $|\Gamma_{Sopt}|$ [9] at a given frequency f requires solving

$$\sum_{n=0}^{4} c_n x^n = 0 \tag{2}$$

where the coefficients c_n depend on the noise parameters of the device in transmission matrix representation [10]; the unknown x is the lossless reactive feedback X_S normalized to a real impedance Z_o.

It is straightforward to extend (2) to the case of a lossy feedback by assigning the feedback a given quality factor

$$Q = \frac{X_S}{R_S} \tag{3}$$

and expressing the feedback impedance Z_S as

$$Z_S = \left(\frac{1}{Q} + j\right) X_S \tag{4}$$

Only the positive solutions X_S from (2) are considered in this paper.

According to (3), the quality factor is related to a loss represented by R_S; the loss is associated with a source of thermal noise [11], whose average power within a bandwidth $\Delta f << f$ at the ambient temperature T_o is

$$\overline{|v_S|^2} = 4kT_o R_S \Delta f \tag{5}$$

Equations (3) and (4) along with (5), define the signal and noise characteristics of the feedback branch. No noise correlation exists between the feedback impedance and the internal noise sources of the device [12]. The quality factor affects the coefficients c_n but the procedure outlined in [9] in order to get (2) remains the same.

3. RESULTS AND DISCUSSION

The solution of (2) after modifying the coefficients c_n has been applied to three Hewlett-Packard devices [13]: two MESFETs (ATF21186 and ATF10136) and one BJT (AT41486). The noise and scattering parameters have been taken from the data book;

the frequency at which the solution is sought, is 1 GHz for ATF21186 and AT41486, and 2 GHz for ATF10136. The required magnitude of Γ_{Sopt} is 0.1; this value ensures that a 20 dB input return loss may be obtained when a simultaneous noise and power match is delivered by properly choosing the load [4], [9]. The smallest value of Q has been selected in order to ensure that a solution for (2) exists. Figures 1, 3 and 5 show the locus of $|\Gamma_{Sopt}| \leq 0.1$ vs. the lossy feedback Z_S on the Γ_{Sopt} plane for some values of the quality factor Q.

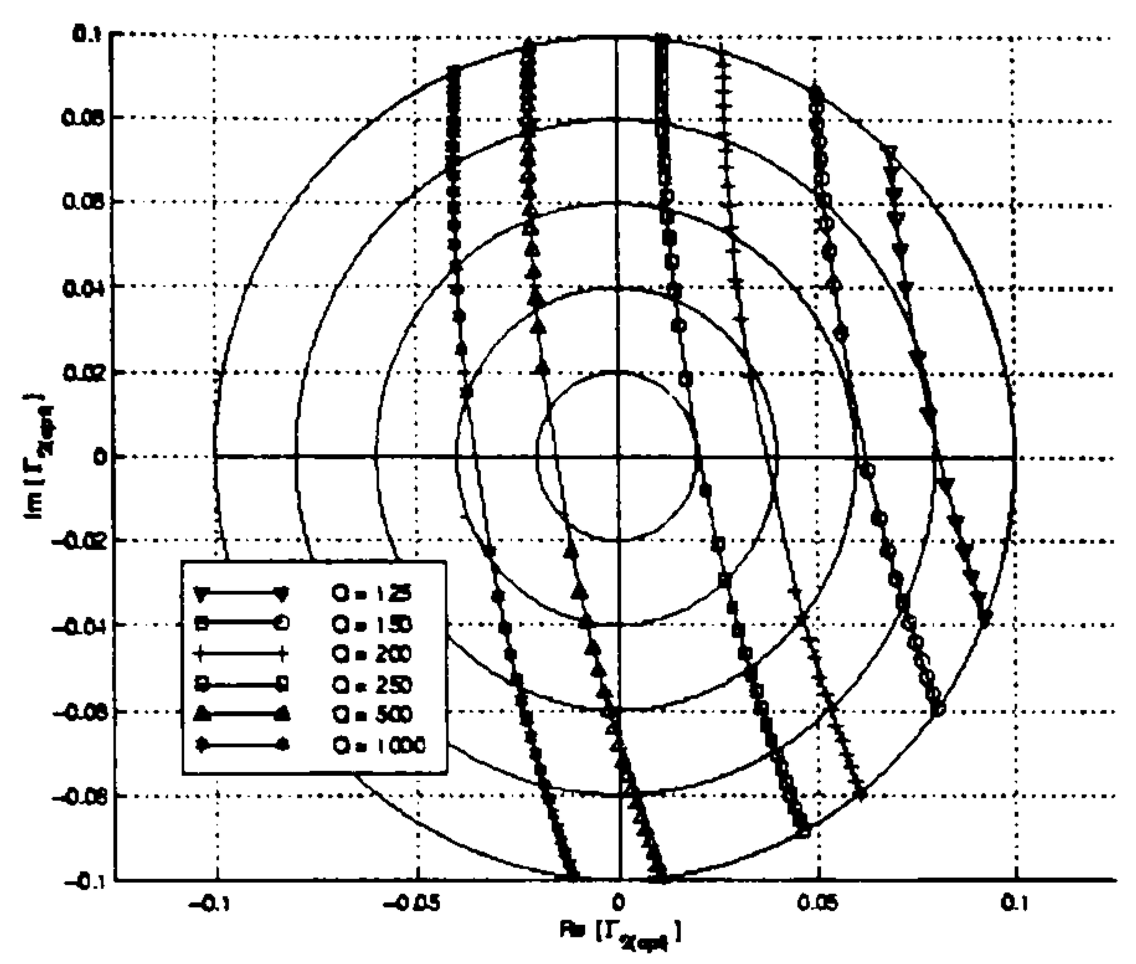

Figure 1: $|\Gamma_{Sopt}| \leq 0.1$ vs. series feedback X_S for different Q; for any curve, as X_S increases, the imaginary part of Γ_{Sopt} moves from positive to negative values. (Device: Hewlett Packard ATF21186 MESFET).

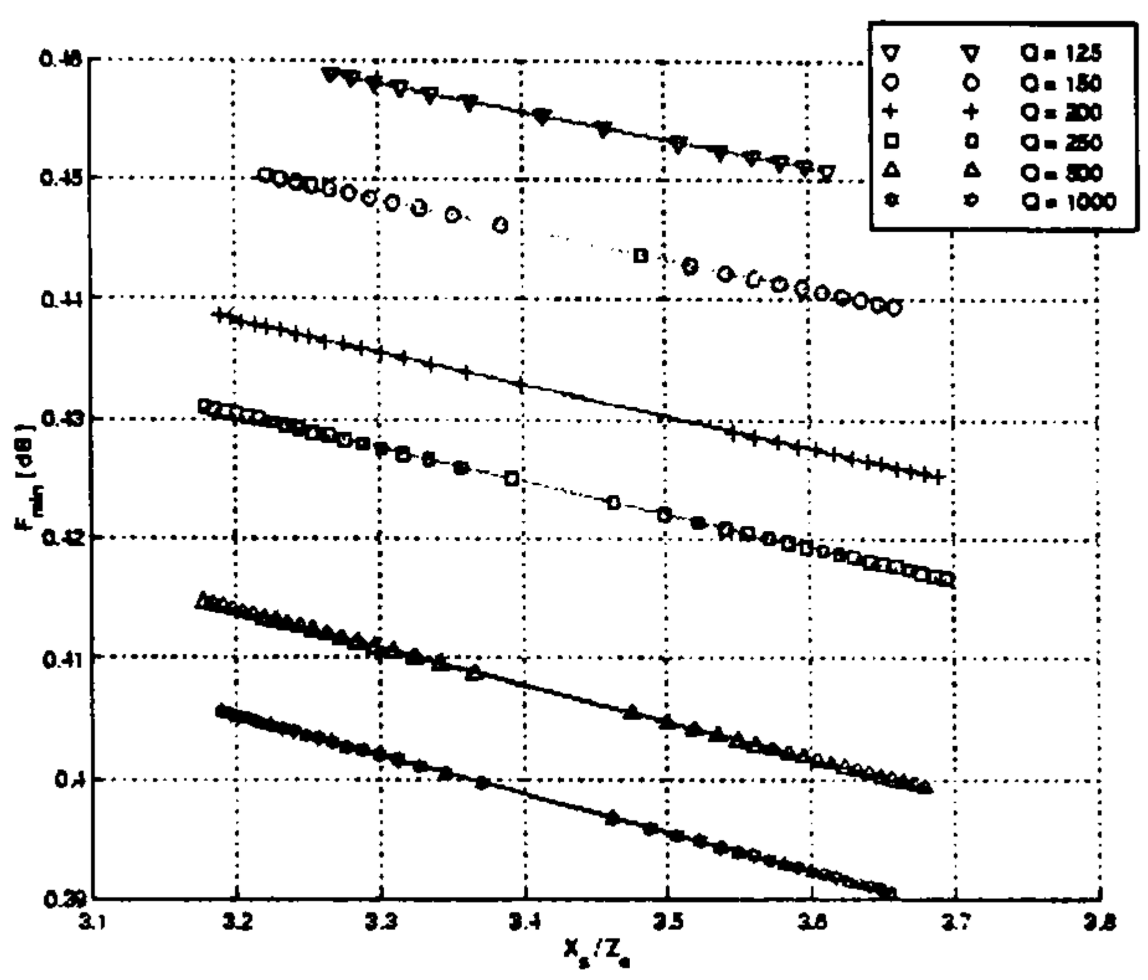

Figure 2: $F_{\min}$ vs. series feedback X_S/Z_o ($Z_o = 50\ \Omega$) for different Q. (Device: Hewlett Packard ATF21186 MESFET).

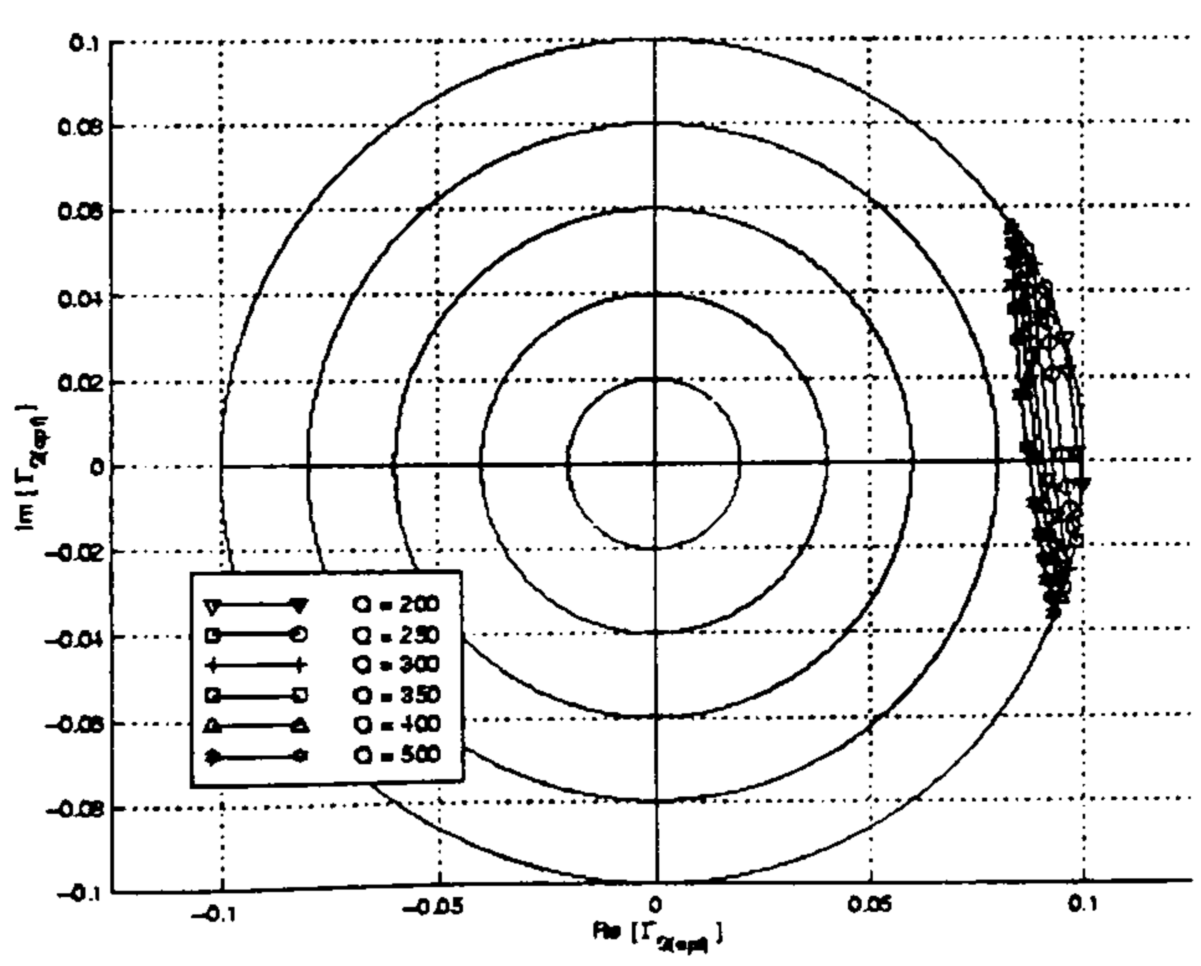

Figure 3: $|\Gamma_{Sopt}| \leq 0.1$ vs. series feedback X_S for different Q for any curve, as X_S increases, the imaginary part of Γ_{Sopt} moves from positive to negative values. (Device: Hewlett Packard ATF10136 MESFET).

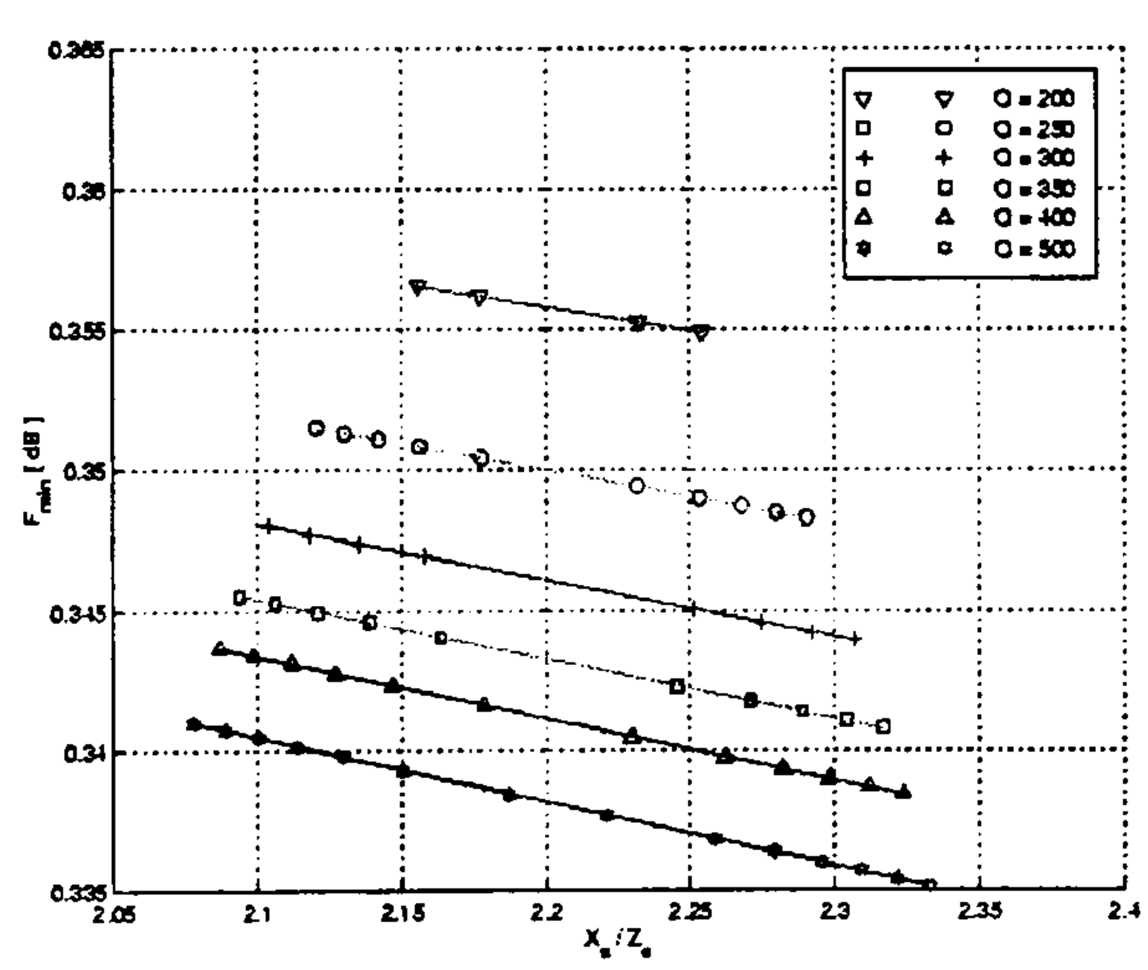

Figure 4: $F_{\min}$ vs. series feedback X_S/Z_o ($Z_o = 50\ \Omega$) for different Q. (Device: Hewlett Packard ATF10136 MESFET).

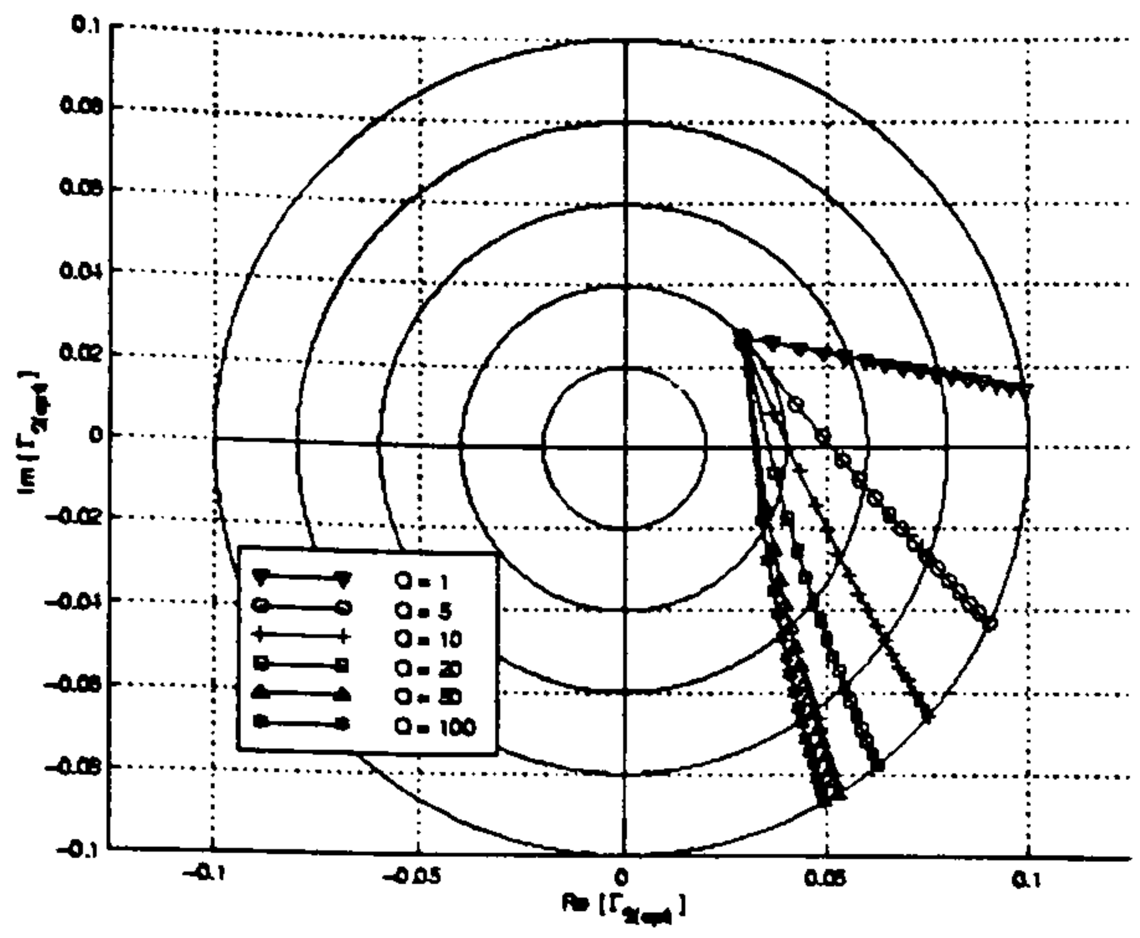

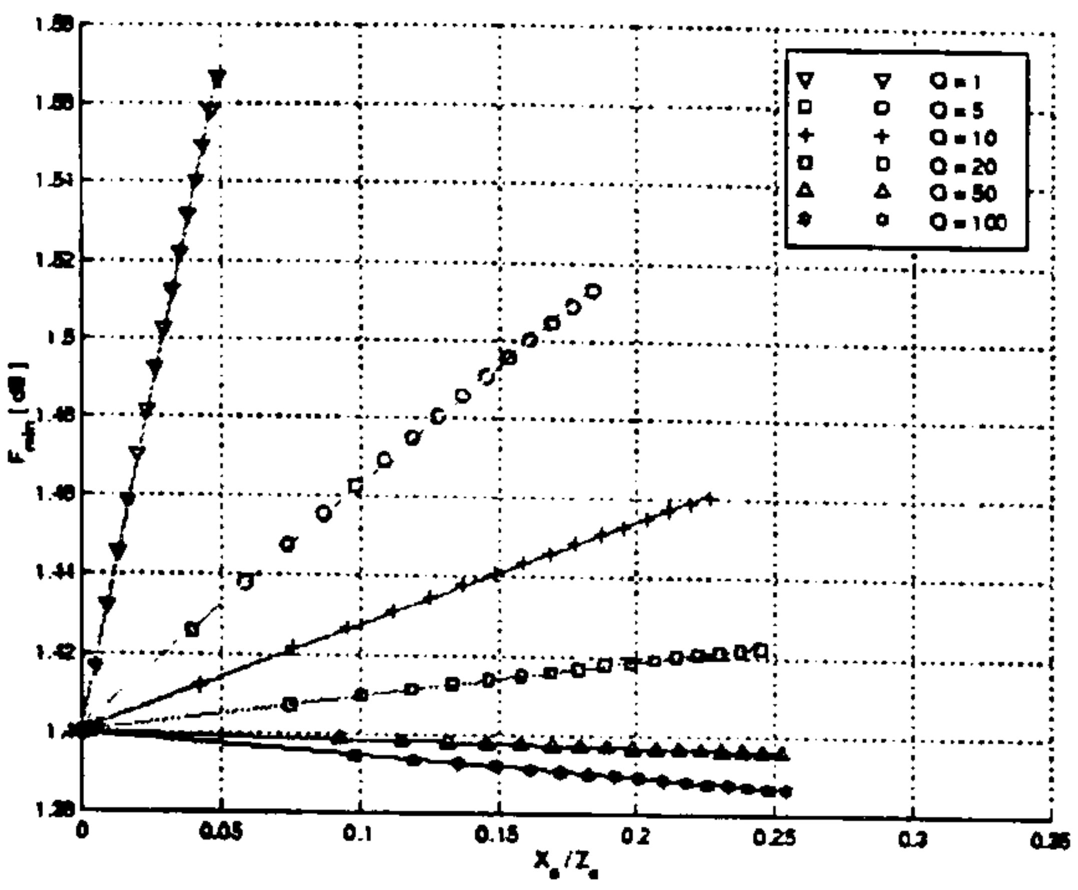

Figure 5: $|\Gamma_{Sopt}| \leq 0.1$ vs. series feedback X_S for different Q; for any curve, as X_S increases, the imaginary part of Γ_{Sopt} decreases. (Device: Hewlett Packard AT41486 BJT).

Figure 6: $F_{\min}$ vs. series feedback X_S/Z_o ($Z_o = 50\ \ \Omega$) for different Q. (Device: Hewlett Packard AT41486 BJT).

The figures demonstrate that similar devices such as the ATF21186 and ATF10136 MESFETs have different behaviours of Γ_{Sopt} vs. Z_S. Figures 1 and 3 point out that the minimum distance between the centre of the Γ_{Sopt} plane and each curve can be very different: for the ATF21186, a Q between 250 and 500 can make $\Gamma_{Sopt} = 0$; and for the ATF10136, a Q as high as 1000 still keeps the Γ_{Sopt} curve far from the centre. Figure 5 shows that very lossy feedback impedances can make $|\Gamma_{Sopt}|$ smaller than 0.1; however, this device without feedback ($Z_S = 0$) provides $|\Gamma_{Sopt}| \leq 0.1$ as is demonstrated by the intersection of every curve on the Γ_{Sopt} plane.

The issue now is to check whether the loss associated with Q can still improve $F_{\min}$, as a pure reactive feedback $Z_S = jX_S$ does because the noise measure remains constant [1], [14], [15]. Figures 2, 4 and 6 plot the minimum noise figure $F_{\min}$ of the feedback network vs. X_S for a constant Q. Their values without feedback for the ATF21186 and AT41486 at 1 GHz and for the ATF10136 at 2 GHz are respectively 0.55 dB, 1.40 dB and 0.40 dB. Figures 2 and 4 show that the minimum noise figure $F_{\min}$ decreases even if a loss is present. As far as the AT41486 BJT is concerned, Fig. 6 demonstrates that $F_{\min}$ can be lowered if Q is larger than ≈ 50; for very lossy feedback impedances ($Q < 50$), $F_{\min}$ increases as expected.

A common feature of Figures 2, 4 and 6 is that $F_{\min}$ in dB is linearly dependent on the lossy feedback. Tables 1, 2 and 3 collect the resulting coefficient p and q when a least squares fit with $y = px + q$ is carried out on the simulated points of each figures. The term p expresses the improvement on $F_{\min}$ in dB for a unit change in the normalized feedback $x = X_S/Z_o$ ($Z_o = 50\ \ \Omega$) for a given quality factor Q.

Q	p dB·Ω	q dB
125	-0.0234	0.5354
150	-0.0248	0.5300
200	-0.0266	0.5234
250	-0.0278	0.5195
500	-0.0306	0.5119
1000	-0.0322	0.5084

Table 1: Least squares fit with $y = px + q$ of $F_{\min}$ in dB vs. series feedback $x = X_S/Z_o$, where $Z_o = 50\ \Omega$. (Device: Hewlett Packard ATF21186 MESFET).

Q	p dB·Ω	q dB
200	-0.0167	0.3925
250	-0.0188	0.3913
300	-0.0202	0.3904
350	-0.0212	0.3899
400	-0.0219	0.3894
500	-0.0230	0.3888

Table 2: Least squares fit with $y = px + q$ of $F_{\min}$ in dB vs. series feedback $x = X_S/Z_o$, where $Z_o = 50\ \Omega$. (Device: Hewlett Packard ATF10136 MESFET).

Q	p dB·Ω	q dB
1	3.3979	1.4023
5	0.6104	1.4019
10	0.2682	1.4006
20	0.0916	1.4002
50	-0.0169	1.4000
100	-0.0536	1.4000

Table 3: Least squares fit with $y = px + q$ of $F_{\min}$ in dB vs. series feedback $x = X_S/Z_o$, where $Z_o = 50\ \Omega$. (Device: Hewlett Packard AT41486 BJT).

4. CONCLUSIONS

The extension of the design for the optimum source reflection coefficient Γ_{Sopt} to lossy series feedback impedances Z_S has been presented. The issue of minimum $|\Gamma_{Sopt}|$ has been addressed and it has been pointed out that similar devices may show very different behaviours. It has also been shown that the loss in Z_S can reduce the minimum noise figure as expected with lossless reactive feedback X_S; however, the quality factor Q must be large enough. The design for $|\Gamma_{Sopt}|$ can improve if the quality factor Q and the reactive part of the feedback Z_S could be expressed in terms of a common feature, such as the number of turns when dealing with inductors. The analysis can be applied to MMICs, packaged or chip devices and it is not limited by frequency constraints.

5. ACKNOWLEDGEMENTS

This work is part of a Ph.D. project funded by Filtronic Comtek plc, UK, through the University of Leeds.

REFERENCES

[1] Randall E. Lehmann and David D. Heston, "X band monolithic series feedback LNA", *IEEE Trans. on Microwave Theory and Techniques*, vol. 33, No. 12, pp. 1560-1566, December 1985.

[2] Nobuo Shiga, Shigeru Nakajima, Kenji Otobe, Takeshi Sekiguchi, Nobuhiro Kuwata, Ken-ichiro Matsuzaki and Hideki Hayashi, "X band MMIC amplifier with pulsed doped GaAs MESFETs", *IEEE Trans. on Microwave Theory and Techniques*, vol. 39, No. 12, pp. 1987-1993, December 1991.

[3] Y. Tsukahara, S. Chaki, Y. Sasaki, K. Nakahara, N. Andoh, H. Mastubayasi, N. Tanino and O. Ishihara, "A C-band 4-stage low noise miniaturised amplifier using lumped elements", *IEEE S International Symposium Digest*, vol. 3, pp. 1125-1128, Orlando, FL, 1995.

[4] Jackob Engberg, "Simultaneous input power match and noise optimisation using feedback", *4th European Microwave Conference Proc.*, pp. 385-389, Montreux, Switzerland, 1974.

[5] Les Besser, "Stability considerations of low noise transistor amplifiers with simultaneous noise and power match", *IEEE S International Symposium Digest*, pp. 327-329, Palo Alto, CA, May 12-14, 1975.

[6] A. Anastassiou and M. J. O. Strutt, "Effect of the source lead impedance on the noise figure of a GaAs FET", *Proc. IEEE*, vol. 62, pp. 406-408, March 1974.

[7] Svein Iversen, "Comments on 'Effect of the source lead impedance on the noise figure of a GaAs FET'", *Proc. IEEE*, vol. 63, No. 6, pp. 983-984, June 1975.

[8] Svein Iversen, "The effect of feedback on noise figure", *Proc. IEEE*, vol. 63, pp. 540-542, March 1975.

[9] Luciano Boglione, Roger D. Pollard, and Vasil Postoyalko, "Optimum noise source reflection coefficient design with feedback amplifiers", *IEEE Trans. on Microwave Theory and Techniques*, vol. 45, No. 3, pp. 402-407, March 1997.

[10] Herbert Hillbrand and Peter H. Russer, "An efficient method for computer aided noise analysis of linear amplifier networks", *IEEE Trans. on Circuits and Systems*, vol. CAS-23, No. 4, pp. 235-238, April 1976.

[11] H. Nyquist, "Thermal agitation of electric charge in conductors", *Physical Review*, vol. 32, pp. 110-113, July 1928.

[12] H. Rothe and W. Dalke, "Theory of noise four poles", *Proc. IRE*, vol. 44-I, pp. 811-818, June 1956.

[13] Hewlett Packard Company, *Communication Components, Designer's Catalogue, GaAs and Silicon Products*, Hewlett Packard Company, Palo Alto, CA, 1993.

[14] H. A. Haus and R. B. Adler, "Optimum noise performance of linear amplifiers", *Proc. of IRE*, vol. 46, August 1958.

[15] Hatsuaki Fukui, "Available power gain, noise figure and noise measure of two ports and their graphical representation", *IEEE Trans. on Circuit Theory*, vol. CT-13, No. 2, pp. 137-142, June 1966.

The Pospieszalski Noise Model and the Imaginary Part of the Optimum Noise Source Impedance of Extrinsic or Packaged FET's

Luciano Boglione, *Student Member, IEEE*, Roger D. Pollard, *Fellow, IEEE*, and Vasil Postoyalko, *Member, IEEE*

Abstract— **The imaginary part $X_{S_{opt}}$ of the optimum noise impedance for extrinsic or packaged devices is investigated. The analysis modifies the well-known Pospieszalski noise model by applying a series feedback to the source port. A simple expression for $X_{S_{opt}}$ is developed and is verified for extrinsic and packaged devices with a decreasing level of accuracy. The results give further insights into the way the parasitic inductors L_g and L_s affect the noise performance of the transistor and can help to design low-noise amplifier with simultaneous signal and noise power match at the input port.**

Index Terms—**Amplifier noise, circuit modeling, feedback circuits, microwave FET amplifiers, semiconductor device noise.**

I. Introduction

In 1989, Pospieszalski [1] proposed a simple noise model for active devices such as MESFET's or HEMT's. Many researchers have granted experimental validity to this model throughout the years [2]–[4]. Hughes based on it an extensive investigation of the HEMT's noise behavior and proved that the noise figure can be predicted easily [5]. He also applied this model to a wide range of previously published devices [3] and showed that the noise equivalent temperature T_{ds} of the drain-source resistance ranges around 500 K for the extrinsic device while the intrinsic device can be modeled similarly with T_{ds} around 2000 K.

The Pospieszalski model has been applied to extrinsic devices because of its simplicity. However, this causes the model to fail to predict other noise parameters when considering extrinsic or packaged devices. This paper proposes a simple change in the Pospieszalski noise model as Hughes applied it in [3] in order to explain the behavior of $X_{S_{opt}}$.

II. Analysis

The Pospieszalski noise model of the intrinsic device can easily be described with a H matrix because the noise sources T_{gs} and T_{ds} associated with R_{gs} and R_{ds}, respectively, are uncorrelated [1], [6]. In order to improve the model when it is applied to either extrinsic [3] or packaged devices [7], a feedback element is added—the lossy source inductance L_s (Fig. 1). The circuit model is now a feedback network and can be easily analyzed as a particular case of [8]: the parallel feedback admittance is set to zero and the series feedback impedance is $Z_s = R_s + jX_s$ where $X_s = j\,2\pi f L_s$ and $R_s = \Re e[Z_s]$ is source of thermal noise. After transforming the **H** representation into its **T** matrix representation and developing the noise parameters R_n, g_n, and ρ_n as functions of the model components, the optimum noise impedance $Z_{S_{opt}}$ can be obtained. The final expression for $X_{S_{opt}}$ is

$$\frac{X_{S_{opt}}}{Z_o} = \frac{f_t}{f}\,\frac{x^{(e)}_{S_{opt}} + \Delta x_n}{1 + \Delta x_d} \tag{1}$$

where

$$x^{(e)}_{S_{opt}} = \frac{1}{g_m Z_o} - \frac{f}{f_t} x_s$$
$$\Delta x_n = \frac{1}{T_{ds_o}}\left(1 + \frac{1}{g_m Z_o r_{ds}}\,\frac{x_s}{Q_s}\right)$$
$$\Delta x_d = \frac{1}{r_{ds} T_{ds_o}}\,\frac{x_s}{Q_s}.$$

There, $Q_s = \Im m[Z_s]/\Re e[Z_s]$ is the Q of the inductor, $f_t = g_m/(2\pi C_{gs})$ is the frequency where the short circuit gain is unity, $x_s = X_s/Z_o$ is the reactive series feedback value normalized to the characteristic impedance Z_o, and $r_{ds} = R_{ds}/Z_o$, $T_{ds_o} = T_{ds}/T_o$, $T_o = 290$ K are normalized values of elements of the model in Fig. 1. Notice that R_{gs} does not appear in (1). The remaining noise parameters can be worked out similarly but their expansions give rise to much more involved expressions [1].

At the frequency $f = \omega/(2\pi)$, (1) can be simplified to

$$X_{S_{opt}} \simeq \frac{1}{\omega C_{gs}} - \omega L_s \tag{2}$$

if

$$\begin{cases} \Delta x_n & < x^{(e)}_{S_{opt}} \\ \Delta x_d & < 1 \end{cases}$$

is verified. This approximation is a very simple expression whose implications are now developed.

III. Validation

Expression (2) is dependent only on C_{gs} and L_s at the frequency $\omega/(2\pi)$ for the case of either a lossy or a lossless inductor L_s. The result is valid for this model as long as T_{ds} and R_{ds} are large; the exact value of T_{ds} is not really important for the determination of $X_{S_{opt}}$. Hughes has proved that this

Manuscript received March 17, 1997. This work was sponsored by Filtronic Comtek plc.

The authors are with the School of Electronic & Electrical Engineering, Institute of Microwaves and Photonics, The University of Leeds, Leeds LS2 9JT, U.K.

Publisher Item Identifier S 1051-8207(97)06172-2.

TABLE I
COMPARISON BETWEEN MODELS CITED IN [3] WITH $T_{ds} = 2000$ K. EVERY MODEL HAS BEEN EVALUATED AT THE TOP END OF ITS FREQUENCY RANGE. C_{gs}, L_s, L_g, AND R_s ARE THE VALUES AS GIVEN IN EACH REFERENCE

Reference	Range GHz	R_s Ω	C_{gs} fF	L_s pH	L_g pH	f_{max}/f_t	$\Delta x_n / x^{(e)}_{S_{opt}}$	Δx_d $\times 10^{-5}$	C_{opt} fF	L_{opt} pH
[2]	4–18	0.70	224	6.59	42.4	0.4160	0.4631	1.348	259.90	46.78
[9] (FET)	11–13	1.67	300	0	0	0.8168	0.2242	1.422	314.20	0.37
[9] (HEMT)	11–13	3.37	250	0	0	0.3713	0.4118	4.017	259.90	0.64
[16]	40–60	2.20	76	25	10	0.9550	0.3071	1.380	93.85	31.28
[17]	2–18	3.50	270	23	340	0.3563	0.6963	5.006	248.90	362.00
[18]	2–18	3.20	240	30	50	0.6169	0.3626	2.861	239.40	84.59
[19]	12–25	2.98	127	38.6	147	0.9684	0.1751	0.955	129.30	183.80
[20]	1–25.5	2.72	96.4	5	51.6	0.1236	0.9478	9.646	79.51	53.50

is true for T_{ds} [3]. R_{ds} is usually in the range of hundreds of ohms.

In order to validate (2), some references used in [3] have been analyzed (Table I). The references provide a complete list of the values of the components. It is worth pointing out that these models as presented in those papers have been optimized for matching the measured S parameters in a given frequency range. As Hughes highlighted, noise figure and associated gain are often the only published quantities available for characterizing the noise performance. Table I has been developed according to this procedure. The room temperature has been assumed to be $T_{room} = 298$ K; the input resistance R_{gs} has an equivalent noise temperature $T_{gs} = T_{room}$ for quite a large spread of the drain current I_{ds} [2]; the equivalent noise temperature T_{ds} of the output resistance R_{ds} has been set to $T_{ds} = 2000$ K, as [3] suggests. In [2] (not cited in [3]), the simulation has been carried out with $T_{ds} = 2550$ K but the results in Table I for $x^{(e)}_{S_{opt}}/\Delta x_n$ and Δx_d refer to $T_{ds} = 2000$ K. The value $T_{ds} = 2000$ K has been chosen for the analysis because the topology of the device models is available and R_{ds} is therefore part of the intrinsic device embedded within the external components. Reference [9] outlines one MESFET model and one HEMT model; they consist of resistive and capacitive elements only.

The frequency dependence of the optimum noise reactance has been approximated with a least squares fit for each reference of Table I with an expression similar to (2)

$$X^{(i)}_{S_{opt}} = \frac{1}{\omega_i}\frac{1}{C_{opt}} - \omega_i L_{opt}. \tag{3}$$

The models provided by the references of Table I have been used to determine $X^{(i)}_{S_{opt}}$ for each angular frequency ω_i with a circuit simulator; the frequency range $(\omega_i, i = 1 \ldots N)$ varies according to the published reference (Table I). The least squares fit (3) has been applied to packaged devices [10] with some considerable degree of agreement (Fig. 2).

Equation (3) proves that

1) the expression (2) fits the data of the device circuit model;
2) a simple Pospieszalski noise model with feedback can successfully be applied to simulate $X_{S_{opt}}$ of extrinsic or packaged devices.

By comparing the values for C_{opt} and L_{opt} to C_{gs} and L_s respectively (Table I), it is clear that $C_{opt} \simeq C_{gs}$ while the inductance $L_{opt} \neq L_s$. Others [11] have confirmed that the Pospieszalki noise model for the intrinsic device provides $X_{S_{opt}} = 1/(\omega C_{gs})$. In fact, for the Pospieszalki noise model (intrinsic), $X_{S_{opt}} = -\Im\mathrm{m}[Z_{in}]$ where $Z_{in} = R_{gs} + 1/(j\omega C_{gs})$ is the input impedance. This observation suggests that if a series inductor L_g is connected between the source and the gate input, then $-X_{S_{opt}} = \Im\mathrm{m}[Z_{in}] = \omega L_g - 1/(\omega C_{gs})$ or more generally as a first approximation, that $-X_{S_{opt}}$ is the sum of the reactive components through which the current from the input port flows (Fig. 3). Therefore, (2) is modified

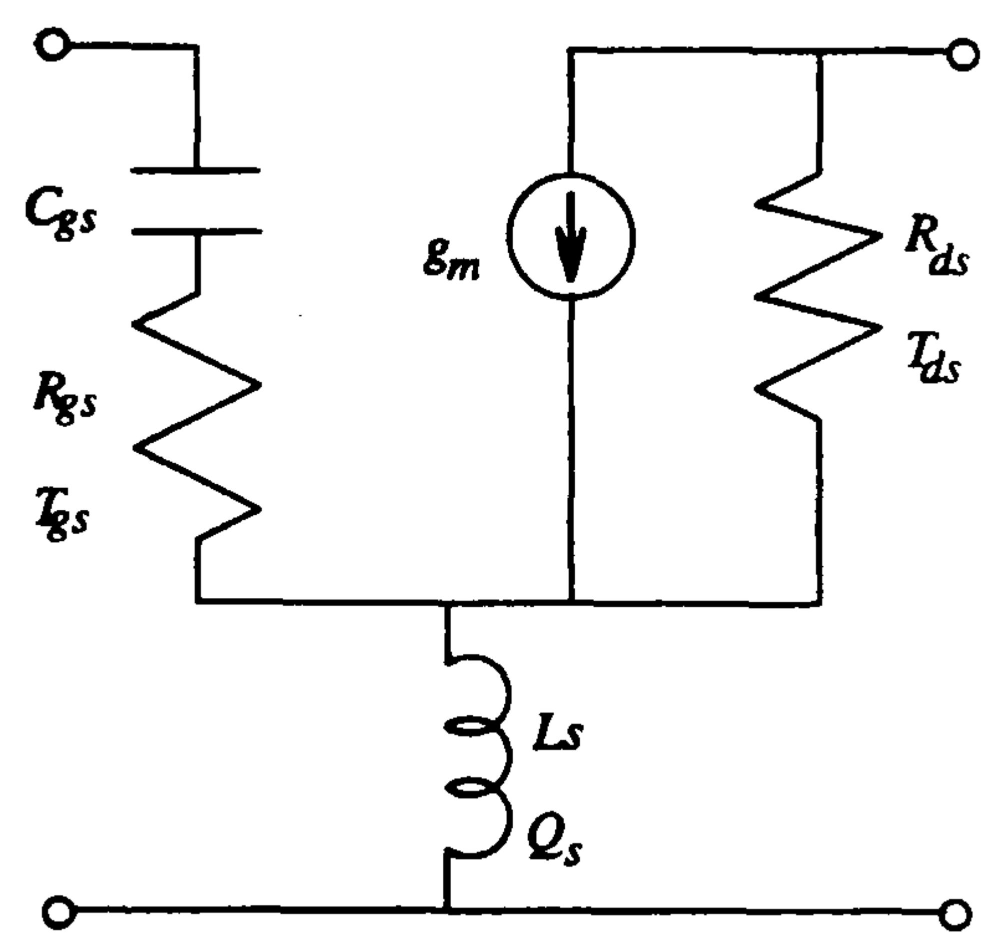

Fig. 1. Noise model for extrinsic or packaged devices. The feedback is a source of thermal noise if Q_s is specified.

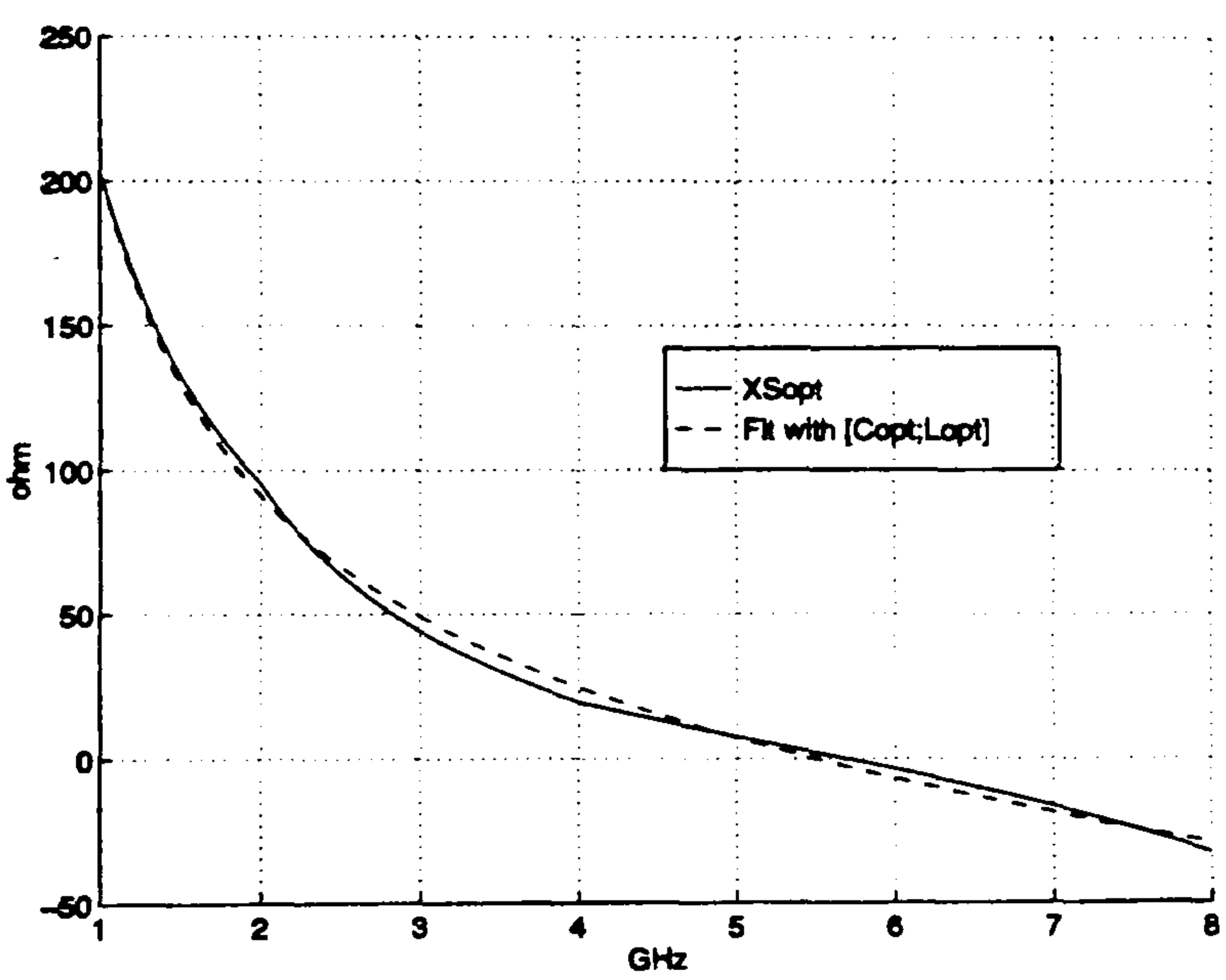

Fig. 2. Comparison between (3) and the simulated $X_{S_{opt}}$ for Hewlett-Packard ATF10136.

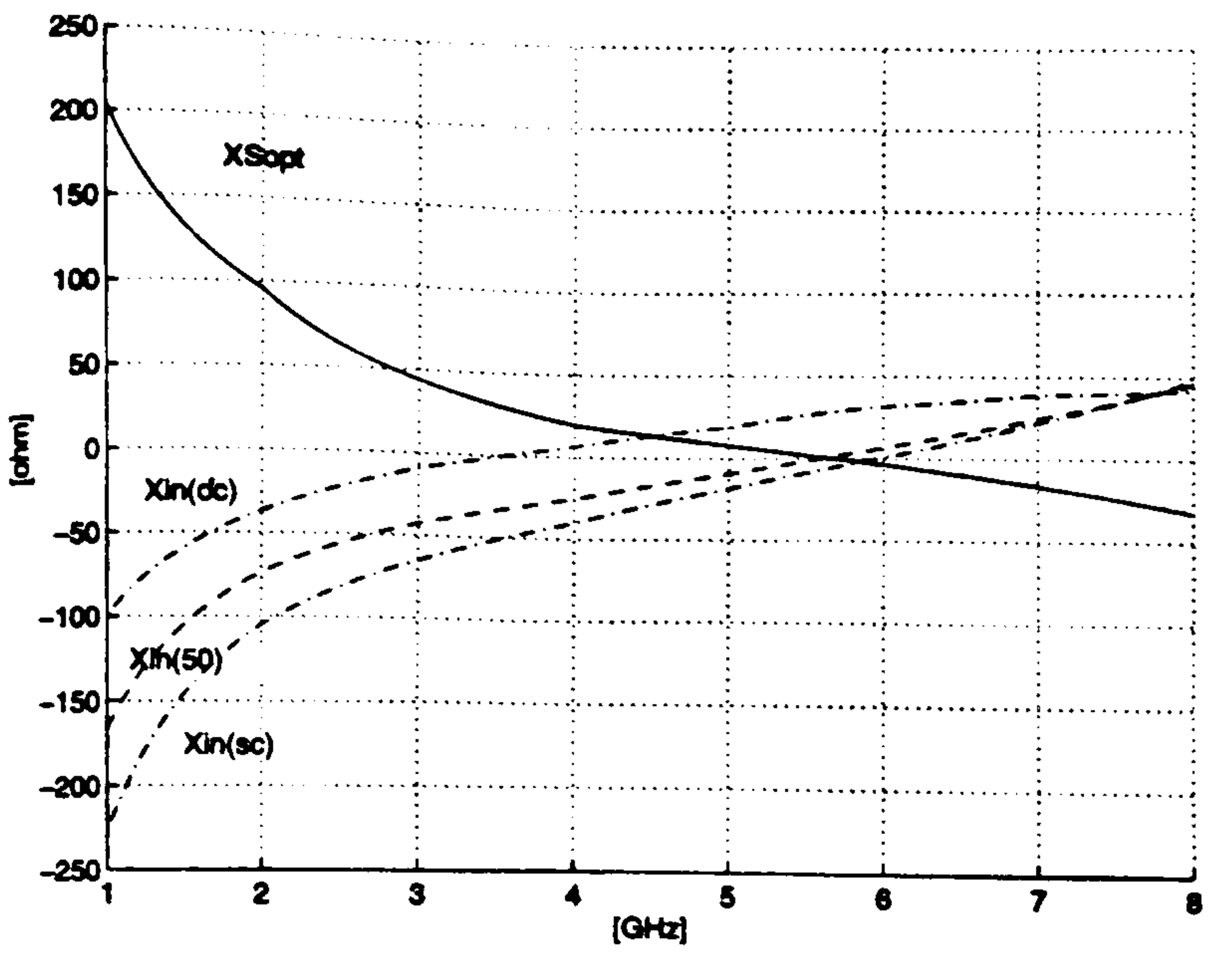

Fig. 3. Simulated imaginary part of $Z_{S_{\rm opt}}$ and $Z_{\rm in}$ for Hewlett-Packard ATF10136 when the output port is terminated by an open circuit (oc). $Z_0 = 50\,\Omega$ (50) or a short circuit (sc).

accordingly:

$$X_{S_{\rm opt}} \simeq \frac{1}{\omega C_{\rm gs}} - \omega(L_s + L_g) \qquad (4)$$

Table I shows that excellent agreement is achieved.

Equation (4) improves the understanding on how parasitic inductances affect the noise performance of the device [12], [13]. L_g is not in the feedback branch and will not have the same effects on device performance as L_s [14], [15]. The two inductors L_g and L_s give the designer the freedom to set $X_{S_{\rm opt}} = 0$ at the frequency where $R_{S_{\rm opt}} = 50\ \Omega$. Explicit equations for $R_{S_{\rm opt}}$ and $X_{S_{\rm opt}}$ allow the designer of either monolithic microwave integrated circuit (MMIC) or surface mounted low-noise amplifiers (LNA's) to determine, at a given frequency, the values of external inductors that provide $R_{S_{\rm opt}} = 50\ \Omega$ and $X_{S_{\rm opt}} = 0$. The MMIC designer has one more degree of freedom because of the ability to control $C_{\rm gs}$.

IV. Conclusion

A simple equation explains the behavior of the imaginary part of the optimum source impedance for minimum noise figure $Z_{S_{\rm opt}}$ of extrinsic or packaged transistors. The result is shown to be consistent with different circuit models previously published and it is based on the widely accepted Pospieszalski noise model. The expression confirms that the Pospieszalski noise model developed for intrinsic devices is well suited for extrinsic as well as packaged transistor for a quick investigation of their noise performance and for design purposes.

References

[1] M. W. Pospieszalski, "Modeling of noise parameters of MESFET's and MODFET's and their frequency and temperature dependence," *IEEE Trans. Microwave Theory Tech.*, vol. 37, pp. 1340–1350, Sept. 1989.

[2] M. W. Pospieszalski and A. C. Niedzwiecki, "FET noise model and on-wafer measurement of noise parameters," in *IEEE MTT-S Int. Symp. Dig.*, Boston, MA, June 10–14, 1991, pp. 1117–1120.

[3] B. Hughes, "A temperature noise model for extrinsic FET's," *IEEE Trans. Microwave Theory Tech.*, vol. 40, pp. 1821–1831, Sept. 1992.

[4] B. Hughes, J. Perdomo, and H. Kondoh, "12 GHz low-noise MMIC amplifier designed with a noise model that scales with MODFET size and bias," *IEEE Trans. Microwave Theory Tech.*, vol. 41, pp. 2311–2316, Dec. 1993.

[5] B. Hughes, "A linear dependence of $f_{\rm min}$ of frequency for FET's," *IEEE Trans. Microwave Theory Tech.*, vol. 41, pp. 979–981, June/July 1993.

[6] H. Hillbrand and P. H. Russer, "An efficient method for computer aided noise analysis of linear amplifier networks," *IEEE Trans. Circuits Syst.*, vol. CAS-23, pp. 235–238, Apr. 1976.

[7] A. Caddemi, A. Di Paola, and M. Sannino, "Microwave noise parameters of HEMT's vs. temperature by a simplified measurement procedure," in *Proc. 1996 High Performance Electron Devices for Microwave and Optoelectronic Applications—EDMO*, Leeds, U.K., Nov. 25–26, 1996, pp. 153–157.

[8] L. Boglione, R. D. Pollard, and V. Postoyalko, "Analytical behavior of the noise resistance and the noise conductance for a network with parallel and series feedback," *IEEE Trans. Microwave Theory Tech.*, vol. 45, pp. 301–304, Feb. 1997.

[9] K. Tanaka, M. Ogawa, K. Togashi, H. Takakuwa, H. Ohke, M. Kanazawa, Y. Kato, and S. Watanabe, "Low-noise HEMT using MOCVD," *IEEE Trans. Microwave Theory Tech.*, vol. MTT-34, pp. 1522–1527, Dec. 1986.

[10] *Communication Components, Designer's Catalogue, GaAs and Silicon Products*, Hewlett-Packard Company, Palo Alto, CA, 1993.

[11] P. J. Tasker, W. Reinert, B. Hughes, J. Braunstein, and M. Schlechtweg, "Transistor noise parameter extraction using a 50 ohm measurement system," in *IEEE MTT-S Int. Symp. Dig.*, Atlanta, GA, 1993, pp. 1251–1254.

[12] J. Engberg, "Simultaneous input power match and noise optimization using feedback," in *4th European Microwave Conf. Proc.*, Montreux, Switzerland, 1974, pp. 385–389.

[13] L. Besser, "Stability considerations of low noise transistor amplifiers with simultaneous noise and power match," in *IEEE MTT-S Int. Symp. Dig.*, Palo Alto, CA, May 12–14, 1975, pp. 327–329.

[14] R. E. Lehmann and D. D. Heston, "X band monolithic series feedback LNA," *IEEE Trans. Microwave Theory Tech.*, vol. MTT-33, pp. 1560–1566, Dec. 1985.

[15] N. Shiga, S. Nakajima, K. Otobe, T. Sekiguchi, N. Kuwata, K.-I. Matsuzaki, and H. Hayashi, "X band MMIC amplifier with pulsed doped GaAs MESFET's," *IEEE Trans. Microwave Theory Tech.*, vol. 39, pp. 1987–1993, Dec. 1991.

[16] N. Camilleri, P. Chye, A. Lee, and P. Gregory, "Monolithic 40 to 60 GHz LNA," in *IEEE MTT-S Int. Symp. Dig.*, Dallas, TX, May 8–10, 1990, pp. 599–602.

[17] P. C. Chao, S. C. Palmateer, P. M. Smith, U. K. Mishra, K. H. G. Duh, and J. C. M. Hwang, "Millimeter-wave low-noise high electron mobility transistor," *IEEE Electron Device Lett.*, vol. 6, pp. 531–533, Oct. 1985.

[18] H. Hida, K. Ohata, Y. Suzuki, and H. Toyoshima, "A new low-noise AlGaAs/GaAs 2DEG FET with a surface undoped layer," *IEEE Trans. Electron Devices*, vol. ED-33, pp. 601–607, May 1986.

[19] P. R. Jay, H. Derewonko, D. Adam, P. Briere, D. Delagebeaudeuf, P. Delescluse, and J.-F. Rochette, "Design of TEGFET devices for optimum low-noise high-frequency operation," *IEEE Trans. Electron Devices*, vol. ED-33, pp. 590–594, May 1986.

[20] L. D. Nguyen, P. J. Tasker, D. C. Radulescu, and L. F. Eastman, "Characterization of ultra-high speed pseudomorphic AlGaAs/InGaAs (on GaAs) MODFET's," *IEEE Trans. Electron Devices*, vol. 36, pp. 2243–2248, Oct. 1989.